Modeling Fire Growth on Combustible Lining Materials in Enclosures

Karlsson, Björn

1992

LUND UNIVERSITY

Department of Fire Safety Engineering

Report TVBB-1009, Lund 1992

Modeling Fire Growth on Combustible Lining Materials in Enclosures

Björn Karlsson

Report TVBB 1009
ISSN 1102-8246
ISRN LUTVDG/TVBB--1009--SE

Modeling Fire Growth on Combustible Lining Materials in Enclosures

Björn Karlsson

Research financed by the Swedish Fire Research Board (BRANDFORSK)

2nd edition

Printed in Sweden
KF-Sigma
Lund 1992

Abstract

An extensive research program, dealing with fire growth on combustible wall lining materials, has been ongoing in Sweden over the last decade. Several lining materials were tested in bench-scale fire tests in order to derive basic material flammability parameters. The same materials were also tested in a full scale room test and a 1/3 scale room test for two different scenarios, A and B. Scenario A refers to the case where walls and ceiling are covered by the lining material, Scenario B where lining materials are mounted on walls only.

This study utilises the results from these experiments and presents mathematical models where material properties derived from standardised bench-scale tests are used as input data. The models predict fire growth in the full or 1/3 scale tests, and consist of sub-models for calculating the rate of heat release, gas temperatures, radiation to walls, wall surface temperatures and flame spread on the wall lining material.

A thermal theory of wind-aided flame spread on thick solids is examined and solutions are given for flame spread velocities under ceilings and in wall-ceiling intersections. Flame extensions under a ceiling, associated with these processes, are discussed and the behaviour of the solutions analysed.

The results from the models are compared with experiments on 22 materials tested in the full scale room and 13 materials tested in the 1/3 scale room for Scenario A. Comparisons for Scenario B are made with 4 materials in full scale and 10 materials in 1/3 scale. The results show reasonably good agreement for most materials between the model and the experiments.

List of symbols

A_f	Flame area (m^2)
A_p	Pyrolysis area (m^2)
A_o	Area of opening (m^2)
A_0	Initial pyrolysing area (m^2)
A_w	Combustible wall area behind the burner (m^2)
A_{tot}	Total surface area of enclosure (m^2)
a	Dimensionless constant (=K Q)
b	Ignition correlation parameter ($s^{-1/2}$)
c	Specific heat capacity (kJ/kg K)
C	Pre-exponential constant in equation (64)
C_1	Constant (m/s) and (m^2/s), depending on units of K
C_2	Constant (s)
C_3	Constant (s^{-1})
D	Characteristic dimension of burner (m)
F	Configuration factor (-)
g	Gravitational acceleration (m/s^2)
h	Convective and radiative heat transfer coefficient (kW/m^2K)
h_c	Convective heat transfer coefficient (kW/m^2K)
h_k	Heat transfer coefficient in equation (65) (kW/m^2K)
h_N	Newtonian cooling coefficient (kW/m^2K)
H	Height (m)
H*	Modified height for flame extension correlations (m)
H_o	Height of opening (m)
ΔH	Change in enthalpy (kJ/kg)
K	Constant in flame length and flame area correlations (m/kW) and (m^2/kW)
K	Constant in non-linear flame length correlations, eqns (22) - (26) (m/kW^n)
k	Thermal conductivity of the solid fuel (kW/mK)
$k\rho c$	Apparent thermal inertia (kW^2 s /m^4 K^2)
L	Length (m)
L_r	Flame extension under ceiling (m)
L_0	Correlation coefficient for flame extension under ceiling (m)
$\dot{m}'_{air}$	Air entrainment per width and unit time (kg / s m)
n	Exponential constant in flame length correlations (-)
$\dot{q}''$	Radiative heat flux per area (kW/m^2)
$\dot{q}''_{0,ig}$	Minimum radiant heat flux per area for piloted ignition (kW/m^2)
$\dot{q}''_e$	External radiant heat flux per area (kW/m^2)

$\dot{q}''_f$	Radiant heat flux from flame per area (kW/m^2)
$\dot{q}''_w$	Radiant heat flux from burner flame per area (kW/m^2)
$\dot{Q}''$	Energy release rate per fuel area (kW/m^2)
$\dot{Q}^*$	Dimensionless energy release rate
$\dot{Q}_b$	Energy release rate from burner (kW)
$\dot{Q}_L$	Combustion energy released in corner (see eqn (47)) (kW)
$\dot{Q}_{tot}$	Total heat release rate (kW)
$\dot{Q}''_{max}$	Maximum heat release rate of the fuel per unit area measured in the Cone Calorimeter at an irradiance level of 50 kWw/m^2 (kW/m^2)
$\dot{Q}''_C$	Heat release rate from the Cone Calorimeter per unit area (kW/m^2)
$\dot{Q}_c$	Total heat release rate from fuel in ceiling (kW)
s	Laplace transform operator
s_1	Constant (s $^{-1}$)
s_2	Constant (s $^{-1}$)
T	Temperature (K or °C)
T_f	Flame temperature (K or °C)
$T_{fl.f}$	Material surface temperature just ahead of the flame front (K or °C)
T_{ig}	Ignition temperature (K or °C)
T_s	Surface temperature (K or °C)
$T_{s,min}$	Minimum surface temperature for opposed flow flame spread (K or °C)
T_0	Initial temperature (K or °C)
t	Time (s)
t_{ig}	Time to piloted ignition in the Cone Calorimeter
t_p	Dummy variable of integration (s)
V	Velocity (m/s)
V_A	Flame spread velocity under ceiling in Model A (m^2/s)
V_d	Downward flame spread velocity (m/s)
V_h	Flame spread velocity in horizontal wall-ceiling intersection (m/s)
V_p	Velocity of the pyrolysis front in (m/s) or (m^2/s) (specified in the text)
W	Width (m)
x_f	Flame height (m)
x_p	Height of the pyrolysis front (m)
x_{p0}	Initial height of the pyrolysis front (m)
y	Distance into solid, perpendicular to surface (m)

α	Entrainment coefficient in eqn. (68)
α	Constant (1/s)
β	Constant (1/s)
Δ	Distance in equations (9) - (14) (m)

Δ	Constant (s^{-2})
δ	Fuel thickness (m)
ε	Emissivity (-)
Φ	Flame heating parameter (kW^2/m^3)
λ	Decay coefficient when simulating results from Cone Calorimeter (s^{-1})
ν	Kinematic viscosity (m^2/s)
ρ	Density (kg/m^3)
τ	Time to ignition (s)
τ_w	Time to ignition of the wall material behind the burner (s)
σ	Stefan-Boltzmann constant (W/m^2K^4)

Subscripts

f	flame
g	gas
gc	gas phase conduction
ig	ignition
lin	lining material
lwc	light weight concrete
p	pyrolysis
∞	ambient

Contents

1 Introduction

This research work has been performed as a partial fulfillment of the Ph.D requirements at the Department of Fire Safety Engineering at Lund University. This first chapter discusses the background of the work and the contents of the thesis.

1.1 Background

The main purpose of fire regulations has been to ensure an acceptable level of fire risk to the population. Up until the turn of the 19th century the regulations were mainly concerned with inhibiting the spread of fire from one building to another by prescribing minimum distances between buildings and by organising fire fighting. Later, fire endurance requirements for certain structural elements were formulated, based on direct testing of the elements. Testing of materials was limited to measurements of thermal properties and strength at high temperatures.

In the 1960's great advancements were made in predicting the influence of high temperature on structural elements, resulting in a performance-based regulatory system for such elements. Furnishings and other non-structural features of the building had been, to a large extent, either non-regulated or simply related to performance in a specified bench scale test. The relationship between the material behaviour in such a test and in a real fire has remained unknown in any general predictive sense.

Only recently has attention been drawn towards the materials used in furnishings and wall linings. Work in this area has included development of bench-scale tests to derive basic flammability characteristics which could rationally be used as classification criteria. Also, full-scale standard tests have been developed to evaluate the fire performance of materials and products in real-life situations. The contribution of a specimen to the fire growth within a previously calibrated compartment can then be used to rate materials and to evaluate the validity of existing bench-scale test methods.

In Sweden, over the last decade, work in this area has been coordinated, mainly within a single research project entitled "Fire Hazard - Fire Growth in Compartments in the Early Stage of Development (Pre-flashover)". The project was carried out jointly by Lund University, the Swedish National Testing and Research Institute and the Swedish Institute for Wood Technology Research. The

project was funded by the Swedish Fire Research Board; an outline of the research program is given by Pettersson /1/. The work contained in this thesis utilises both experimental and theoretical results from the overall project.

Additionally, a second reseach project on combustible wall lining materials has recently been carried out by the National Fire Testing laboratories in Denmark, Finland, Norway and Sweden. The project has been named EUREFIC /2/ and experimental results from this project will also be used in the current study.

1.2 Overview of this dissertation

Over the last two decades, real advances have been made in the understanding of fire phenomena and the interaction of fires with buildings. At the same time the development within modern building technology has resulted in an overall increase of fire hazards; buildings tend towards unconventional sizes and shapes while materials used in furniture, combustible lining materials and other fittings exhibit more hazardous flammability characteristics.

The need to take advantage of the emerging new technology, both with regards to design and regulatory purposes, is therefore obvious. The objective of this work is to contribute in a small way towards that goal by constructing mathematical models which could rationally predict full scale fire growth on combustible lining materials. The input to the models are results from modern bench-scale flammability tests.

Two mathematical models will be described. Model A describes the case where the combustible lining material is mounted on the walls and the ceiling of an enclosure and Model B the case where the lining material is mounted on the walls only. Two room sizes will be considered: the full scale test room with a single door opening in accordance with methods proposed by ISO /6/ and NORDTEST /90/; and, a 1/3 scale model of the full scale compartment.

Chapter 2 gives a summary description of three bench-scale test methods and lists derived flammability parameters for several materials. These parameters are then used as input to the models described in Chapter 4.

In order to predict fire growth on combustible materials, flame spread velocities must be considered. Chapter 3 discusses flame spread over solids, in particular concurrent flow flame spread under ceilings and in wall-ceiling intersections, as well as flame extensions associated with these processes. Limits of flame spread propagation and non-propagation are described as a function of material

flammability parameters. Finally, a simple, analytical model for flame spread under ceilings is presented.

In Chapter 4, two mathematical models for calculating fire growth on combustible lining materials are presented; Model A and Model B. The models consist of sub-models for the calculation of gas temperatures, material surface temperatures, flame spread and heat release rates.

Chapter 5 describes the full scale and 1/3 scale room experiments and presents a comparison of the calculated results from Models A and B with the results from the experiments.

Chapter 6 describes how the mathematical models can be replaced by simple regression equations, where time to flashover is expressed as a function of the material parameters from the bench-scale tests. This allows some preliminary conclusions to be drawn as to the importance of each of the parameters.

Finally, Chapter 7 summarises the conclusions of the work and discusses possible further areas of investigations.

It should be noted that in the course of developing the mathematical models some engineering assumptions will have to be made with respect to many physical phenomena. The study reported here is therefore of a pilot character and should be seen as a first, preliminary attempt to arrive at a rational engineering solution to a recognized and important fire safety problem.

2 Bench-scale tests

2.1 Introduction

There are currently in existence a large number of standardised national and international fire test methods, designed to classify, rank or measure fire properties of materials /3/. Some of these are bench-scale test methods, where only a small sample of the material is tested. Many of these test methods only give as output certain rating terms (class A, etc) or arbitrary numbers (sometimes on a scale of 0 - 100). Such results have often little to do with the actual fire properties of materials.

Set against this is the substantial progress which has been made during the last decade in the understanding of fire processes and their interaction with buildings and humans. Many computer models have been developed (Friedman, /4/), successfully predicting the fire environment in a room, given that the energy release rate in the room is known and used as input to the model.

It would be advantageous if results from bench-scale tests on materials could be used as input to such models in order to estimate the contribution from internal lining materials to the fire growth in a full-scale room. This is possible only if the output from the bench-scale test is an actual or estimated property of the material and not just a rating or an arbitrary number.

Due to the improved understanding of fire physics, a number of physically based modern test methods for flammability have been developed in recent years. Babrauskas /5/ summarises these test methods, including the ISO Ignitability Test (ISO 5657) /6/, the Cone Calorimeter (ISO DIS 5660) /7/ and both the American and International version of the Lateral Ignition and Flame Spread Test (LIFT) /8/, /9/.

In this chapter we shall describe the three above mentioned bench-scale test methods and report the derived flammability parameters for the materials listed in Table I. These parameters are then used as input to the fire growth models described in Chapter 4. It should be noted that some of these models only need as input results from the Cone Calorimeter; others also need results from the Lateral Ignition and Flame Spread Test, depending on the scenario being treated and the modelling accuracy required.

The ISO Ignitability Test is also discussed since some results from this test method will be used here to complement ignitability data for some of the materials listed in Table I.

Table I Combustible wall lining materials considered in this work

Material No.	Material name	Approximate thickness (mm)	Apparent weight (kg/m^2 or kg/m^3)
S1	Insulating fibreboard	13	3.25 kg/m^2
S2	Medium density fibreboard	12	7.2 kg/m^2
S3	Particle board	10	7.5 kg/m^2
S4	Gypsum plaster board	13	9.1 kg/m^2
S5	PVC wallcovering on gypsum plaster board	13.7	9.34 kg/m^2
S6	Paper wallcovering on gypsum plaster board	13.6	9.3 kg/m^2
S7	Textile wallcovering on gypsum plaster board	13.7	9.47 kg/m^2
S8	Textile wallcovering on mineral wool	42.7	7.87 kg/m^2
S9	Melamine faced particle board	14.2	11.5 kg/m^2
S10	Expanded polystyrene	50	1.0 kg/m^2
S11	Rigid polyurethane foam	30	0.9 kg/m^2
S12	Wood panel, spruce	11	5.8 kg/m^2
S13	Paper wallcovering on particle board	10.6	7.7 kg/m^2
E1	Painted gypsum paper plaster board	13	9.5 kg/m^2
E2	Ordinary plywood	12	725 kg/m^3
E3	Textile wallcovering on gypsum paper plaster board	13	9.8 kg/m^2
E4	Melamine faced high density non-combustible board	13	14.0 kg/m^2
E5	Plastic faced steel sheet on mineral wool	25	16.3 kg/m^2
E6	FR particle board type B1	16	630 kg/m^3
E7	Faced rockwool	30	2.6 kg/m^2
E8	FR particle board	12	755 kg/m^3
E9	Polyurethane foam covered with steel sheet	80	12.6 kg/m^2
E10	PVC-wall carpet on gypsum paper plaster board	13	10.6 kg/m^2
E11	FR polystyrene	25	37 kg/m^3

It should be noted that other modern bench-scale tests have been proposed, for example, a test which takes account of the radiant emission from the material's own flames (deRis, /10/). This test has not yet been standardised and will not be considered in this study.

For a more thorough discussion on the theoretical and practical aspects of bench-scale testing, the recent work of Jansenss /11/ is recommended.

2.2 The Cone Calorimeter

In order to estimate the fire hazard in a room where a wall lining material is burning one has to be able to predict the energy release rate from the material. Many attempts have been made to calculate this from first principles, by setting up and solving the conservation equations for mass and energy and taking account of oxygen concentrations, charring, gas phase chemistry, moisture content, etc. These attempts have met with some success in well-defined small scale experiments, but have been restricted to consider only a few materials. The methods typically require extensive bench-scale testing by both standardised and non-standardised test methods. A recent review of such models is given by Parker /12/.

The Cone Calorimeter provides a somewhat more empirical approach to this problem, where heat release from a small sample of material under a constant heat flux is assumed to represent the heat release rate from the material in a full-scale test. This approach will be used in the current work.

The Cone Calorimeter (Figure 1) makes use of an electric heater in the form of a truncated cone, hence its name (Babrauskas, /13/). A square sample of material, 100mm * 100mm, is subjected to a constant radiant flux from the cone heater, typically in the range 20 - 75 kW/m^2. A spark igniter is used for piloted ignition. A complete description of the design of the apparatus and test methodology is given in /7/.

The material surface temperature rises due to the external radiation and pyrolyses begins. Once the mixture of fuel vapors and air above the sample exceeds the lower flammability limit the sample ignites and the time to ignition is recorded. The combustion products are collected in a hood system and the oxygen concentration and air flow are measured. The apparatus utilises the principle of oxygen consumption to calculate the heat released by the material. Mass loss rate from the sample is also measured. The results from the test are thus, for each exposure level, time to ignition, mass loss rate and rate of heat release (RHR).

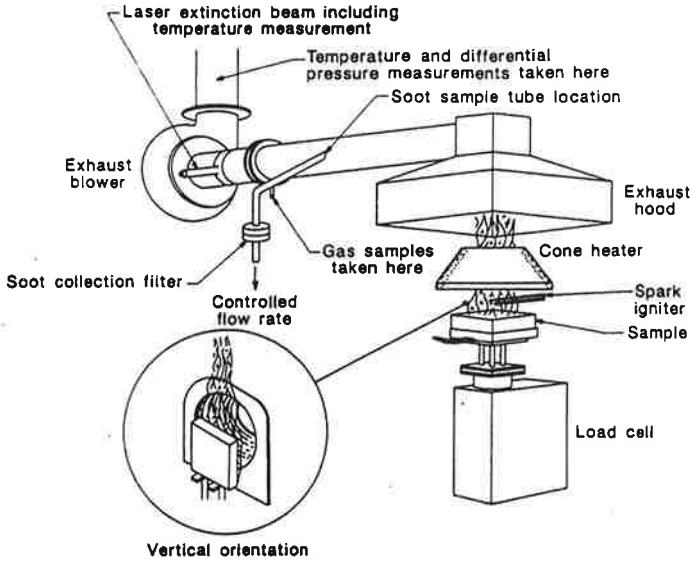

Fig. 1. A Schematic view of the Cone Calorimeter (from /5/)

The Cone Calorimeter data used in this study are the results of two tests series. The first 13 materials given in Table I (denoted S1 - S13) were tested by Tsantaridis and Östman /14/ at the Swedish Institute for Wood Technology Research. The materials listed as E1 - E11 in Table I were tested within a joint Nordic fire research program, EUREFIC, and the results were reported by Thureson /15/.

2.2.1 The "Swedish" materials

The first 13 materials in Table I (sometimes referred to as the "Swedish" materials) were originally tested in three different RHR apparatuses; the Ohio State University apparatus /16/; an open configuration /17/ based on a design originally developed by the National Institute of Standards and Technology (formerly National Bureau of Standards) /18/; and the Cone Calorimeter /19/. The measurements used here are from the Cone Calorimeter and were reported in /14/. The samples were tested at an irradiance level of 25, 50 and 75 kW/m^2. An example of the test output is given in Figure 2 for material no. 3.

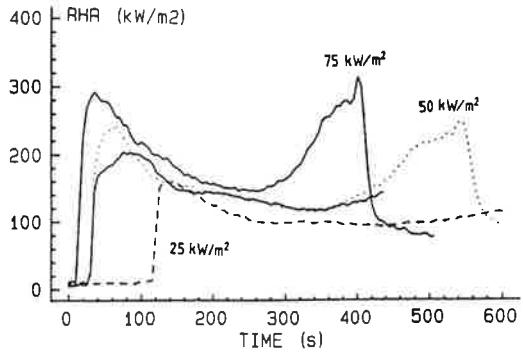

Fig. 2. Rate of heat release results from the Cone Calorimeter (from /14/).

2.2.2 The EUREFIC materials

Materials No. E1 - E11 in Table I were tested in the Cone Calorimeter in two orientations, vertical and horizontal /15/. The irradiance levels were 25, 35, 50 and 75 kW/m^2. In an attempt to use the same full-scale calculation methodology for both the "Swedish" and the EUREFIC materials we have only used the results from the horizontal orientation, since the "Swedish" materials were only tested in this way.

Further, we have chosen to use the results from the 50 kW/m^2 irradiance level for the same reason. The "Swedish" materials were only tested at an irradiance level of 25, 50 and 75 kW/m^2, the 50 kW/m^2 irradiance level being the most representative in a full-scale test. There is, however, some evidence that this value may be too high, a level of 35 kW/m^2 is perhaps the more suitable /19/.

2.2.3 Mathematical representation of the Cone Calorimeter results

One of the mathematical models described in Chapter 4 is numerically based and can therefore use as input the whole heat release rate curve from the Cone Calorimeter. Other models, described in Chapters 3 and 4, are based on analytical solutions of the flame spread equations and cannot use these results directly as input. The rate of heat release curve from the cone must be expressed in mathematical terms in order to allow analytical solutions.

Several workers have proposed schemes for such mathematical representations of the heat release rate from the Cone Calorimeter /20/, /21/, /22/, /23/. The most

simple of these are the approaches described by Cleary et al. /23/ and Magnusson et.al. /20/. The former approximates the heat release rate as an average constant value with a certain duration, taking account of the area under the actual heat release curve. The latter, which is the approach we will use in this work, idealised the experimental curves as seen in Fig. 3, resulting in the expression

$$\dot{Q}''(t) = \dot{Q}''_{max}\, e^{-\lambda t} \qquad (1)$$

Equation (1) assumes semi-infinite sample (no returning heatwave) so that no account is taken of the last part of the curve (where heat release rate can be seen (Figure 2) to be increasing). This assumption has been partly justified by Thomas and Karlsson /24/ who found that the initial part of the heat release rate curve has a much greater influence on the fire growth than the final part of the curve, particularly when modeling concurrent flow flame spread.

Also, the peak heat release is often rounded off in the experiments due to the delay time of the measuring system. Kokkala /25/ has shown that, having taken account of the delay time in the experimental apparatus, there is a sharp peak in the curve and a subsequent decay, resulting in a shape very similar to the one seen in Fig. 3.

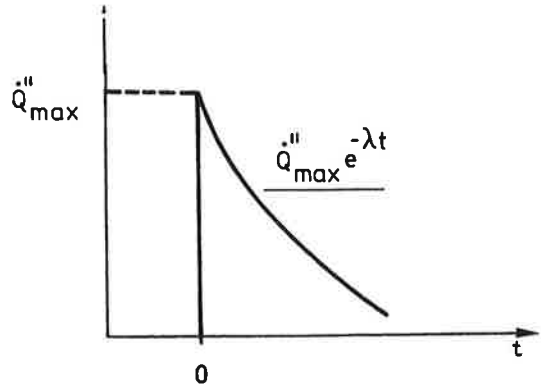

Fig. 3. Principle for analytical approximation of experimental RHR curves.

The $\dot{Q}''_{max}$ values were taken directly from Cone Calorimeter measurements at 50 kW/m^2 irradiance and are given, together with the corresponding regression values of λ, in Table II. Equation (1) seemed phenomenologically correct except for materials 9 and 10. Section 3.5.3 summarises the methodology, a full description of its background is given by Magnusson et al. /20/.

Table II: Heat Release parameters $\dot{Q}''_{max}$ and λ derived from Cone Calorimeter experiments 50 kW/m^2 irradiance level

Mat No.	Material name	$\dot{Q}''_{max}$ kW/m^2	λ s^{-1}
S1	Insulating fiberboard	184	0.0090
S2	Medium density fiberboard	208	0.0027
S3	Particle board	204	0.0030
S4	Gypsum plasterboard	151	0.0390
S5	PVC cover on gypsum pl. board	210	0.0600
S6	Paper cover on gypsum pl. board	254	0.0600
S7	Textile cover on gypsum pl. board	408	0.0700
S8	Textile cover on mineral wool	466	0.0800
S9	Melamine-faced particle board	150	0.0016
S10	Expanded polystyren	-	-
S11	Rigid polyurethane foam	247	0.0200
S12	Wood panel, spruce	168	0.0075
S13	Paper cover on particle board	197	0.0041

2.3 The ISO Ignitability Test

Under normal circumstances, bench-scale data from the ISO Ignitability Test /6/ would not be needed; ignitability can be measured both in the Cone Calorimeter and the Lateral Ignition and Flame Spread Test. However, the "Swedish" materials in Table I were tested according to an old version of the Lateral Ignition and Flame spread Test (Sundström, /26/) where no time to ignition was recorded for the different flux levels and ignitability data from other sources must therefore be used.

Ignitability data for these materials are available from the Cone Calorimeter tests, but only at three heat flux levels. More data is needed to derive the flammability parameters used as input to the fire growth models discussed in Chapter 4. We will attempt to reconstruct the ignitability data for these materials by using data on ignition from both the Cone Calorimeter and the ISO Ignitability Test. The data is taken from Östman and Tsantaridis /27/ who compared ignitability data from these two test methods, concluding that the two methods were compatible and gave similar results.

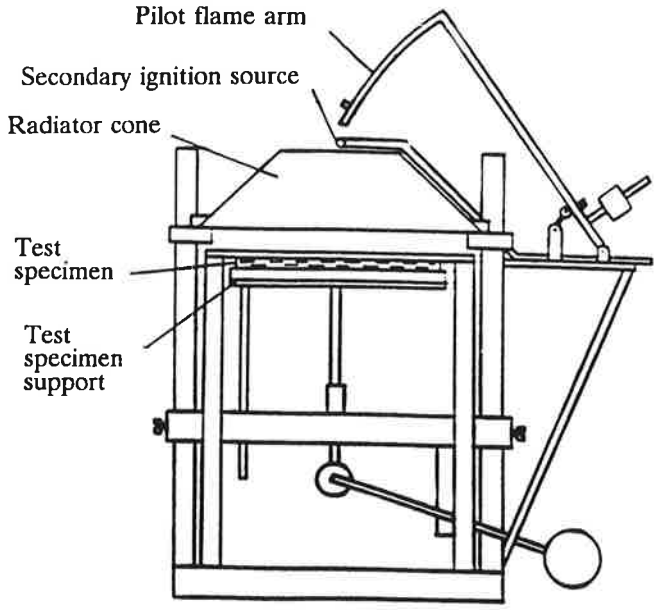

Fig. 4. A schematic view of the ISO radiant ignition apparatus.

The ISO Ignitability Test apparatus is somewhat similar to the Cone Calorimeter with respect to its heater; it is an electrical heater in the shape of a truncated cone (see Figure 4). The specimen is orientated horizontally upwards and its size is

165 mm * 165 mm. A pilot flame is introduced at regular intervals at a position 10 mm above the sample in order to ignite any volatile gases emerging from the surface. Heat fluxes for testing should be 10, 20, 30, 40, and 50 kW/m^2 and results are the time to ignition at these heat flux levels.

The ignitability data used in this study is given in Tables III and IV /27/ in Appendix A and the way in which it is used to develop material flammability parameters is discussed in the following section.

2.4 Lateral Ignition and Flame Spread Test (LIFT)

Both the International Standards Organization (ISO) and the American Society for Testing and Materials (ASTM) have developed test methods to characterise flame spread properties of materials /8/, /9/. These are based on the method originally developed by the International Maritime Organization (IMO) /28/ but in the ASTM and the ISO method the data treatment and analysis are carried out according to a theory of flame spread developed by Quintiere /29/.

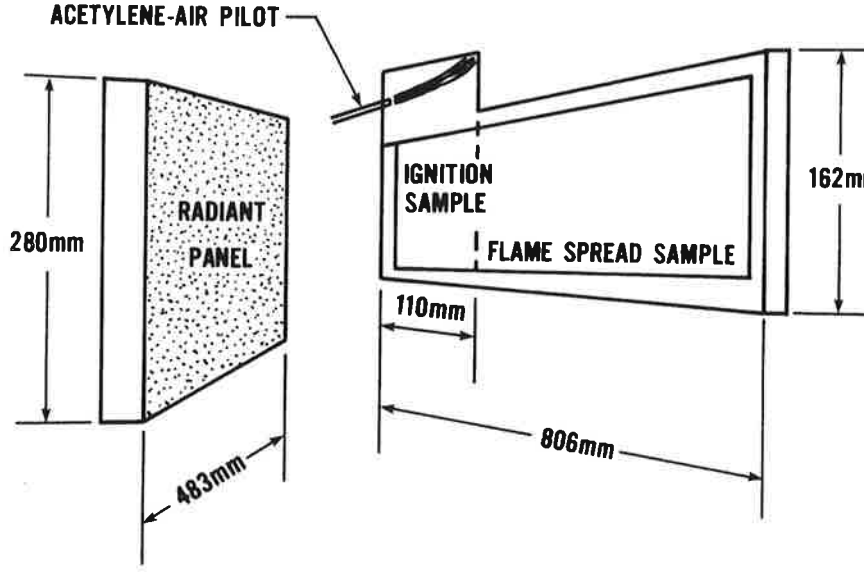

Fig. 5. A schematic view of the LIFT apparatus.

The test consists of two procedures: one to measure ignition and one to measure lateral flame spread, sometimes referred to as opposed flow flame spread. The test apparatus has been named LIFT, for Lateral Ignition and Flame spread Test and is shown in Figure 5. Vertically mounted specimens are exposed to the heat from a vertical air-gas fuelled radiant-heat energy source inclined at 15° to the specimen.

For the ignition test, a series of 155 mm * 155 mm specimens are exposed to a nearly uniform heat flux and the time to ignition, using a pilot flame as igniter, is recorded. For the flame spread test, a specimen measuring 155 mm * 800 mm is exposed to a heat flux, gradually decreasing along the horizontal length of the sample. After ignition, the flame spread velocity along this length of the specimen is recorded. The data from the two procedures is then correlated with a theory of ignition and flame spread for the derivation of material flammability properties.

The theoretical aspects of opposed flow flame spread are discussed in Chapter 3. The following is a short description of how the flammability properties are derived; a full and accurate description is provided in the ASTM /8/ and ISO /9/ standards. The flammability properties we are interested in deriving are:

$\dot{q}''_{0,ig}$	the critical heat flux for ignition, per unit area of specimen
T_{ig}	the ignition temperature
$k\rho c$	the apparent thermal inertia
Φ	the flame heating parameter

An additional parameter, the minimum surface temperature for flame spread, $T_{s,min}$ can also be derived from this test and can be useful when modeling the initiation of downward, opposed flow flame spread. In the models presented in Chapter 4, this phenomenon is presently solved in an alternative manner and this parameter is thus not used here.

Quintiere et al. /30/ have shown that, for flat vertical surfaces heated by a constant flux, the heat flux and the ignition time can be related by the semi-empirical expression

$$(\dot{q}''_{0,ig} / \dot{q}''_e) = b\sqrt{t} \qquad (2)$$

where $\dot{q}''_e$ is the external heat flux per unit area, t is the time to ignition and b is an empirical coefficient, related to the apparent thermal inertia, $k\rho c$. The critical heat flux for ignition, $\dot{q}''_{0,ig}$, is simply measured by repeated measurements, decreasing the incident heat flux step by step until no ignition occurs.

The ignition temperature, T_{ig}, is calculated by iteration, using the relationship

$$\dot{q}''_{0,ig} = h_c(T_{ig} - T_\infty) + \sigma(T_{ig}^4 - T_\infty^4) \equiv h(T_{ig} - T_\infty) \quad (3)$$

where h_c is the convective heat loss coefficient, taken to be 15 W/m^2 in this test. Thus, the total heat loss coefficient, h, can also be calculated.

By plotting $(q''_{0,ig} / q''_e)$ versus $\sqrt{t}$ and drawing a straight fit line through the data, up to the point where $(q''_{0,ig} / q''_e) = 1$, the ignition correlation parameter, b, can be determined. The apparent thermal inertia is then calculated from

$$k\rho c = \frac{4h^2}{\pi b^2} \quad (4)$$

The flame heating parameter, Φ, can be derived using the second procedure of the test, the Flame Spread Test. The flame spread velocity, V, is calculated by applying a running three-point least squares fit to the measured flame front position-time data. By plotting $V^{-1/2}$ versus $q''_e F(t)$ where

$$F(t) = \begin{cases} b\sqrt{t}, & t \le t^* \\ 1, & t \ge t^* \end{cases} \quad (5)$$

the flame spread parameter, C, is obtained as the slope of the straight line fitted to the data. t^* is the characteristic equilibrium time. The flame heating parameter, Φ, is then calculated from

$$\Phi = \frac{4}{\pi(Cb)^2} \quad (6)$$

A more complete description of the methodology is given in the ASTM standard /8/ and an in depth discussion on the theory by Quintiere et al. /30/.

It should be noted that Jansenss /31/ has recently proposed that essentially the same methodology could be applied to data from the Cone Calorimeter with a slight modification in the equations.

2.4.1 The "Swedish" data

As mentioned earlier, the "Swedish" materials were tested according to an old version of the Lateral Ignition and Flame spread Test /22/ where no time to ignition was recorded for the different flux levels. Therefore, the ignitability parameters ($\dot{q}''_{0,ig}$, T_{ig} and $k\rho c$) could not be derived according to the standardised methods. In order to reconstruct the ignitability data for these materials we have used data on ignition from both the Cone Calorimeter and the ISO Ignitability Test (see Tables III and IV in Appendix A).

Figure 6 shows, as an example, a plot of time to ignition versus external heat flux for material S3. The resulting critical heat flux for ignition is determined to be 19 kW/m^2. Figure 7 shows, for the same material, a plot of $(\dot{q}''_{0,ig} / \dot{q}''_e)$ versus $\sqrt{t}$, the slope of the straight line fit giving a value of the ignition correlation parameter, b. The ignition temperature and the apparent thermal inertia were then calculated according to the procedure outlined above and the results are given in Table V. Corresponding graphs for all of the "Swedish" materials are given in appendix A-1 and A-2, showing a reasonable consistency between the data from the Cone Calorimeter and the Ignitability Test.

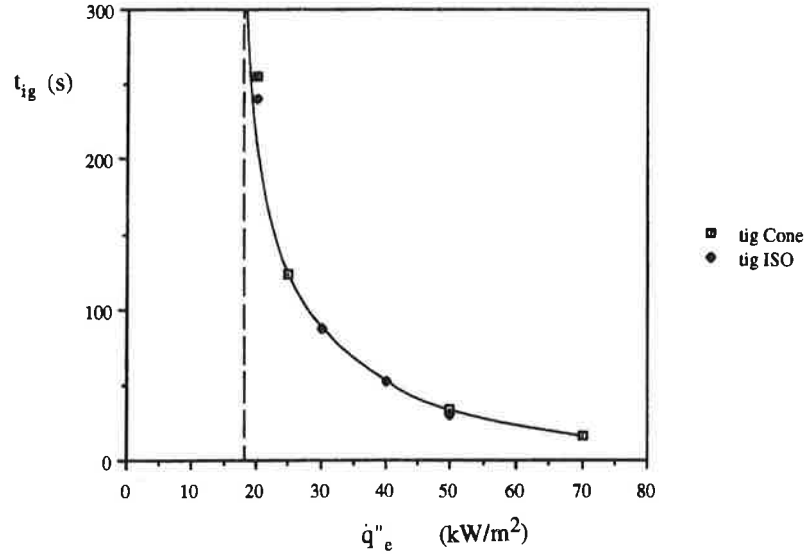

Fig. 6. Time to ignition versus external heat flux for material S3

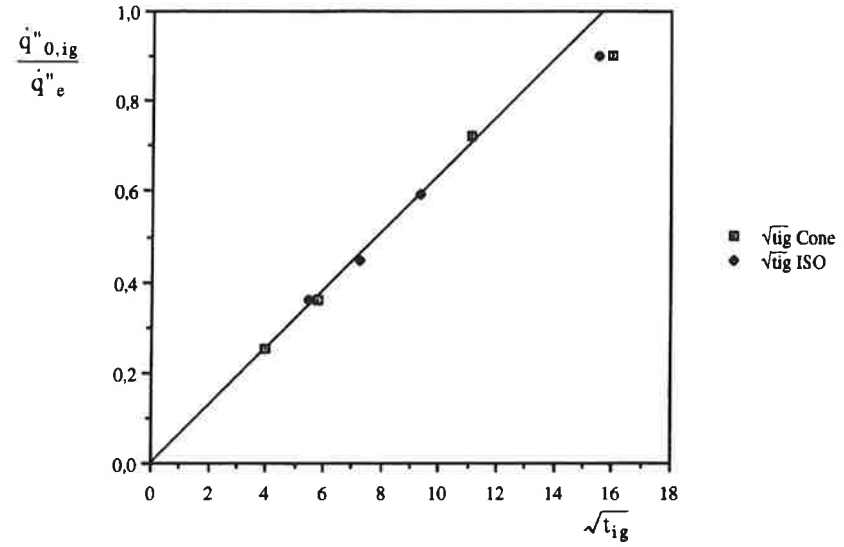

Fig. 7. A plot of ($q''_{0,ig}$ / q''_e) versus $\sqrt{t_{ig}}$ for material S3

Cleary and Quintiere /23/ have also reported ignitability parameters for these materials. A description of the procedure they followed and the data used has not yet been published but there is a very good agreement with the values reported here. Figures 8 and 9 show the difference between values of kρc and T_{ig} reported in /23/ and in this work, respectively.

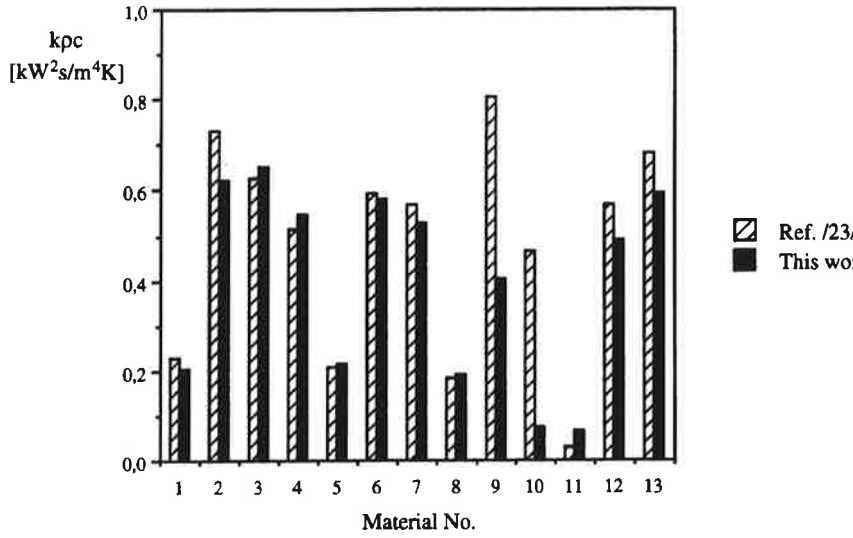

Fig. 8. Apparent thermal inertia, kρc, reported here and in /23/

Table V Parameters derived from the Ignitability test and the LIFT apparatus for the "Swedish" materials.

Mat. No.	$\dot{q}''_{o,ig}$ [kW/m²]	T_{ig} [°C]	kρc [kW²s/m⁴K²]	Φ [kW²/m³]
S1	19	423	0.204	12.9
S2	17.5	406	0.621	9.3
S3	18.0	412	0.653	9.1
S4	27.5	503	0.546	14.7[b]
S5	17.5	406	0.217	12.6[c]
S6	18.0	412	0.580	0.6
S7	18.0	412	0.570	9.1
S8	16.6	396	0.190	8.7
S9	27.0	500	0.403	0.5[b]
S10	20.0	434	0.372[a]	24.9[b]
S11	10.0	302	0.068	6.7[b]
S12	19.5	429	0.489	20.5[b]
S13	19.0	423	0.595	4.9[c]

[a] Average of two values, 0.074 and 0.670, see Appendix A-2.
[b] Data from Cleary et al. /23/, evaluated for the above kρc data.
[c] Reevaluation of data from Karlsson /85/.

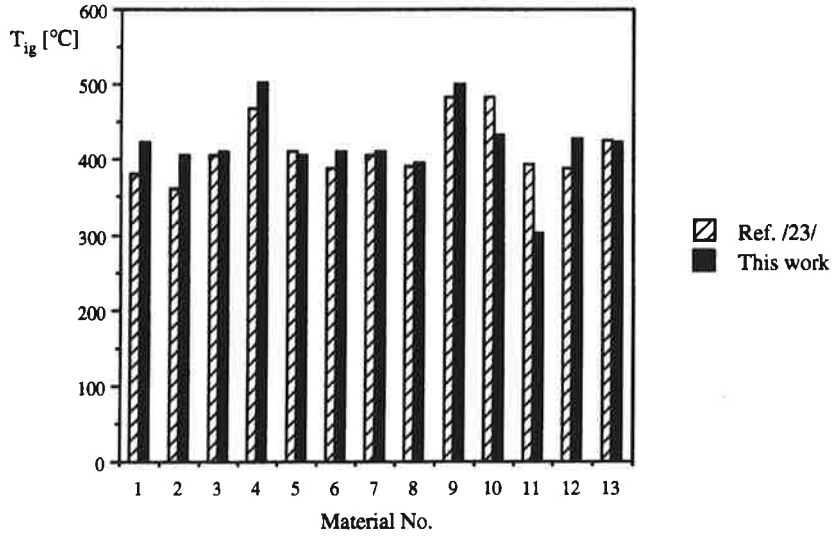

Fig. 9. Ignition temperature, T_{ig}, reported here and in /23/.

2.4.2 The EUREFIC materials

The EUREFIC materials were tested in the LIFT apparatus according the ASTM E 1321 standard /8/. The results were reported by Nisted /32/. Only 9 out of 11 materials ignited in the LIFT; material parameters were therefore only determined for 9 of the materials.

Unfortunately, some of the slopes in the $(\dot{q}''_{0,ig} / \dot{q}''_e)$ versus $\sqrt{t}$ diagrams in /32/ seem to have been drawn incorrectly, resulting in incorrect values for $k\rho c$. This seems to be the case for Materials No. E2, E3, E9, E10 and E11. For very long times (i.e. points with high $\sqrt{t}$ and close to the line $(\dot{q}''_{0,ig} / \dot{q}''_e) = 1$) some influence of a returning heat wave may be present and the slope should therefore be drawn with emphasis on the points with lower values of $\sqrt{t}$. We reproduce these graphs in Appendix A-3 with new slopes drawn in. The results are given in Table VI.

Table VI Parameters derived from the LIFT apparatus for the EUREFIC materials, from /32/ and Appendix A-3

Material No.	$\dot{q}''_{o,ig}$ kW/m²	T_{ig} °C	kρc (kW/m²K)²· s
E1	33.8	552	0.7206
E2	16.3	392	0.9746[a]
E3	15.9	387	0.77147[a]
E4	46.7	631	0.3036
E5	35.4	563	0.5707
E6	[b]	[b]	[b]
E7	13.4	355	0.0815
E8	[b]	[b]	[b]
E9	26.4	495	0.5390[a]
E10	16.2	391	0.5451[a]
E11	32.3	541	0.4892[a]

[a] Reevaluated data, due to incorrectly drawn slopes in the graphs of $(\dot{q}''_{o,ig} / \dot{q}''_{e})$ versus $\sqrt{t_{ig}}$ (see Appendix A3).

[b] Values not derived due to the fact, that the material did not ignite.

3 Flame spread over solids

3.1 Introduction

The ignition of a combustible material and the subsequent spread of flame over its surface is a most important phenomenon regarding the growth of compartment fires. Many theories of flame spread have been presented, most of them qualitative rather than quantitative. These can be divided into two groups: theories that consider flame spread in terms of chemical kinetics and regard the thermal fluxes and flame temperature as dependent variables to be determined; and those that regard these as given quantities, thus ignoring chemical kinetics and only considering energy conservation (so called thermal theories).

Here, we shall not present an extensive review of the different flame spread phenomena and the physical processes involved, since several authors have already given excellent reviews, for example Williams /33/, Fernandez-Pello and Hirano /34/, Quintiere /35/, and more recently Janssens /11/, Wichman /36/ and Di Blasi /37/.

We shall here only present a short overview of the various modes of flame spread over solids in order to orientate the reader and establish a basis for the more detailed discussion that follows.

Williams /33/ gave a comprehensive review of flame spread where he discussed the processes involved in terms of a simple energy conservation principle and gave "the fundamental equation of fire spread". The equation states that the heat transferred to the virgin fuel needed to heat the fuel from T_0 to T_{ig} equals its change in enthalpy and is given as

$$\rho V \Delta H = \dot{q}'' \qquad (7)$$

where ρ is the density of the fuel heated to ignition, V is the spread rate, ΔH the change in enthalpy per unit mass of unburnt fuel in going from temperature T_0 to T_{ig} and q" is the heat transferred to the unburnt fuel needed to increase its temperature from T_0 to T_{ig}. With respect to solid fuels, the ignition temperature, T_{ig}, is assumed to be the temperature at which the solid emits sufficient amounts of flammable gas to support piloted ignition in the gas phase.

Usually the density of the fuel is known and assuming that its specific heat capacity, c, is constant with temperature, the increase in enthalpy can be written as

$$\Delta H = c(T_{ig} - T_0) \tag{8}$$

Williams /33/ systematically discussed the influence of fuel geometry, orientation and state on the quantities given in equation (7). He defined the dominant mode at which heat is transferred to the unburnt fuel as the one that produces the largest contribution to q". There are mainly three mechanisms of heat transfer between the flame and the virgin fuel: convection (gas phase conduction), radiation and solid phase conduction.

Normally, all of the above modes of heat transfer would be present, to a varying degree, when flame spreads over a surface. It can therefore be problematic to set up and solve analytically exact expressions for the flame velocity. If one, however, as Williams /33/ did, only takes account of the mode which is considered to be dominant, then approximate expressions for flame spread velocity are easily developed and solved using equation (7).

The orientation of the solid fuel and wind conditions are important when determining the dominant mode of forward heat transfer. A vertically oriented sample with an ignition source at the top will spread flame upwind (opposed flow flame spread) and when the ignition source is at the bottom of the sample the spread is downwind (wind aided flame spread). The spread rate will also depend on whether the fuel can be considered to be thermally thick or thin. For thermally thin fuels the temperature is assumed to be uniform over its thickness, leading to an equation for the heat balance, written as

$$\rho c \delta (T_{ig} - T_0) V = \dot{q}'' \Delta \tag{9}$$

where δ is the fuel thickness and Δ is the length over which heat is transferred. No heat is assumed to be lost through the unexposed side. The heat flux, q", is assumed to be constant over the length Δ. A similar expression for the thermally thick case can be obtained by considering heat conduction theory and substituting the physical material thickness with the thermal penetration thickness

$$\delta \sim \sqrt{\frac{k}{\rho c} t} = \sqrt{\frac{k}{\rho c} \frac{\Delta}{V}} \tag{10}$$

which leads to the following equation for flame spread velocity

$$V = \frac{\dot{q}''^2 \Delta}{k \rho c (T_{ig} - T_0)^2} \tag{11}$$

This work is mainly concerned with solid materials which can be considered to be thermally thick for the time period of interest. The remainder of this chapter will therefore discuss the application of equation (11) to wind aided flame spread and opposed flow flame spread over thick solids.

3.2 Opposed flow flame spread over thick solids

Flame spread over a horizontal surface where the entrained air flow direction is against the flame spread is commonly termed opposed-flow flame spread. We shall here consider the case of opposed-flow flame spread over a thick solid, illustrated by Figure 10. The theory originates from Quintiere /29/ and has been reviewed extensively by several authors (for example /11/, /38/, /35/), we shall therefore only summarise the theory here, in order to orientate the reader.

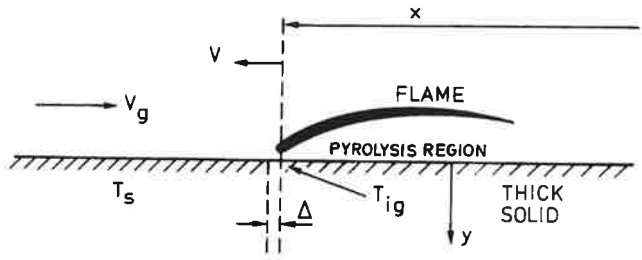

Fig. 10. Energy conservation analysis in opposed flow flame spread.

The dominant mode of heat transfer in this case is considered to be gas phase conduction over a short distance Δ, near the pyrolysis front. The flame is tilted, resulting in a very small view factor between the flame and the non-burning fuel and far field flame radiation can thus be neglected. The gas phase conduction heat flux, q''_{gc}, is assumed to be constant over the distance Δ and zero beyond. Equation (11) can thus be rewritten as

$$V = \frac{(\dot{q}''_{gc})^2 \Delta}{k\rho c (T_{ig} - T_g)^2} \qquad (12)$$

The net forward flame heat flux, characterised as conduction in the gas phase suggests that

$$\dot{q}''_{gc} \sim k_g \left(\frac{T_f - T_{ig}}{\Delta} \right) \qquad (13)$$

where the k_g refers to the properties of the gas. The length Δ must also be described. Quintiere argues that in opposed flow flame spread the forward gas phase conduction must be balanced out by opposed flow convection, i.e.

$$\rho_g c_g V_g \frac{\partial T}{\partial x} \sim k_g \frac{\partial^2 T}{\partial x^2}$$

As a consequence

$$\Delta \sim \frac{k_g}{\rho_g c_g V_g} \tag{14}$$

Combining equations (12), (13) and (14), the "ideal" velocity /35/ of the flame front can be written as

$$V = \frac{V_g (k\rho c)_g (T_f - T_{ig})^2}{k\rho c (T_{ig} - T_s)^2} \tag{15}$$

This equation is identical to the theoretically derived result by de Ris /39/. It should be noted that chemical kinetics are ignored in equation (15) and that Wichman /40/ has developed an alternative model, including the effects of finite kinetics in the gas phase. His analysis modifies the "ideal" velocity by a function of the Damköhler number, bringing into play the needed kinetic data for the fuel. Roughly, it can be said /8/ that if chemical kinetics are important, then the actual flame spread velocity is lower than that given by equation (15).

The problem with using equation (15) is the difficulty in determining the flame temperatures when various materials are burning. Quintiere et. al. /30/ rewrote equation (15) as

$$V = \frac{\Phi}{k\rho c (T_{ig} - T_s)^2} \tag{16}$$

where Φ is essentially a material property which can be determined in a bench scale test. Consequently, they developed a methodology to derive this parameter from the LIFT apparatus, where $k\rho c$ and T_{ig} are derived from the ignitability part of the test and Φ from the flame spread procedure. The methodology was briefly discussed in Chapter 2 of this work, an in depth discussion is found in /30/ and a complete description of the methodology in the ASTM 1321-90 standard /8/.

3.3 Wind aided flame spread

3.3.1 General considerations

We will in this section consider wind aided flame spread on a thermally thick material, or a thin material with a backing board. The theory developed is built on a quasi-steady thermal model; no account is taken of chemical kinetics. Also, we assume that the fuel is sufficiently thick so that it is not completely consumed during the spread process, i.e. we assume no burn-out.

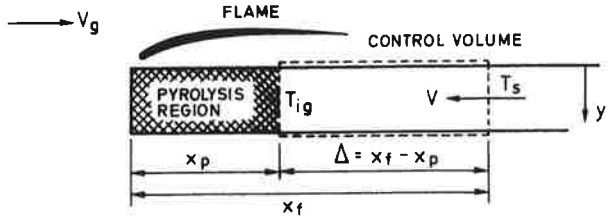

Fig. 11. Energy conservation in wind-aided flame spread.

The configuration is shown in Figure 11. Starting with the general heat conduction equation, the initial condition $T(y,0) = T_0$ and the boundary condition $\dot{q}''(0,t) = \dot{q}''_e = -k\frac{dT}{dy}$ at $y = 0$ (thus ignoring convective and radiative cooling and other heat losses) we arrive at the well known, simple expression for ignition temperature

$$T_{ig} - T_0 = \frac{2\dot{q}''_e}{\sqrt{\pi}}\sqrt{\frac{\tau}{k\rho c}} \qquad (17)$$

where τ denotes time to ignition. Replacing this time with a heating distance (assumed to be equal to $x_f - x_p$) divided by a velocity of the pyrolysis front we arrive at an expression similar to equation (11)

$$V = \frac{4\dot{q}''^2_e(x_f - x_p)}{\pi k\rho c(T_{ig} - T_0)^2} \qquad (18)$$

Saito, Quintiere and Williams /41/ (SQW) discussed a thermal theory of concurrent flow flame spread on thick solids which lead to an integral equation of the Volterra type for the velocity of spread. Following SQW we rewrite equation (18) as

$$V(t) = \frac{x_f - x_p}{\tau} = \frac{dx_p}{dt} \tag{19}$$

$$\text{where } \tau = \frac{\pi k \rho c (T_{ig} - T_0)^2}{4 \dot{q}''^2_e} \tag{20}$$

Here, τ is ignition time and depends only on fuel properties, the ambient temperature and the level of heat flux from the flame to the fuel. Inherent in the equations is the assumption that τ is approximately constant while $x_f - x_p$ varies.

In order to write down a complete expression for V(t) we must have an expression for both x_f and x_p. SQW did this and discussed the solution of the resulting integral equation at short times and at long times. Thomas and Karlsson /42/ obtained an analytical solution and evaluated it for various conditions.

Certain approximations were required for the integral equation to be obtained. The main assumptions are:

1) The material is thermally thick, homogeneous and its thermal properties are constant with temperature.
2) Chemical kinetics are excluded, so very fast (as well as very slow) rates of spread are not fully dealt with and extinction conditions are therefore only discussed approximately.
3) The flame length, x_f, depends on a power of $\dot{Q}$, the rate of heat release.
4) Heat flux from the flame only occurs at constant flux within the region $x_p < x < x_f$ (see Figure 12).

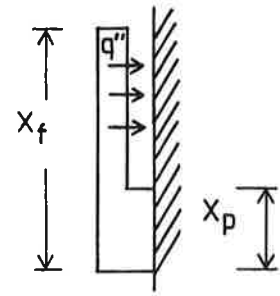

Fig. 12. Heat flux from the flame is assumed to be constant in the region $x_p < x < x_f$.

For setting up the integral equation for flame velocity we also need an expression for x_p and x_f. The height of the pyrolysis zone as a function of time is written as

$$x_p(t) = x_{po} + \int_0^t V_p(t_p)\, dt_p \tag{21}$$

where x_{po} is the value of x_p at an initial time t = 0 and t_p is the dummy variable of integration.

Flame heights are most commonly correlated with energy release rate, $\dot{Q}$, and are of the form

$$x_f(t) = K\left(\dot{Q}_{tot}(t)\right)^n \tag{22}$$

where K and n are constants derived from experiments and $\dot{Q}_{tot}(t)$ is the total heat release rate at time t. The values of K and n are dependent on the choice of scenario, i.e. whether the flames are under a ceiling, in a corner or on open walls. Some experiments and correlations are given in section 3.4.

In order to set up the equation for the velocity of the pyrolysis front we assume a steady-state initial condition, i.e. a constant burner output, $\dot{Q}_b$, producing a constant, steady flame height in front of the virgin fuel. This flame height at t = 0 is thus given by

$$x_f = K\dot{Q}_b^{\,n} = x_{po} \tag{23}$$

The flame produces a heat flux which is assumed to be constant over the flame height and zero above it. After a certain time the material behind the flame ignites, the pyrolysis height is then also given by equation (23). This initial pyrolysis height is termed x_{po} and the time at which ignition occurs is taken to be t = 0.

The flame height at time t = 0, termed x_{fo}, is due to the energy released by the burner and the energy released from the initially burning material. This initial flame height at time t = 0 (as opposed to the flame height before t = 0, given by equation (23)) is given by

$$x_{fo} = K\left(\dot{Q}_b + x_{po} W \dot{Q}''(0)\right)^n \tag{24}$$

In this equation $\dot{Q}''(0)$ is the energy released per unit area by the material at ignition and W is the width of the flame front, here assumed to be equal to the width of the burner.

Now we need expressions for the flame height at an arbitrary time t, after the pyrolysis front has started to move upwards. In principle, this height is given by equation (22) but we need an expression for the total heat release, $\dot{Q}_{tot}(t)$. This energy release rate is from three sources: the constant output from the gas burner; the initially burning material at time t = 0; and the contribution which results from the pyrolysis front moving upward. This total rate of heat release is given by

$$\dot{Q}_{tot}(t) = \dot{Q}_b + x_{po} W \dot{Q}''(t) + \int_0^t \dot{Q}''(t - t_p) W V(t_p) dt_p \qquad (25)$$

The heat release rate from the burning material is assumed to change with time so $\dot{Q}''(t)$ is the material heat release rate at time t and t_p is the dummy variable of integration.

Substituting $\dot{Q}_{tot}(t)$ in equation (22) with equation (25) we have an expression for $x_f(t)$. Putting this and equation (21) into equation (19) we finally arrive at the following Volterra integral equation of the second kind for the flame spread velocity:

$$V(t) = \frac{1}{\tau}\left[K\left(\dot{Q}_b + x_{po} W \dot{Q}''(t) + \int_0^t W \dot{Q}''(t - t_p) V(t_p) dt_p\right)^n - \left(x_{po} + \int_0^t V(t_p) dt_p\right)\right] \qquad (26)$$

where the two terms in the brackets on the r.h.s. represent x_f and x_p respectively. As before, t_p is the dummy variable of integration, K and n are coefficients for flame length, $\dot{Q}_b$ is the gas burner output, W is the (assumed) constant width of flame front and $\dot{Q}''(t)$ is the rate of heat release per unit area from the material at time t.

3.3.2 Solving equation (26) for wind aided flame spread

To solve equation (26) analytically one has to mathematically represent both the time dependence of the material heat release rate and the flame length as a function of heat release rate. Also, no account can be taken of pre-heating of the material beyond the flame front, i.e. T_s in equation (20) must be given a constant value, typically = T_0. This means that the time to ignition, τ, is constant.

Equation (26) expresses the velocity in one direction only, assuming that the width of the burning strip of material is constant. However, similar equations can be set up, expressing the velocity in terms of areas, thus allowing flame spread velocity to be calculated under a ceiling, where the width of the flame front is not constant. A simple, analytical model for flame spread under ceilings will be presented in section 3.5 of this work but presently we shall discuss wind aided flame spread in one direction.

These equations can, of course, be solved numerically, using one of many possible numerical algorithms /43/ and this has been done in one of the room fire growth models presented in Chapter 4 . The advantages of a numerical solution are that material heat release rate can be taken directly from the Cone Calorimeter, flame height can be expressed as a non-linear function of heat release rate and pre-heating of the material by the gas layer can be taken into account.

The disadvantages of a numerical solution are that the physical meaning of the terms in equation (26) gets somewhat clouded and the behaviour of the solution can not be directly analysed. Thomas and Karlsson /42/ discussed the assumptions and limitations of the equation and gave analytical solutions for certain conditions, depending on flame length correlations, initial gas burner output and heat release history of the burning material. In this section, we shall examine the most simple case they presented in order to throw some light on the importance of the ingoing parameters and the behaviour of the solution.

In addition to the assumptions listed in the previous section, the following assumptions were made in order to facilitate an analytical solution:

1) The heat release rate from the burning material can be expressed mathematically as $\dot{Q}''_{max}\ e^{-\lambda t}$ where $\dot{Q}''_{max}$ is the maximum rate of heat release from the Cone Calorimeter test and λ is the decay coefficient (see Figures 3 and 13). Observe that many other types of mathematical representations of the heat release rate can be made, some of which were analysed by Thomas and Karlsson /42/. Also, Saito, Quintiere and Williams /41/ analysed the case of a constant heat release rate with a certain duration.

2) We assume that the flame length is linearly dependent upon the heat release rate and can be written as $x_f = K\dot{Q}_{tot}$, where K is a constant (in m/kW) and $\dot{Q}_{tot}$ is the total heat release rate. The coefficient n in equations (22), (24) and (26) is thus = 1. K is often expressed in m^2/kW, the choice of units depends entirely on the type of flame length correlation used and on how the flame spread velocity equation is set up. In section 3.5 we shall use flame area correlations and express K in m^2/kW.

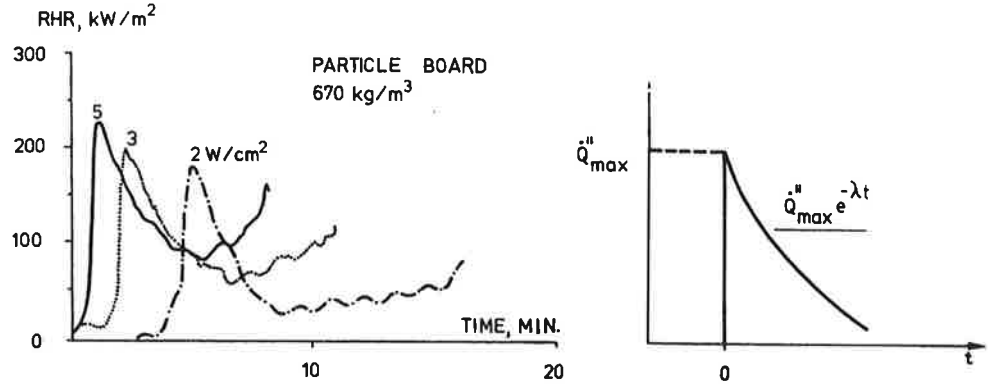

Fig. 13. Cone Calorimeter test results and a mathematical representation of the material heat release rate.

3) The initial pyrolysing length, x_{po}, is dependent on the burner output, $\dot{Q}_b$ (see equation (23). Burner output is here assumed to be constant for all times.

4) Pre-heating of the combustible material beyond the flame tip is not accounted for (such as pre-heating by a hot gas layer). The flame is assumed to be the only source of heat and therefore T_s in equation (20) is set equal to T_0.

The numerical values of K, $\dot{Q}_b$, $\dot{Q}''_{max}$, λ and τ will be discussed in the following chapters where specific scenarios will be considered. In this section we shall only give an analytical solution and discuss its implications.

Applying these assumptions in equation (26), the flame spread velocity is expressed as

$$V(t) = \frac{1}{\tau}\left[K\left(\dot{Q}_b + x_{po} W \dot{Q}''_{max} e^{-\lambda t} + \int_0^t W \dot{Q}''_{max} e^{-\lambda (t - t_p)} V(t_p)\, dt_p \right) \right]$$

$$- \frac{1}{\tau}\left(x_{po} + \int_0^t V(t_p)\, dt_p \right) \qquad (27)$$

The first term in the brackets on the r.h.s. is = x_f and the Laplace transform of this term is

$$\bar{x}_f(s) = K\left(\frac{\dot{Q}_b}{s} + \frac{x_{po} W \dot{Q}''_{max}}{s+\lambda} + \frac{W \dot{Q}''_{max}}{s+\lambda}\bar{V}(s)\right) \tag{28}$$

where $\bar{V}(s)$ and $\bar{x}_f(s)$ denote the Laplace transforms of V(t) and $x_f(t)$ respectively and s is the Laplace transform operator.

The second term in the brackets on the r.h.s. of equation (27) is = x_p and the Laplace transform is

$$\bar{x}_p(s) = \frac{x_{po}}{s} + \frac{\bar{V}(s)}{s} \tag{29}$$

resulting in

$$\bar{V}(s)\,\tau = K\left(\frac{\dot{Q}_b}{s} + \frac{x_{po} W \dot{Q}''_{max}}{s+\lambda} + \frac{W \dot{Q}''_{max}}{s+\lambda}\bar{V}(s)\right) - \left(\frac{x_{po}}{s} + \frac{\bar{V}(s)}{s}\right) \tag{30}$$

Isolating $\bar{V}(s)$, recognizing that $K\dot{Q}_b = x_{po}$ and rearranging gives

$$\bar{V}(s) = \frac{1}{\tau} \frac{s\, K \dot{Q}''_{max} x_{po} W}{s^2 + s\frac{1}{\tau}\left(1 - K \dot{Q}''_{max} + \lambda\tau\right) + \frac{\lambda}{\tau}} \tag{31}$$

For simplification we let $a = K \dot{Q}''_{max}$ and $C_1 = \frac{K \dot{Q}''_{max} x_{po} W}{\tau}$

The inverse Laplace transform is then given as

$$V(t) = \frac{C_1}{s_2 - s_1}\left[s_2 e^{s_2 t} - s_1 e^{s_1 t}\right] \tag{32}$$

where s_1 and s_2 are the real simple roots of the quadratic equation (the denominator of equation (31))

$$s^2 + s\frac{1}{\tau}\left(1 - a + \lambda\tau\right) + \frac{\lambda}{\tau} = 0$$

Therefore

$$s_{1,2} = -\frac{1}{2\tau}(1 - a + \lambda\tau) \pm \frac{1}{2}\sqrt{\Delta}$$

where the determinant $\Delta = \frac{1}{\tau^2}(1 - a + \lambda\tau)^2 - \frac{4\lambda}{\tau}$

The conditions for the velocity to accelerate are that s_1 or s_2 or both are positive, otherwise the velocity decelerates.

If the determinant is negative, i.e. $(1 - \sqrt{a})^2 < \lambda\tau < (1 + \sqrt{a})^2$, a real solution can be achieved by using complex numbers, the factors $e^{s_1 t}$ and $e^{s_2 t}$ then become trigonometric functions. Writing s_1 and s_2 as $\alpha \pm i\beta$ the solution is given as

$$V(t) = \frac{C_1 e^{\alpha t}}{\beta}(\alpha \sin(\beta t) + \beta \cos(\beta t)) \qquad (33)$$

Thomas and Karlsson /42/ identified the above limits of propagation and non-propagation for concurrent flow flame spread. They expressed the velocity in terms of length, following the work of SQW /41/. Baroudi and Kokkala /44/ represented these limits graphically in terms of τ, λ and a, as seen in Figure 14.

The characteristic behavior of the solution for different parameters $K\dot{Q}''_{max}$ (= a) and $\lambda\tau$ is shown in Figure 14. Note that the solutions given above are only valid for a positive velocity since the flame height is always considered to be positive. Exponentially accelerating flame spread appears in region I below line A. In regions II and III the solutions are trigonometric and for long times the velocity oscillates between positive and negative values. In region II, V(t) -> $\pm\infty$ as t -> ∞ and in region III, V(t) -> $\pm$ zero as t -> ∞. These solutions, however, cease to be valid for flame spread once the velocity has become negative for the first time. In region IV the flame spread decelerates for all times.

Observe that burn-out has only been partially treated, i.e. burn-out is achieved for a certain part of the pyrolysing material when the heat release rate there goes to zero. This is assumed to have no influence on the base of the flame, which is at all times considered to be at x = 0.

This assumption on burn-out must be examined critically for certain scenarios, for example, the case of flame spread up a wall on a relatively thin material, where the burner output is small. The pyrolysis- and flame fronts can then move quite rapidly away from the burner flame and burn-out will significantly influence flame height.

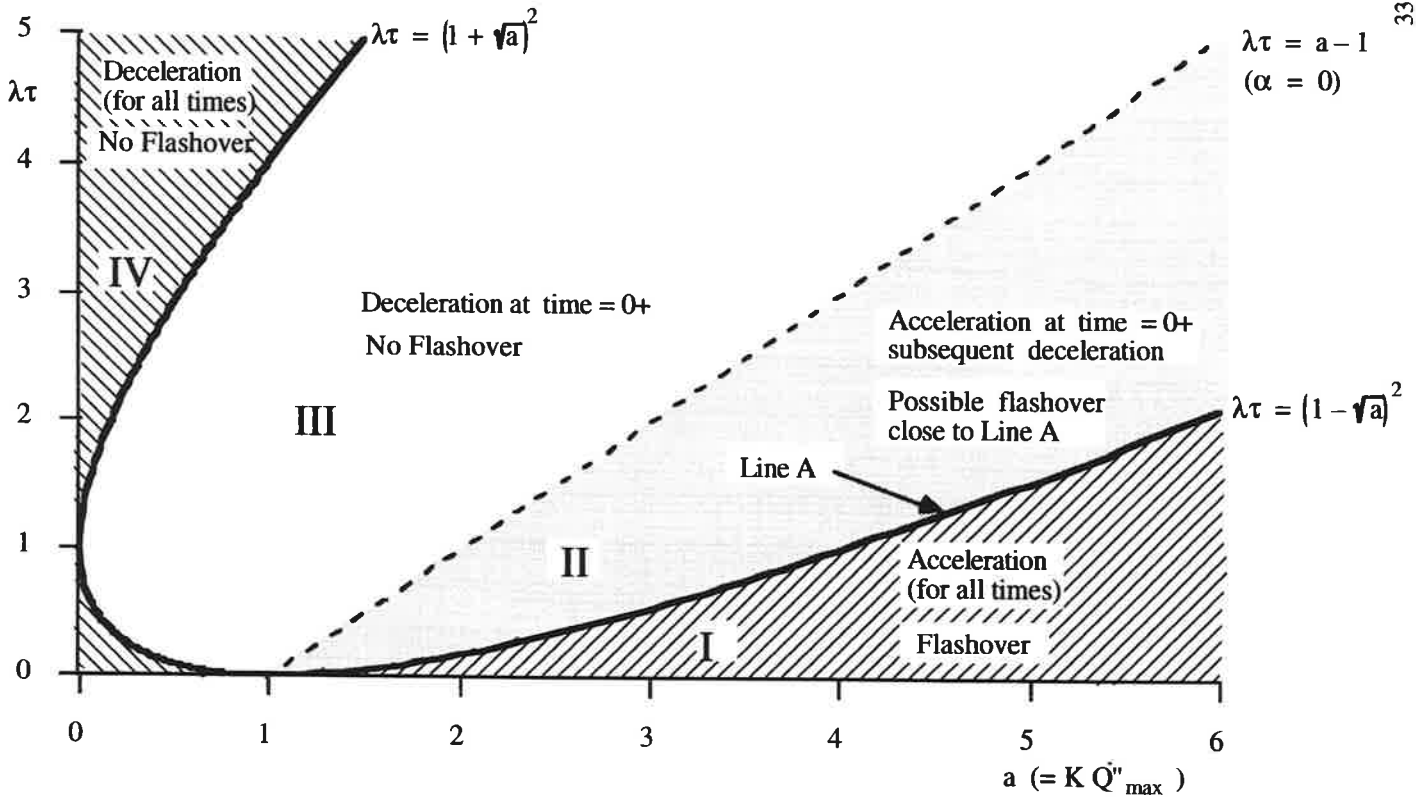

Fig. 14. Regions of flame front acceleration and deceleration

This treatment of burn-out can be partly justified in the scenarios that we will consider here, since the burner outputs in these scenarios are very high. This means that even if a part of the material has ceased to pyrolyse, the burner flame is covering it, and the base of the flame can still be assumed to be at $x = 0$ and the flame to be continuous up to $x = x_f$. Also, for thin materials, where heat release rate decreases very rapidly to zero, the flame velocity usually decelerates to zero before any burn-out occurs at $x = 0$. There may, however, exist material property combinations for which the above burn-out assumptions must be re-examined.

In section 3.5 we shall discuss the limits of propagation and non-propagation further, giving concrete examples of 12 different materials spreading flame in a certain scenario. All 12 materials were found to behave as predicted by the limits given in Figure 14.

3.4 Flame extension and flame area under ceilings

3.4.1 General considerations

Consider a surface that can be a solid, liquid, the exit plane of a burner or some orifice issuing fuel gas with a characteristic dimension D. This can be a diameter in the case of a circular source or the length of one side in the case of a square source.

The height of diffusion flames from such sources have traditionally been discussed in terms of the Froude number, i.e. the ratio of inertia and buoyancy forces. The Froude number can be written in terms of energy as depending on $\dot{Q}^2/D^5$, where $\dot{Q}$ is the energy release rate. Thomas et. al. /45/ used dimensional analysis of the geometry of turbulent diffusion flames and established the dependence of flame height on $\dot{Q}^2/D^5$ and Steward /46/ found some theoretical justification for this.

More generally, flame height normalised by diameter, L/D, has traditionally been correlated as (McCaffrey /47/, Heskestad /48/)

$$\frac{L}{D} \sim K \dot{Q}^{*^n} \tag{34}$$

where K is a constant (not the same as in Chapter 3.3) and n has been found to be 2/5 for a wide range of Froude numbers (Heskestad /48/, Zukoski /49/). For small Froude numbers n increases and is reported to range from 2/3 to 2 (Zukoski /49/, Cox and Chitty /50/). Zukoski /49/ used the non-dimensional heat release rate, $\dot{Q}^*$ (the square root of the Froude number), and defined it as

$$\dot{Q}^* = \frac{\dot{Q}}{\rho_0 c_p T_0 D^2 \sqrt{g D}} \tag{35}$$

where ρ_0, c_p and T_0 are the density, specific heat and temperature of the ambient air respectively and g is the acceleration due to gravity.

Several authors have analysed data on flame heights and many correlation equations, in the form of equation (34), exist for unconfined flames (some of which have been referred to above) and flames close to a wall. Tu and Quintiere /51/ gave a summary of the data on wall flames from Delichatsios /52/, Hasemi /53/, Kulkarni et.al. /54/ and Tu et.al. /51/ where the flame length was correlated with heat release rate per unit width of burning wall.

Some data also exists for flame heights in a corner, which is not confined by a ceiling. Hasemi /55/ and Kokkala /56/ have both reported correlation equations for this scenario, where n in equation (34) is given as 2/3 and the constant K as 4.3 (Hasemi) and 4.96 (Kokkala).

In this study we are interested in flames in a corner of a room, confined by a ceiling and two perpendicular walls. Once the flames reach the ceiling the "T" pattern flame morphology described by Williamson et.al. /57/ is clearly evident, see Figure 15. We are interested mainly in two scenarios: firstly, where there is combustible material on walls only and, secondly, where the combustible material is mounted on both walls and ceiling.

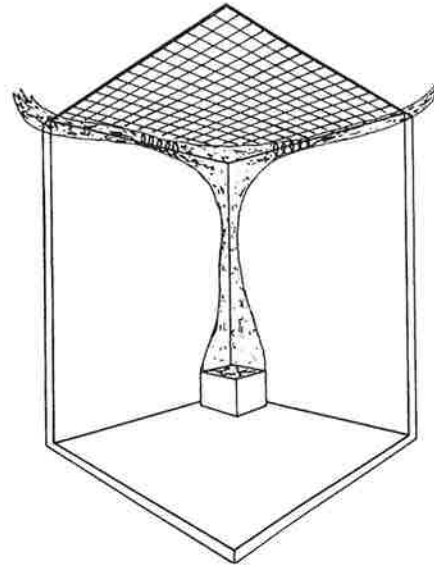

Fig. 15. A schematic representation of flame extensions in a corner, under a ceiling (from /57/).

In the first case we are mainly interested in the flame extensions along the wall-ceiling intersection and particularly in the flame length along the wall, since this is where the combustible material is mounted and where the flame will spread. In this case the flame extension is expressed as a length and is a function of heat release rate.

In the second case we are interested in both the flame extension in the wall-ceiling intersection and the flame area under the ceiling, since the combustible material is mounted on both walls and ceiling. The geometry of the flames, relevant to flame spread, is in this case rather complex and, for convenience, flame extensions will therefore be expressed as an area of no specific geometry.

Experimental data on flame heights in a corner where the flames are confined by a ceiling is scarce. Thomas and Karlsson /58/ analysed data from Andersson and Giacomelli /59/ and Gross /60/ in order to estimate the flame extension along the wall-ceiling intersection. A summary of their work is given in the following section. Flame area under a ceiling will be discussed in section 3.4.3.

3.4.2 Flame extensions in a wall-ceiling intersection

Consider a point source, in an open corner with 2 infinite perpendicular walls, a distance H below a ceiling, but without a floor (see Figure 16)

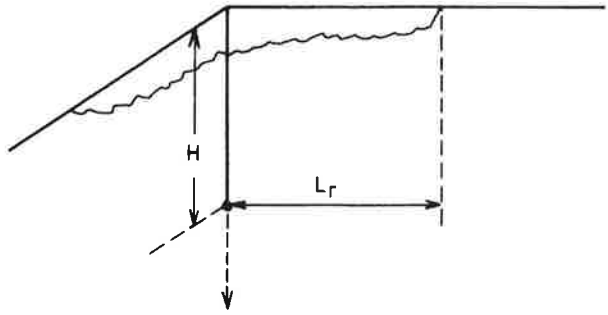

Fig. 16. Point source in an open corner a distance H below a ceiling.

Here, H is the only independent dimension in the system and we should expect the flame extension under the ceiling, L_r, to be a function of

$$\frac{L_r}{H} = \mathrm{Fnc}\left[\frac{\dot{Q}}{\rho_0 c_p T_0 H^2 \sqrt{g H}}\right] \qquad (36)$$

A second term could be added in the brackets above, i.e. a Reynolds number ($=\sqrt{gH}\,H/\nu$), the ratio of a characteristic turbulent eddy viscosity to the molecular kinematic viscosity, ν. Such a variable should be considered because of the bounding surfaces and the stratification occurring in horizontal flow which dissipates turbulence. However, this term is often ignored, assuming that the bounding surfaces are adiabatic and perfectly smooth (Hasemi /55/, Kokkala /56/, Babrauskas /61/).

Now consider a finite source of size D, either a diameter of a circular source or a length of one side of a square source. It is commonplace when discussing plumes to introduce an addition to H to represent a virtual source. In general we need to

introduce the ratio D/H but we shall, as a first approach, include D only as an addition to H and thus represent a virtual source.

For vertical plumes in free space Morton et. al. /62/ estimated this addition to be $1.5\sqrt{A_f}$ where A_f was the source area. In a corner the burner is 1/4 of the apparent equivalent area (see Figure 17) and the correction is therefore 3D. Babrauskas /61/ used the flame length data obtained by You and Faith /63/ and proposed a method of scaling flames under ceilings based on the assumption that flames in different geometric orientations entrain the same quantity of air, i.e. that their dilution is the same. He used the correction 2.9D.

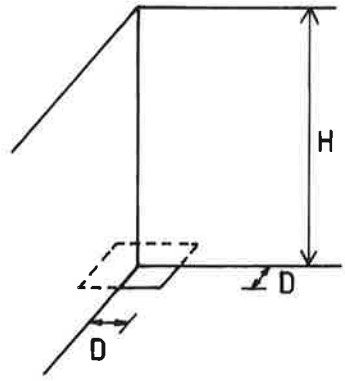

Fig. 17. Apparent equivalent source area.

Here we follow Morton et. al. and Babrauskas and incorporate the burner size into H by replacing H in equation (36) by

$$H^* = H + 3D \tag{37}$$

Hence, the following scaling law for the flame extension under a ceiling is proposed

$$\frac{L_r}{H^*} = Fnc\left[\frac{\dot{Q}}{\rho_0 c_p T_0 H^{*2}\sqrt{g H^*}}\right] \tag{38}$$

as a first approximation; other geometric terms may have to be added later to improve the correlation with the data.

Andersson and Giacomelli /59/ performed experiments in an 0.8 m high enclosure, 1.2 m long by 0.8 m wide with a 0.07 m square burner, positioned in a corner on the floor and half way up the corner. The values of H* are 0.94 and 0.61

respectively. The flame extension along the wall - ceiling intersection was determined visually with a range of $\dot{Q}$ from 5 kW - 33 kW. Their data is plotted as L_r versus $\dot{Q}$ in Figure 18.

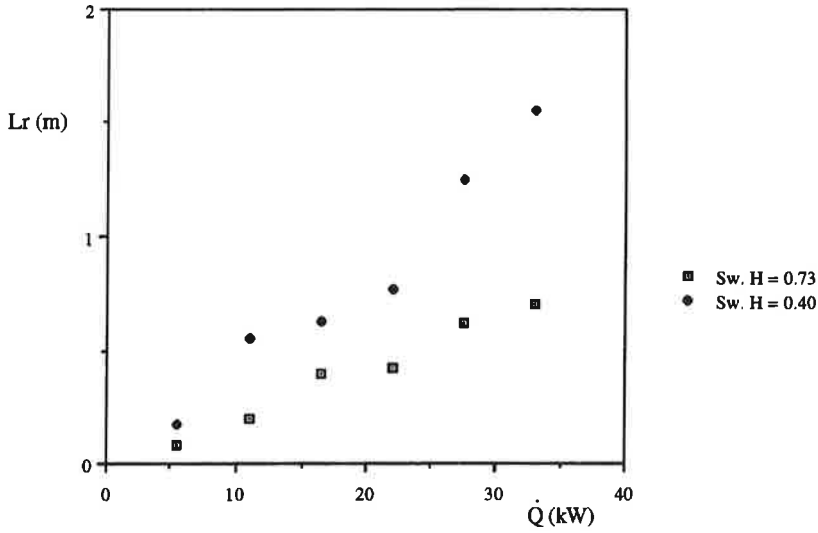

Fig. 18. Flame extension under ceiling vs. energy release rate, Swedish data /59/.

There is some suggestion of a small discontinuity from 15 kW to 25 kW but a direct proportionality between L_r and $\dot{Q}$ appears to be a reasonable summary of their data. Experimentally, the ratios of the slopes in Figure 18 is 2.05 and based on

$$\frac{L_r}{H^*} \sim \frac{\dot{Q}}{H^{*5/2}}$$

it should be $(0.96/0.61)^{3/2}$, that is 1.97.

On the basis of only two flow conditions the ~ 5% difference is possibly fortuitous. There is, however, no justification for refining the scaling law without further data and the form of equation (35) is therefore used for correlating the data. Figure 19 shows the plot of L_r/H^* versus $\dot{Q}^*$ where $\dot{Q}^*$ has been redefined as

$$\dot{Q}^* = \frac{\dot{Q}}{\rho_0 c_p T_0 H^{*2} \sqrt{g H^*}} \qquad (39)$$

In the figure Sw stands for Swedish data (from Andersson and Giacomelli /59/).

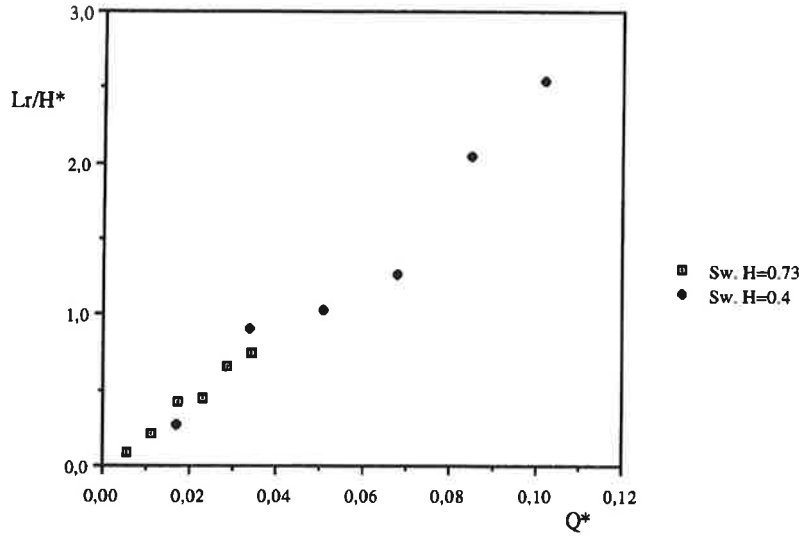

Fig. 19. Correlation of flame extensions under ceiling, Swedish data.

The best linear fit to the data is

$$\frac{L_r}{H^*} = -0.078 + 24.3\,\dot{Q}^* \qquad (40)$$

with a coefficient of determination $r^2 = 0.99$. The constant -0.078 indicates that L_r is zero when $\dot{Q}^*$ is less than 0.0032. For the experiments mentioned above (where $H^* = 0.73 + 3D$ and $D = 0.07$) the horizontal flame extension under the ceiling is zero when $\dot{Q}$ is less than 3.2 kW.

Gross /60/ measured luminous flame extensions in the corner - wall - ceiling configuration. Combining his data and the Swedish data referred to above and plotting L_r/H^* versus $\dot{Q}^*$ (as defined by equation (39)) gives results shown in Figure 20. The best linear fit through the data is

$$\frac{L_r}{H^*} = -0.15 + 25\,\dot{Q}^* \qquad (41)$$

Some curvature is apparent at low $\dot{Q}^*$ as well as a possible discontinuity at $\dot{Q}^* \sim 0.07$.

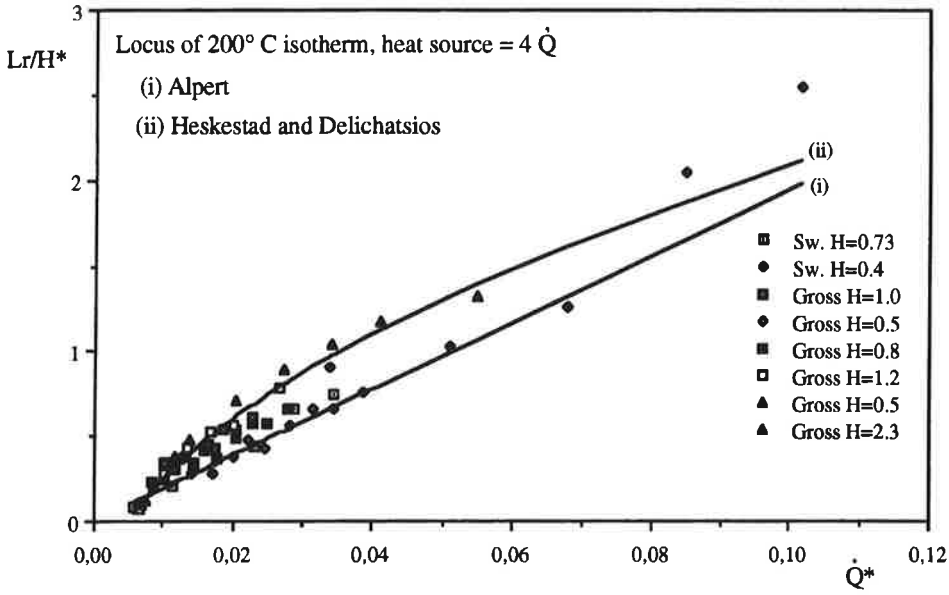

Fig. 20. Correlation of flame extensions under ceilings in a corner configuration.

The early identification by Yokoi /64/ of flame length with the distance to a particular isotherm in non-combusting systems, allowed Thomas and Karlsson /58/ to compare the above correlation with existing plume and ceiling jet correlations.

Alpert /65/ gives the temperature rise at a radial distance "r" from the center of a plume deflected by a flat ceiling as

$$\Delta T = \frac{5.38}{H}\left(\frac{\dot{Q}}{r}\right)^{2/3} \qquad \left(\text{valid for } \frac{r}{H} > 0.18\right) \tag{42}$$

Heskestad and Delichatsios /66/ later, on the basis of additional experiments, gave

$$\Delta T = \frac{T_0\left(\dot{Q}/\rho_0 c_p T_0 H^2 \sqrt{g H}\right)^{2/3}}{\left(0.188 + 0.313\, r/H\right)^{4/3}} \tag{43}$$

Following Yokoi's identification of flame length as the distance to an isotherm (or degree of dilution), Thomas and Karlsson /58/ replaced H by H*, r by L_r and $\dot{Q}$ by $4\dot{Q}$ in equations (42) and (43) ($\dot{Q}$ is thus heat released in one quadrant). Assuming ambient conditions, i.e. $\rho_o = 1.2$ kg/m^3, $c_p = 1$ kJ /kg K, $T_o = 293$ K and $g = 9.81$ m/s^2 enables us to rewrite equations (42) and (43). The ambient values used here are slightly different from those used by Thomas and Karlsson /58/ resulting in the equations

$$\frac{L_r}{H^*} = \left(\frac{1450}{\Delta T}\right)^{3/2} \dot{Q}^* \qquad (44)$$

and

$$\frac{L_r}{H^*} = -0.6 + \left(\frac{3470}{\Delta T}\right)^{3/4} \sqrt{\dot{Q}^*} \qquad (45)$$

Assuming that the tip of the flames correspond with the 200°C isotherm (over ambient, i.e. $\Delta T = 200$°C) gave the results shown as lines (i) and (ii) in Figure 20. The correlation given by equation (41) can therefore be said to have a close similarity to established ceiling plume correlations.

3.4.3 Flame extension correlations to be used in the present work

In Scenario B, the concurrent flow flame spread in the ceiling-wall intersection occurs relatively early on in the test. This corresponds to heat release rates ranging from 11 kW - 30 kW in the 1/3 scale tests and 100 kW - 300 kW in the full scale tests. The range of values for $\dot{Q}^*$ is thus 0.012 - 0.032 and 0.008 - 0.024 respectively. Observe that the range of $\dot{Q}^*$ values for the 1/3 scale tests is quite a bit higher than the same range for the full scale test, due to the much higher value of H* in the full scale test.

The slope of equation (41) seems to fit the flame extensions in the 1/3 scale room quite well in the $\dot{Q}^*$ range 0.02 - 0.03. and this equation is therefore used for flame extensions in the 1/3 scale tests.

For the full scale test, however, due to the increasing curvature as $\dot{Q}^*$ approaches zero, the slope given in equation (41) is too low in the $\dot{Q}^*$ range 0.01 - 0.02. A best fit, for this range of $\dot{Q}^*$, to the data in Figure 20 gives a slope of 40. For the full scale tests, equation (41) is rewritten as

$$L_r / H^* = -0.15 + 40\,\dot{Q}^* \qquad (46)$$

3.4.4 Flame areas under a ceiling corner

In order to express flame propagation on the underside of a ceiling in terms of area, some assumption must be made on how flame area increases as a function of heat release rate. The flame extension area shown schematically in Figure 15 depicts a rather complex geometry and there seems to be very little data available where the area of flames, under a corner of a ceiling, is reported.

The only such data available are a few visual observations made by Andersson and Giacomelly /59/ from the 1/3 scale room experiments mentioned in the previous section. In their report the data is presented as rough sketches and must therefore be considered to be very inaccurate. The few data points are presented in Figure 21 only to establish the order of magnitude of K, the flame area coefficient. The slope of the line in Figure 21 is ≈ 0.0083 showing a reasonably linear dependence on heat release rate. The linear dependence can, to a limited extent, be justified by observing that flame lengths are usually considered to be a function of $\dot{Q}^n$ where n is 2/5 - 2/3. Squaring $\dot{Q}^n$ gives approximately a linear relationship between flame area and heat release rate $\dot{Q}$.

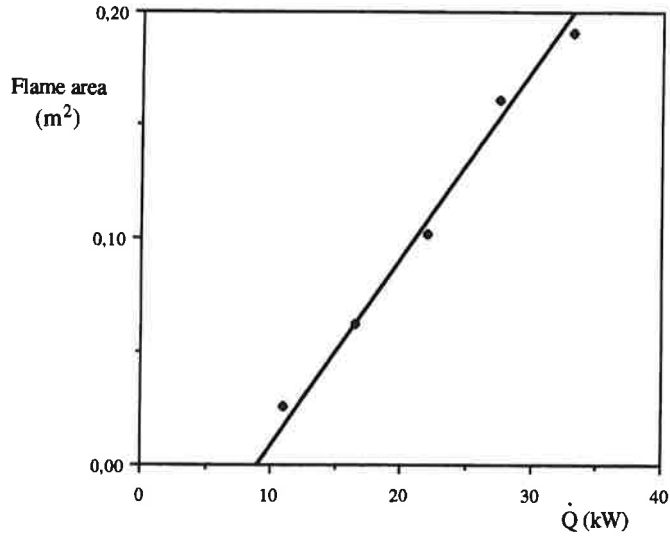

Fig. 21. Visually observed, approximate flame area under a ceiling as a function of heat release rate in the 1/3 scale room test.

Cleary and Quintiere /23/ have used the value 0.01 when calculating flame spread under a ceiling; this value is extrapolated from experiments on wall flames (Tu and Quintiere /51/). Karlsson /67/ has earlier used a value of 0.015 when calculating flame spread and resulting heat release rates under a ceiling, showing reasonable agreement with experimentally measured heat release rate.

Until more experimental data exist on flame extensions and flame areas in this rather complex geometry we shall have to make some simple engineering approximations and assume that flame area, in a corner under a ceiling, can be expressed as a linear function of heat release with a growth constant, K, in the range of 0.008 - 0.015 m^2/kW.

Also, some account must be taken of the fact that the flames do not reach the ceiling at low heat release rates in the corner. Again, due to the lack of both experimental data and previous theoretical work pertaining to the scenario under consideration, we must resort to simple engineering judgements. A relationship for the initial flame area in the ceiling of the form

$$A_0 = K\,(\dot{Q}_{corner} - \dot{Q}_L) \tag{47}$$

is proposed here, where $\dot{Q}_{corner}$ is the total heat release from the burner and the burning material behind the burner flame, $\dot{Q}_L$ is the combustion energy released over the flame height from the burner to the ceiling and K is a constant in the range 0.008 - 0.015.

An expression for the flame area as a function of heat release rate can then be written as

$$A_f = K\,(\dot{Q}_{corner} - \dot{Q}_L + \dot{Q}_{ceiling}) = A_0 + K\,\dot{Q}_{ceiling} \tag{48}$$

where $\dot{Q}_{ceiling}$ is the calculated energy released by the burning material in the ceiling.

The expressions for A_0 and A_f can of course have different forms than those given above and equations (47) and (48) must be seen as being preliminary. However, this form of the equations seemed to give reasonable results when calculated heat release rates were compared with experimental ones.

Magnusson and Sundström /20/ have estimated the amount of energy lost in the corner plume to be in the range of 60 - 150 kW in the full scale test room. A good fit to the experimental data was achieved by choosing $\dot{Q}_L$ = 150 kW for the full scale room and $\dot{Q}_L$ = 18 kW for the 1/3 scale room.

3.5 A simple, analytical model for flame spread and heat release rate in the Room Corner Test

3.5.1 General

We shall in this section give an example of how analytical solutions of the flame spread equations discussed in the previous sections can be used to calculate flame spread on the underside of a ceiling. In this section we ignore pre-heating by a gas layer and, essentially, we assume the configuration shown in Figure 15, i.e. ignition by a burner in an open corner with two infinite perpendicular walls and an infinite ceiling at a height H above the floor. This simple model has previously been described by Karlsson /67/.

In Chapter 4 more complex models will be presented where account is taken of the fire environment in the enclosure.

We shall assume that combustible material is mounted on both walls and ceiling and that heat release rate and time to flashover are mainly governed by the advancement of the flame under the ceiling. Downward and lateral flame spread will thus be ignored. We will use experiments on 12 different materials in the Room Corner Test, carried out by Sundström /68/, to compare with the calculated heat release rates.

Further, we shall make simple assumptions with regard to time to ignition, τ, where τ is directly linked to a measured time to ignition in the Cone Calorimeter. The only bench-scale test results needed as input are thus heat release rate and time to ignition in the Cone Calorimeter at one specified incident heat flux.

3.5.2 The theories of Parker and Saito, Quintiere and Williams

The thermal theories of wind-aided flame spread velocity presented by Saito, Quintiere and Williams /41/ have been discussed in section 3.3. The equations were written in terms of lengths, giving the velocity in [m/s].

Parker /69/ considered the one-dimensional flame spread problem for the underside of a surface, in the ASTM E-84 test configuration. He wrote the velocity of the pyrolysis front (in [m^2/s]) as

$$V(t) = \frac{A_f - A_p}{\tau} \qquad (49)$$

where A_f represents the flame area, A_p the pyrolysing area and τ time to ignition.

Since the aim of this section is to model the concurrent flow flame spread under a ceiling we shall follow Parker's example and express the velocity of the pyrolysis front in terms of area. We will make similar assumptions as in section 3.3 to facilitate an analytic solution of equation (49), i.e:

1) The heat release rate from the burning material can be expressed mathematically as $\dot{Q}''_{max}\ e^{-\lambda t}$ where $\dot{Q}''_{max}$ is the maximum rate of heat release from the Cone Calorimeter test and λ is the decay coefficient (see Fig. 13).
2) We assume that the flame area is linearly dependent upon the heat release rate and can be written as $A_f = A_0 + K\,\dot{Q}_{ceiling}$, where K is a constant (in m^2/kW) and $\dot{Q}_{ceiling}$ is the heat release rate from the ceiling material (see equation (48)).
3) The initial pyrolysing area under the ceiling, A_0, depends on the burner output and the energy released from the material in the corner behind the burner. An expression for A_0 is given in section 3.5.5.

The work of Andersson and Giacomelli /59/ was discussed in the previous section. They found that the shape of the flame in the ceiling sometimes resembled a quarter circle and sometimes a triangle. Regarding the shape of the flame and the pyrolysing area considered here, we simply assume that the flame area correlation is valid for an area of undefined shape.

The resulting integral equation then becomes, with $V(t) = \frac{dA_p}{dt}$ (in m^2/s):

$$V(t) = \frac{1}{\tau}\left[A_0 + K\left(A_0\dot{Q}''_{max}e^{-\lambda t} + \int_0^t \dot{Q}''_{max}e^{-\lambda(t-t_p)}V(t_p)\,dt_p\right) - \left(A_0 + \int_0^t V(t_p)\,dt_p\right)\right] \quad (50)$$

where the first two terms in the brackets on the r.h.s. represent A_f and the last term represents A_p and t_p is the dummy variable of integration. Rearranging equation (50) and taking the Laplace transform gives:

$$\overline{V}(s) = \frac{1}{\tau}\,\frac{s\,K\dot{Q}''_{max}A_0}{s^2 + s\frac{1}{\tau}\left(1 - K\dot{Q}''_{max} + \lambda\tau\right) + \frac{\lambda}{\tau}} \quad (51)$$

We see that this is the same as equation (31) except that $W\,x_{po}$ (where W is width and x_{po} is initial pyrolysis height) has been replaced by A_0, the initial pyrolysing area in the ceiling.

Again we let $a = K\dot{Q}''_{max}$ but the constant C_1 is now given by $C_1 = \frac{K\dot{Q}''_{max} A_0}{\tau}$

Here, the velocity is expressed in terms of area, but the roots of the quadratic in the denominator of equation (51) are the same as in section 3.3, so the same limits apply and are shown, as before, in Figure 14.

Also, the two expressions for flame spread velocity given by equations (32) and (33), are valid here with the exception that the constant C_1 has been redefined as above.

3.5.3 Data needed from bench-scale tests

Table VII lists 13 materials which were both tested in the Cone Calorimeter /7/ and in the Room Corner test /68/. It lists the parameters $\dot{Q}''_{max}$ and t_{ig}, measured at an irradiance level of 50 kW/m^2 by Tsantaridis et al. /14/. The heat release rate measured in the Cone Calorimeter is modelled mathematically as $\dot{Q}(t) = \dot{Q}''_{max}\, e^{-\lambda t}$. The decay coefficient, λ, can therefore be calculated from the expression

$$\lambda = \text{average of} \left[- \frac{\ln\left(\dot{Q}''_C(t) / \dot{Q}''_{max} \right)}{t} \right] \qquad (52)$$

where $\dot{Q}''_C(t)$ is the time dependent heat release rate from the Cone Calorimeter. This allows the average value of λ to be calculated; this value is listed in Table VII (Table II in Chapter 2 lists the same values of $\dot{Q}''_{max}$ and λ). This way of determining λ is, however, not straight forward since only the first, decaying part of the heat release curve from the Cone is used in order to get a "best fit" (see Figure 13).

This problem can be avoided by solving equation (49) numerically, as will be shown in Chapter 4, thus allowing the results from the Cone to be used directly. The drawback is that no analytical solutions can be obtained, thus clouding the physical meaning behind the equations and figures such as Figure 14 cannot be obtained.

The equations above assume that the materials are thermally thick; the properties of composite materials are thus assumed to reflect their bulk properties.

Table VII also lists the parameters $\lambda\tau$ and a (= $K\dot{Q}''_{max}$). These parameters are plotted in Figure 22, which is similar to Figure 14. The figure shows the regions of flame front acceleration and deceleration, identified by Thomas and Karlsson /42/. Baroudi and Kokkala /44/ originally used their results to construct such figures.

Table VII: Values of $\dot{Q}''_{max}$ and t_{ig} measured at an irradiance level of 50 kW/m^2 /14/, λ is an average of the values obtained by equation (52). The parameters $K\dot{Q}''_{max}$ and $\lambda\tau$ are used in Figure 22.

Mat. no.	Material name	$\dot{Q}''_{max}$ [kW/m^2]	λ [s^{-1}]	t_{ig} [s]	$K\dot{Q}''_{max}$ [-]	$\lambda\tau$ [-]
S1	Insulating fib.board	184	0.0090	12	2.76	0.18
S2	Medium density fib.board	208	0.0027	28	3.12	0.13
S3	Particle board	204	0.0030	34	3.06	0.17
S4	Gypsum plasterboard	151	0.0390	34	2.26	2.25
S5	PVC cover on gyps. pl. b.	210	0.0600	10	3.15	1.02
S6	Paper cover on gyps. pl. b.	254	0.0600	21	3.81	2.14
S7	Textile cover on gyps. pl. b	408	0.0700	20	6.12	2.38
S8	Textile cover on min. wool	466	0.0800	11	6.99	1.50
S9	Melamine-faced particle b.	150	0.0016	40	2.25	0.11
S10	Expanded polystyren	-	-	-	-	-
S11	Rigid polyurethane foam	247	0.0200	2	3.71	0.68
S12	Wood panel, spruce	168	0.0075	21	2.52	0.27
S13	Paper cover on particle b.	197	0.0041	27	2.96	0.18

Exponentially accelerating flame spread appears in region I below line A. Materials No. S1, S2, S3, S8, S9, S11, S12 and S13 (see Table VII) fall into this category and all of them go to flashover in the Room Corner test.

In region II the flame starts accelerating but then decelerates and stops at a finite time. A position just above Line A can therefore result in flashover since the flame can spread over a considerable area before it decelerates and finally stops. Material No. S7 (see Table VII) shows such behavior, and is quite close to causing flashover in the Room Corner test. Materials No. S5 and S6 are much further away from Line A and the flame starts decelerating much earlier, showing a low risk for flashover.

In region III the solution of the above equations shows an initial deceleration. There is no acceleration until the velocity has been negative for some time. The equation for the velocity is only valid until the velocity has decelerated to zero and

for all practical purposes materials in this region do not go to flashover in the Room Corner Test (Material No. 4, see Table VII). The same is true for region IV, except that the velocity decelerates for all times.

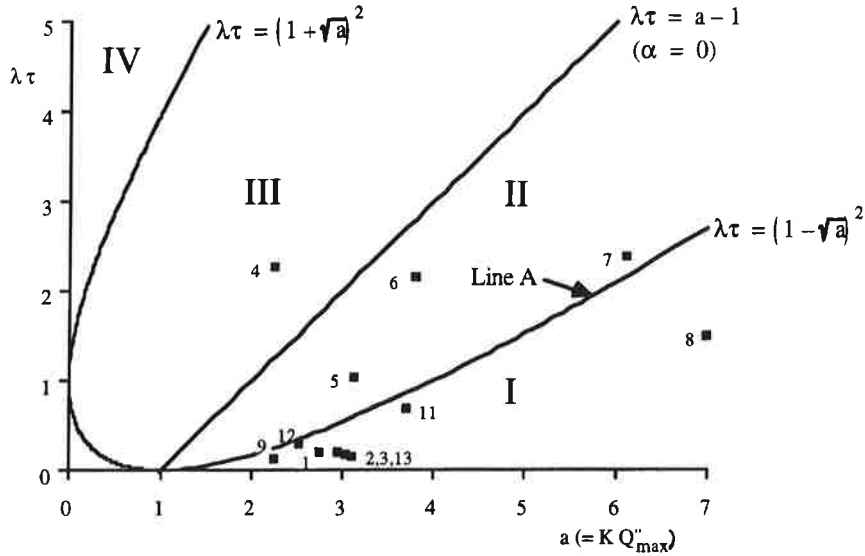

Fig. 22. Regions of flame front acceleration and deceleration. Numbers on the graph represent material numbers given in Table VII.

The roots of the quadratic in the denominator of equation (51) are the same whether the equations are set up for velocity in terms of areas under ceilings or linear velocities up a wall. Figure 22 is thus valid for other configurations than the Room Corner test and flame spread under a ceiling. The value and the units of K, the flame length or flame area coefficient, change in each configuration (flame spread up a corner, on a wall or under a ceiling) and so does the initial pyrolysing area, A_0, or pyrolysing length, x_p. Also, τ, the time to ignition, depends on the configuration.

3.5.4. Expressions for heat release rate and pyrolysing area

In order to calculate how far the flame front has travelled and the resulting heat release rate we must set up expressions, in terms of velocity, for the pyrolysing area, A_p, and the heat release from the ceiling, $\dot{Q}_c$. The solutions are given in two parts, one for the region $\lambda\tau < (1-\sqrt{a})^2$, $\lambda\tau > (1+\sqrt{a})^2$, when the flame

accelerates or decelerates monotonously and another for the region $(1-\sqrt{a})^2 < \lambda\tau < (1+\sqrt{a})^2$, where flame spread will eventually cease.

The pyrolysing area as a function of time can be written as

$$A_p(t) = A_0 + \int_0^t V(t_p)\, dt_p \tag{53}$$

For $\lambda\tau < (1-\sqrt{a})^2$, $\lambda\tau > (1+\sqrt{a})^2$ the solution is given as (see eqn. (32))

$$A_p(t) = A_0 + \frac{C_1}{s_2 - s_1}\left(e^{s_2 t} - e^{s_1 t}\right) \tag{54}$$

and for $(1-\sqrt{a})^2 < \lambda\tau < (1+\sqrt{a})^2$ the solution is (see eqn. (33))

$$A_p(t) = A_0 + \frac{C_1 e^{\alpha t}}{\beta}\sin(\beta t) \tag{55}$$

Similarly, the heat release rate from the ceiling material can be written

$$Q_c(t) = A_0 \dot{Q}''_{max} e^{-\lambda t} + \int_0^t \dot{Q}''_{max} e^{-\lambda (t - t_p)} V(t_p)\, dt_p \tag{56}$$

For $\lambda\tau < (1-\sqrt{a})^2$, $\lambda\tau > (1+\sqrt{a})^2$ the solution is given as

$$Q_c(t) = A_0 \dot{Q}''_{max} e^{-\lambda t} + \frac{C_1}{s_2 - s_1}\left(\frac{s_2 \dot{Q}''_{max}\left(e^{s_2 t} - e^{-\lambda t}\right)}{s_2 + \lambda} - \frac{s_1 \dot{Q}''_{max}\left(e^{s_1 t} - e^{-\lambda t}\right)}{s_1 + \lambda}\right) \tag{57}$$

and for $(1-\sqrt{a})^2 < \lambda\tau < (1+\sqrt{a})^2$ the solution is given as

$$Q_c(t) = A_0 \dot{Q}''_{max} e^{-\lambda t} + C_1 C_2 \dot{Q}''_{max}\left[e^{\alpha t}\left(\cos(\beta t) + \frac{C_3}{\beta}\sin(\beta t)\right) - e^{-\lambda t}\right] \tag{58}$$

where $C_2 = \left(\frac{1}{\lambda}\left(\alpha^2+\beta^2\right)+2\alpha+\lambda\right)^{-1}$ and $C_3 = \frac{1}{\lambda}\left(\alpha^2+\beta^2\right)+\alpha$

3.5.5 Some further assumptions on time to ignition and flame area under ceiling

In the ISO 9705 procedure combustible lining materials are placed on both walls and ceiling. Time to flashover is, however, mainly due to ignition of the wall material behind the burner and a subsequent ignition and flame spread over the material in the ceiling. We shall therefore not consider the combustible material on the walls, other than that behind the burner and in the wall-ceiling intersection.

The heat released in the Room Corner test is thus assumed to come from three sources. First, the gas burner releases around 100 kW, with flame heights that nearly reach the ceiling. After an ignition time τ, the material behind the burner ignites. This causes the flames to hit the ceiling, the flame area in the ceiling being equal to A_0. After yet another ignition period τ, this ceiling area ignites and the flames spread along the ceiling.

The procedure for calculating the heat release rate is the following:

1) For $t < \tau$ $\quad \dot{Q}(t) = \dot{Q}_b$ (59)

2) For $\tau < t < 2\tau$ $\quad \dot{Q}(t) = \dot{Q}_b + \dot{Q}''_{max} * A_w * e^{-\lambda(t-\tau)}$ (60)

3) For $t > 2\tau$ $\quad \dot{Q}(t) = \dot{Q}_b + \dot{Q}''_{max} * A_w * e^{-\lambda(t-\tau)} + \dot{Q}_c(t-2\tau)$ (61)

where $\dot{Q}_c$ is calculated from equations (57) and (58).

Here, A_w stands for the wall area behind the burner, an area assumed to be equal to twice the burner width times the height from the burner to the ceiling (≈ 0.65 m^2 in the Room Corner test). $\dot{Q}_b$ is the burner output ($\approx$ 100 kW in the Room Corner test).

In order to determine the constants s_1, s_2, α and β and solve equations (57) and (58) there are three parameters which have not yet been defined numerically, viz. A_0, K and τ.

The time to ignition in the room corner test, τ, correlates strongly with time to

ignition in the Cone Calorimeter (t_{ig}) at an irradiance level of 50 kW/m^2. It was found that a value of $\tau \approx 1.7\ t_{ig}$ gave a reasonable representation of both time to ignition of the material behind the burner as well as the ignition time in the ceiling. Alternatively, time to ignition can be calculated from equation (20) where τ is a function of $k\rho c$, T_{ig} and the heat flux from the flame, $\dot{q}''_f$. This procedure will be used in the more complex models described in Chapter 4. However, taking q''_f equal to 35kW/m^2 gave iginition times and calculated heat release rates very similar to the results achived by using the more simple approach above, where τ is assumed to be $1.7\ t_{ig}$.

It is difficult to determine the numerical value of the flame area coefficient, K, from experiments, as discussed in section 3.4. Saito, Quintiere and Williams /41/ report a value of 0.010 [m^2/kW] for upward flame spread on a wall. When taking account of pre-heating by the hot gas layer this value seems to give good results for flame spread under a ceiling and this value will be used for the more sophisticated model presented in Chapter 4. Here, however, we cannot take account of pre-heating by the hot gas layer since analytical solutions are being used. We must therefore choose a somewhat higher value to be used here. A good fit was obtained by choosing K = 0.015 [m^2/kW].

It can be noted that the flame length coefficient has been expressed by Baroudi and Kokkala /44/ as E" = 1/K, where E" has a real physical meaning: the heat release rate per unit area of flame. The dimensionless parameter $a = \dot{Q}''_{max}/E''$ is then easier to comprehend.

The form of the equations for initial pyrolysis area and flame area as a function of heat release rate was discussed in section 3.4.3. The initial pyrolysis area, A_0, depends on the amount of energy carried by the plume to the ceiling. We have assumed this amount of energy to be the burner output and the energy released by the material behind the burner, minus the energy lost in the wall corner plume.

Magnusson and Sundström /20/ have estimated the amount of energy lost in the plume to be in the area of 60 - 150 kW. When $\dot{Q}$ = 100 kW the flames do not quite reach the ceiling, so we have here used the value 150 kW for the energy lost in the plume and thus write (see equation (48))

$$A_0 = K*[\dot{Q}_b + \dot{Q}''_{max}*A_w*e^{-\lambda\tau} - 150] \qquad (62)$$

Since there are difficulties in determining both A_0 and K experimentally, a proper parameter study should be carried out. The above values and expressions for these parameters must therefore be considered to be preliminary.

3.5.6 Results of heat release rate calculations

The above procedure was applied to all these materials except Material No. S10, expanded polystyrene, since this material melts in both the bench scale and full scale test and the theory is not considered to be valid for such materials. Using the model on this material results in a longer time to flashover than in the experiments.

The complete series of results are shown in Appendix B, as examples the results for particle board and paper wallcovering on gypsum plaster board is shown in Figures 23 and 24. The agreement with experimental data is good, except for Material No. S9, melamine faced particle board. This is due to the way this material behaves in the Cone Calorimeter; there is a sharp pulse of heat release at time = 40 seconds ($=t_{ig}$), but then the material releases no more heat until time $\approx$ 200 seconds, thereafter showing a typical curve for the heat release rate.

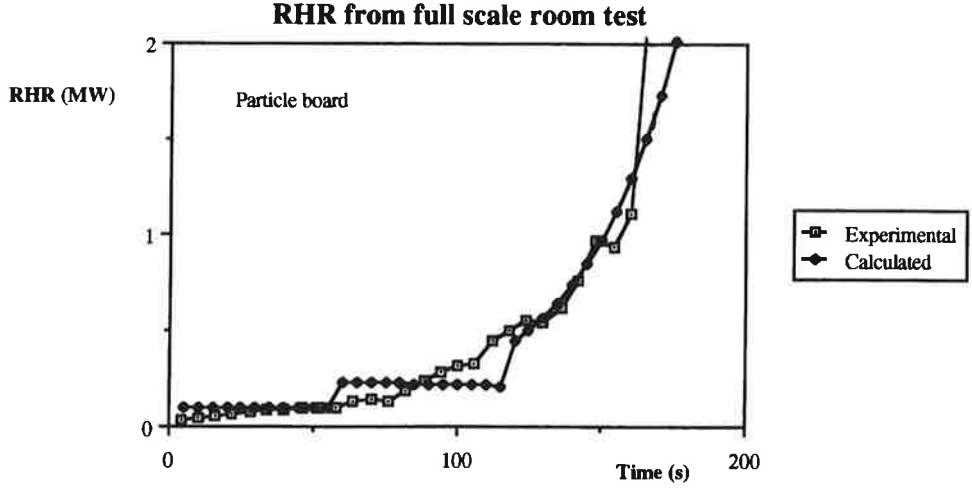

Fig. 23. Material No. S3.

3.5.7 Discussion

Among the earlier efforts to model heat release rate in the Room Corner test is the work of Magnusson and Sundström /20/, who presented a model for calculating the heat release in the same scenario as has been discussed above. The regression equation was capable of predicting heat release rates in both a full scale and a 1/3 scale of the Room Corner test, showing good agreement with experiments. The drawback with their approach was that materials which did not go to flashover could not be modelled, since no mechanism for a retreating flame was included.

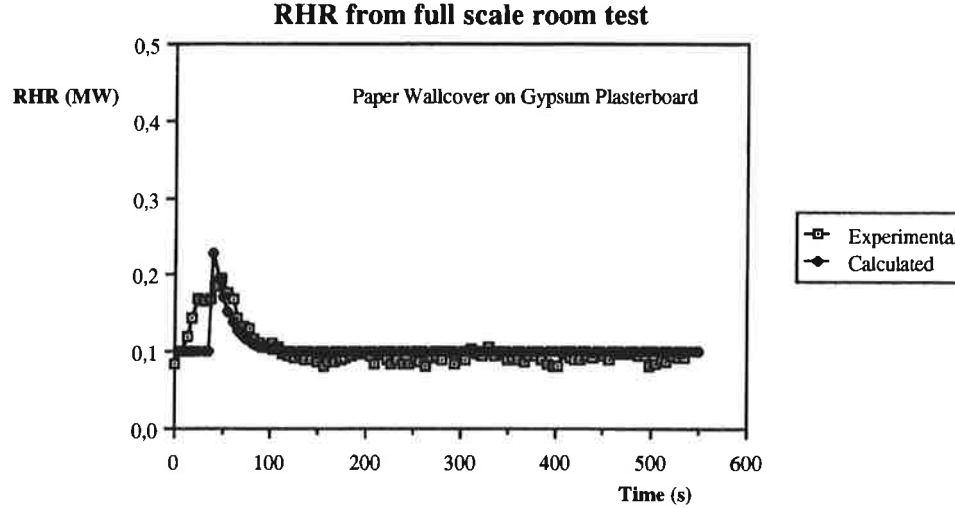

Fig. 24. Material No. S6.

Here, this drawback has been amended by applying a thermal theory for concurrent flow flame spread to the underside of a ceiling, thus including a possible retreat of the flame. However, pre-heating of the material is assumed to be due to radiation from the advancing flame only, no account is taken of heating from other sources. Further, the radiation from the flame is assumed to be of a constant intensity over the flame length and zero beyond that.

Several other assumptions are made with respect to flame lengths, heat release rate and time to ignition. In spite of the simplicity of the model and the numerous assumptions, the results show good agreement with experiments. However, a parameter study should be carried out to determine the value of the flame length coefficient, K, and the initial pyrolysing area, A_0.

The models presented in Chapter 4 will remove some of the above assumptions. The main purpose of this section has been to exemplify the usefulness of analytical solutions of the flame spread velocity equations where simple, but physically sound, engineering approximations can give a good indication of material behaviour with respect to fire growth on lining materials.

Finally, the interested reader may wish to consult a recent paper by Thomas /70/, where he discusses the differences in using a fractional power relationship (such as 2/3) between flame length and heat release rate as opposed to using proportionality, as we have done here.

4 Modeling room fire growth on combustible lining materials

Fires in enclosures, where surface lining materials are the main source of combustibles, can occur under a wide range of circumstances with respect to the geometry of the enclosure , the geometry of the lining materials and the strength, type and position of the ignition source. We will, in this chapter, define the scenarios to be modelled, give a short review of earlier work and set up the assumptions and equations which will be used to construct mathematical models for calculating flame spread and heat release rate in the chosen scenarios.

4.1 Selecting scenarios

It is generally more or less accepted that real-life, full scale scenarios which have to be investigated include /71/

i) fire development in a room of limited dimensions, where heat release from an item first ignited may result in the involvement of the building fabric and a substantial increase in the temperature of the compartment and, therefore, a reduction in the time to flashover,

ii) fire spread in a large volume compartment (e.g. an industrial building, theatre, exhibition arena) where the heat release from an item first ignited may result in the involvement of the building fabric but without any significant increase of temperature within the compartment,

iii) fire propagation down a corridor resulting from radiative and convective heat transfer from a room adjoining the corridor, possibly involving the wall, ceiling and floor coverings.

The list above gives only the outline or frame for a scenario specification; factors that have to be specified include geometry and location of burner or ignition source, burner programme or heat output from ignition source, size and geometry of room and openings, application of the lining material to walls and/or ceiling, etc.

Internationally, a number of large scale fire test methods have been developed /72/, /73/, /74/ to allow evaluation of the performance of wall and ceiling linings in configurations and under circumstances representative of end use. These test methods all apply an ignition source in the corner of a room which is considered

to be the most severe ignition configuration plausible. The strength of the ignition source, however, is not the same in these test methods. The gas burners used as ignition sources have been placed in contact with both walls of a corner. Williamson et al. /75/ have argued that an ignition source a short distance from the corner may be more representative as a "real world" scenario.

Consequently, a wide range of possible scenarios exist and we must clearly limit ourselves to a few of these in our modeling efforts. One of the limiting factors is access to experimental data and for many of the scenarios enumerated above the required combination of full scale experiments and bench-scale tests are very scarce.

We shall in this work limit our modeling efforts to two basic scenarios for which extensive experimental work has been carried out in the Scandinavian countries /1/, /2/, both with respect to bench-scale tests and full scale experiments. In these experiments the ignition source was a gas burner in the corner of an enclosure where lining materials were mounted on three walls only, or on three walls and the ceiling. The enclosures had the dimensions of the Room Corner test, as defined in the ISO 9705 standard /72/, or a 1/3 scale of that room.

We shall consider two basic scenarios; Scenario A, where the lining material is mounted on three walls and the ceiling; and Scenario B, where the lining material is mounted on three walls only. This will result in two separate mathematical models being presented, Model A and Model B, respectively.

The reason for distinguishing between these two scenarios is that fire growth in Scenario A is dominated by concurrent flow flame spread on the material in the ceiling but in Scenario B the fire growth is dominated by concurrent flow flame spread in the ceiling-wall intersection and subsequent downward flame spread on the walls.

Furthermore, two compartment geometries will be considered for both scenarios; the full scale room, as defined by /72/, and a 1/3 scale copy of it. The results from the calculations will thus be compared with four series of experiments, described in Chapter 5.

4.2 Earlier modeling efforts

Quintiere /76/ has given a description of the conceptual formulation of wall fire spread in a room. It is evident from this description that a solution of the wall fire growth phenomena on a fundamental basis requires a modelling structure involving a number of heat transfer, fluid dynamics and combustion phenomena. In order to use analytical or numerical calculation methods a number of simplifications will have to be introduced.

Basically two approaches have been employed. In the first one, there is no explicit linking between flame spread and radiative feedback from the upper gas layer; flame spread is modelled independently of the room fire process. The adjustable parameters in the expressions for the growing fire are fitted in such a way that the model describes a closely defined scenario, usually the ISO 9705 room corner standard test, and the main output of the model is the HRR-curve describing the room test. This approach is usually linked to the classification problem with classification of the product determined by its behaviour in the full scale test scenario.

The validity of the model outside this scenario is unknown and for fire engineering design a more physically based methodology becomes necessary. This second approach is usually founded in the zone modelling technique. Ideally it consists of solving conservative equations for distinct control volumes which characterise the room fire, including calculation of the heat transfer from the upper gas layer and the flame region to the surface lining areas. These two approaches are discussed below, giving examples of existing models.

4.2.1 Calculation models, where heat release is not influenced by room fire process

In this category, three different models have been generated within the Swedish project "The pre-flashover fire" /1/. These models, of Östman et al. /77/, Magnusson et al. /20/ and Wickström et al. /78/, vary with respect to the amount of physics contained in the model structure and the method used for the estimation of parameters.

In /77/, time to flashover in ISO 9705 has been correlated, using straighforward statistical analysis, with a simple expression containing time to ignition and peak heat release rate from Cone Calorimeter, and the material density.

In /20/, heat release rate in the full scale room was assumed to follow an exponential curve. The undetermined parameters in the model, which used non-dimensional quantities, were calculated by regression analysis. The main limitation of the model was that the heat release curve from the Cone Calorimeter was assumed exponentially decaying and that the model was not extended to cover the case when fire growth stopped before flashover.

In /78/, heat release rate in the ISO 9705 standard test is modelled by using ignition times and the heat release rate curve from the Cone Calorimeter. The growth rate of the burning area is assumed to follow specified expressions, flame propagation to be determined by a calculated fictitious surface temperature at a point beyond the flame front and total heat release rate calculated by a superposition procedure.

A number of parameters are determined by comparing the model output with experiments and the model extended to cover the burner programme (with burner output 100 kW for the first 10 minutes of the test, 300 kW after 10 minutes) specified in ISO 9705. The empirical nature of the model permits it to give good agreement with experiments, a more recent publication /79/ shows a favourable comparison with full scale experiments on 16 different materials.

A very recently published model is probably the most advanced so far with respect to using available fire physics (Karlsson, /67/). A short description of this model was given in Chapter 3.5. It should be emphasized that all four models mentioned above are semi-empirical and applicable to a scenario with the combustible lining material on both walls and ceiling and with a gas burner in the room corner as an ignition source.

4.2.2 Calculation models, where account is taken of the interaction between the room fire process and the flame spread

This second category of models must be more comprehensive and flexible than the models described in section 4.2.1. A number of models in this category exist or are being developed. The early modeling effort by Smith et al. /80/ has been followed by Tran and Janssens /81/, who have recently carried out extensive experimental and theoretical work on fire growth on combustible linings. A description of the model they have developed, and some validation studies, will be published shortly /82/, /83/.

Here we will summarise only one model of this category; the one presented by Quintiere /84/. This is an improved version of the model originally presented by

Cleary and Quintiere /23/. We shall also, in later sections of this chapter, give detailed descriptions of two additional models in this category, Model A and Model B, which are improvements on the models previously presented by Karlsson /85/.

The model described in /84/ treats the case of ISO 9705 room with combustible linings on walls and ceilings. It simulates the ignition, flame spread, burn-out, and burning rate of wall and ceiling materials subject to a corner fire ignition source in a room.

The flame pyrolysis and burn-out fronts are computed with respect to two modes of flame spread. One mode includes upward spread, spread along the ceiling, and spread along the wall-ceiling jet region in accordance with the theories given in Chapter 3. At this time, no distinction for these different configurations is made in the model and they are universally treated as governed by upward flame spread.

The second mode of spread is composed of lateral spread along the wall and subsequent downward spread from the ceiling jet. Again, the same relationship will be considered for both. In this fashion, the pyrolysis and burn-out areas are computed.

The energy release rate per unit area is considered as a function of time. The energy release rate per unit area is governed by the flame heat flux and the radiative feedback from the heated room. Flame heat flux is considered uniform over the pyrolysis area, and uniform over the extended flame length. Two values are selected: 60 kW/m^2 over the pyrolysis area and the area associated with the square burner corner ignition flame, and 30 kW/m^2 for the extended flame spread which governs upward flame spread.

The room thermal feedback controls both the rate of spread through a computation of the material surface temperature ahead of the flame, and the rate of energy release per unit area through radiative heat transfer from the gas layer in the room. Gas layer temperature calculations are based on the methodology proposed by McCaffrey et al. /86/, with a revised pre-exponential constant. The model accuracy has been tested against a series of ISO 9705 Room Corner tests, performed on 13 different materials (tabulated as the "Swedish" materials in Chapter 2), showing good agreement with experiments.

It should also be mentioned that several specialised flame spread models have been developed (for example Delichatsios et al. /87/, Mitler /88/ and Kulkarni /89/), using flame spread theories considerably more sophisticated than those described in Chapter 3. Some of these models take account of a variable heat flux

over the flame height, radiative and convective heating, oxygen concentration, flame spread in vitiated atmosphere, etc.

Efforts are now under way to link these flame spread models to two-zone models to get information on pre-heating of the material, oxygen concentration, smoke layer height and temperature and other environmental factors. Examples are the models described in /87/ and /88/ , which are now being linked to the special version of the well known two-zone model CFAST /90/ . Input to the flame spread models can be the results from both standard and non-standard bench-scale tests.

4.3 Structure of the models presented in this work

4.3.1 Model A

Model A simulates the case where lining material is mounted on both walls and ceiling. The total rate of heat release in the room is assumed to come from three sources: the gas burner, the vertical wall area behind the burner and, finally, the ceiling and the ceiling-wall intersection.

The ignition source in the corner ignites the wall material behind the burner and spreads rapidly upward on an area, A_w, approximately equal to the width of the burner times the distance from the burner to the ceiling. This results in a flame under the ceiling, with a "T" pattern flame morphology as described in Chapter 3.4.1 (see Figure 15). The flames spread both in the ceiling-wall intersection and under the ceiling itself in the mode of concurrent flow flame propagation.

When the fire in the corner starts and the lining material in the corner ignites, combustion products and plume entrained air are transferred to the ceiling. The hot gas layer forms, descends and increases in temperature with time. Relatively early in the test the layer reaches the top of the opening, stabilises and hot gases start flowing out through the opening.

The hot layer is in contact with the lining material in the upper part of the room. Heat from the layer is transferred to the lining material, increasing its surface temperature and thus allowing the flame to spread more rapidly.

The heat released from the material causes the flames to stretch over the unburnt material. If the heat released by the material is small or its time to ignition is long, the velocity of the flame front may at some point start to decelerate and, eventually stop. A high rate of heat release and a short ignition time might, on the other hand, result in exponentially increasing flame front velocity and relatively rapid flashover.

In the case of no flashover, the strength of the ignition source may be increased, causing the flame to stretch over unburnt material, not reached by the earlier ceiling flames. This again can cause rapid flashover or an eventual deceleration of the flame velocity and no flashover.

Lateral and downward flame spread is ignored in the current version of this model since the flame spread and the resulting heat released is very much dominated by concurrent flow flame spread. Both Quintiere /84/ and Karlsson and Magnusson /91/ have found that this flame spread mode is not significant

until close to the onset of flashover. Also, no account is taken of the relatively low oxygen concentration in the upper layer.

The following sub-models will have to be included in the total simulation model:

1. Ignition of the wall area behind the burner
2. Upper layer hot gas temperature calculation based on calculated heat release rate
3. Heating up of the ceiling and wall areas immersed in the gas layer
4. Ignition and flame spread under the ceiling and in the ceiling-wall intersection.
5. Calculation of total heat release rate, based on areas pyrolysing and time dependence of bench-scale heat release rate curves.

If flashover is not achieved within 10 minutes, the burner output is increased to 300 kW in the full scale test. This increase is also accounted for in the present version of Model A. The input to this model is the heat release rate curve from the Cone Calorimeter at 50 kW/m^2 irradiance and material parameters kρc and T_{ig} from bench-scale tests.

4.3.2 Model B

Model B simulates the case where lining material is mounted on walls only. The total rate of heat release in the room is assumed to come from five sources: the gas burner, a horizontal strip of material at the ceiling-wall intersection corresponding to the vertical height of the ceiling jet and, when downward flame spread has started, the wall material in the upper layer and from the wall linings below the hot gas layer respectively.

As in Model A, the ignition source in the corner ignites the wall material behind the burner and spreads rapidly upward on the material behind the burner with an area A_w. The resulting ceiling jet, or flame, spreads along the intersections between the walls and the ceiling in the mode of concurrent flow flame propagation.

After a time the pyrolysing area has propagated quite far along the two ceiling-wall intersections and a strip of material at the top of the walls is pyrolysing. In the experiments discussed here this strip has a height of 5 - 10% of the room height, a value of 7.5% has been chosen for Model B. In this time period there are thus three major sources that contribute to the total heat release: the gas burner, the diminishing effect of the pyrolysing area behind the gas burner and

the increasing pyrolysis area of the horizontal strip at the ceiling-wall intersection.

As described in the previous section, the hot gas layer forms, descends, increases in temperature and stabilises just below the top of the opening. The wall lining area below the strip covered by the horizontal ceiling-wall jet flame is simultaneously being heated up from the hot gas volume. As a consequence, the downward flame spread in the upper layer starts and a fourth source of released energy is being added to the three mentioned above.

The flame spread is quite slow at first since the wall material has a relatively low surface temperature. It then accelerates until it reaches the interface of the smoke layer and walls, which is assumed to be at a height equal to the height of the opening.

At this point the flame spread slows down since the walls beneath the smoke layer have a lower surface temperature than the walls immersed in the hot layer. The downward spread then accelerates again as the wall lining surface temperature rises.

The following sub-models will have to be included in the total simulation model:

1. Ignition of the wall area behind the burner
2. Upper layer hot gas temperature calculation based on calculated heat release rate
3. Heating up of wall areas, both below and above the thermal discontinuity, by convection and radiation
4. Horizontal, concurrent flow flame spread along the ceiling-wall intersection
5. Downward, against the wind, flame spread
6. Calculation of total heat release rate, based on areas pyrolysing and time dependence of bench-scale heat release rate curves.

The inputs to this model are heat release rate parameters $\dot{Q}''_{max}$ and λ (these allow mathematical representation of the heat release rate curve from the Cone Calorimeter at 50 kW/m^2 irradiance) and material parameters kpc, T_{ig} and Φ from bench-scale tests.

4.4 Ignition of the material immediately behind the gas burner

In the scenarios considered here, the ignition source is a gas burner with a relatively high energy output, 100 kW in the full scale tests and 11 kW in the 1/3 scale tests. This results in a corner flame which nearly reaches the ceiling of the compartment. For simplicity, we assume that the burner flame causes a constant irradiant heat flux to the material behind the burner over an area A_w, equal to twice the burner width times the height from the top of the burner to the ceiling. The approximate value of A_w is thus 0.75 m^2 for the full scale tests and 0.1 m^2 for the 1/3 scale tests. We are interested in calculating the time it takes to ignite this area of material.

The solution of the general heat conduction equation with simple boundary conditions (ignoring convective and radiative cooling) was given in Chapter 3.

Time to ignition of the wall material behind the burner, τ_w, can then be calculated from - cf equation (20)

$$\tau_w = \frac{\pi \, k\rho c \, (T_{ig} - T_o)^2}{4 \, \dot{q}''^2_w} \qquad (63)$$

where $\dot{q}''_w$ denotes the net heat flux from the burner flame. The values of $k\rho c$ and T_{ig} are available from the bench-scale tests described in Chapter 2.

We would expect the heat flux from the burner flame to be higher in the full scale tests than in the 1/3 scale tests, since the burner output and burner size in the latter tests are much smaller and the flames therefore thinner.

Recent experiments carried out using the same burner size (0.17m*0.17m) and heat output (100 kW) as used in the full scale room test were presented and discussed by Kokkala et al. /56/. They found that the incident heat flux on the material behind the burner was around 40 kW/m^2 over a height ≈ 1.6 m above the floor. Williamson et al. /75/ report values of 50 - 60 kW/m^2 for burner output of 150 kW and burner size 0.3m*0.3m.

Choosing $\dot{q}''_w$ = 45 kW/m^2 for the full scale tests and $\dot{q}''_w$ = 25 kW/m^2 for the 1/3 scale tests seemed to give good results in both Model A and Model B and these values were therefore used in the calculations.

4.5 Calculation of gas temperatures

The basic principle used to calculate the temperature in a compartment fire is the conservation of mass and energy. Since the energy release rate and the compartment temperature change with time, the application of the conservation laws will lead to a series of differential equations.

By making certain assumptions on the energy and mass transfer in and out of the compartment boundaries, the laws of mass and energy conservation can result in a relatively complete set of equations. Due to the complexity and the large number of equations involved, a complete solution of the set of equations would usually only be obtained from computer programs.

However, there exist regression formulae which, with a number of limiting assumptions, allow the gas temperature in a naturally or mechanically ventilated compartment to be calculated by hand.

McCaffrey, Quintiere and Harkleroad /86/ used a simple conservation of energy expression and a correlation of a relatively wide range of data to develop a hand-calculation formula for the hot layer temperature in a naturally ventilated compartment.

The upper layer temperature was written as a function of two dimensionless groups

$$\frac{\Delta T}{T_0} = C \cdot X_1^N \cdot X_2^M \qquad (64)$$

The constants C, N and M were determined from a wide range of experimental data; the final form of the regression equation in /86/ was given as

$$\frac{\Delta T}{T_0} = 1.63 \left(\frac{\dot{Q}}{\sqrt{g}\, c_p \rho_o T_o A_o \sqrt{H_o}} \right)^{2/3} \left(\frac{h_k A_w}{\sqrt{g}\, c_p \rho_o A_o \sqrt{H_o}} \right)^{-1/3} \qquad (65)$$

The heat transfer coefficient, h_k, depends on the duration of the fire and the thermal characteristics of the compartment boundaries. The thickness of the lining materials treated here and the short duration of the corner test is such that the outer boundaries of the test compartment do not have an effect on the heat transfer coefficient. It can therefore be written as:

$$h_k = \sqrt{\frac{k\rho c}{t}} \qquad (66)$$

The experimental data upon which equation (65) is based comes from tests where the fire and the plume are in the centre of the enclosure, allowing relatively cold air to entrain into the plume from all directions. In the corner fire scenario much less cold air can entrain into the plume and we can expect higher gas temperatures in this scenario.

4.5.1. Determination of a modified pre-exponential factor, C

The method developed by McCaffrey et al. /86/ was followed by Karlsson /85/ to calculate the upper layer gas temperatures in a series of four corner test experiments. The experiments were carried out for Scenario A and Scenario B in both the full scale and the 1/3 scale room corner test geometry, making a total of 41 experiments. The two constants, N and M, as they appear in equation (65) did seem to describe the slope and shape of the experimental curves well. The constant C was determined, resulting in values for each of the experimental series ranging from 2.0 - 2.7.

The work in this earlier study /85/ was, however, based on values of apparent thermal inertia for the lining materials which were determined, some time ago, by a procedure quite different from the standardised procedure described in Chapter 2. The two procedures give the same ranking of materials but the order of magnitude of kρc is different, resulting in much higher values from the standardised procedure.

We will base all our calculations in this study on kρc values determined by the standardised procedure described in Chapter 2. This necessitates a re-evaluation of the pre-exponential constant C in equation (65).

The non-dimensional groups X_1 and X_2 were calculated, knowing the geometry of the full scale and the 1/3 scale enclosure and taking the heat release rate as a function of time from the experiments. The heat transfer coefficient in each scenario was calculated according to the methodology described in /86/, i.e.

$$h_k = \left(\sqrt{\frac{[k\rho c]_{lin}}{t}}\, A_{lin} + \sqrt{\frac{[k\rho c]_{lwc}}{t}}\, A_{lwc} \right) \Big/ A_{tot} \qquad (67)$$

where the subscripts $_{lin}$ and $_{lwc}$ stand for lining material and light weight concrete respectively and A_{tot} is the total enclosure surface area. The thermal inertia of the light weight concrete was taken to be 0.125 [$(kW/m^2K)^2$ s]. Data below 50°C and above 600°C were not included in the calculations. The resulting average values of the pre-exponential constant C are given in Table VIII.

Table VIII. Average values of the pre-exponential constant C for a series of four corner test experiments. A and B stand for Scenario A and Scenario B respectively.

Series	No. of materials	No. of exp. values	$C_{average}$	Standard deviation
Full scale, A	13	300	3.10	0.553
1/3 scale, A	13	474	3.15	0.691
Full scale, B	4	223	4.05	0.596
1/3 scale, B	11	208	3.54	0.879

Figure 25 shows the distribution of the calculated values of C for all the measured points in the 13 experiments carried out in full scale, Scenario A. The distribution for the other experimental series is similar, although $C_{average}$ may be different.

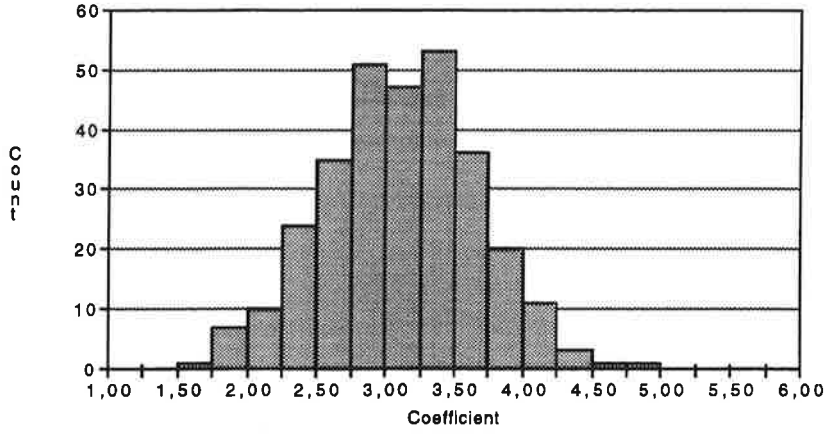

Fig. 25. Distribution of the calculated values of C for all the measured points in the 13 experiments carried out in full scale, Scenario A.

The experimental gas temperature was measured by thermocouples 5 cm from the ceiling in both 1/3 scale tests series and 30 cm from the ceiling in full scale test, scenario A. But in the full scale B test series the gas temperature was measured only 10 cm from the ceiling, resulting in relatively much higher gas

temperature values than in the other test series. This may to a certain degree account for the much higher $C_{average}$ in the last mentioned test series, as well as the fact that this series was carried out 4 years after the others and different experimental apparatus (such as thermocouples) was used. In general, the constant for the Scenario B experiments seems to be higher than that for Scenario A. This is due to the diffferent flame spread processes in the two scenarios. The greater turbulence in Scenario A as the flame spreads across the ceiling may, for example, cause greater mixing and lower gas temperatures.

Mowrer and Williamson /92/ discussed how the methodology described in /86/ could be used for corner fires. They observed that mass entrainment into the plume varied as a 1/3 power of the heat release rate. Using the analogy of equivalent source diameter (as seen in Figure 17) and replacing $\dot{Q}$ with $4\dot{Q}$ they found that the excess temperature over ambient in the corner plume should be 2.5 times higher than in the conventional plume.

However, the hot layer will not descend as rapidly in the corner fire as in the case of a conventional plume. The entrainment height in the corner plume will therefore be greater and the mass flow out through the opening will be altered. Mowrer et al. /92/ also included this consideration and concluded that the temperatures calculated by equation (65) should be multiplied by 1.7 in the case of a corner fire. This gives a pre-exponential factor $C \approx 2.8$.

4.5.2 Taking account of high heat release rates, close to flashover

Some account must be taken of the fact that the correlation above is not valid when the fire in the enclosure is approaching flashover. The energy released within the compartment in flame and upper layer combustion is restricted by the availability of oxygen. The heat release measured in the experiments includes the energy released in the flames coming out through the opening. This part of the heat release does not influence the gas temperature within the compartment. The availability of oxygen in the upper layer can be approximated by using a simple flame formula /93/, calculating the entrainment of air into the corner flame

$$\dot{m}'_{air} = \frac{2}{3} \alpha \rho_0 \sqrt{2g (1 - T_0/T_f)} \, x_f^{3/2} \qquad (68)$$

where x_f is the effective entrainment flame height, α is the entrainment coefficient and T_f is the flame temperature. Thus, the maximum rate of heat release inside the compartment was found to be approximately 600 kW for the full scale room and 60 kW for the 1/3 scale room.

4.5.3 Results

The procedure of limiting the heat release rate by the air entrainment into the corner flame and finding a pre-exponential factor for each test series proved to be very robust. Using experimental heat release rate to calculate gas temperatures shows very good agreement with measured gas temperatures. These results are not shown here but the results from the complete calculation procedure, where calculated heat release rate is used as input, are shown in Appendices C, D, E and F and are discussed in Chapter 5.

4.6. Heat transfer to walls and wall surface temperatures

When the fire in the corner starts and the lining material in the corner ignites, combustion products and plume entrained air are transferred to the ceiling. The hot gas layer forms, descends and increases in temperature with time. Relatively early in the test the layer reaches the top of the opening, stabilises and hot gases start flowing out through the opening.

Classical heat transfer provides expressions for quantities such as view factors, radiation and temperature fields in semi-infinite bodies. The lining materials studied here were treated as semi-infinite bodies since the test duration is relatively short and the thin materials tested all have a reasonably thick backing board.

No account is taken of downward flame spread in Scenario A, since the dominating physical process leading to flashover is concurrent flow flame spread under the ceiling. In that model the wall lining surface temperature below the gas layer is therefore not calculated.

This is, however, of considerable importance in Scenario B, since the downward flame spread velocity is the process leading to flashover. The velocity of the pyrolysis front is a function of the wall surface temperature, which will have to be calculated as a function of time and height above floor level. The pre-heating of this surface is mainly due to radiation from the hot gas layer above it, and, once the flames start travelling down the wall, radiation from the wall flames and the pyrolysing lining material behind these flames.

The pre-heating is also, but to a lesser extent, due to radiation from the flames in the corner. Because of the rather complex geometry we shall ignore the radiation from the flames in the corner and only consider the heat flux from the hot gas layer and the burning walls.

4.6.1 Heat flux calculations

One long side of the compartment wall is split into a large number of thin, horizontal strips (≈ 100 strips in the full scale test) and the instantaneous heat flux from the gas layer to the centre of each strip calculated using the expression

$$\dot{q}'' = \varepsilon F \sigma (T_g^4 - T_0^4) \qquad (69)$$

The emission coefficient is taken to be a constant value close to unity. The configuration factor, F, is calculated in a conventional way, treating the centre of each strip as a point at a certain height below the gas layer. Once the downward flame spread has started the radiation from the wall flames and the pyrolysing lining material behind the flames is added to the smoke layer radiation. The instantaneous heat flux to the walls can then be calculated from the expression

$$\dot{q}'' = \varepsilon_g F_g \sigma (T_g^4 - T_0^4) + \varepsilon_f F_f \sigma (T_f^4 - T_0^4) + \varepsilon_p F_p \sigma (T_p^4 - T_0^4) \qquad (70)$$

where the subscript $_g$ refers to the gas layer, $_f$ to the flame and $_p$ to the pyrolysing wall material. The view factors from the flame and the pyrolysing wall material are assumed to be identical, half the radiation coming from the flame and the other half from the pyrolysing material beneath the flames. The downward flame spread velocity is assumed to be the same, at any one time, on all three walls. All walls will thus experience radiation from one opposite wall flame and one perpendicular wall flame.

It remains to give values for the flame temperature and the pyrolysing material surface temperature. Little experimental work can be referred to in this respect for the scenarios and configurations considered here and some engineering assumptions must be made. The flame temperature was taken to be ≈ 1100 K and the pyrolysing material surface temperature was assumed to be ≈ 750 K. Further, the flame emission coefficient was taken to be 0.5, as was the surface of the pyrolysing material, giving a total emissivity of unity for the flames and the pyrolysing area.

4.6.2 Temperatures of wall surfaces beneath the hot gas layer

As discussed above, one long side of the compartment wall is split into a large number of thin strips and the heat flux to the centre of each strip calculated. The general one-dimensional heat conduction equation can be solved by means of Laplace transformations /94/, with conventional initial and boundary conditions

$$T = T_0 \text{ for } t = 0 \text{ and all } y > 0$$

and

$$k \left.\frac{\delta T}{\delta y}\right|_{y=0} = \dot{q}'' - h_N (T - T_0)$$

where h_N is the Newtonian cooling coefficient. If this coefficient is assumed to be a constant and independent of temperature, and reradiation is ignored, the wall surface temperature at time t can be calculated from

$$T_s - T_0 = \frac{\dot{q}''}{h_N}\left(1 - \exp(h_N^2 t / k\rho c)\, \mathrm{erfc}\left(\sqrt{h_N^2 t / k\rho c}\right)\right) \qquad (71)$$

The above equation also assumes a semi-infinite wall and a constant heat flux $\dot{q}''$.

Knowing the heat flux as a function of time, at the centre of each strip, the wall surface temperature at time step n can be calculated using the superposition principle. Equation (71) then becomes

$$T_s(n) - T_0 = \sum_{i=1}^{n} \frac{\dot{q}''(i) - \dot{q}''(i-1)}{h_N} \exp\left(h_N^2 (n - i)dt / k\rho c\right)\, \mathrm{erfc}\left(h_N \sqrt{(n - i)dt / k\rho c}\right) \qquad (72)$$

where dt is the size of the time step.

The surface temperature can thus be calculated as a function of time and height from the floor. An explicit form of the superposition integrals can be found in /95/ and /96/.

4.6.3 Surface temperature of ceiling and walls immersed in the hot gas layer

For both Model A and Model B we require the surface temperature of the ceiling and the walls immersed in the hot gas layer. These areas are assumed to be heated up by the hot gas layer alone and therefore, to have one surface temperature for each time step. No account is taken of the fact that the ceiling corner, being heated also by the corner plume, has a higher surface temperature than, say, the material in the centre of the ceiling.

As above, a solution of the general one-dimensional heat conduction equation by means of Laplace transformations can be achieved, with conventional initial and

boundary conditions

$$T = T_0 \text{ for } t = 0 \text{ and all } y > 0$$

and

$$k \left.\frac{\delta T}{\delta y}\right|_{y=0} = h\left(T_g - T_0\right)$$

Again, assuming h (the convective and radiative heat transfer coefficient) to be constant and using the superposition principle, the surface temperature of the wall material emerged in the hot layer can be calculated from the expression

$$T_s(n) - T_0 = \sum_{i=1}^{n}\left[T_g(i) - T_g(i-1)\right] \exp\left(h^2 (n - i)dt/k\rho c\right) \operatorname{erfc}\left(h\sqrt{(n - i)dt/k\rho c}\right) \quad (73)$$

Putting the Newtonian cooling coefficient in (72) and the heat transfer coefficient in (73) equal to a constant value is of course an oversimplification and is seen only as a temporary measure.

4.7 Concurrent flow flame spread

In Scenario A, the concurrent flow flame spread velocity equations presented in Chapter 3 are used to calculate the pyrolysing area under the ceiling at each time step and thus, the rate of heat release contribution from the ceiling material. In order to take account of pre-heating by the hot gas layer, these equations must be solved numerically. A numerical solution also allows us to use directly as input the heat release curve from the Cone Calorimeter. No mathematical representation of the bench-scale heat release rate is therefore needed.

In Scenario B, however, the concurrent flow flame spread only occurs at a small strip of material in the ceiling-wall intersection, relatively early in the test when gas temperatures are still reasonably low. Neglecting pre-heating by the hot gas layer will therefore not cause excessive errors and allows us to use the analytical solutions to the equations presented in Chapter 3. However, such solutions require a mathematical representation of the bench-scale heat release rates.

4.7.1 Concurrent flow flame spread in Model A

Concurrent flow flame spread under a ceiling can be calculated using the equation for pyrolysis front velocity (expressed in areas) given as equation (50). We rewrite this equation, in order to use directly the heat release rates from the Cone Calorimeter, as

$$V_A(t) = \frac{1}{\tau}\left[A_o + K\left(A_o\dot{Q}''_C(t) + \int_0^t \dot{Q}''_C(t - t_p)\, V_A(t_p)\, dt_p\right) - \left(A_o + \int_0^t V_A(t_p)\, dt_p\right)\right] \quad (74)$$

where $\dot{Q}''_C(t)$ represents the heat release rate in the Cone Calorimeter at time t after ignition and V_A represents flame spread velocity under the ceiling in Model A. The assumptions and limitations behind the above equation are discussed in some detail in Chapter 3.

In order to take account of pre-heating by the gas layer we must rewrite the equation for ignition time as

$$\tau = \frac{\pi\, k\rho c\, (T_{ig} - T_s)^2}{4\, \dot{q}''^2_f} \quad (75)$$

where ambient temperature has been replaced by surface temperature, T_s. This surface temperature is calculated as described in section 4.6.3.

Equation (74) is a Volterra integral equation of the second kind and several sophisticated numerical solution mechanisms for such equations exist /43/. In Model A, however, the equation is solved by iteration, usually only requiring 4-5 cycles to reduce the numerical error to less than 0.1%. The stability of the numerical solution was tested, for a constant τ, against analytical solutions, showing no irregularities.

The above equations assume quasi-steady state and second order derivatives have thus been ignored. Several test runs were made, varying the time step and comparing the results. The time step used in Model A of 0.1 seconds gives good results but a time step of 1 second may be adequate since the influence on the calculated time to flashover is small for the cases tested.

In equations (74) and (75) there are three parameters which have not yet been defined numerically, viz. A_0, K and $\dot{q}''_f$.

The numerical values of the flame length coefficient, K, and the initial pyrolysing area, A_0, were discussed in Chapter 3.5. In Model A we follow Quintiere /84/ and set the value of K to be 0.01 [m^2/kW]. An expression for the initial pyrolysing area was given in Chapter 3.5 as equation (62). During the time needed for ignition of the ceiling, the value of A_0 decreases somewhat, due to the decrease in energy release rate from the material behind the burner. An average value of this energy release rate is therefore used when calculating A_0.

It should, however, be noted that very little experimental data exist for flame area extensions under a ceiling corner and the above mentioned values and expressions will probably have to be replaced when new data becomes available.

Quintiere, Harkleroad and Hasemi /97/ found that, for vertical wall flame spread, the heat flux from the flame to the virgin fuel was $\approx 25 \pm 5$ kW/m^2. The heat flux from the flames under the ceiling in a full scale test can be considered to be slightly above this value. In the 1/3 scale test the flames are thinner and this heat flux should therefore be somewhat less than in the full scale test. Here, we have chosen $\dot{q}''_f = 35$ kW/m^2 for the full scale test and $\dot{q}''_f = 25$ kW/m^2 for the 1/3 scale test.

4.7.2 Concurrent flow flame spread in Model B

In Model B, we wish to calculate the velocity of the pyrolyses front in the ceiling-wall intersection, resulting from the extension of the corner flames along the intersection. An analytical solution of the concurrent flow flame spread equation is used, similar to the solutions presented in section 3.3.2. There, the relationship between flame length and heat release was assumed to be described as $x_f = K\dot{Q}_{tot}$ but here we will make use of the flame extension correlations presented in Chapter 3.4.2 and write

$$x_f = - L_o + K\dot{Q}_{tot} \tag{76}$$

Replacing $\dot{Q}_{tot}$ we get

$$x_f = -L_o + K\left(\dot{Q}_b + A_w \dot{Q}''_{max} e^{-\lambda(\tau + t)} + x_{po} W \dot{Q}''_{max} e^{-\lambda t}\right) +$$

$$K\left(\int_0^t W \dot{Q}''_{max} e^{-\lambda(t - t_p)} V_h(t_p)\, dt_p\right) \tag{77}$$

where V_h represents the flame spread velocity in the horizontal ceiling-wall intersection.

Inserting this into equation (19) in Chapter 3 we get solutions which are slightly more involved than before; the solution is

$$V_h(t) = \frac{1}{s_1 - s_2}\left[(B + As_1) e^{s_1 t} - (B + As_2) e^{s_2 t}\right] \tag{78}$$

where

$$A = \frac{1}{\tau}\left(- L_o + K\left(\dot{Q}_b + A_w \dot{Q}''_{max} e^{-\lambda\tau} + \dot{Q}''_{max} W x_{po}\right) - x_{po}\right)$$

$$B = \frac{\lambda}{\tau}\left(- L_o + K\dot{Q}_b - x_{po}\right)$$

$$C = \frac{1}{\tau}\left(1 - K \dot{Q}''_{max} W + \tau\lambda\right)$$

$$D = \frac{\lambda}{\tau}$$

$$s_1 = \frac{1}{2}\left(- C + \sqrt{C^2 - 4\,D}\right)$$

and $$s_2 = \frac{1}{2}\left(- C - \sqrt{C^2 - 4\,D}\right)$$

The above equations can be simplified using relationships between L_0, x_{po} and $\dot{Q}_b$.

$\dot{Q}''_{max}\, A_w\, e^{-\lambda t}$ is the heat release rate of the wall area A_w behind the burner at the onset of concurrent flame propagation and W is the width of the burning strip in the ceiling-wall intersection, taken to be 7.5% of the room height. The above equation can be solved for the case $C^2 - 4D < 0$ by using complex numbers. Also, analytical solutions are available for the length of the pyrolysis front, $x_p(t)$, and the resulting heat release rate from the horizontal ceiling-wall intersection, $\dot{Q}_h(t)$, by rewriting and integrating equation (78). This was done for a different scenario in Chapter 3.5.4. The analytical solutions for this scenario are rather cumbersome and are not shown here.

The flame extension coefficients, L_0 and K, were discussed in Chapter 3, where the extension of flames under ceilings was expressed as a function of nondimensional heat release rate, burner diameter and ceiling height. Rewriting equations (41) and (46) in terms of $\dot{Q}$ (instead of $\dot{Q}^*$) gives the values $L_0 = 0.14$ and $K = 0.025$ for the 1/3 scale room test and the values $L_0 = 0.4$ and $K = 0.008$ for the full scale test.

The ignition time, τ, is calculated as in Model A, using equation (75). In Model B, however, we do not take account of pre-heating by the hot gas layer and so T_s is replaced by T_0 in equation (75). The flame heat flux, $\dot{q}''_f$, is taken to be 35 kW/m^2 for the full scale test and 25 kW/m^2 for the 1/3 scale test, as was done in Model A.

4.8 Downward, opposed flow flame spread (Model B only)

When ignition of the material in the ceiling-wall intersection has occurred the flames spread relatively rapidly towards an opposite corner in the compartment. This results in a thin strip of pyrolysing material at the top of the walls.

When this flame spread has come to a halt or reached an opposite corner, the downward, opposed flow flame spread is assumed to start. The initiation of the downward flame spread is, in fact, governed by a certain minimum surface temperature, $T_{s,min}$, a material property which can be approximated reasonably well in bench-scale tests. This temperature compares well with the calculated surface temperatures at the top of the wall at the time when the concurrent flow flame spread ceases and $T_{s,min}$ is therefore not used in the current version of Model B, but may well be included in later versions.

The downward, opposed flame spread is quite slow at first since the wall material has a relatively low surface temperature. It then accelerates until it reaches the interface of the smoke layer and walls.

At this point the flame spread slows down since the walls beneath the smoke layer have a lower surface temperature than the walls immersed in the hot layer. The downward spread then accelerates again. The flame spread velocity is calculated from an expression similar to equation (16) in Chapter 3

$$V_d = \frac{\Phi}{k\rho c \left(T_{ig} - T_{fl.f}\right)} \qquad (79)$$

where T_{ig} and Φ are obtained from the bench-scale tests discussed in Chapter 2. $T_{fl.f}$ is the material surface temperature just ahead of the flame front. If the position of the flame front is known, this surface temperature at a certain wall height and certain time, can be extrapolated from the surface temperatures calculated at the centre of each wall strip at each time step. The downward flame spread velocity can thus be calculated.

4.9 Calculation of heat release rate

In both Model A and Model B we distinguish between two ignition times. Firstly, there is τ_w, which is the time calculated from equation (63) and refers to the time it takes the gas burner ignitor to start pyrolysing the material behind it. Before this time the only heat being released is from the gas burner.

Secondly, τ is the time it takes to ignite the material in the ceiling or in the ceiling-wall intersection, and thus initiating the concurrent flow flame spread. Figure 26 is a characteristic sketch of the heat release rate versus time.

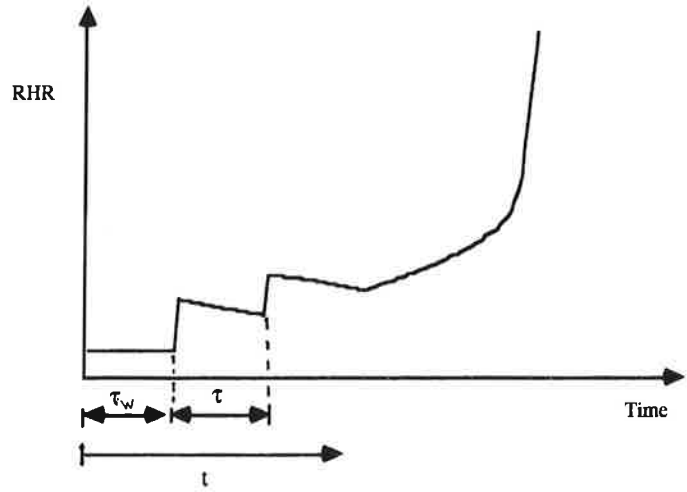

Fig. 26. Characteristic sketch of the heat release rate as a function of time.

For the period $0 < t < \tau_w$ the heat release rate is constant in both Model A and Model B and is taken to be the effect output from the gas burner, $\dot{Q}_b$. This is specified as 100 kW for the full scale tests and 11 kW in the 1/3 scale tests.

In Model A, we also simulate an increase in the burner energy release when no flashover has occurred in the first 10 minutes of the test. The burner effect output is thus set to 300 kW and 33 kW in the full scale tests and the 1/3 scale tests, respectively, if no flashover occurs during the first 10 minutes.

4.9.1 Rate of heat release in Model A

The heat release rate in the period $\tau_w < t < (\tau_w + \tau)$ is modelled in the following way: An area A_w, (equal to twice the width of the burner and the height from the top of the burner to the ceiling) is assumed to ignite and the heat release as a function of time, for the above period, is written as

$$\dot{Q}_{tot}(t) = \dot{Q}_b + A_w \dot{Q}''_C(t - \tau_w) \qquad (80)$$

where $\dot{Q}''_C$ stands for measured heat release rate per unit area from the Cone Calorimeter at a flux level of 50 kW/m^2.

This is a rather crude way of modelling the initial heat release rate. Fundamentally, one would wish to take account of the varying incident heat flux over this area, calculate flame spread velocity up the corner and take account of the burning rate variation as a function of incident heat flux. Such an approach requires the wall to be divided into a large number of nodes, following the heat flux history at each node, and a method of using Cone Calorimeter results where burning rate has been measured at various heat flux levels. Consequently, an advanced numerical solution mechanism would be required and we shall at the present stage of development accept the rather crude form of equation (80).

Once this area ignites, the flames reach the ceiling and start heating the unburnt material there. We shall assume that there is no pyrolysis front present at the intersection of the corner and the ceiling and treat the heat release calculated from equation (80) as a burner ignition source.

The flame extensions under the ceiling will eventually, after a time τ, cause the ignition of an initial pyrolysing area in the ceiling, A_o and consequently, concurrent flow flame spread. The addition to the heat release rate calculated by equation (80) is (where $t_1 = t - (\tau_w + \tau)$ to simplify the following equation)

$$A_o \dot{Q}''_C(t_1) + \int_0^{t_1} \dot{Q}''_C(t_1 - t_p)\, V_A(t_p) dt_p$$

The total heat release rate is thus calculated from

$$\dot{Q}_{tot}(t) = \dot{Q}_b + A_w \dot{Q}''_C(t - \tau_w) + A_o \dot{Q}''_C(t_1) + \int_0^{t_1} \dot{Q}''_C(t_1 - t_p)\, V_A(t_p) dt_p \qquad (81)$$

where $V_A(t)$ is calculated numerically from equation (74).

4.9.2 Rate of heat release in Model B

In Model B we will use an analytical solution of the flame spread equation and must therefore replace $\dot{Q}''_C(t)$, the heat release rate from the Cone Calorimeter, with a mathematical representation of this heat release rate, i.e. $\dot{Q}''_{max}\, e^{-\lambda t}$.

For the time interval $\tau_w < t < (\tau_w + \tau)$ the same procedure as described for Model A is followed and the form of equation (80) is used, resulting in

$$\dot{Q}_{tot}(t) = \dot{Q}_b + A_w \dot{Q}''_{max}\, e^{-\lambda(t - \tau_w)} \qquad (82)$$

At time $t = \tau_w + \tau$ an initial pyrolysis area, x_{po}, ignites in the ceiling-wall intersection and the term

$$x_{po} W \dot{Q}''_{max}\, e^{-\lambda t_1} + W \int_0^{t_1} \dot{Q}''_{max} e^{-\lambda(t_1 - t_p)} V_h(t_p) dt_p$$

is added to equation (82). Here, $t_1 = t - (\tau_w + \tau)$, W is the width of the strip in the ceiling-wall intersection (taken to be = 7.5% of the compartment height) and V_h is the horizontal flame spread velocity along the strip. When this flame front has come to a halt, or reached the nearest corner, the downward flame spread is assumed to start. We define the time t_d as the onset of downward flame propagation and the complete equation for heat release rate in Model B is then written as

$$\dot{Q}_{tot}(t) = \dot{Q}_b + A_w \dot{Q}''_{max}\, e^{-\lambda(t - \tau_w)} + x_{po} W \dot{Q}''_{max}\, e^{-\lambda t_1}$$

$$+ W \int_0^{t_1} \dot{Q}''_{max} e^{-\lambda(t_1 - t_p)} V_h(t_p) dt_p + L \int_0^{t_2} \dot{Q}''_{max} e^{-\lambda(t_2 - t_p)} V_d(t_p) dt_p \qquad (83)$$

Here, $t_2 = t - t_d$ and L is the length of the downward burning strips, taken to be equal to the length of three walls in the compartment. V_d is calculated from equation (79) and includes the downward flame spread on materials both above and below the thermal discontinuity.

In Chapter 5 we shall compare the results from using the above methodologies and compare them to experimentally measured values.

5 Results from calculations and experiments

In this chapter we shall summarise five series of room corner experiments, carried out in four different scenarios. These are:

Full scale test, Scenario A, 24 materials tested (2 series of experiments)
1/3 scale test, Scenario A, 13 materials tested
Full scale test, Scenario B, 4 materials tested
1/3 scale test, Scenario B, 11 materials tested

The measured rate of heat release and gas temperatures from these experiments will then be compared with calculations performed using Model A and Model B.

5.1 Full scale tests, Scenario A

5.1.1 Experimental set up

The full scale tests, Scenario A, were carried out according to the standard test method NT FIRE 025 /73/. The fire test room is 3.6 m long, 2.4 m wide and 2.4 m high with a doorway measuring 0.8 m wide and 2.0 m high (see Figure 27). The walls are of lightweight concrete, 150 mm thick, with a thermal inertia $(k\rho c)_{lwc} = 0.15$ [kW^2s/m^4K^2]. The lining materials were fixed to the ceiling and to three walls, excluding the doorway wall.

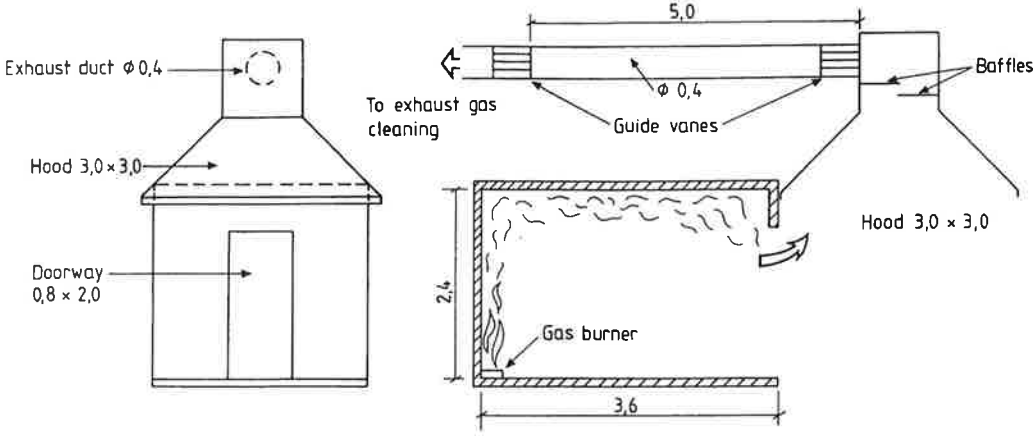

Fig. 27. Front view and section of the full scale room corner test compartment (dimensions in meters).

The ignition source was a propane gas burner situated on the floor, in a corner of the room, with an effect of 100 kW. If this effect did not cause flashover in 10 minutes the effect was raised to 300 kW for another 10 minutes.

The combustion products leaving the room were collected in a hood connected to an exhaust system and the rate of heat release from the fire calculated using the principle of oxygen consumption /13/.

Two series of experiments were carried out for this scenario. Sundström /68/ described the first test series, carried out at the Swedish National Testing Institute in Borås. The 13 different lining materials tested in this series are listed as Materials S1 -S13 in Table I, Chapter 2. The second test series was carried out within the EURIFIC research programme /2/, a cooperative project managed by fire laboratories in Sweden, Norway, Danmark and Finland. 11 different lining materials were tested in this series and are listed as Materials E1 - E11 in Table I, Chapter 2. The experimental test results are available in digital form from a software package named DCS (Data Converting System) developed by Lønvik and Opstad /98/

A detailed description of the two test series are given by Sundström /68/ and Söderblom /99/.

5.1.2 Results

A total of 24 materials have been tested in the bench scale tests described in Chapter 2 and in the full scale room experiments described above. However, Materials E6 and E8 did not ignite in the bench scale LIFT apparatus and the essential material parameters $k\rho c$ and T_{ig} could not be determined. The full scale fire test of these two materials were therefore not simulated.

As a result, 22 of the experiments described above were simulated using Model A. Material properties input data and geometric input data to Model A is:

1) RHR (Rate of Heat Release) as a function of time from the Cone Calorimeter at an incident heat flux of 50 kW/m^2. For the Materials S1 - S13 this data is available from Tsantaridis and Östman /14/. For Materials E1 - E11 the tests are described by Thureson /15/ and the data is available from Lønvik and Opstad /98/. The early part of the Cone Calorimeter data describes conditions before the material ignites; this part of the data is not used in Model A. Ignition is assumed to have occurred when the heat release rate reaches 50 kW/m^2 and the time when this occurs is taken to be t = 0. An example of the data is shown in Figure 28.

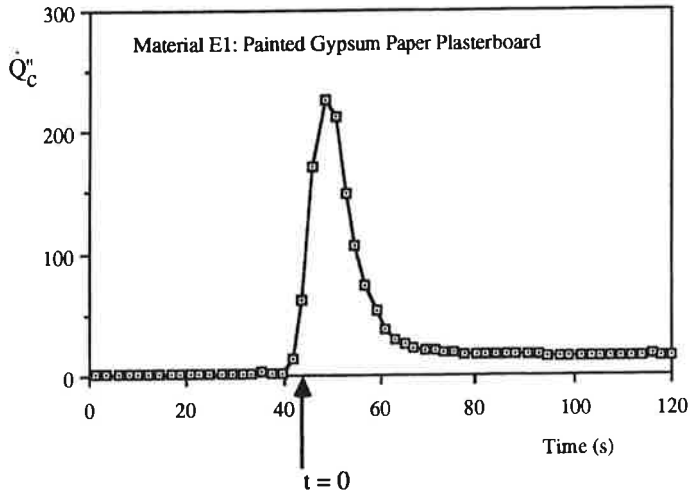

Fig. 28. RHR from the Cone Calorimeter for Material E1 at an incident heat flux of 50 kW/m^2.

2) Material parameters (kpc) and T_{ig} as determined from the bench scale tests in Chapter 2. The data used here is given in Tables V and VI, Chapter 2.

3) Length, breadth, and height of room, area and height of opening, height and width of gas burner, as given above. This data is used in calculations of gas temperatures, view factors, flame extensions and heat release rate.

4) Modeling parameters relevant to the full scale room, i.e. $\dot{q}''_w$ = 45 kW/m^2 and $\dot{q}''_f$ = 35 kW/m^2. These parameters have lower values in the 1/3 scale test room due to, amongst other factors, thinner and less radiative flames.

The above data was used as input to Model A. A summary of the heat release rate calculations is given in Figure 29, where calculated times to flashover are compared with experimental ones.

The complete results for rate of heat release and hot layer gas temperatures for all 22 materials are given in Appendix C. Examples of the heat release results for 4 materials are given in Figure 30. The results show good agreement with the experiments. Two materials, S9 (melamine faced particle board) and E7 (combustible faced mineral wool) show poor results.

Material S9 behaves rather uniquely in the Cone Calorimeter; there is a sharp pulse of heat release at time = 40 seconds (=t_{ig}), but then the material releases no more heat until time $\approx$ 200 seconds, thereafter showing a typical curve for the heat release rate. We have, as input to the model, only used the latter part of the

heat release curve from the Cone Calorimeter; using the whole curve will not cause flashover until after ≈ 800 seconds.

The experimental results for Material E7 show very rapid flame spread and heat release in excess of 1.5 MW early on in the test and therefore an early flashover. The flame subsequently retreats and there is no "second" flashover when the burner output is increased to 300 kW. The model, however, fails to predict the extremely fast flame spread in the beginning of the test. This is because the material releases heat in the Cone Calorimeter for a very short duration, only 20 seconds, and because burn-out is ignored in the model.

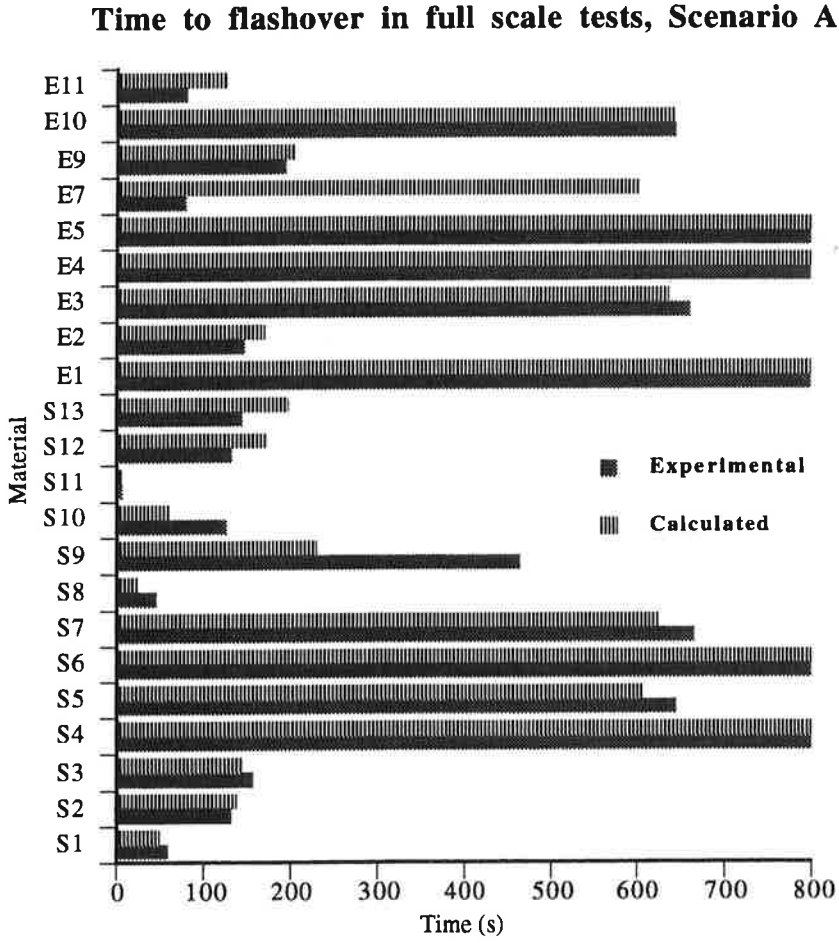

Fig 29. Calculated and experimental time to flashover for the full scale tests, Scenario A (no flashover past 800 seconds).

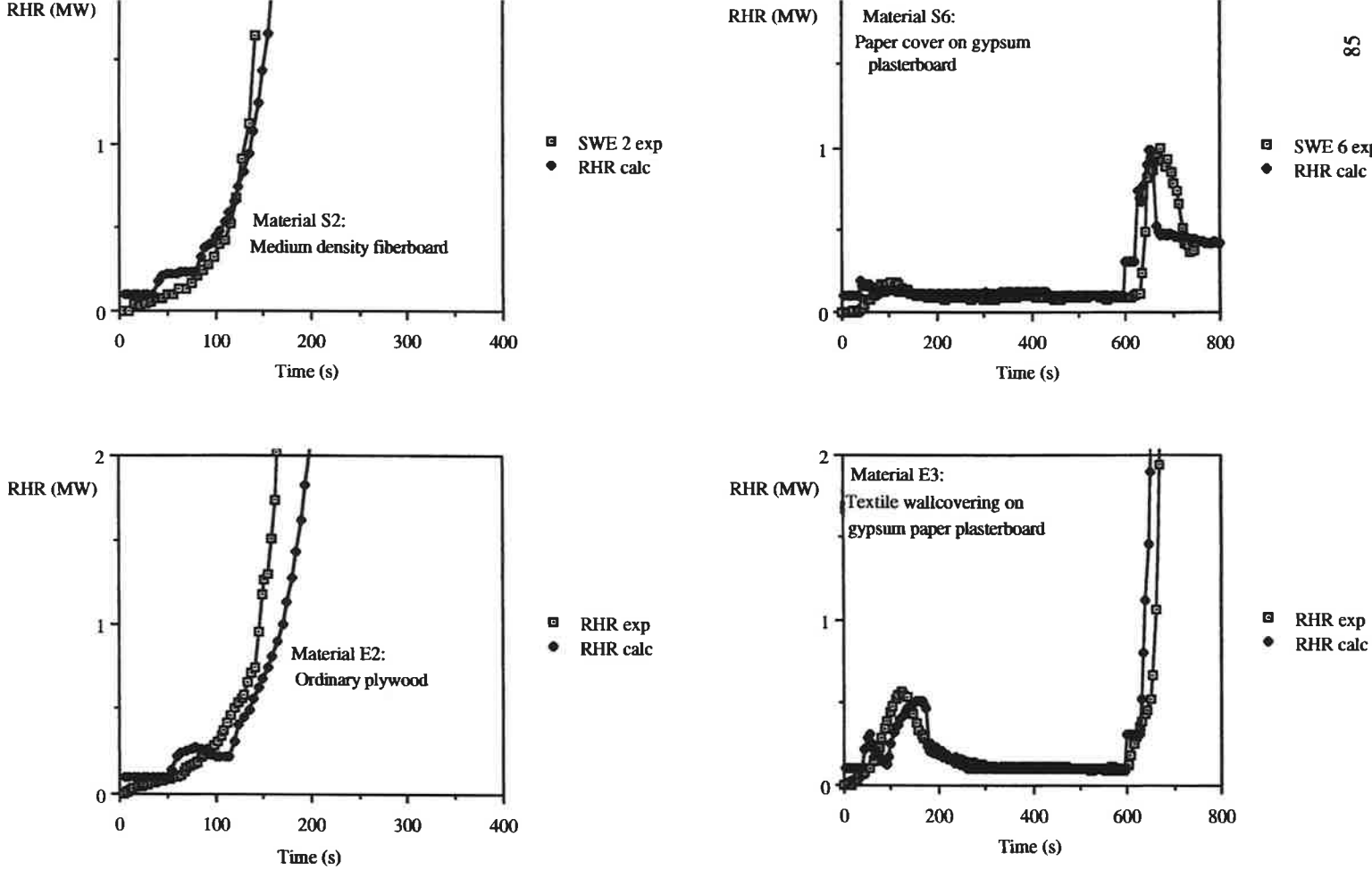

Fig. 30. Comparison of experimental and calculated heat release rates for materials S2, S6, E2 and E3.

5.2 1/3 scale tests, Scenario A

5.2.1 Experimental set up

The experiments were carried out in a room with a length of 1.2 m, width of 0.8m and height of 0.8 m. A description of the test procedure and results is given by Andersson /100/. The room is a 1/3 scale model of the full scale compartment described in section 5.1.1. Scaling criteria were to achieve the same upper layer gas temperature in full- and 1/3 scale. The ignition source was a gas burner with an effect of 11 kW for 10 minutes and, if no flashover occurred, 33 kW for another 10 minutes.

For Scenario A, where lining material was mounted on both ceiling and walls, the doorway measured 0.56 m wide and 0.67 m high. The experimental set up is shown in Figure 31.

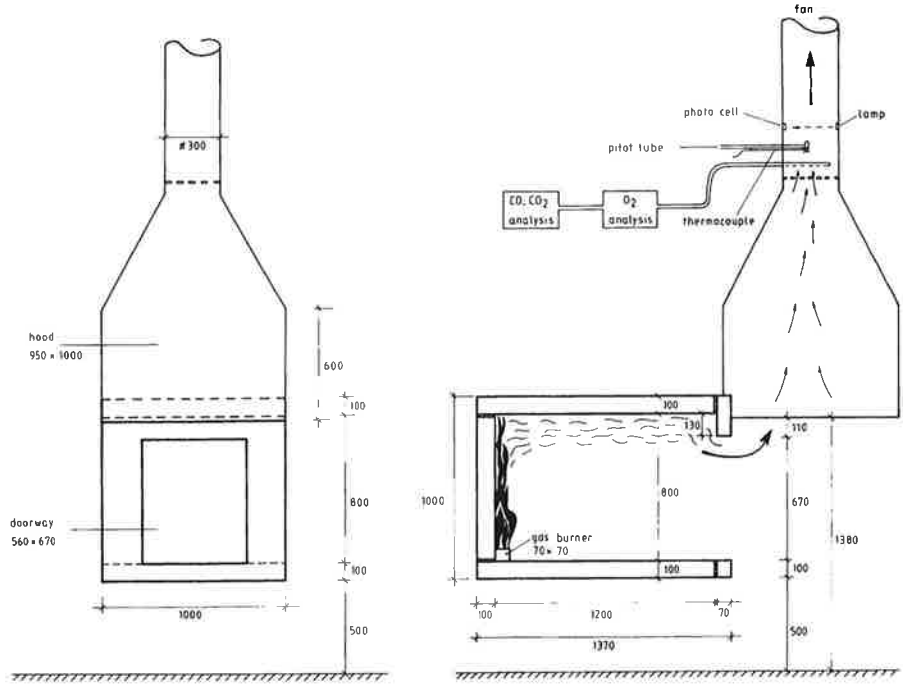

Fig. 31. Configuration of 1/3 scale room test (dimensions in mm).

5.2.2 Results

All of the "Swedish" materials were tested in the 1/3 scale room experiments described above. The materials are listed as S1 - S13 in Table I.

Material properties input data and geometric input data to Model A are:

1) The same rate of heat release data from the Cone Calorimeter as were described in section 5.1.2.

2) The same material parameters (kρc) and T_{ig} as described in section 5.1.2. The data is given in Table V, Chapter 2.

3) Length, breadth, and height of room, area and height of opening, height and width of gas burner, as given above (see Figure 31).

4) Modeling parameters relevant to the 1/3 scale room, i.e. $\dot{q}''_w = 25$ kW/m^2 and $\dot{q}''_f = 25$ kW/m^2. These parameters have lower values in the 1/3 scale test room than in the full scale test due to, amongst other factors, thinner and less radiative flames.

The above data was used as input to Model A; a summary of the heat release rate calculations is given in Figure 32, where calculated times to flashover are compared with experimental ones.

The complete results for rate of heat release and hot layer gas temperatures for all 13 materials are given in Appendix D. Examples of the heat release results for 2 materials are given in Figure 33.

The results are reasonable, but not as good as for the full scale tests. Again, Material S9 (Melamine faced particle board) shows a much earlier time to flashover then in the experiments, for the same reasons as enumerated in section 5.1.2. Material S10 (expanded polystyrene) does not go to flashover in the 1/3 scale test which is rather surprising, since it goes to flashover rather rapidly in the full scale test. This is no doubt due to the lower heat fluxes experienced in the 1/3 scale test; at low fluxes this material tends to melt; at higher fluxes it spreads flame rapidly and releases considerable energy. The model predicts relatively rapid flashover, since melting of materials is not accounted for.

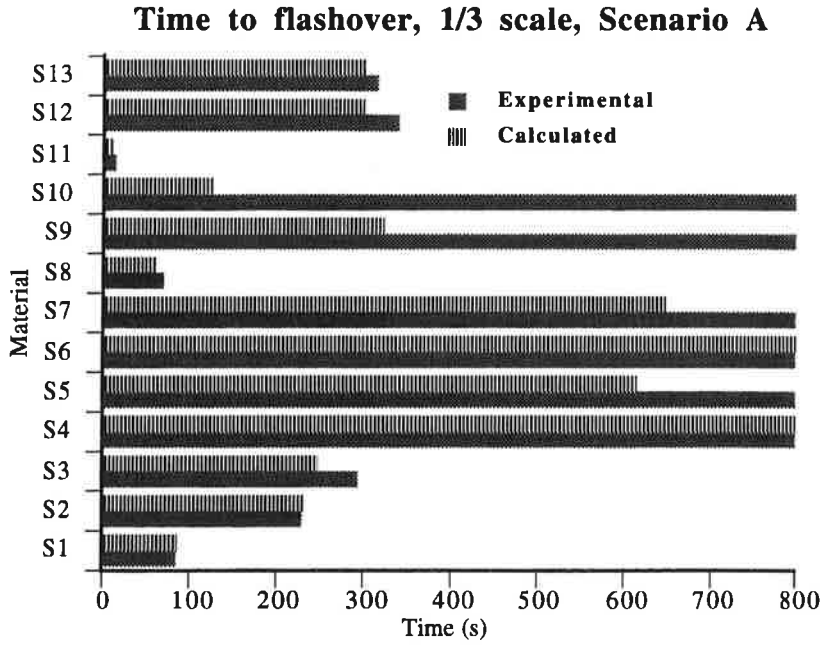

Fig. 32. Calculated and experimental time to flashover for the 1/3 scale tests, Scenario A (no flashover past 800 seconds).

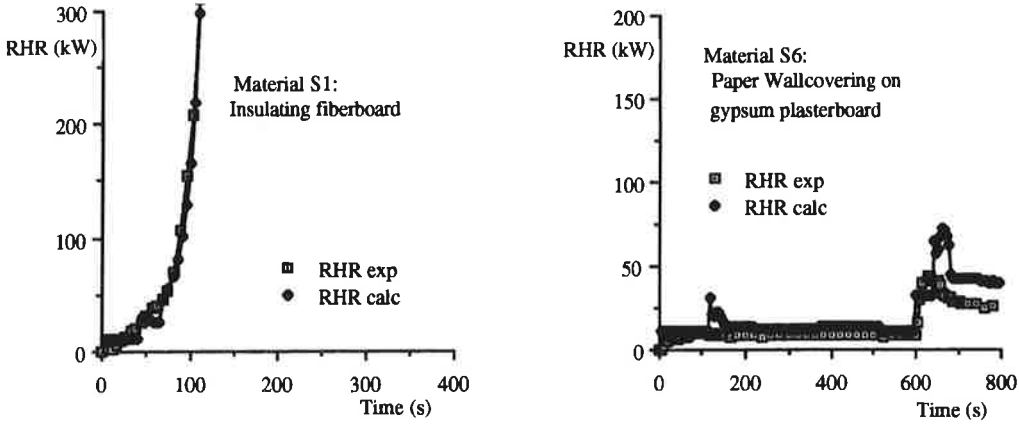

Fig. 33. Comparison of calculated and measured heat release rates for Materials S1 and S6

Also, Materials S5 and S7 are predicted to go to flashover after the energy release from the ignition source is increased to 33 kW; this is not the case in the experiments. Both materials have some potential to spread flame in the concurrent flow mode as seen in Figure 14, Chapter 3 (they are both close to "Line A" in Fig. 14). Further, the modeling of this phenomenon (increasing the ignition source substantially in one step, causing flame spread over material which has been pre-heated by the gas layer over a long period) is to a considerable degree dependent on the heating history of the ceiling surface material. The predicted hot layer gas temperatures in both these tests are quite a bit higher than the measured ones for the entire duration of the test, resulting in high surface temperatures and rapid concurrent flow flame spread.

5.3 Full scale tests, Scenario B

5.3.1 Experimental set up

Scenario B refers to the case where the lining materials are fixed only to three walls of the compartment, excluding the doorway wall. The full scale tests were carried out in the standard room corner test compartment described in section 5.1 (see Figure 27), with the same gas burner configuration and an initial burner heat output of 100 kW. If this effect did not cause flashover in 5 minutes the effect was raised to 300 kW. Only 4 materials were tested in this test series and 3 of them went to flashover within 5 minutes. These materials are listed in Table I, Chapter 2, as Materials S2, S3, S6 and S8. The test series is described by Ondrus /101/ and Karlsson /85/.

5.3.2 Results

The fundamental difference between Model A and Model B, with respect to input data, is that the latter does not use the heat release rate results from the Cone Calorimeter directly, but needs a mathematical representation of these results. Model B utilises analytical solutions of the concurrent flow flame spread equations, thereby making such a representation necessary. Also, one more material parameter from the bench scale test methods is needed, i.e. the opposed flow flame spread parameter, Φ.

Material properties input data and geometric input data to Model B are:

1) RHR (Rate of Heat Release) as a function of time from the Cone Calorimeter at an incident heat flux of 50 kW/m^2. This data is then represented mathematically according to the procedures described in Chapter 2 (see Figures 2 and 3 in Chapter 2). The two RHR parameters needed are thus $\dot{Q}''_{max}$ and λ and these are listed in Table II, Chapter 2.

2) Material parameters ($k\rho c$), T_{ig} and Φ as determined from the bench scale tests in Chapter 2. The data used is given in Table V, Chapter 2.

3) Length, breadth, and height of room, area and height of opening, height and width of gas burner (see Figure 27).

4) Modeling parameters relevant to the full scale room, i.e. $\dot{q}''_w$ = 45 kW/m^2 and $\dot{q}''_f$ = 35 kW/m^2.

5) When using the above data in the model it became apparent that the heating up of surfaces in the room was far too slow, causing slow flame spread and long times to flashover. When discussing hot gas temperatures in Chapter 4, we found that the pre-exponential coefficient for calculating gas temperatures was around 3.0 for all the test series, except for the scenario discussed here, where it was found to be just above 4.0. The value of 4.0 was therefore used here, whereas the value 3.0 was used for all the other series. Additionally, the total heat transfer coefficient, governing the surface temperatures of the materials immersed in the hot gas layer, had to be increased to the rather high value of 50 W/m^{2}K, whereas it was fixed at 25 W/m^{2}K for all the other test series. This test series is thus "the odd one out" and the materials here seem to need more heating than the ones in the other test series.

Calculated and experimental times to flasover are shown in Figure 34. No general conclusion can be drawn as to the validity of the model since only 4 materials were tested. The complete results for rate of heat release and hot layer gas temperatures for all 4 materials are given in Appendix E.

In Model B no account is taken of the increased burner output to 300 kW, after 5 minutes, since analytical solutions are used for concurrent flow flame spread; numerical solutions are needed to describe this phenomenon. The only material affected by this is Material S6 (paper wallcovering on gypsum plaster board) and the predicted values are therefore only shown for the first 5 minutes of the test.

The results for Material S2 (medium density fiberboard) are shown in Figure 35.

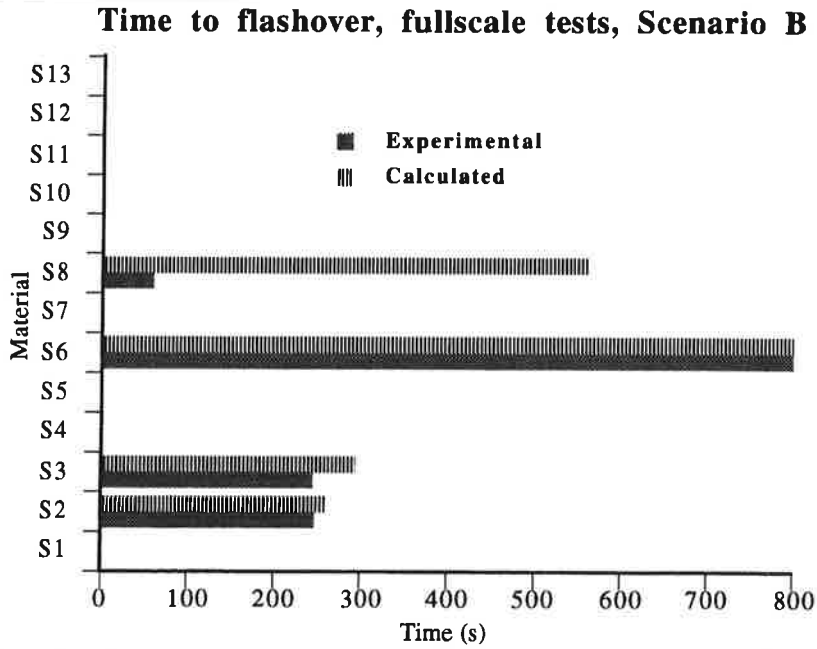

Fig. 34. Calculated and experimental time to flashover for the full scale tests, Scenario B

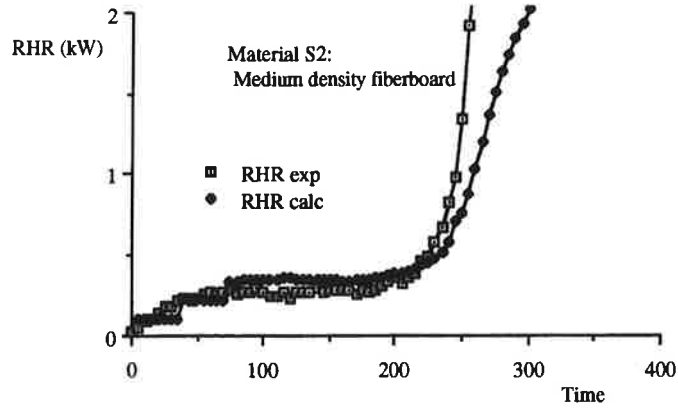

Fig. 35. Comparison of calculated and measured heat release rates for Material S2.

The results for Material S8 (textile wallcovering on mineral wool) are somewhat curious (see Appendix E). The experimental data shows a rapid flashover but in the predictions the wall surface temperatures are too low to allow downward flame spread early on in the test. This results in low heat output which in turn

results in too low surface temperatures and so on. The material is, however, very close to going to flashover in the model. Decreasing the value of kρc by 20% results in rapid flashover. The same effect could be achieved by slightly altering parameters governing heat flux to walls, the heat transfer coefficient in the upper layer or the cooling coefficient for the lower walls. Such a calibration procedure must be based on more experimental data.

5.4 1/3 scale tests, Scenario B

5.4.1 Experimental set up

Again, Scenario B refers to the case where the lining materials are fixed only to three walls of the compartment, excluding the doorway wall. The 1/3 scale tests were carried out in the test compartment described in section 5.2 (see Figure 31), with the exception that the the door opening width measured 0.46 m (as opposed to 0.56 m in the 1/3 scale test series for Scenario A). The same burner configuration was used with a burner heat output of 11 kW. 10 materials were tested in this scenario; they are listed in Table I, Chapter 2, as Materials S1, S2, S3, S5, S7, S8, S9, S11, S12 and S13. A description of the test procedure and results is given by Andersson /100/.

5.4.2 Results

Material properties input data and geometric input data to Model B are:

1) The two RHR parameters described in section 5.3.2. above, i.e. $\dot{Q}''_{max}$ and λ. These are listed in Table II, Chapter 2.

2) The same material parameters, kρc, T_{ig} and Φ as described in section 5.3.2. The data is given in Table V, Chapter 2.

3) Length, breadth, and height of room, area and height of opening, height and width of gas burner (see Figure 31, except that width of opening is 0.46m).

4) Modeling parameters relevant to the 1/3 scale room, i.e. $\dot{q}''_w = 25$ kW/m^2 and $\dot{q}''_f = 25$ kW/m^2.

A summary of the heat release rate calculations is given in Figure 36, where calculated times to flashover are compared with experimental ones. The complete results for rate of heat release and hot layer gas temperatures for all 10

materials are given in Appendix F. The gas burner output was increased to 33 kW after 10 minutes for only three Materials; S5, S7 and S9 and the predicted values are therefore only shown for the first 10 minutes. Figure 37 shows examples of the results for Materials S3 and S12.

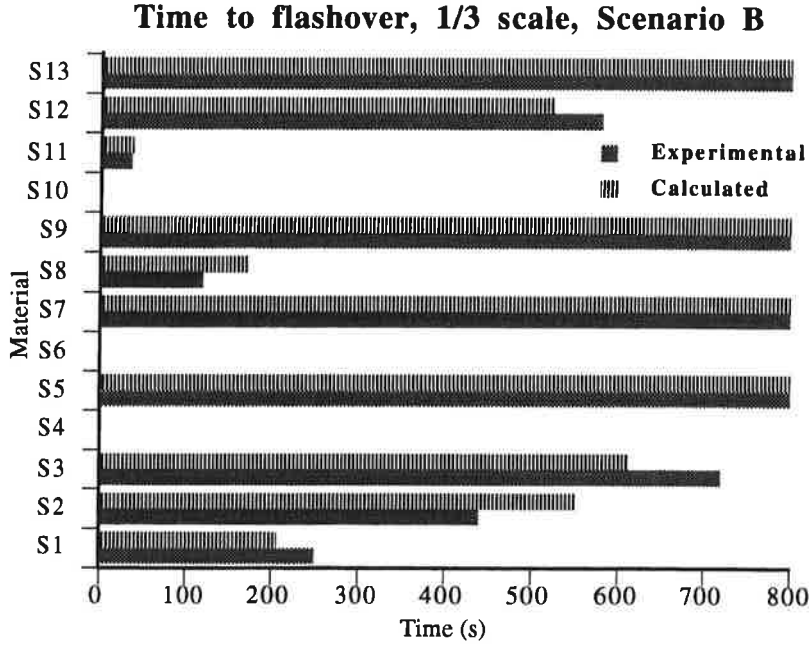

Fig. 36. Calculated and experimental time to flashover for the 1/3 scale tests, Scenario B.

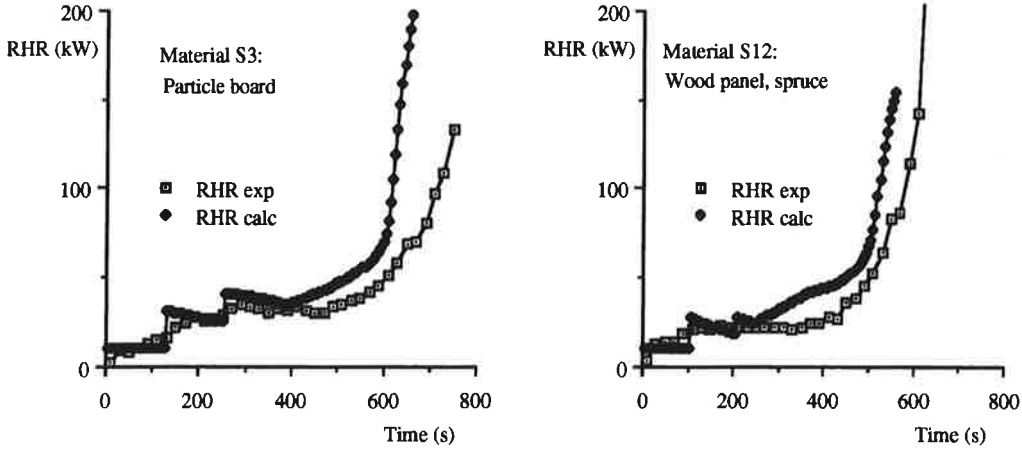

Fig. 37. Comparison of calculated and measured heat release rates for Materials S3 and S12.

5.5 Discussion

We have only compared the results from two of the sub-models here, i.e. calculations of heat release rate and calculations of gastemperatures. The results from the sub-models for calculating surface temperatures, heat fluxes and downward flame spread velocities, have, in earlier studies (/85/, /102/), been compared to experimental results. Summarising those results, it can be said that there is a fair agreement between calculated and experimental surface temperatures, heat fluxes and downward flame spread velocities, given that the calculated heat release rate (used as input to the sub-models) compares well with experiments.

It should be noted that the four experimental series discussed above were carried out over a period of five years at two different locations and are therefore not very coherent. Different types of thermocouples and other measuring equipment were used. Also, some of the parameters derived from bench scale data, used as input to the models, were arrived at by non-standardized means.

Furthermore, the models themselves must be seen as rather crude, engineering attempts to model a physically very complex reality. However, the results indicate that the basic structure of the models may seem acceptable for arriving at approximate times to flashover in the four scenarios treated.

These issues will be discussed further in Chapter 7.

6 Replacing models with power law correlations

6.1. General

Mitler /103/ has listed several reasons for developing mathematical fire models and ways in which these can be useful for classification, design and research purposes. He mentions that expensive full-scale testing can in some cases be avoided, flammability of materials (in certain configurations) can be established and research needs can be identified.

Karlsson and Magnusson /91/, /104/ have utilized the models presented in previous chapters to address some of the above issues. They outlined a methodology where a certain limit state could be expressed as an analytical function of design parameters.

The most natural choice of a limit state in this instance is time to flashover, which is a good measure of hazard in the room corner test. Similarly, the natural choice of design parameters are the results from bench-scale tests, which are also input to the mathematical models. Further, in order to construct such analytical expressions, the results from the bench-scale tests must be expressed as constant value parameters and cannot be a function of time. This means that the results from the Cone Calorimeter must be replaced by a mathematical expression. Karlsson and Magnusson /91/ used the parameters $\dot{Q}''_{max}$ and λ to represent the time-dependent results from the Cone Calorimeter, as has been done earlier in this work.

Consequently, they proposed the following response surface expression for time to flashover

$$t_{fo} = a_0 \, (\dot{Q}''_{max})^{b_1} \, (\lambda)^{b_2} \, (k\rho c)^{b_3} \, (T_{ig})^{b_4} \, (\Phi)^{b_5} \qquad (84)$$

where the constant a_0 and the exponents $b_1 ... b_5$ were to be determined by linear regression analysis, using computer programs to calculate several hundreds of values of t_{fo} as a function of a wide range of fictitious bench-scale test results.

Replacing the rather complex models described earlier with a single analytical expression for time to flashover of the above form, has several advantages. The points which are of particular interest here are:

a) relevant flammability parameters measured in the bench-scale tests can be identified and ranked according to their importance.

b) the influence of uncertainty and variability in bench-scale test results on the overall reliability of the calculation procedures can be estimated.

We shall, in the following sections, give two examples of how such equations can be constructed, one for the full scale test, Scenario A and another for the 1/3 scale test, Scenario B. This work must be seen to be of a preliminary nature since no sensitivity testing has been carried out for various modeling parameters.

6.2 Scenario A

In order to construct a regression equation of the above type we must represent the results from the Cone Calorimeter mathematically. Several such representations have been suggested (Mowrer et al. /21/, Baroudi et al. /44/) but we shall use the representation discussed earlier, i.e. $\dot{Q}''_C(t) = \dot{Q}''_{max}\, e^{-\lambda t}$.

We shall therefore not use heat release data directly from the Cone Calorimeter but will use as input to Model A a range of $\dot{Q}''_{max}$ and λ values to represent a large number of fictitious heat release curves. Additional input parameters are the apparent $k\rho c$ and the ignition temperature, T_{ig}.

The model was run with 600 combinations of input parameters and the resulting regression equation was

$$t_{fo} = 0.326\, (\dot{Q}''_{max})^{-1.14}\, (\lambda)^{0.085}\, (k\rho c)^{1.07}\, (T_{ig})^{2.19} \qquad (85)$$

with a coefficient of determination, $R^2 = 99.0\%$. The units of the parameters are the same as in Tables II and V. Figure 38 shows the calculated times to flashover from equation (85) and from the model.

The rather high exponential for ignition temperature is not to be seen as a measure of the importance of T_{ig} but rather expresses the importance of time to ignition, which can be said to be a function of $(k\rho c\, T_{ig}^2)$ for a certain constant irradiant heat flux. Omitting T_{ig} from the regression gives a coefficient of determination $R^2 = 93.7\%$. Omitting λ and $\dot{Q}''_{max}$ give R^2 as 97.5% and 82.2% respectively. However, if $k\rho c$ is omitted the regression breaks down and the coefficient of determination is $R^2 = 18.5\%$.

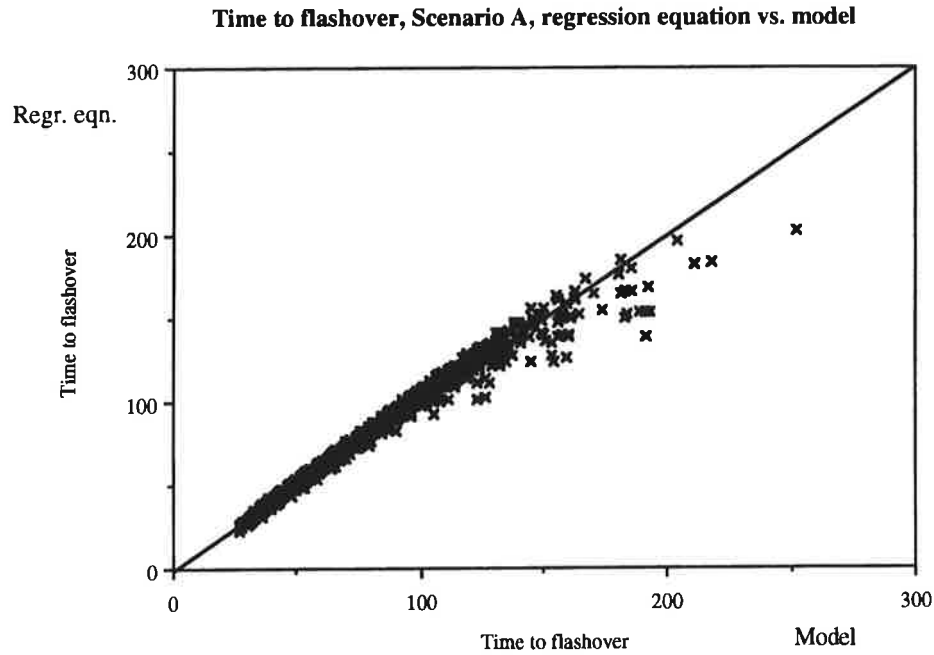

Fig. 38. Time to flashover in Scenario A, calculated by equation (85) and by the model.

The range of input parameters used were:

$\dot{Q}''_{max}$	=	150 - 300	kW/m^2
λ	=	0.002 - 0.012	1/s
T_{ig}	=	380 - 440	°C
$k\rho c$	=	0.1 - 0.6	$kW^2s/m^4 K^2$

The values of the coefficients of determination mentioned above change somewhat when the range of input parameters is increased. Using over 5000 calculated times to flashover, with a considerably increased range of input parameters, lowers this coefficient to ≈ 90%. This is partly because equation (85) is only valid for materials which do go to flashover and some of the input parameter combinations will not cause flashover. The exponents in equation (85) however, remain roughly the same.

The equation can therefore be said to be valid only for material parameter combinations which fall under "Line A" in Figure 14, i.e. materials which will cause exponentially accelerating flame spread. Before applying equation (85) a check should thus be made on whether $\lambda\tau < (1 - \sqrt{a})^2$, where $a = K \dot{Q}''_{max}$ and τ is calculated from equation (75) in Chapter 4.

6.3 Scenario B

We shall use Model B when applied to the 1/3 scale room test as a basis for our calculations. The model is described in Chapter 4 and in this case the results from the Cone Calorimeter are modelled mathematically using $\dot{Q}''_{max}$ and λ. Other input parameters are $k\rho c$, T_{ig} and Φ. Since the range of ignition temperatures for the materials which do go to flashover in this Scenario is somewhat small and the values relatively uncertain in relation to their range, we shall omit T_{ig} in the regression equation. The resulting equation is then

$$t_{fo} = 8.2*10^4 \, (\dot{Q}''_{max})^{-0.52} \, (\lambda)^{0.11} \, (k\rho c)^{0.75} \, (\Phi)^{-0.37} \qquad (86)$$

with the coefficient of determination $R^2 = 96.0\%$. Figure 39 shows the calculated times to flashover from equation (86) and from the model.

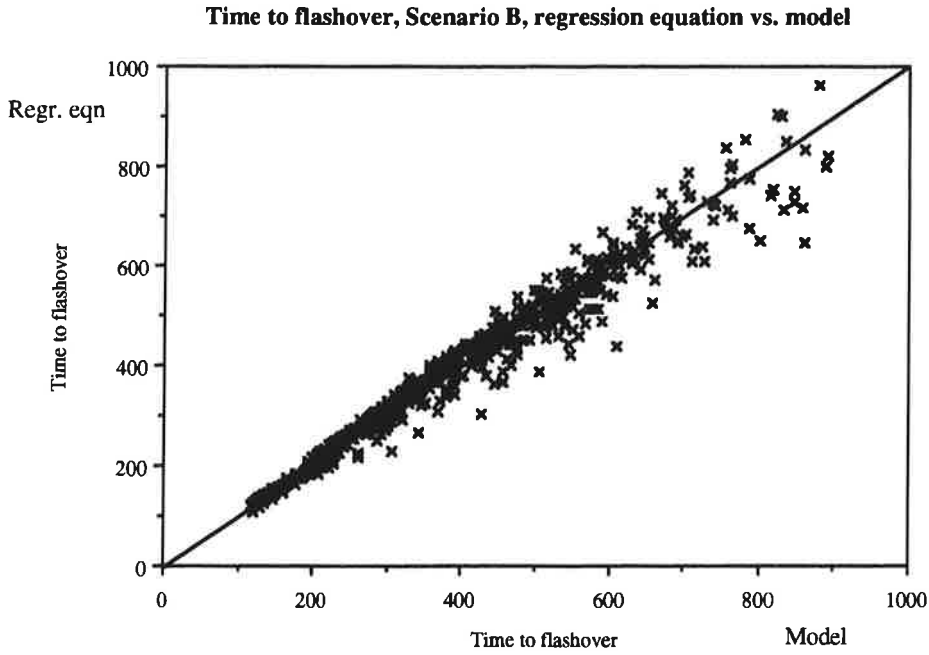

Fig. 39. Time to flashover in Scenario B, calculated by equation (86) and by the model.

The main difference between time to flashover in Scenario A and Scenario B is that in the former this time is typically in the range 100 - 300 seconds while in the latter it is typically 300 - 900 seconds. Also, in the regression equation for Scenario A, we omitted the opposed flow flame spread parameter, Φ, since

opposed flow flame spread does not seem to have significant influence on time to flashover in that scenario. However, in Scenario B, this mode of flame spread is obviously important. Omitting the parameter Φ from the regression equation for this scenario gives a coefficient of determination $R^2 = 79.0\%$.

In other words, excluding Φ in Scenario B leads to a marked increase in variability of uncertainty (assuming that the selection of material parameters corresponds to the distribution these parameters have in real life). The final influence of the increased variability on predictive capacity can be assessed only in the context of a proper and general reliability study of the calculation models and the bench-scale test results.

6.4. Discussion

Earlier work of the above nature includes the work of Karlsson and Magnusson /91/, /104/, Thomas and Karlsson /24/ and Kokkala et al. /22/. Thomas and Karlsson /24/ discussed Model B and set up groups of dimensionless variables governing ignition, gas temperature rise, surface temperature rise, flame spread and heat generation. Simplifying these groups of dimensionless variables and assuming geometrical factors to be constants, they expressed time to flashover in a similar expression to equation (84).

The derivation procedure of the heat release rate parameters $\dot{Q}''_{max}$ and λ is rather ambiguous and a direct use of $\dot{Q}''_C(t)$ from the Cone Calorimeter would clearly be preferable. Thomas, in /24/, pointed out that in equation (86) the combination of $\dot{Q}''_{max}$ and λ is

$$t_{fo} \sim \left[\frac{\dot{Q}''_{max}}{\lambda^{0.21}} \right]^{-0.52} \tag{87}$$

Since the integral

$$\int_0^\infty t^b e^{-\lambda t} dt = \frac{\Gamma(b+1)}{\lambda^{b+1}} \tag{88}$$

where Γ denotes the gamma-function, he observed that the bracketed term in equation (87) is obtained by integrating a time-weighted heat release rate

$$\int_0^{\infty} \frac{\dot{Q}''_{max}\, e^{-\lambda t}}{t^{0.79}}\, dt \qquad (89)$$

This strongly suggests (Kokkala et al. /22/) that instead of using the parameters $\dot{Q}''_{max}$ and λ, the heat release rate from the Cone Calorimeter could be represented as a time-weighted integral of the results from the Cone Calorimeter, I_Q, written as

$$I_Q = \int_0^{\infty} \frac{\dot{Q}''_C(t)}{t^{0.79}}\, dt \qquad (90)$$

with $\dot{Q}''_C(t)$ directly taken from the Cone Calorimeter.

Kokkala, in /22/, further suggested that the parameters kρc and T_{ig} could possibly be replaced by an ignition time measured in the Cone Calorimeter under a certain irradiant heat flux. Time to flashover in Scenario A could thus be calculated as a function of two indices, a rate of heat release index, I_Q, and an ignitability index, t_{ig}. For Scenario B a third parameter, Φ, will probably have to be included.

Work along these lines is now continuing as well as efforts, in a wider context, to implement these results in a classification procedure with regard taken to uncertainty, reliability and economy.

Finally, one must keep in mind that the models which are the bases of the regression equations consist of sub-models which are in some cases crude and need to be improved. Even though Model A has been assessed favourably against 22 full scale experiments, there is considerable room for improvement. Model B has only been assessed against 10 experiments in the 1/3 scale room and the resulting regression equation must be seen as being preliminary.

7 Summary and conclusions

This work has discussed bench-scale test methods and how results from these can be used to predict flame spread on combustible wall and ceiling lining materials. Two mathematical models have been described, where Model A treats the case where lining materials are attached to walls and ceiling and Model B, where lining materials are mounted on the walls only.

The results from the models have been compared with experiments carried out in a full scale room corner test compartment and a 1/3 scale of the same compartment. Model A has been tested against 22 different lining materials in the full scale room and 13 materials in the 1/3 scale room. Model B has only been tested against 4 materials in the full scale room and 10 materials in the 1/3 scale room. The models, in their present form, can only be said to have been validated for cases where the ignition source is on the floor in the corner of a room and has a relatively high energy output.

In this chapter we shall comment upon the applicability of the bench-scale test results for modeling purposes, discuss the analytical solutions of the concurrent flame spread equations, review some of the assumptions behind Models A and B and point out improvements to be made in future work.

7.1 Bench-scale tests

We have used data from three bench-scale test methods; the Cone Calorimeter; the LIFT apparatus and the ISO ignitability test. Results from the last mentioned test was only used here to complement some missing data from the LIFT apparatus tests. As a consequence, results from only two bench-scale tests are needed as input data to mathematical models of the type presented here. Future developments may require a third test method to take account of the radiant emission from the material's own flames.

Depending on the scenario under consideration and on the model accuracy required, this can even be narrowed down to one test only: the Cone Calorimeter. This will limit the accuracy and applicability of the model and requires the following to be considered:

a) that downward or lateral, opposed flow flame spread does not influence time to flashover significantly, which seems to be the case in Scenario A for the materials examined here.

b) that the apparent material properties ($\dot{q}''_{o,ig}$, $k\rho c$ and T_{ig}), traditionally derived from the LIFT apparatus, can be derived using the Cone Calorimeter. This, however, requires ignition measurements to be carried out at many different heat flux levels, especially at levels close to $\dot{q}''_{o,ig}$. Janssens /31/ has done this for several materials using the Cone Calorimeter in the vertical orientation.

c) if the effects of the enclosure can be ignored, for example by ignoring the pre-heating by the hot gas layer, then time to ignition in the Cone Calorimeter at a certain irradiant heat flux can possibly replace the above apparent material properties. This was done for the simple, analytical model discussed in Chapter 3.5 where time to ignition in the full scale test, τ, seemed to correlate reasonably well with t_{ig} in the Cone Calorimeter at an irradiant flux of 50 kW/m^2. The advantage is that the Cone Calorimeter test only needs to be carried out at one, specified irradiant heat flux level. The disadvantage is that the model becomes very scenario-dependant and no account can be taken of the room fire environment. Also, no physically sound procedure can be used in order to take account of increased burner output to 300 kW after 10 minutes, as was the case for the 22 materials tested in the full scale room, Scenario A.

It should be noted that the methodology of replacing the LIFT apparatus with the Cone Calorimeter in order to derive ignitability parameters ($k\rho c$ and T_{ig}) has not been standardised. Extensive calibration studies need therefore to be undertaken to harmonize results from both apparatuses, before the results are used in modeling.

If one is considering Scenario B, or some other scenario where downward or lateral, opposed flow flame spread does influence time to flashover significantly, the flame heating parameter, Φ, and the minimum surface temperature for spread, $T_{s,min}$, will have to be included as input parameters for the mathematical models. This means that the LIFT apparatus must be used and the ignitability parameters $k\rho c$ and T_{ig} can be obtained in the traditional, standardised manner.

Therefore, both the Cone Calorimeter and the LIFT apparatus should be used in any serious experimental work, where modeling of fire growth on combustible wall lining materials is to be attempted.

Alternatively, attempts could be made to mathematically model the flame spread part of the LIFT apparatus procedure, using Cone Calorimeter results as input. However, to date, no sound theoretical bases for such work has been presented.

We have shown in this work that using the material parameters measured in these bench-scale tests to mathematically model fire growth on lining materials in full scale tests was quite successful. It can be concluded that these material parameters do indeed reflect the basic material properties pertaining to ignition, heat release rate and flame spread. In other words, the physical processes of ignition, heat release rate and flame spread in reasonably well defined full scale scenarios, can me modelled using the derived material properties as input data.

7.2 Concurrent flow flame spread and flame extensions

In Chapter 3 we mainly examined concurrent flow flame spread under ceilings and in wall-ceiling intersections as well as flame extensions associated with these processes. The analytical solutions to the flame spread equations were derived and the behaviour of these solutions analysed.

The equations were set up in terms of the flame length coefficient, K, ignition time, τ, and time dependent heat release rate, using the parameters $\dot{Q}''_{max}$ and λ. The limits of propagation and non-propagation given in Figure 14 are valid for many configurations, provided that the assumptions listed in Chapter 3 can be justified.

Figure 14 can then be said to be valid for flame spread under a ceiling, up a straight wall, up the corner of two perpendicular walls and in a wall-ceiling intersection. The value of the flame length coefficient, K, will be different in each configuration. So will the time to ignition, τ, since the (assumed) constant heat flux from the flame, $\dot{q}''_f$, will depend upon the configuration. In other words, if K is known for the configuration Figure 14 can be used to assess whether a material with certain material properties ($k\rho c$, T_{ig}, $\dot{Q}''_{max}$ and λ) will cause exponential flame spread or not.

Observe, though, that burn-out has only been partially treated, i.e. burn-out is achieved for a certain part of the pyrolysing material when the heat release rate there approaches zero. This is assumed to have no influence on the base of the flame, which is at all times considered to be at $x = 0$.

This treatment of burn-out can be justified for the scenarios and most of the materials we have considered in this work (see section 3.3.2) but must be examined critically for other scenarios. For example, in the case of flame spread up a wall where the burner output is very low, the flame may become discontinuous (one flame from the burner, another, higher up, from the burning material) and burn-out will very significantly influence flame height and spread rates.

Flame extensions in wall-ceiling intersections were expressed as a function of the height from the burner to the ceiling, the characteristic dimension of the burner and heat release rate. Further, the dependence on heat release rate was assumed to be linear. Thomas /70/ has found some justification for linearisation. However, some curvature can be seen in Figure 20, Chapter 3, for small values of $\dot{Q}^*$ (where $\dot{Q}^*$ is defined by equation (39)). If a range of low values of $\dot{Q}^*$ is to be considered, the slope in Figure 20 can be increased, but care must be taken in not applying the increased slope for higher values of Q^*.

Due to the lack of both experimental data and previous theoretical work on flame areas in a corner under a ceiling, some simple engineering assumptions had to be made. The flame area coefficient quoted in this work must therefore be considered preliminary, but the value used is consistent with the few observations available and with the values used by other workers.

Chapter 3 is concluded by presenting a simple, analytical model for flame spread under ceilings. No account is taken of enclosure fire environment and input to the model is simply heat release rate and time to ignition from the Cone Calorimeter at one specified incident heat flux. The model compares favourably with 11 out of 12 experiments carried out in the full scale room test. This rather simple model is only presented to exemplify the usefulness of analytical solutions of the flame spread velocity equations. Due to its simplicity, it can take no account of the increased burner output to 300 kW after 10 minutes, as opposed to Model A, presented in Chapter 4.

7.3 Models for room fire growth on combustible linings

Fires in enclosures, where surface lining materials are the main source of combustibles, can occur under a wide range of circumstances with respect to the geometry of the enclosure , the geometry of the lining materials and the strength, type and position of the ignition source. We have, in this work, concentrated on a small room scenario where the ignition source is placed in a corner of the room and has a relatively high energy output.

Two calculation models were presented in Chapter 4: Model A, where the lining material is mounted on three walls and the ceiling; and Model B, where the lining material is mounted on three walls only. The simulation procedure included ignition by the gas burner, calculation of hot gas temperatures, surface temperatures, concurrent flow flame spread and, in Model B, downward flame spread.

The ignition of the wall area behind the burner is simulated in a very crude way in both models. This material is simply assumed to ignite simultaneously over the whole height of the wall after a certain calculated ignition time. There exist a considerable amount of experimental and theoretical work with regard to flame heights in a corner, heat fluxes and mass flows in a corner plume. More accurate modeling of ignition and subsequent flame spread up the corner should thus be reasonably straightforward.

The approach used in Models A and B must therefore be seen as being unnecessarily crude and will be improved in later versions of the models. However, in the scenarios considered here, the initial burner flame nearly reaches the ceiling and, for our purposes, the errors induced by this simple assumption are not considered to be grave.

The energy release rate from the burner and the material behind the burner is then treated as an ignition source for the ceiling and the wall-ceiling intersection. The presence of a pyrolysis front on the material behind the burner is thus ignored. This secondary ignition of the ceiling material becomes unnecessary once the flame spread on the material behind the burner is treated in a more sound manner.

Hot layer gas temperatures are calculated using a well known regression equation with a modified pre-exponential coefficient to account for restricted entrainment into the corner plume. This approach seems to give results which compare quite well with experiments. An alternative would be to use classical zone-modeling techniques with plume equations valid for corner flames. Such an approach would also allow the descent of the hot layer to be calculated.

Presently, the layer is assumed to be stabilised at the height of the door opening from the start of the calculations. This assumption is justified by the fact that the smoke layer stabilises relatively early in the tests and its temperature is not very high in the early stages. Using a zone-modeling technique is, however, clearly preferable.

Wall and ceiling surface temperatures are calculated using classical heat transfer. The total heat transfer coefficient is assumed to be constant for the case where the surface is immersed in the hot gas layer. Similarly, the Newtonian cooling coefficient is assumed to be constant when the surface is heated up by radiation from the gas layer and the burning walls. The calculation procedures should be improved by assuming these coefficients to be a linear function of surface temperatures, as is often done in conventional zone-models.

Downward flame spread in Model B is calculated using a well known expression where the velocity is a function of Φ, $k\rho c$, and the surface temperature at the flame front. The initiation of downward flame spread is modelled rather crudely and should be improved by using the material parameter $T_{s,min}$, the minimum surface temperature for downward flame spread.

In Model B, the concurrent flow flame spread equations are solved analytically. In Model A, however, these equations are solved numerically, allowing greater flexibility with regard to input parameters and pre-heating by the hot gas layer. The analytical solutions used in Model B should therefore be replaced by numerical solutions.

The many assumptions behind the concurrent flow flame spread equations are enumerated in Chapter 3 and were summarised in the previous section. Several possible improvements to the modeling could be made, such as taking account of burn-out and using non-linear flame length correlations. However, the complexity of the flame morphology under the ceiling can not be accounted for accurately in the foreseeable future and some of these improvements may be considered to be negligible in comparison to the crude assumptions which will have to be made with respect to flame morphology.

The same is valid for predicting the thermal decomposition and mass flow of volatile gases from a burning wall lining specimen, which has undergone a history of heat fluxes in a full scale fire. Assuming that the heat release rate from such a specimen can be taken directly from the Cone Calorimeter is a crude approximation. However, although much of the physics involved in burning is well understood, the complexity of the problem is such that modeling all aspects of it from first principles is as yet an impossible task.

Therefore, heat release rate from the Cone Calorimeter at an irradiance level of 50 kW/m^2 was assumed to represent material heat release rates in the calculations. The heat flux from the flame in the full scale test was, however, assumed to be only 35 kW/m^2 and this heat flux should therefore be used as a basis for the heat release rate calculations. This inconsistency is due to the fact that some of the tested materials did not ignite at lower heat flux levels in the Cone Calorimeter. The problem could possibly be solved by a scheme of interpolations and extrapolations of data from the Cone Calorimeter and might improve the results somewhat. Such a scheme has not been tried or investigated here. Similarly, work should be undertaken to investigate the differences in using data from the Cone Calorimeter where the material is tested in the horizontal and the vertical orientation respectively.

7.4 Final remarks

It has been shown that the analytical solutions to the concurrent flow flame spread equations, discussed in Chapter 3, in combination with material flammability parameters, can be used to rank combustible lining materials according to their flame spread propensities. Further, numerical solutions to these equations can be used in mathematical models to calculate flame spread velocity and fire growth on combustible lining materials in enclosures.

The results from the somewhat simple and, in some respects, rather crude models discussed in this work show that more detailed modeling is indeed feasible and will improve predictive capabilities and enhance applicability to various scenarios. However, problems in predicting, from first principles, the mass flow of volatile gases and heat release rate from a burning wall lining specimen, will limit such models considerably. Also, predicting flame morphology and varying heat flux over the flame area will demand simple, engineering judgements to be made for a considerable number of years to come.

The assessment of the models presented here shows that the material properties derived from the Cone Calorimeter and the LIFT apparatus are sound, thermophysical properties which can be used as input to engineering models simulating fire growth on lining materials in "real world" enclosure fires. The assessment also shows that making simple, engineering assumptions with respect to some of the more obscure physical phenomena does not limit model applicability or accuracy excessively.

In recent years, increasing interest for assessing fire hazards of combustible surface materials has resulted in several research projects being launched. The latest addition, and probably the most comprehensive, is the pre-normative research program supported by the Commission of the European Communities /105/. Its objective is to, within 3 years, develop a sound, scientific basis for the test methods needed to evaluate the reaction-to-fire of construction products, including combustible surface lining materials.

It is the hope of the author that this thesis will, in some small way, contribute towards such a basis and, eventually, towards a rational engineering solution to a recognised and important fire safety problem.

Acknowledgements

I wish to express my profound gratitude to Professor Sven Erik Magnusson for his untiring guidance and encouragement and his continual interest in my work. His fatherly concern for my personal and professional welfare, throughout my years as a graduate student, is deeply appreciated.

I have had the great privilege of working with Dr. Philip Thomas on some of the topics which are an essential part of this thesis. Our discussions have been invaluable in providing insight and new approaches to a number of problems, which to me seemed unsolvable. I sincerely appreciate his kind guidance and generosity.

I am also indebted to Professor Matti Kokkala (VTT, Finland) for his many interesting ideas and to Dr. Yuji Hasemi (BRI, Japan), who assisted me in the initial stages of the work on wind-aided flame spread.

The Head of Department, Robert Jönsson, and all the staff at the Department of Fire Safety Engineering deserve a special mention for creating a friendly, supportive and stimulating working environment.

Funding for this work was provided by the Swedish Fire Research Board (BRANDFORSK), whose assistance is gratefully acknowledged.

Last, but not least, I would like to dedicate this work to my parents, who have always stood by me.

Lund, September, 1992

Björn Karlsson

References

1. Petterson, O., "Fire Hazards and the Compartment Fire Growth Process", FoU-brand, Swedish Fire Protection Association, Stockholm, Sweden:1 1980.
2. Proceedings of the International EUREFIC Seminar, held in Copenhagen 11-12 September 1991, Interscience Communications Limited, London, 1991.
3. Fire Test Standards, Second Ed., ASTM, Philadelphia, 1988.
4. Friedman, R., "Survey of Computer Models for Fire and Smoke", Factory Mutual Research Corporation, Norwood, MA 1991.
5. Babrauskas, V., "Modern Test Methods for Flammability", NISTR 4326, NIST, CFR, Gaithersburg, MD 1990.
6. ISO 5657, Fire Tests - Reaction to Fire - Ignitability of Building Products, International Standards Organization, Geneva, Switzerland, 1986
7. ISO 5660, Fire Tests - Reaction to Fire - Rate of Heat Release from Building Products, International Standards Organization, Geneva, Switzerland, 1991.
8. ASTM E 1321-90, Standard Test Method for Determining Material Ignition and Flame Spread Properties, Annual Book of ASTM Standards, ASTM, Philadelphia, 1990.
9. ISO DP 5658, Fire Tests - Reaction to Fire - Surface Spread of Flame of Building Products - Part I, Vertical Specimen, International Standards Organization, Geneva, Switzerland, 1986.
10. de Ris, J., "Flammability Testing State-of-the-Art", Report FMRC J.I.OHJ2.BU, Factory Mutual Research Corporation, Norwood, MA, 1983.
11. Janssens, M.L., "Fundamental Thermophysical Characteristics of Wood and their Role in Enclosure Fire Growth", National Forest Products Association, Washington DC, 1991.
12. Parker, W.J., "Prediction of the Heat Release Rate from Basic Measurements", Heat Release in Fires, Ed., Babrauskas, V., Grayson, S.J., Elsevier Applied Science, London, 1992.
13. Babrauskas, V., "Development of the Cone Calorimeter - A Bench-Scale Heat Release Apparatus Based on Oxygen Consumption" NBSIR 82-2611, National Bureau of Standards, Washington DC, 1982.
14. Tsantaridis, L., Östman, B., "Smoke, Gas and Heat Release Data for Building Products in the Cone Calorimeter", Trätek Rapport I 8903013, TräteknikCentrum, Stockholm, Sweden 1989.
15. Thureson, P., "EUREFIC - Cone Calorimeter Test Results", SP REPORT 1991:24, SP, Borås, Sweden 1991.
16. Blomqvist, J., "RHR of Building Materials - Experiments with an OSU Apparatus Using Oxygen Consumption", Report LUTVDG/(TVBB-3017), Division of Building Fire Safety and Technology, Lund University, Lund, Sweden, 1983.

17. Svensson, G., Östman, B., "Rate of Heat Release By Oxygen Consumption Testing of Building Materials", Meddelande Serie A Nr 812, Swedish Institute for Wood Research, Stockholm, 1983.
18. Sensenig, D. L., "An Oxygen Consumption Method for Determining the Contribution of Interior Wall Finishes to Room Fires", NBS Technical Note 1128, National Bureau of Standards, Washington DC, 1980.
19. Wickström, U., Personal Communication, SP, Borås, Sweden, 1992.
20. Magnusson, S.E., Sundström, B., "Combustible Linings and Room Fire Growth - A First Analysis", REPORT LUTVDG/TVBB-3030, Dept of Fire Safety Eng, Lund University, Lund, Sweden 1985.
21. Mowrer, F.W., Williamson, R.B., "Methods to Characterize Heat Release Rate Data", Fire Safety Journal, Vol 16, pp 367-387, 1990.
22. Kokkala, M., Thomas, P.H., Karlsson, B., "Rate of Heat Release and Ignitability Indices for Surface Linings", submitted for publication in Fire and Materials, 1992.
23. Cleary, T.G., Quintiere, J.G., "A Framework for Utilizing Fire Property Tests", Proc. Third Int. Symposium on Fire Safety Science, Elsevier Science Publishers Ltd, London, 1991.
24. Thomas, P., Karlsson, B., "Dimensionless Quantities in Fire Growth: The Weighting of Heat Release Rate", CODEN: SE-LUTVDG/TVBB-3057, Dept of Fire Safety Eng, Lund University, Lund, Sweden 1990
25. Kokkala, M., "Sensitivity of the Room Corner Test to Variations in the Test System and Product Properties", submitted for publication in Fire and Materials, July,1992.
26. Sundström, B., "Results and Analysis of Building Materials Tested According to ISO and IMO Spread of Flame Tests", SP-RAPP 1984:36, SP, Borås, Sweden, 1984.
27. Östman, B.A., Tsantaridis, L.D., "Ignitability in the Cone Calorimeter and the ISO Ignitability Test", Proceedings of the Fifth Interflam Conference, Interscience Communications Limited, London, 1990.
28. Rec. on Fire Test Procedures for Surface Flammability of Bulkhead and Deck Finish Materials. Res. A546 (14), suppl. Res. A516 (13), A166(ES.IV), International Maritime Organization, London, 1986.
29. Quintiere,, J., "A Simplified Theory for Generalizing Results from a Radiant Panel Rate of Flame Spread Apparatus", Fire and Materials, Vol 5, No 2, 1981.
30. Quintiere, J.G., Harkleroad, M., "New Concepts for Measuring Flame Spread Properties", NBSIR 84-2943, NBS, CFR, Gaithersburg, MD, 1984.
31. Janssens, M., "Piloted Ignition of Wood: A Review", Fire and Materials, Vol 15, pp 151-167, 1991.
32. Nisted, T., "Flame Spread Experiments in Bench Scale", Dantest, Fire Technology, Copenhagen, Denmark, 1991.

33. Williams, F.A., "Mechanisms of Fire Spread", Symposium (Int) of Combustion, 1975.
34. Fernandez-Pello, A.C., Hirano, T., "Controlling Mechanisms of Flame Spread", Combustion Science and Tech, Vol 32, 1983.
35. Quintiere, J., "Surface Flame Spread", The SFPE Handbook of Fire Protection Engineering, Ed. Di Nenno et. al., NFPA, Quincy, MA, 1988.
36. Wichman, I.S., Agrawal, S., "Wind-Aided Flame Spread Over Thick Solids", Combustion and Flame, Vol. 83, pp 127-145, 1991.
37. Di Blasi, C., "Ignition and Flame Spread Across Solid Fuels", Numerical Approaches to Combustion Modeling, Ed. Oran, S.E., Boris, J.P, AIAA, Washington, DC, 1991.
38. Olhemiller, T., "Assessing the Flammability of Composite Materials", NISTIR 89-4032, NIST, CFR, Gaithersburg, MD, 1989.
39. de Ris, J.N., "Spread of a Laminar Diffusion Flame", 12th Symposium (Int) on Combustion, The Combustion Institute, Pittsburgh, PA, 1969.
40. Wichman, I.S., "A Model Describing the Influences of Finite-Rate-Gas-Phase Chemistry on Rates of Flame Spread Over Solid Combustibles", Combustion Science and Tech, Vol 40, 1984.
41. Saito, K., Quintiere, J.G., Williams, F.A., "Upward Turbulent Flame Spread", Proc. First Int Symposium on Fire Safety Science, Hemisphere Publishing Corporation, New York, 1984.
42. Thomas, P., Karlsson, B., "On Upward Flame Spread on Thick Fuels", CODEN: SE-LUTVDG/TVBB-3058, Dept of Fire Safety Eng, Lund University, Lund, Sweden, 1990.
43. Brunner, H., van der Houwen, P.J., "The Numerical Solution of Volterra Equations", CWI Monograph;3, Elsevier Science Publishers, Amsterdam, 1986.
44. Baroudi, D., Kokkala, M., "Analysis of Upward Flame Spread", VTT Publications 89, VTT, Espoo, Finland 1992
45. Thomas, P.H., Webster, C.I., Raftery, M.M., "Some Experiments on Buoyant Diffusion Flames", Combustion and Flame, Vol. 5, p 359, 1961.
46. Steward, F.R., "Prediction of the Height of Turbulent Diffusion Flames", Combustion Science and Technology, Vol. 2, p 203, 1970.
47. McCaffrey, B., "Flame Height", The SFPE Handbook of Fire Protection Engineering, Ed. Di Nenno et. al., NFPA, Quincy, MA, 1988.
48. Heskestad, G., "Luminous Heights of Turbulent Diffusion Flames", Fire Safety Journal, Vol. 5, No. 2, pp 103-108, 1983.
49. Zukoski, E.E., "Fluid Dynamic Aspects of Room Fires", Fire Safety Science, Proc. of the First Int. Symposium, Ed. Grand, C.E., Pagni, P.J., Hemisphere, New York, 1984.
50. Cox, G., Chitty, R., "Some Source-Dependent Effects on Unbounded Fires", Combustion and Flames, Vol. 60, pp219-232, 1985.

51. Tu, K.M., Quintiere, J.Q., "Wall Flame Heights with External Radiation", Fire Technology, August 1991.
52. Delichatsios, M.A., "Flame Heights in Turbulent Wall Fires with Significant Flame Radiation", Combustion Science and Technology, Vol. 39, p 195, 1984.
53. Hasemi, Y., "Thermal Modeling of Upward Wall Flame Spread", Fire Safety Science, Proc. of the First Int. Symposium, Ed. Grand, C.E., Pagni, P.J., Hemisphere, New York, 1984.
54. Kulkarni, A., Quintiere, J.G., Harkleroad, M., "Heat Feedback and Flame Height Measurements on Burning Vertical Surfaces", Combustion Institute Eastern States Section, Chemical and Physical Process in Combustion, Fall Technical Meeting, Providence, RI, 1983.
55. Hasemi, Y., Tokunaga, T., "Some Experimental Aspects of Turbulent Diffusion Flames and Buoyant Plumes from Fire Sources Against a Wall and in a Corner of Walls", Combustion Science and Technology, Vol 40, pp1-17, 1984.
56. Kokkala, M., Heinilä, M., "Flame Height, Temperature and Heat Flux Measurements on a Flame in an Open Corner of Walls" (DRAFT Report), VTT, Fire Technology Laboratory, Espoo, Finland, 1991.
57. Williamson, R.B., Mowrer, F.W., Fisher, F.L., "Observations of Large Scale Turbulence in Corner-Wall Experiments", Combustion Science and Tech, Vol 41, Nos. 1 and 2, pp 83-99, 1984.
58. Thomas, P., Karlsson, B., "On the Length of Flames Under Ceilings", Journal of Fire Sciences, Vol 9, 1991.
59. Andersson, C., Giacomelli, C., "Ett Modellrum i Lågor", Dept of Fire Safety Eng, Lund University, Lund, Sweden 1985.
60. Gross, D., "Measurements of Flame Lengths Under Ceilings", NISTR 88-3835, NIST, CFR, Gaithersburg, MD 1988.
61. Babrauskas, V., "Flame Lengths Under Ceilings", Fire and Materials, Vol 4, No 3, 1980.
62. Morton, B.R., Taylor, G., Turner, J.S., "Turbulent Gravitational Convection From Maintained and Instantaneous Sources", Proc Roy Soc A, Vol 234, pp 1-23, 1956.
63. You, H.Z., Faeth, G.M., "An Investigation on Fire Impingement on a Horizontal Ceiling", NBS-GCR-81-304, NBS, CFR, Gaithersburg, MD, 1981.
64. Yokoi, S., "Study on the Prevention of Fire Spread Caused by Upward Current ", Ministry of Construction, Building Research Institute, Report No 34, Tokyo, 1960.
65. Alpert, R.L., "Calculation of Response Time of Ceiling-Mounted Fire Detectors", Fire and Technology, Vol. 8, pp 181-195, 1972.

66. Heskestad, G., Delichatsios, M.A., "The Initial Convective Flow in Fire", 17th Symposium (International) Combustion Institute, Pittsburgh, 1978.
67. Karlsson, B., "A Mathematical Model for Calculating Heat Release Rate in the Room Corner Test", accepted (November, 1991) for publication in the Fire Safety Journal.
68. Sundström, B., "Full Scale Fire Testing of Surface Materials", SP-RAPP 1986:45, SP, Borås, Sweden, 1986.
69. Parker, W.J., "An Assessment of Correlations Between Laboratory and Full Scale Experiments for the FAA Aircraft Fire Safety Program, Part 3; ASTM E 84", NBSIR 82-2564, NBS, CFR, Gaithersburg, MD, 1982.
70. Thomas, P.H., "On Concurrent Upward Surface Spread of Flame" (draft report), Department of Fire Safety Engineering, Lund University, Lund, 1992.
71. Vandevelde, P., "Transitional Arrangements for Reaction to Fire Testing in Europe", Annex 1, CEC III B-5 Document TC2/002, Brussels, January, 1990.
72. ISO 9705, Fire Tests - Reaction to Fire - Full-scale Room Fire Test for Surface Products, International Standards Organization, Geneva, Switzerland, 1991.
73. Room Fire Test in Full Scale for Surface Products, NORDTEST Fire Test Method. NT FIRE 025, 1986.
74. Standard Test Method for Evaluating Room Fire Growth Contribution of Textile Wall Covering, in Uniform Building Code Standards No. 42-2, pp 1195-1213, International Conferance of Building Officials, Whittter, CA, 1988.
75. Williamson, R.B., Revenaugh, A., Mowrer, F.W, "Ignition Sources in Room Fire Tests and Some Implications for Flame Spread Evaluation", Fire Safety Science Proceedings of the Third International Symposium, Elsevier Applied Science, London 1991.
76. Quintiere, J.Q., "An Approach to Modeling Wall Fire Spread in a Room", Fire Safety Journal, Vol. 3, pp 201-214, 1981.
77. Östman, B., Nussbaum, R.M., "Correlation Between Small-Scale Rate of Heat Release and Full Scale Room Flashover for Surface Linings", Proc Second Int Symposium on Fire Safety Science, pp 823-832, Hemisphere Publishing Corp, Tokyo, Japan ,1988.
78. Wickström, U., Göransson, U., "Prediction of Heat Release Rates of Surface Materials in Large-Scale Fire Test Based on Cone Calorimeter Results", Authorized Reprint from Journal of Testing and Evaluation, November 1987, SP REPORT 1988:11, SP, Borås, 1988.
79. Wickström, U., Göransson, U., "Full-scale/Bench-scale Correlations of Wall and Ceiling Linings", Fire and Materials, Vol 16, pp 15-22, 1992.
80. Smith, E., Satija, S., "Release Rate Model for Developing Fires", ASME Journal of Heat Transfer, 105, pp 282-287, 1983.

81. Tran, H.C., Janssens, M.L., "Wall and Corner Fire Tests on Selected Wood Products", Journal of Fire Sciences, Vol. 9, No. 2, 1991.
82. Tran, H.C., "Simulating Wall and Corner Fire Tests on Wood Products with the OSU Room Fire Model", to be presented at the Int. Symp. on Fire and Flammability of Furnishings and Contents of Buildings, to be held in Miami, FL, December 7, 1992.
83. Janssens, M.L, "MOSURF: A Modified OSU Room Fire Model for Simulating Corner Fires",to be presented at the Int. Symp. on Fire and Flammability of Furnishings and Contents of Buildings, to be held in Miami, FL, December 7, 1992.
84. Quintiere, J., "A Simulation Model for Fire Growth on Materials Subject to a Room-Corner Test", Presentation at the Fire Retardant Chemicals Ass. Spring Conference, Orlando, FL 1992.
85. Karlsson, B., "Room Fires and Combustible Linings", SE-LUTVDG/TVBB-3050, Dept of Fire Safety Eng, Lund University, Lund, Sweden, 1989.
86. McCaffrey, B.J., Quintiere, J.Q., Harkleroad, M.F., "Estimating Room Temperatures and the Likelihood of Flashover Using Fire Test Data Correlations", Fire Technology, Vol 17, pp 98-119, 1981.
87. Delichatsios, M.M., Mathews, M.K., Delichatsios, M.A., "An Upward Flame Spread and Growth Simulation", Proc Third Int Symposium on Fire Safety Science, Elsevier Science Publishers Ltd, London, 1991.
88. Mitler, H.E., "Predicting the Spread Rates of Fires on Vertical Surfaces", 23rd (Int) Symposium on Combustion, 1990.
89. Kulkarni, A.K., Kim, C.I., Kuo, C.H., "Turbulent Upward Flame Spread for Burning Vertical Walls Made of Finite Thickness", NIST-GCR-91-597, NIST, BFRL, Gaithersburg, MD, 1991.
90. Jones, W.W., Forney, G.P., "A Programmers Reference Manual for CFAST, The Unified Model of Fire Growth and Smoke Transport", NIST, Tech. Note 1283, Gaithersburg, MD, 1990.
91. Karlsson, B., Magnusson, S.E., "Internal Linings, the Interim Solution and a Simplified Classification System", ISRN LUTVDG/TVBB-3066-SE, Dept of Fire Safety Eng, Lund University, Lund, 1991.
92. Mowrer, F.W., Williamson, R.B., "Estimating Room Temperatures from Fires along Walls and in Corners", Fire Technology, Vol. 23, No. 2, 1987.
93. Quintiere, J.G., "An Assessment of Correlations Between Laboratory and Full Scale Experiments for the FAA Aircraft Fire Safety Program, Part 2: Rate of Energy Release in fire", NBSIR 82-2536, National Bureau of Standards, Washington DC, 1982.
94. Carslaw, H.S., Jaeger, J.S., "Conduction of Heat in Solids", Oxford University, Oxford, 1959.
95. Rockett, J.A., Conduction of Heat in Solids", The SFPE Handbook of Fire Protection Engineering, Ed. Di Nenno et. al., NFPA, Quincy, MA, 1988.

96. Mitler, H.E., "The Physical Bases for the Harvard Computer Fire Code", Division of Applied Sciences, Harvard University, Home Fire Project Technical Report No. 34, Oct. 1978.
97. Quintiere, J., Harkleroad, M., Hasemi, Y., "Wall Flame Implications for Upward Flame Spread", Combustion Science and Technology, Vol 48, pp 191-222, 1986.
98. Lønvik, L.E., Opstad, K., "Software User's Guide for DCS, a Data Converting System", Report No. STF25 A90003, SINTEF, Trondheim, Norway, 1991.
99. Söderblom, J., "EUREFIC - Large Scale Tests According to ISO DIS 9705", SP REPORT 1991:27, SP, Borås, Sweden, 1991.
100. Andersson, B., "Model Scale Compartment Fire Tests With Wall Lining Materials", Report LUTVDG/(TVBB-3041), Department of Fire Safety Engineering, Lund University, Lund, 1988.
101. Ondrus, J., Internal Memorandum, Department of Fire Safety Engineering, Lund University, Lund, 1988.
102. Karlsson, B., Magnusson, S.E., "An Example Room Fire Model", Heat Release in Fires, Ed., Babrauskas, V., Grayson, S.J., Elsevier Applied Science, London, 1992.
103. Mitler, H.E., "Mathematical Modeling of Enclosure Fires", NISTR 90-4294, NIST, BFRL, Gaithersburg, MD, 1990.
104. Karlsson, B., Magnusson, S.E., "Combustible Wall Lining Materials: Numerical Simulation of Room Fire Growth and the Outline of a Reliability Based Classification Procedure", Fire Safety Science Proceedings of the Third International Symposium, Elsevier Applied Science, London, 1991.
105. Pre-normative Research on the Reaction to Fire of Construction Products, Information for Proposers, Commission of the European Communities, DG XII, Brussels, May, 1992.

Appendix A

Bench-scale test results

Tables III and IV

Appendix A-1, "Swedish" materials, graphs of $\dot{q}''_e$ versus t_{ig}.

Appendix A-2, "Swedish" materials, graphs of $(\dot{q}''_{0,ig} / \dot{q}''_e)$ versus $\sqrt{t_{ig}}$.

Appendix A-3, EUREFIC materials, corrected slope of $(\dot{q}''_{0,ig} / \dot{q}''_e)$ versus $\sqrt{t_{ig}}$.

Table III Cone Calorimeter time to ignition (s). From Reference /27/

Mat. No.	Building material	Heat flux level (kW/m^2) 20	25	30	35	50	75
S1	Insulating fiber board	92	43	-	-	12	6
S2	Medium density fiber board	223	123	-	-	28	14
S3	Particle board	255	123	-	-	34	16
S4	Gypsum board	-	NI	NI	112	34	13
S5	Plastic wall-covering on gypsum board	126	41	28	-	10	4
S6	Paper wall-covering on gypsum board	NI	106	101	-	21	6
S7	Textile wall-covering on gypsum board	NI	115	82	-	20	7
S8	Textile wall-covering on rock-wool	49	30	-	-	11	9
S9	Melamine-faced particle board	-	NI	498	-	42	12
S10	Expanded polystyrene	873	223	-	-	39	-
S11	Rigid polyurethane foam	12	4	-	-	2	-
S12	Wood panel (spruce)	525	169	79	-	21	11
S13	Paper wall-covering on particle board	603	139	111	-	27	12

NI = No ignition
\- = Not tested

Table IV ISO Ignitability time to ignition (s). From Reference /27/

Mat. No.	Building material	Heat flux level (kW/m^2) 10	20	30	40	50
S1	Insulating fiber board	NI	63	22	13	12
S2	Medium density fiber board	NI	209	66	34	22
S3	Particle board	NI	240	87	52	30
S4	Gypsum board	NI	NI	151	60	35
S5	Plastic wall-covering on gypsum board	NI	79	20	13	9
S6	Paper wall-covering on gypsum board	NI	501	76	35	14
S7	Textile wall-covering on gypsum board	NI	363	76	32	22
S8	Textile wall-covering on rock-wool	NI	48	21	17	13
S9	Melamine-faced particle board	NI	NI	174	28	26
S10	Expanded polystyrene	NI	NI	NI	5	2
S11	Rigid polyurethane foam	52	8	5	6	2
S12	Wood panel (spruce)	NI	661	58	28	18
S13	Paper wall-covering on particle board	NI	692	115	55	19

NI = No ignition

Data from "S1.ign"

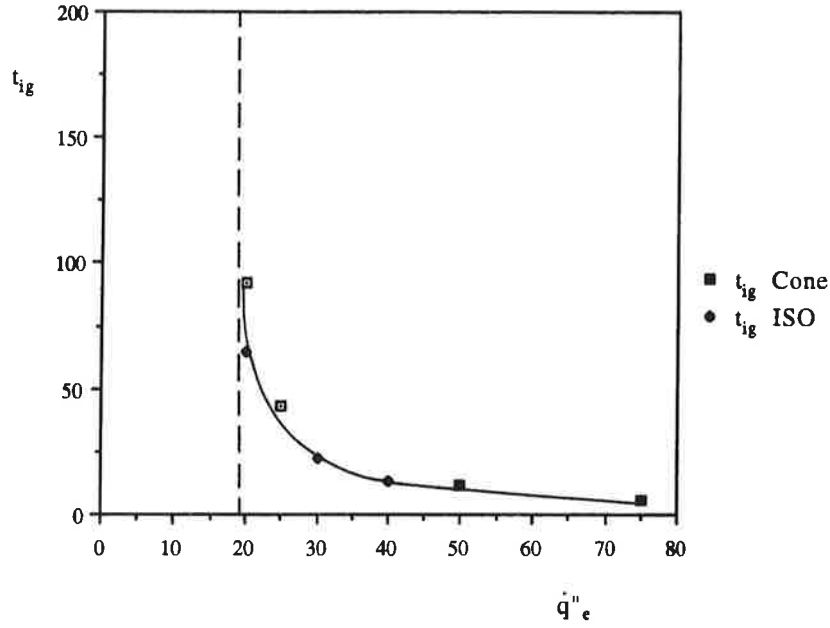

Data from "S2.ign"

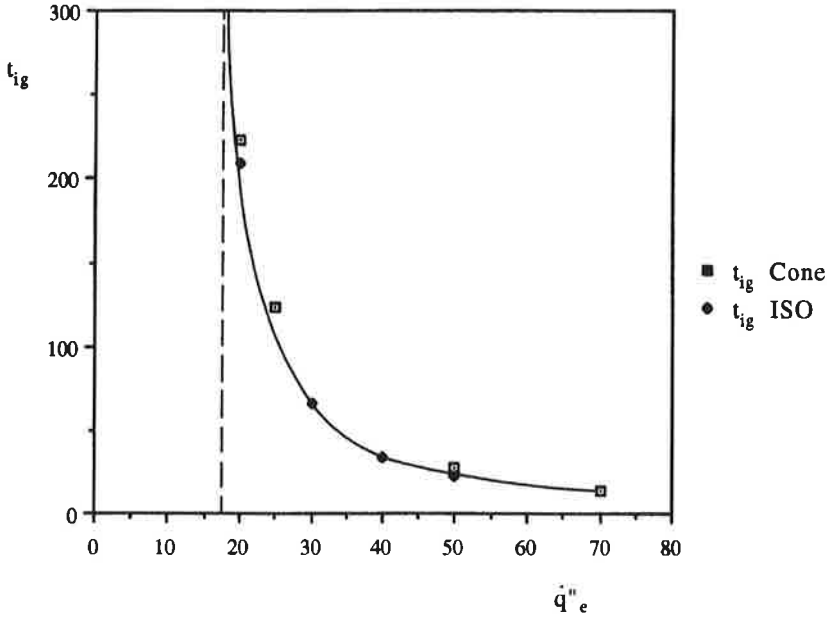

Data from "S3.ign"

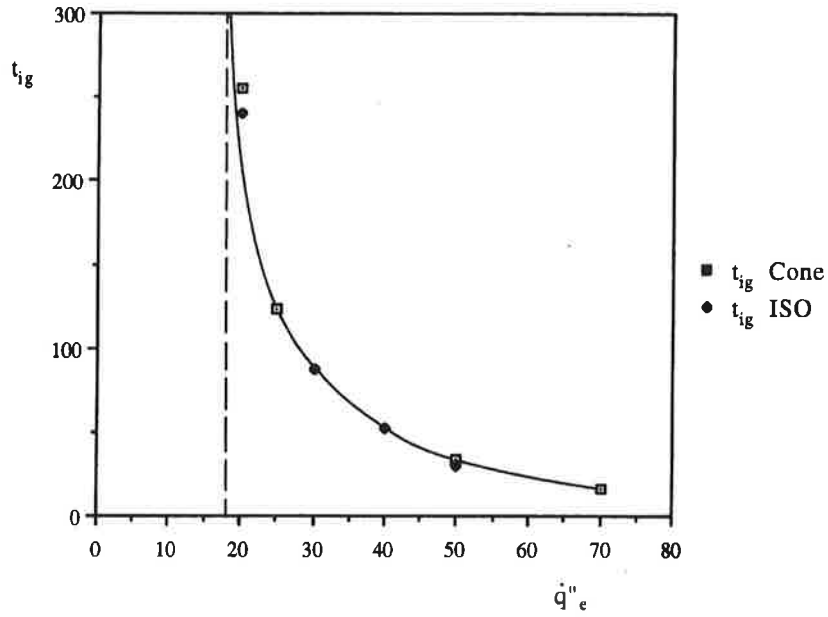

Data from "S4.ign"

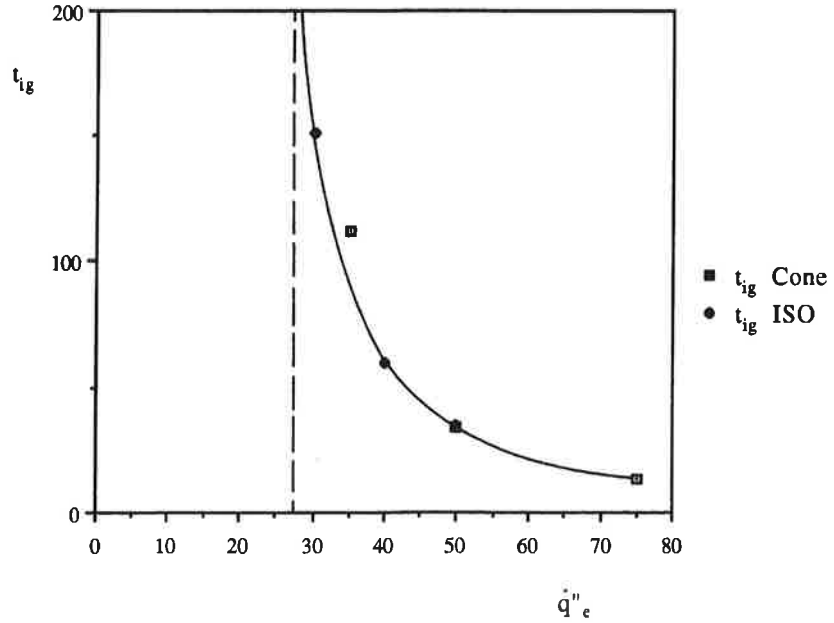

Data from "S5.ign"

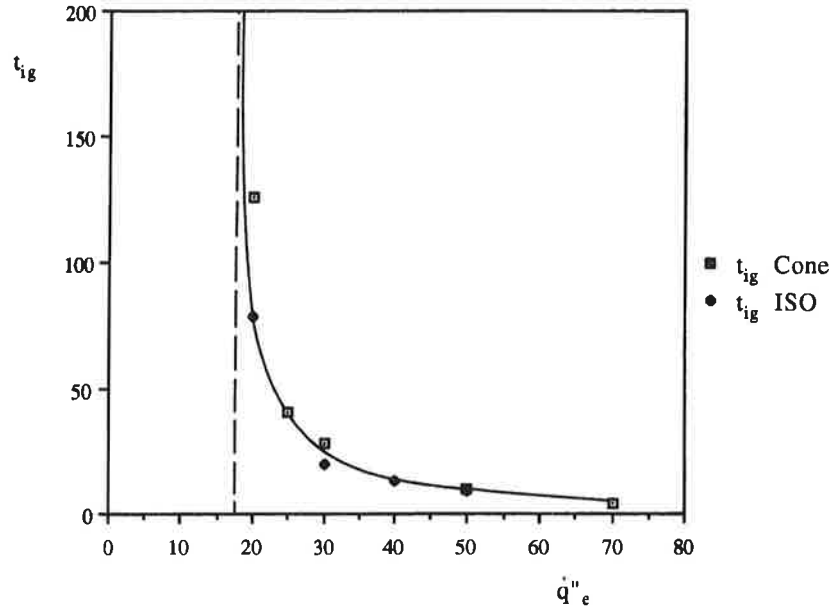

Data from "S6.ign"

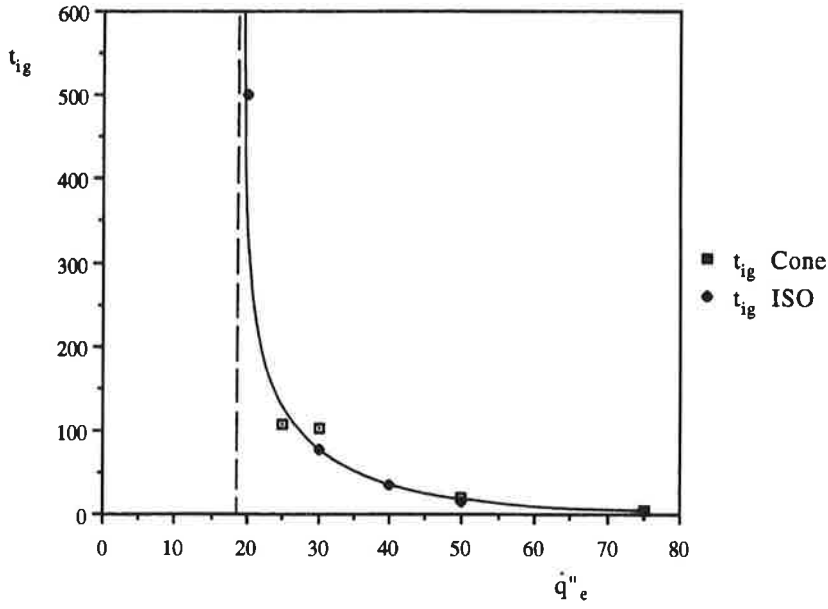

Data from "S7.ign"

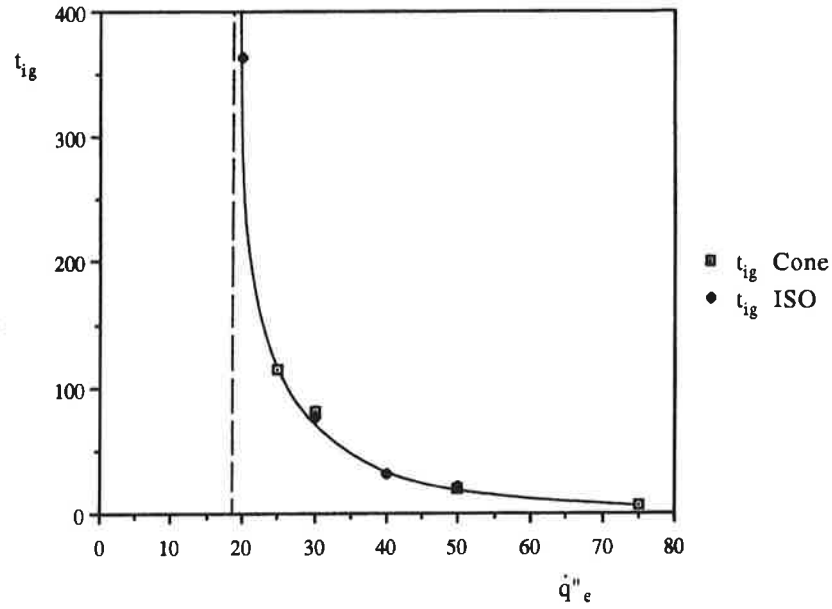

Data from "S8.ign"

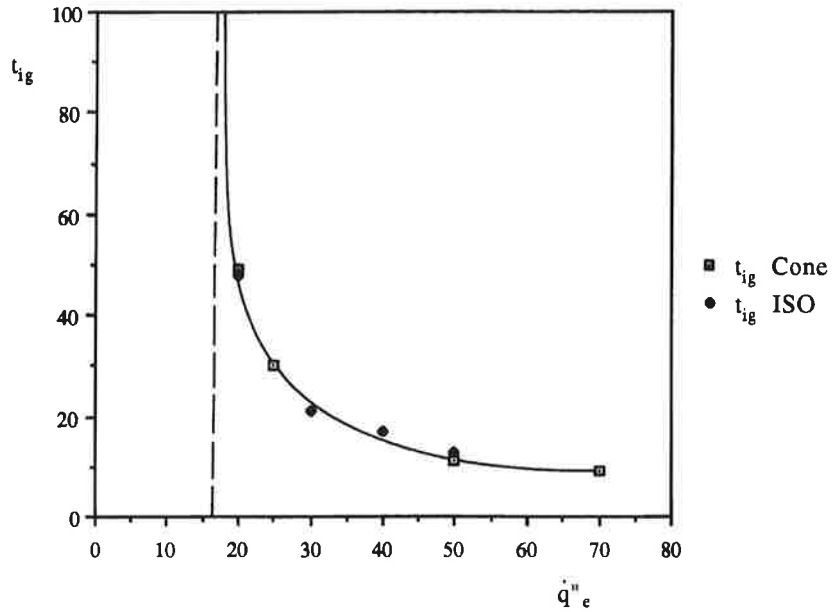

Data from "S9.ign"

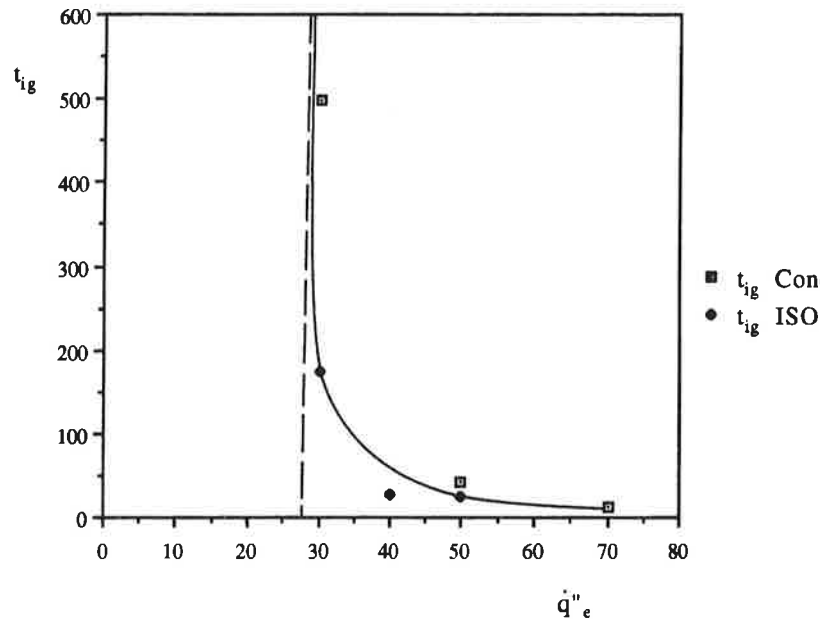

Data from "swe10.ign"

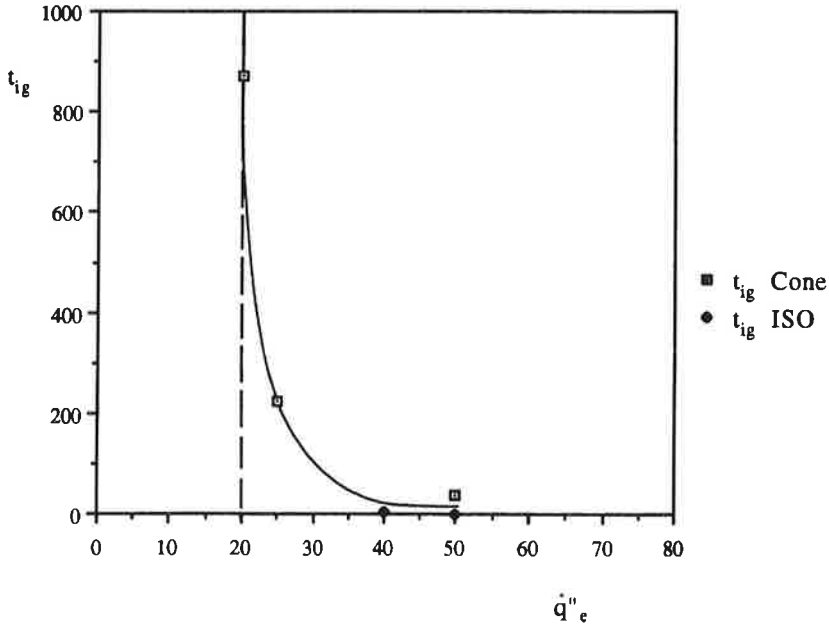

Data from "S11.ign"

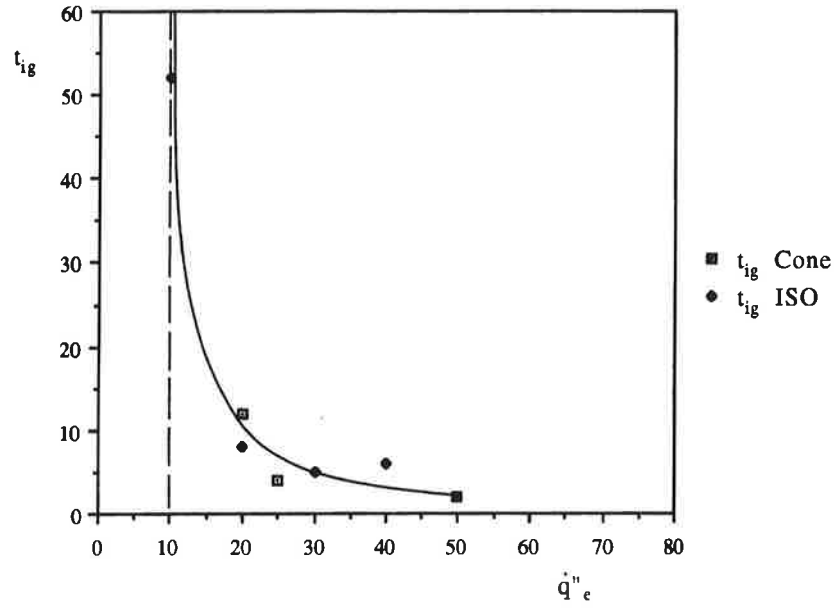

Data from "S12.ign"

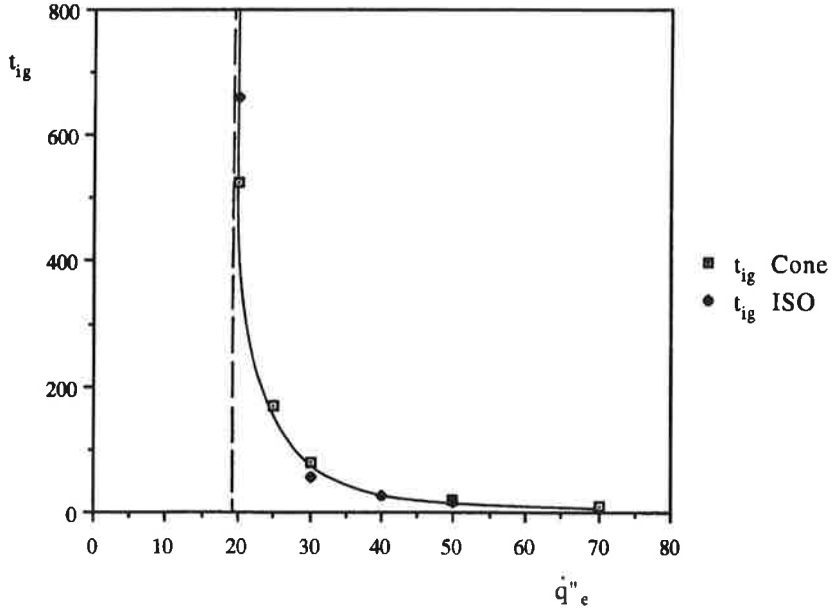

Data from "S13.ign"

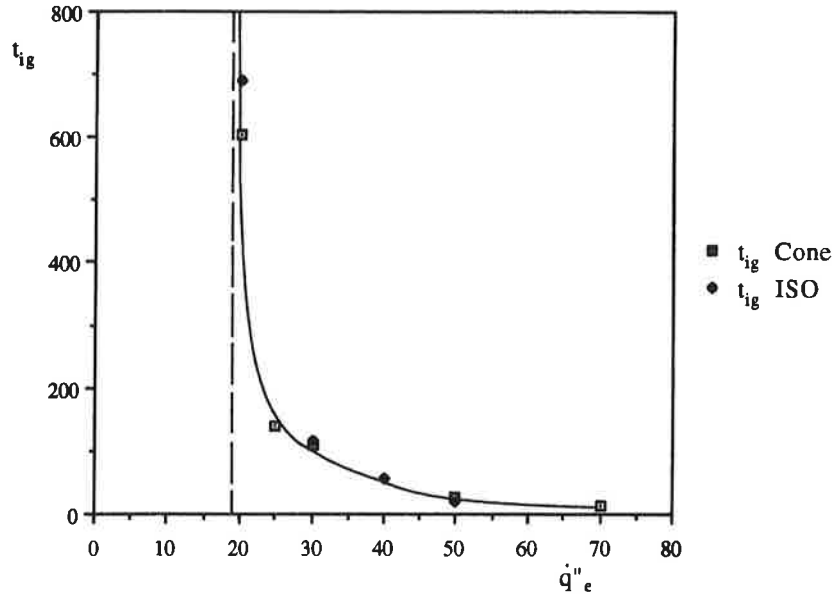

Data from "S1.ign"

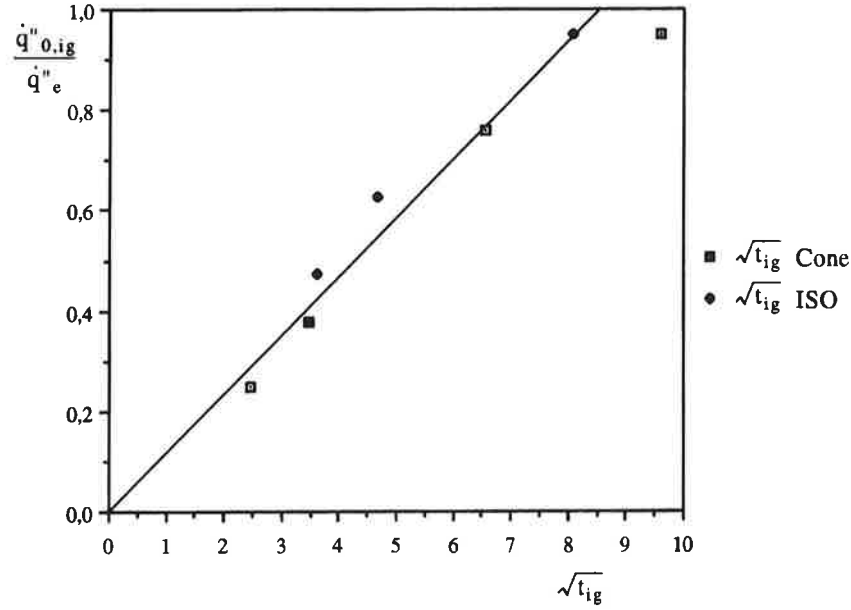

Data from "S2.ign"

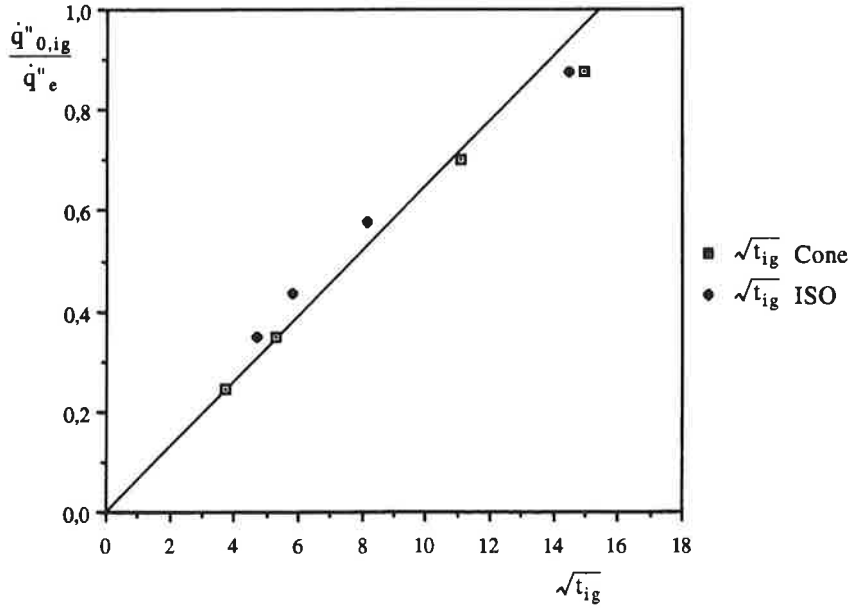

Data from "S3.ign"

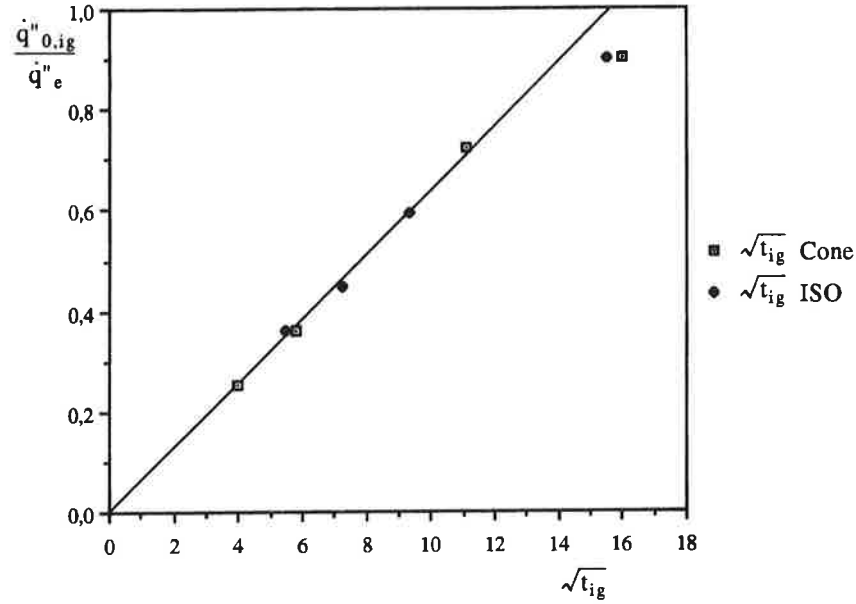

Data from "S4.ign"

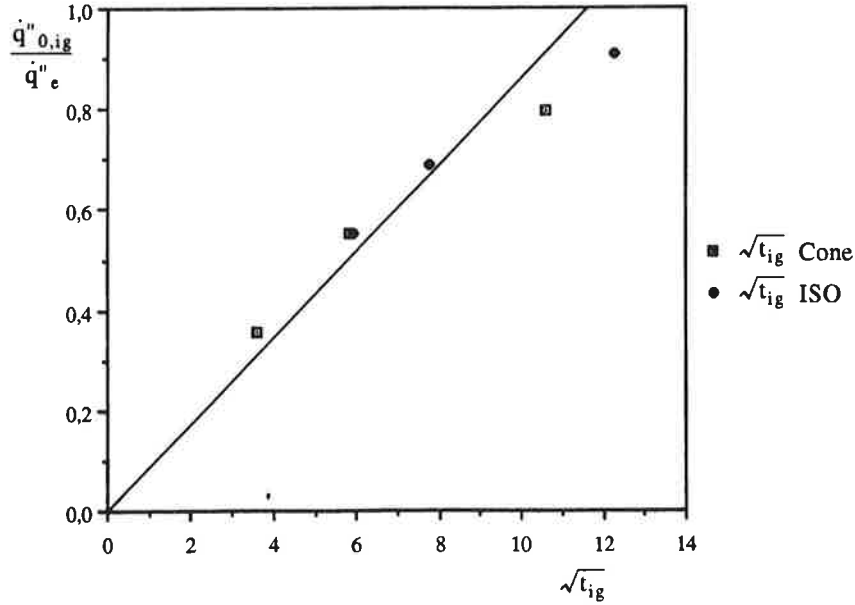

Data from "S5.ign"

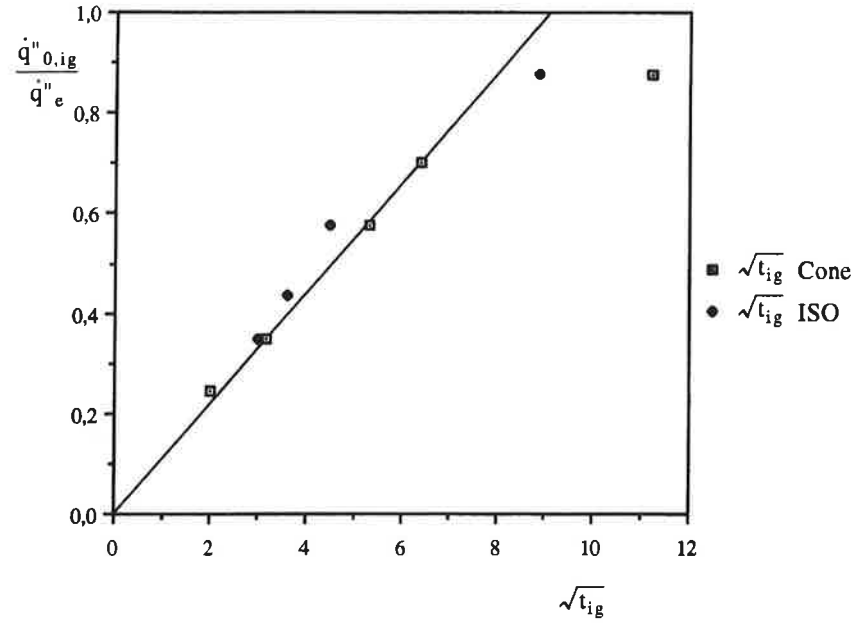

Data from "S6.ign"

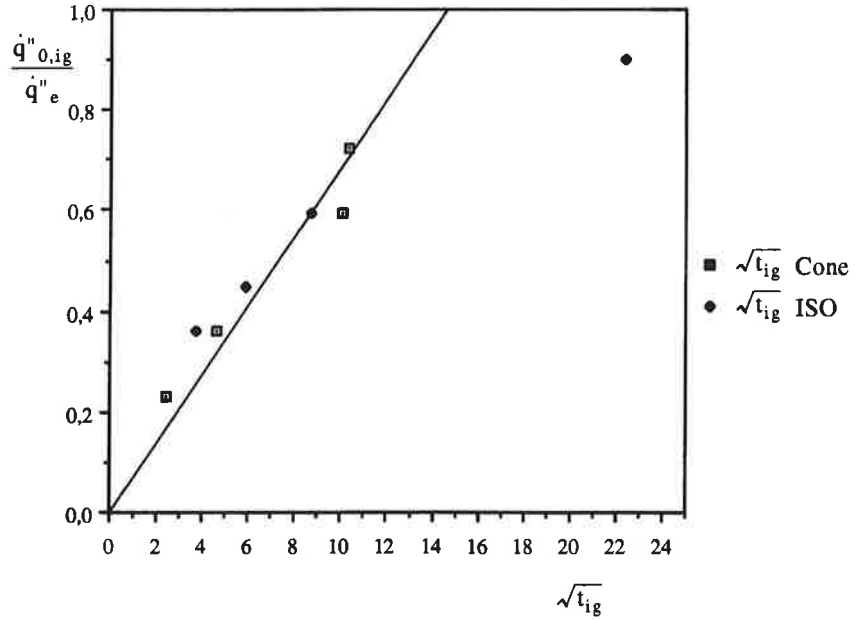

Data from "S7.ign"

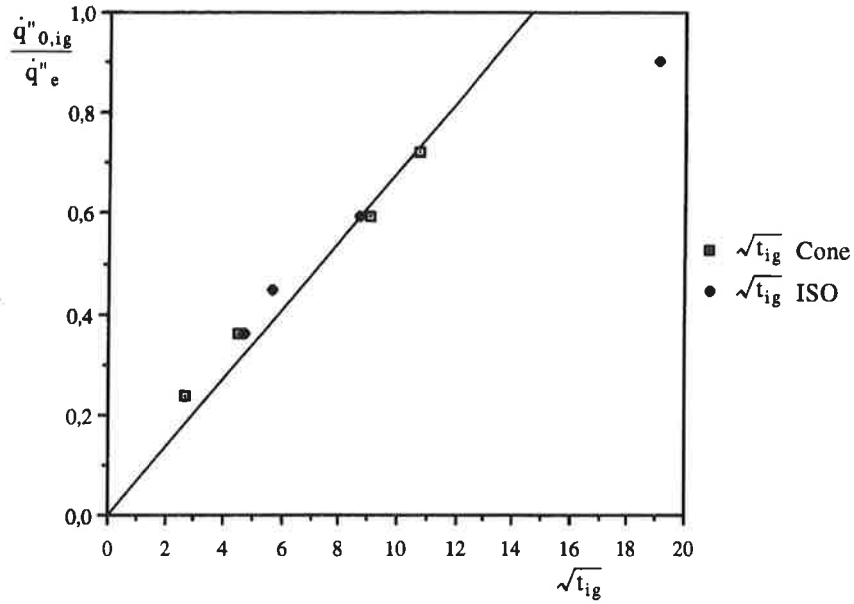

Data from "S8.ign"

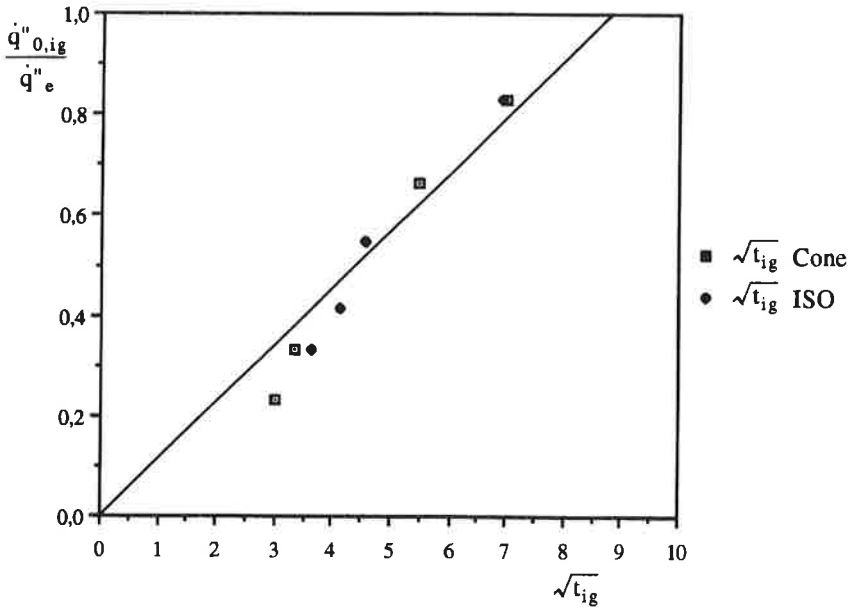

Data from "S9.ign"

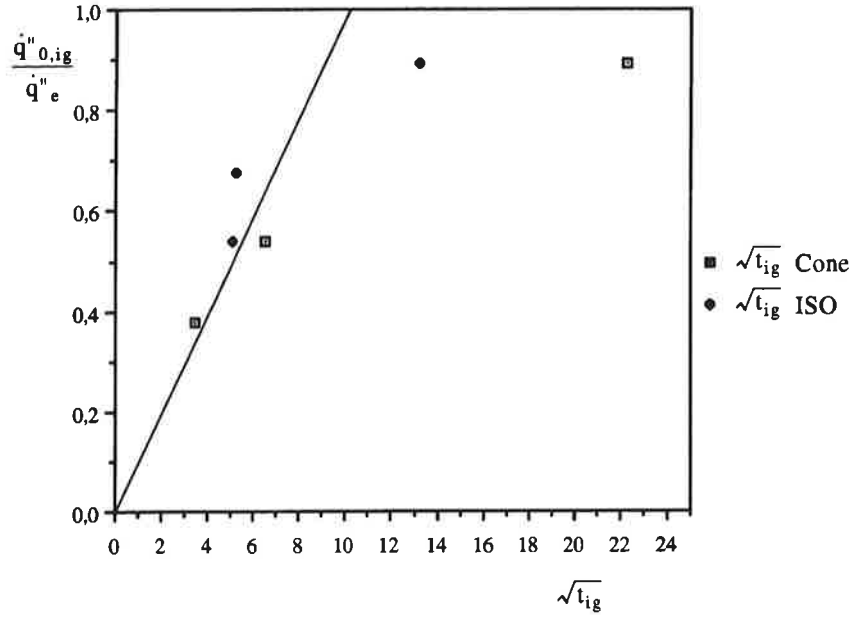

Data from "S10.ign"

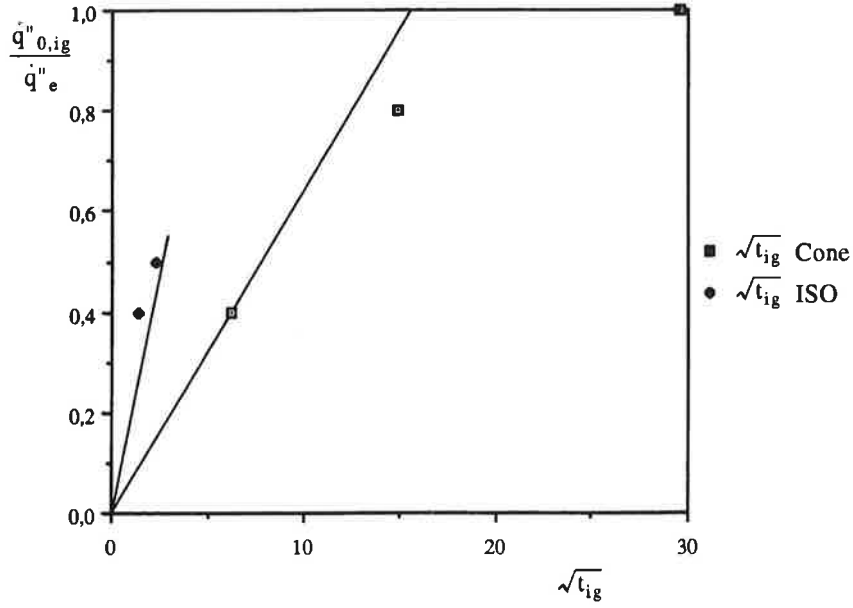

Data from "S11.ign"

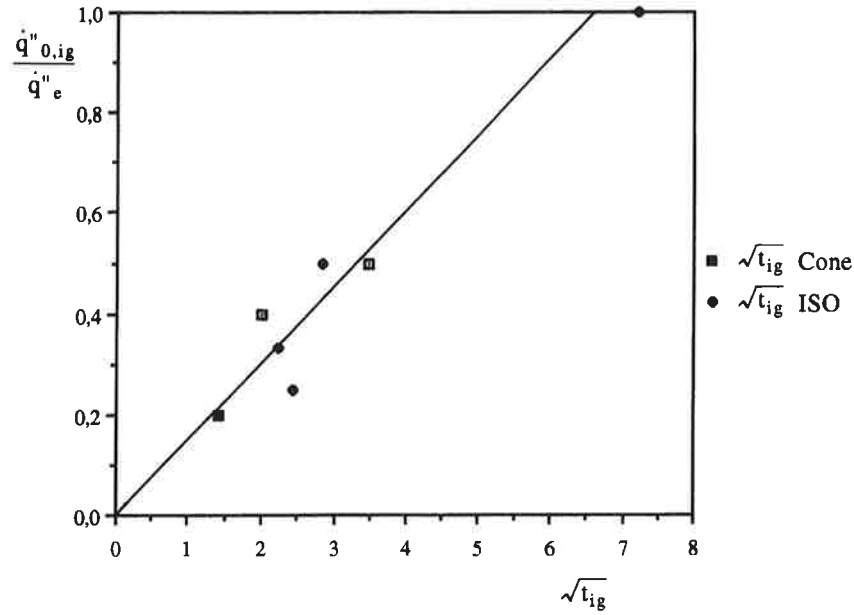

Data from "S12.ign"

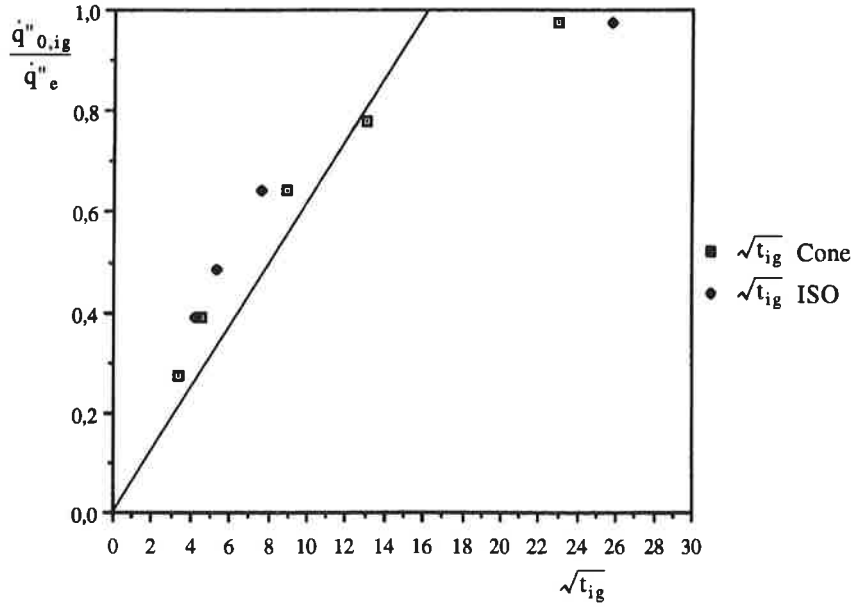

Data from "S13.ign"

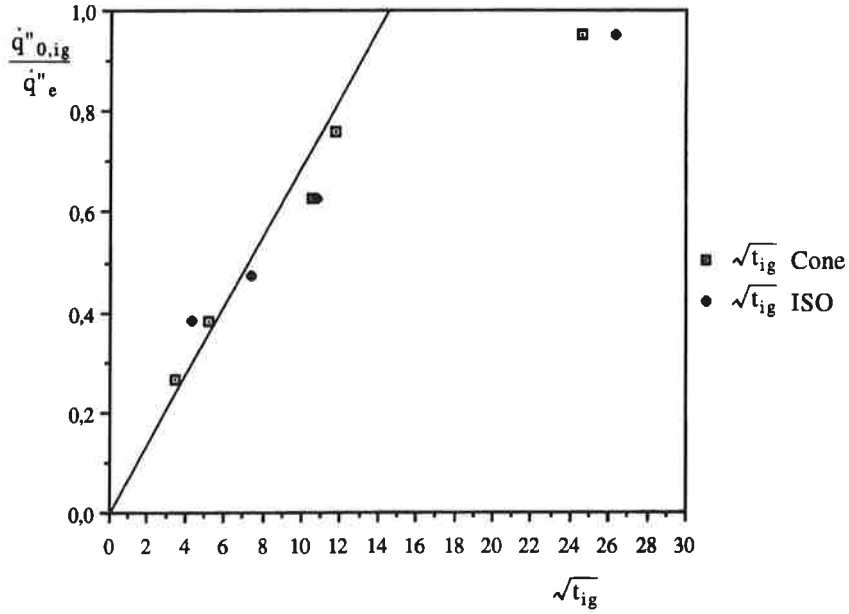

Material E2, corrected parameter b

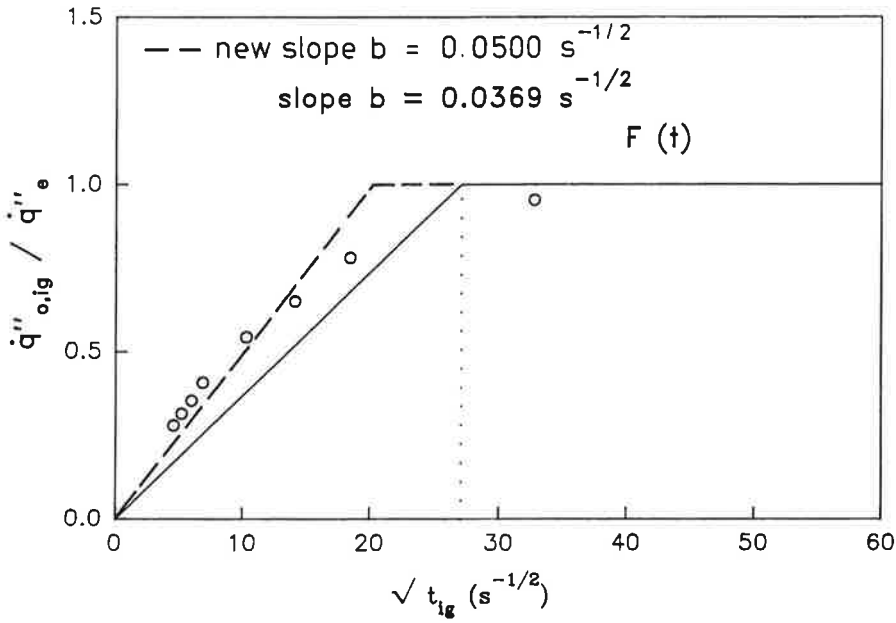

Material E3, corrected parameter b

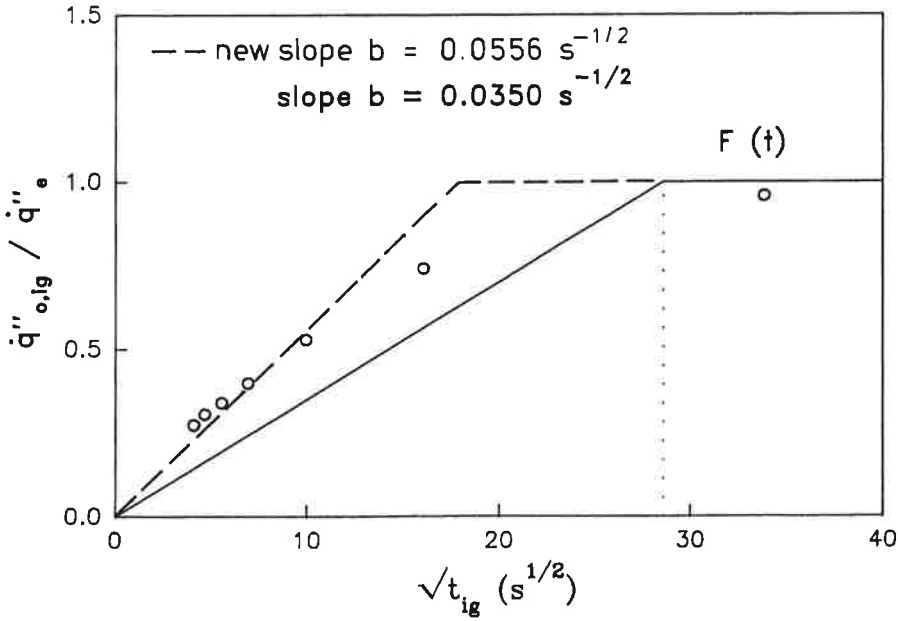

Material E9, corrected parameter b

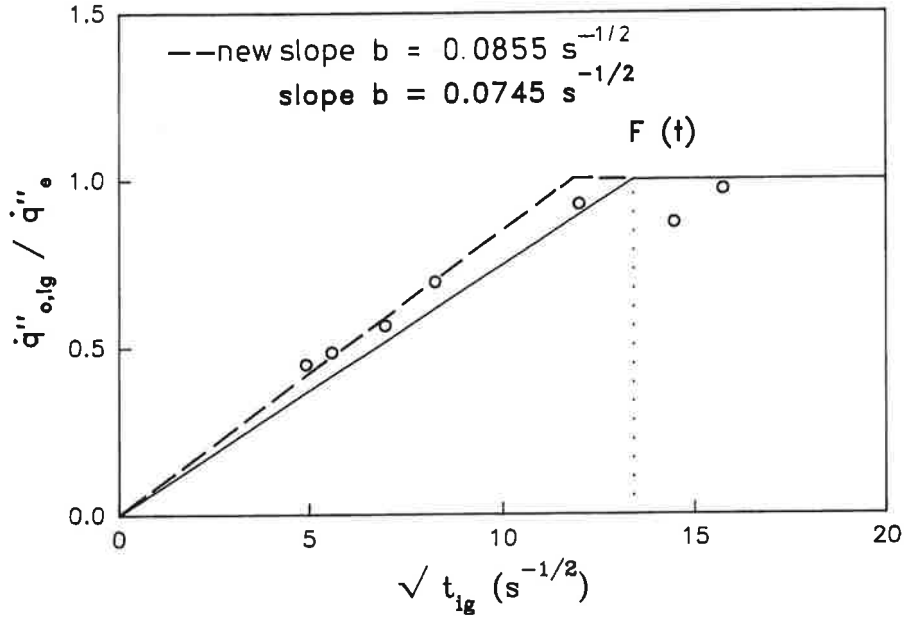

Material E10, corrected parameter b

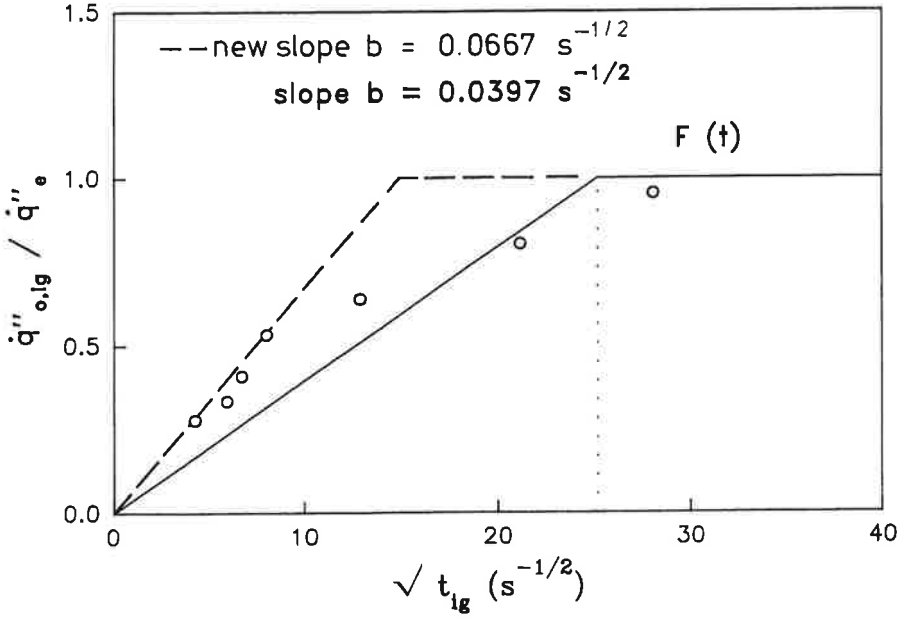

Material E11, corrected parameter b

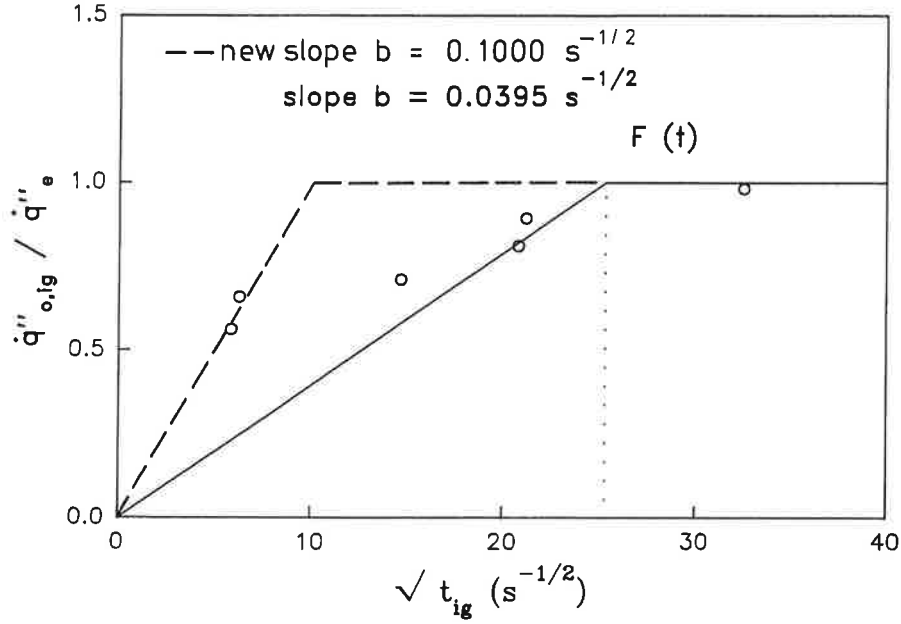

Appendix B

Results from simple, analytical model for Scenario A

Comparison of experimental and calculated RHR from full scale test series, Scenario A, 12 materials.

Material S1, RHR from full scale room test

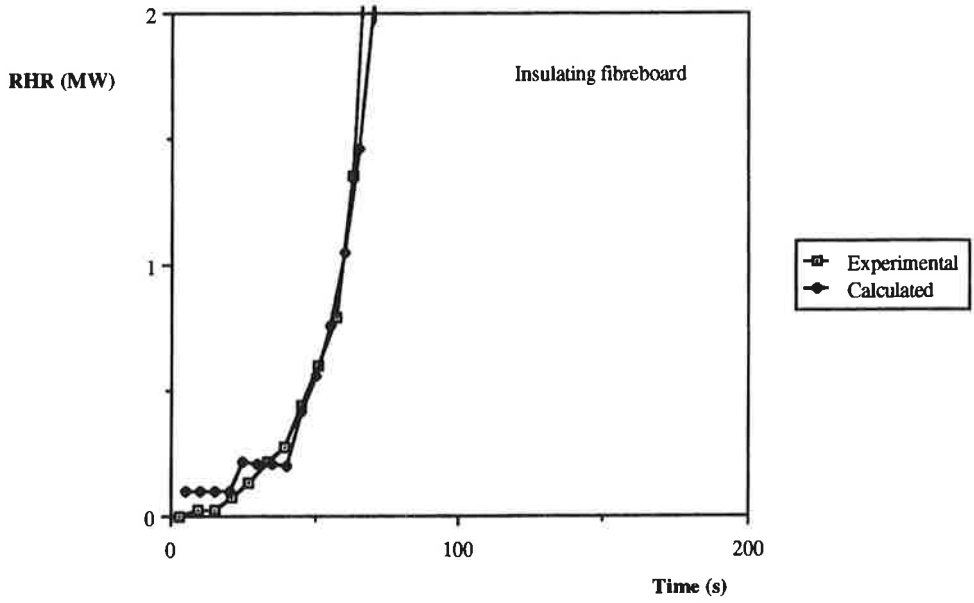

Material S2, RHR from full scale room test

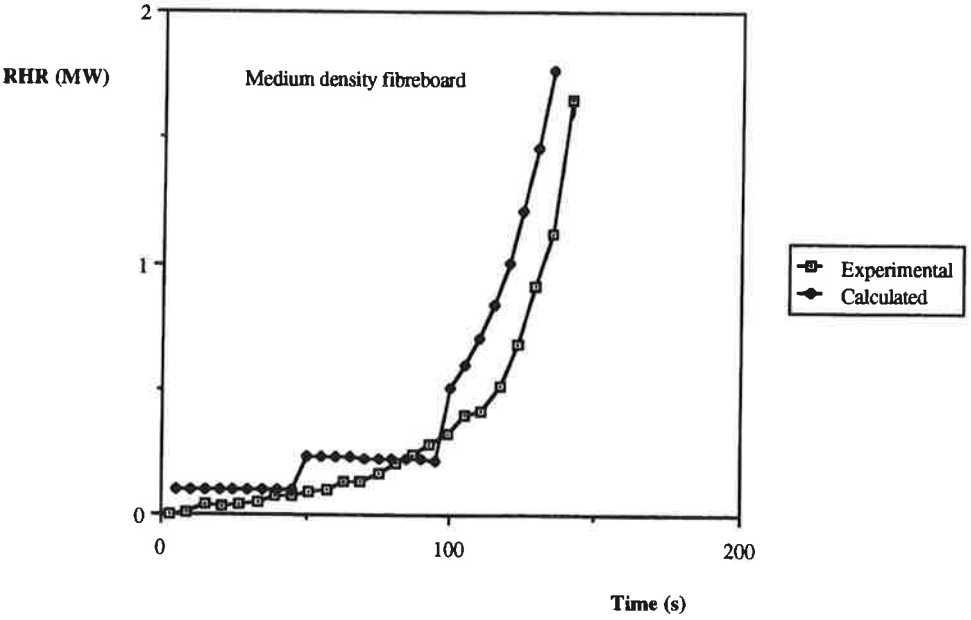

Material S3, RHR from full scale room test

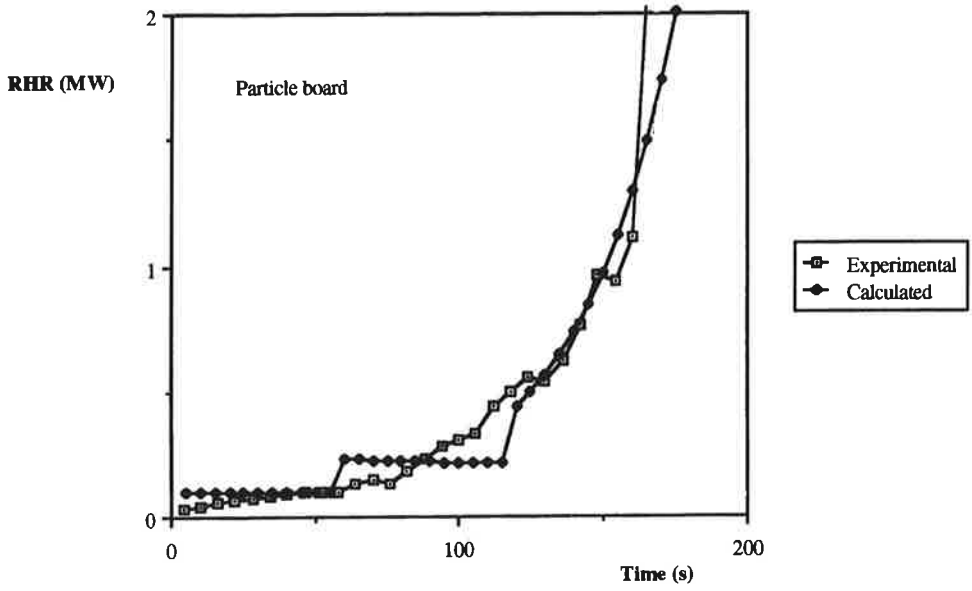

Material S4, RHR from full scale room test

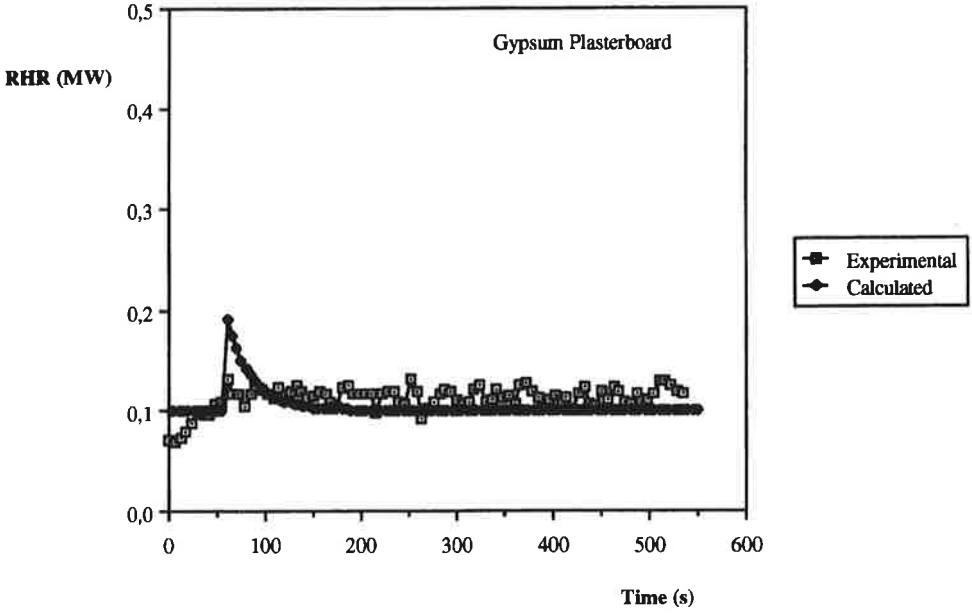

Material S5, RHR from full scale room test

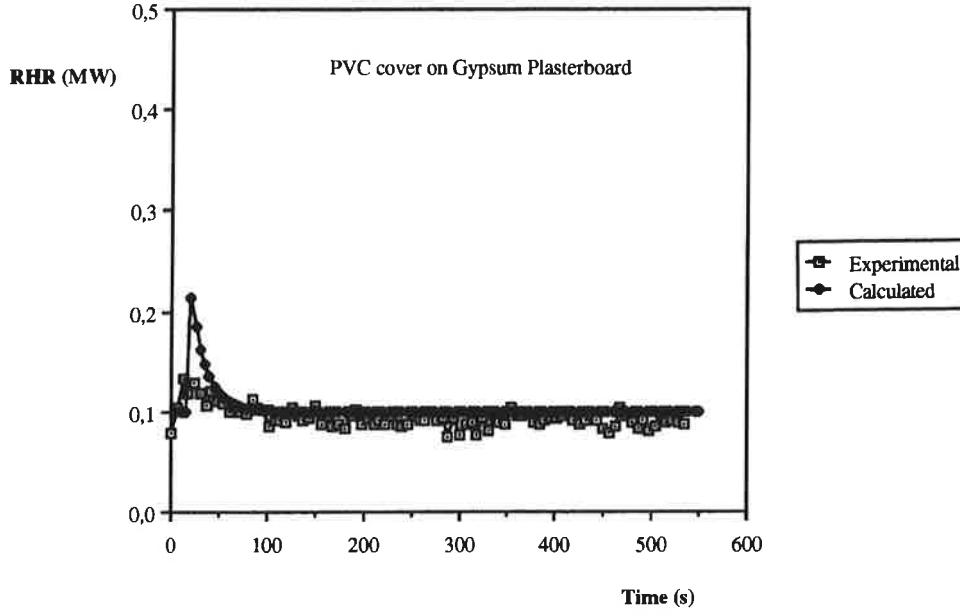

Material S6, RHR from full scale room test

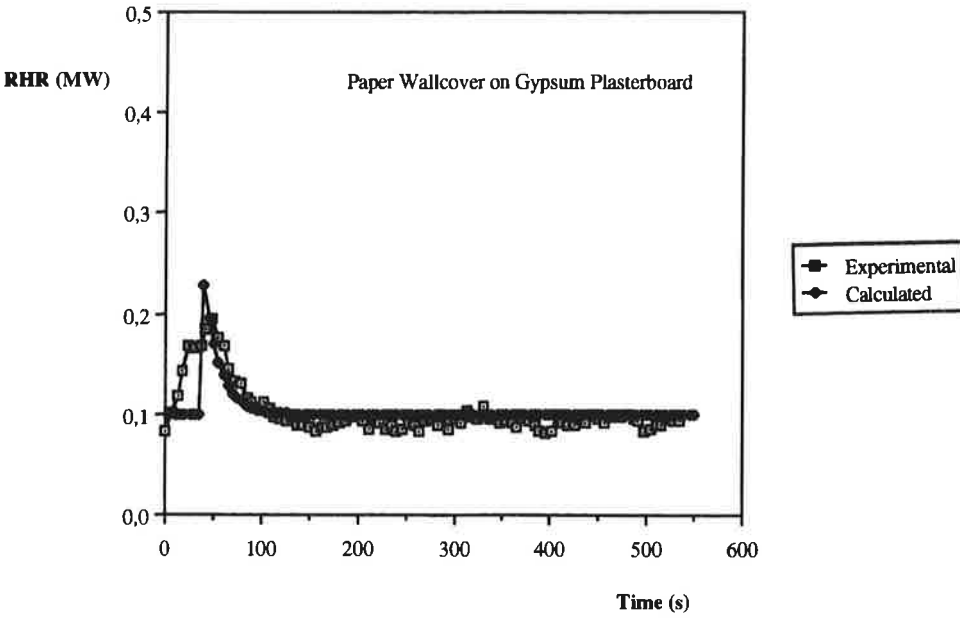

Material S7, RHR from full scale room test

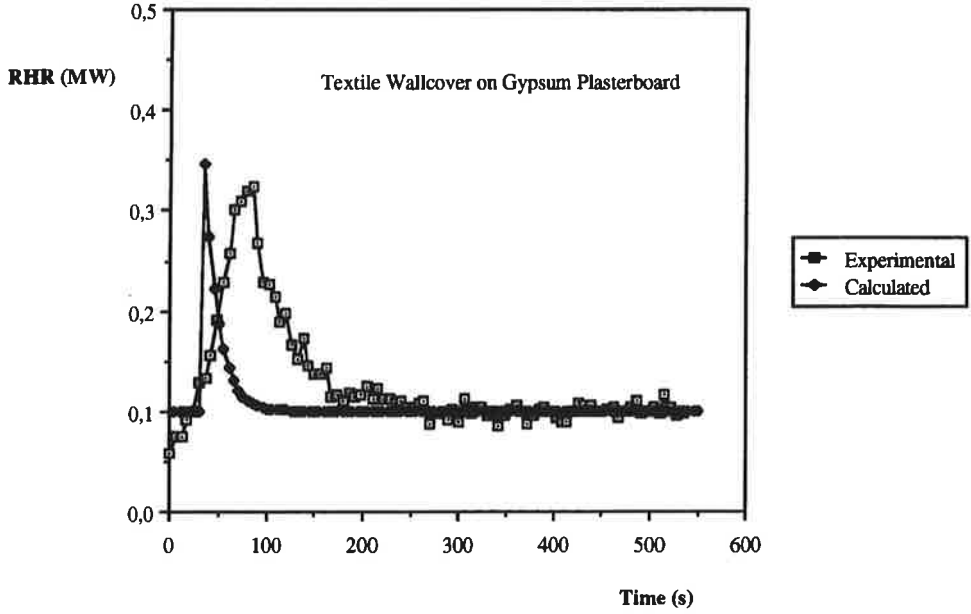

Material S8, RHR from full scale room test

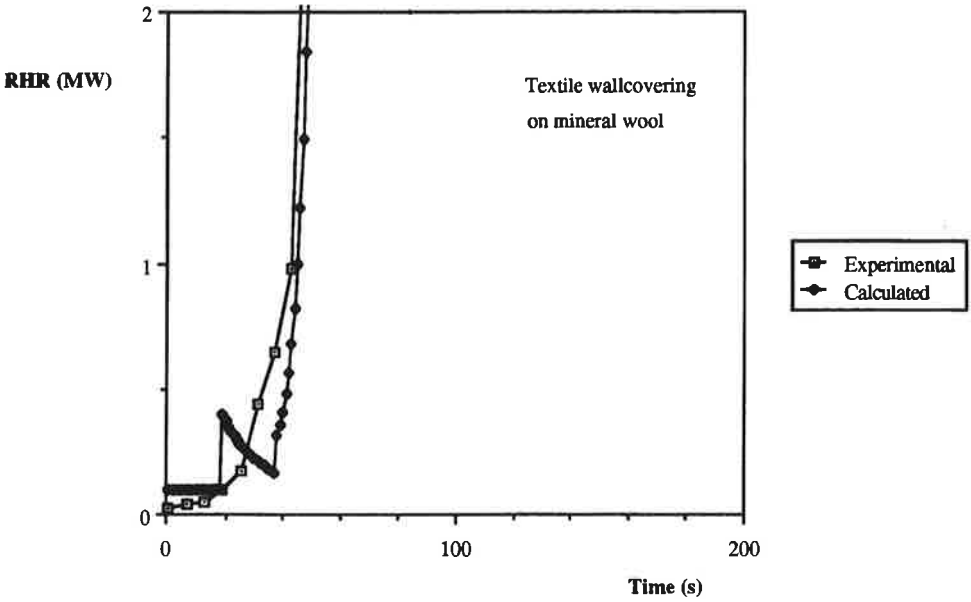

Material S9, RHR from full scale room test

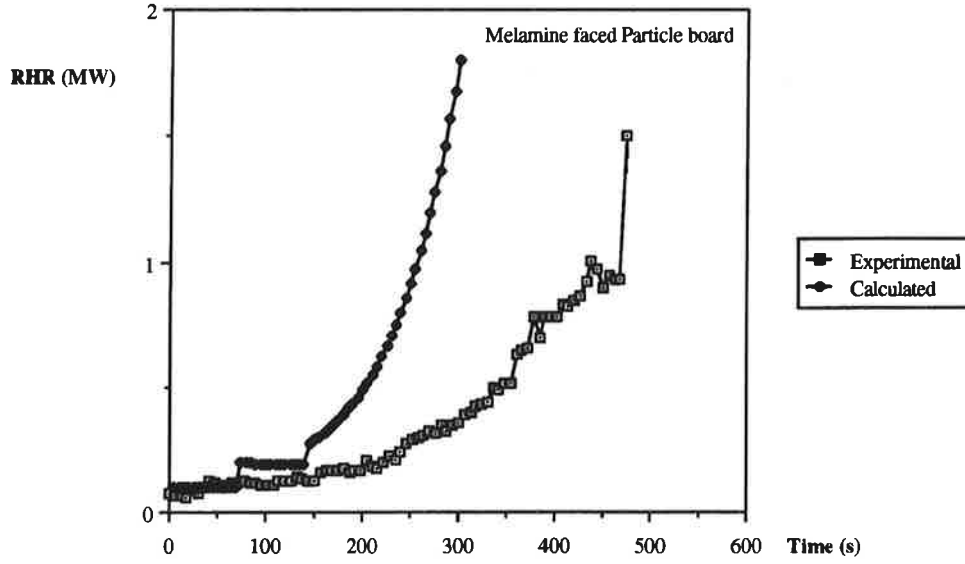

Material S11, RHR from full scale room test

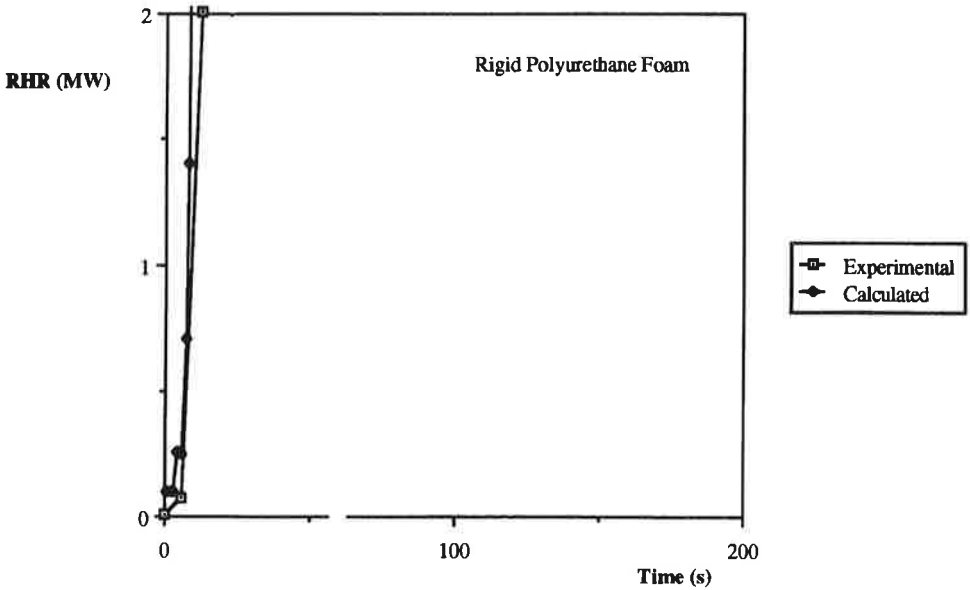

Material S12, RHR from full scale room test

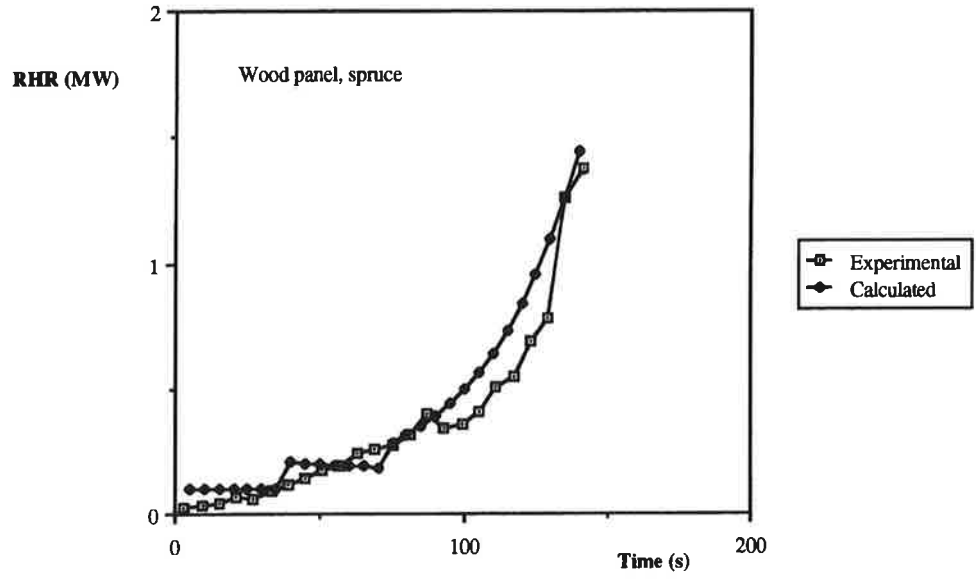

Material S13, RHR from full scale room test

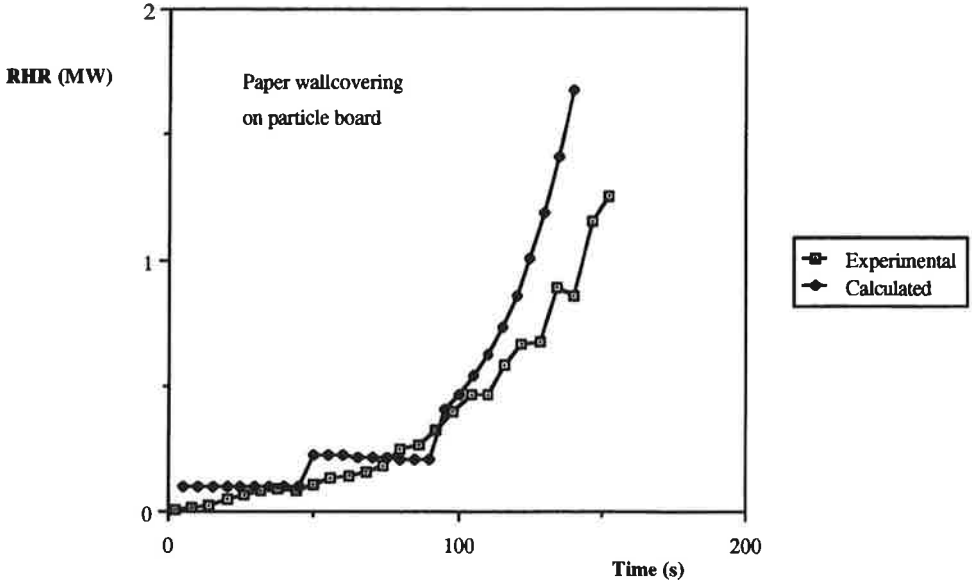

Appendix C

Results from Model A, Full scale experiments

Comparison of experimental and calculated data from full scale test series, Scenario A.

Rate of heat release and gas temperatures, 22 materials.

Material S1, full scale test, Model A
Rate of heat release

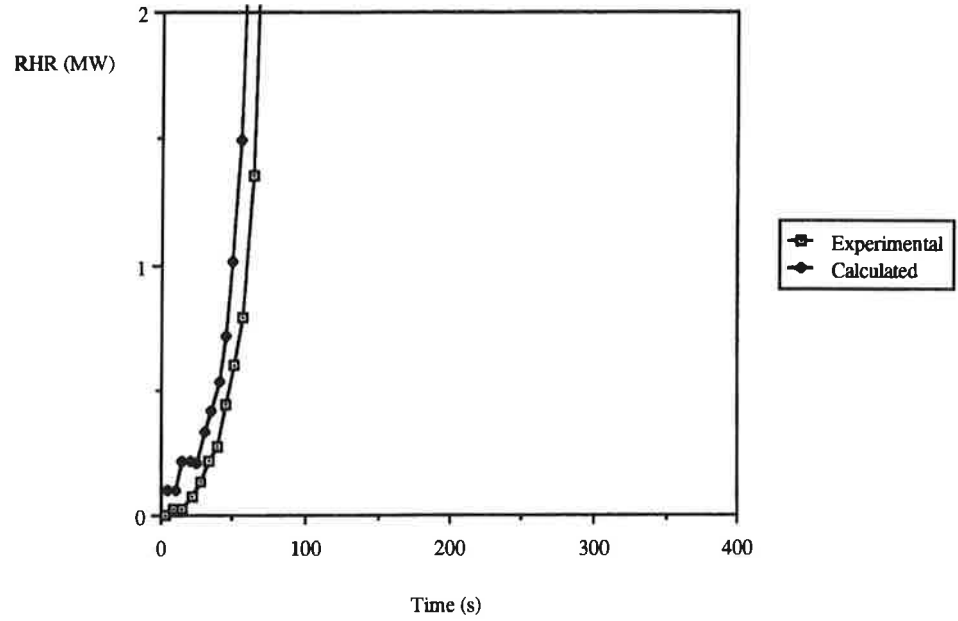

Material S1, full scale test, Model A
Gas temperature

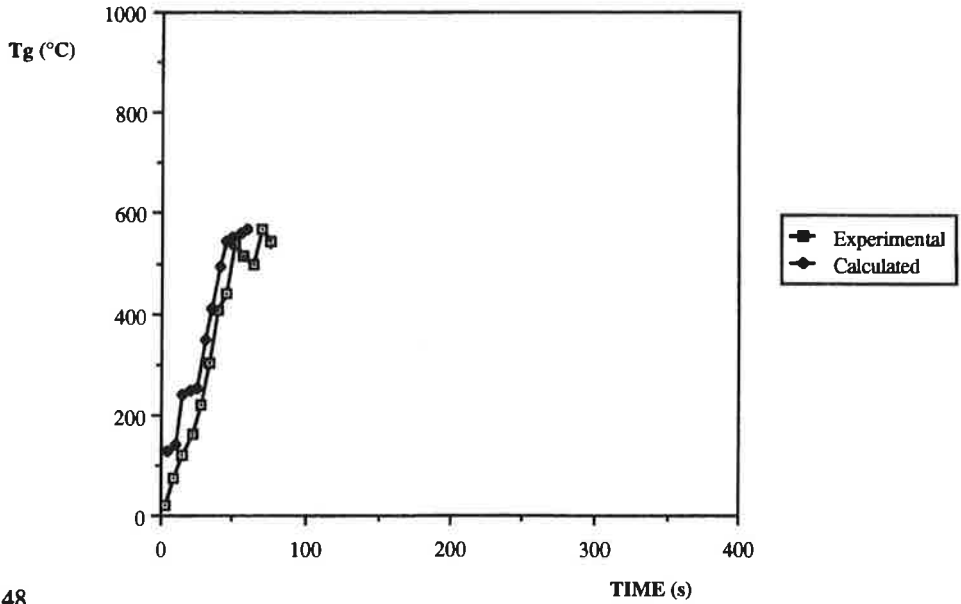

Material S2, full scale test, Model A
Rate of heat release

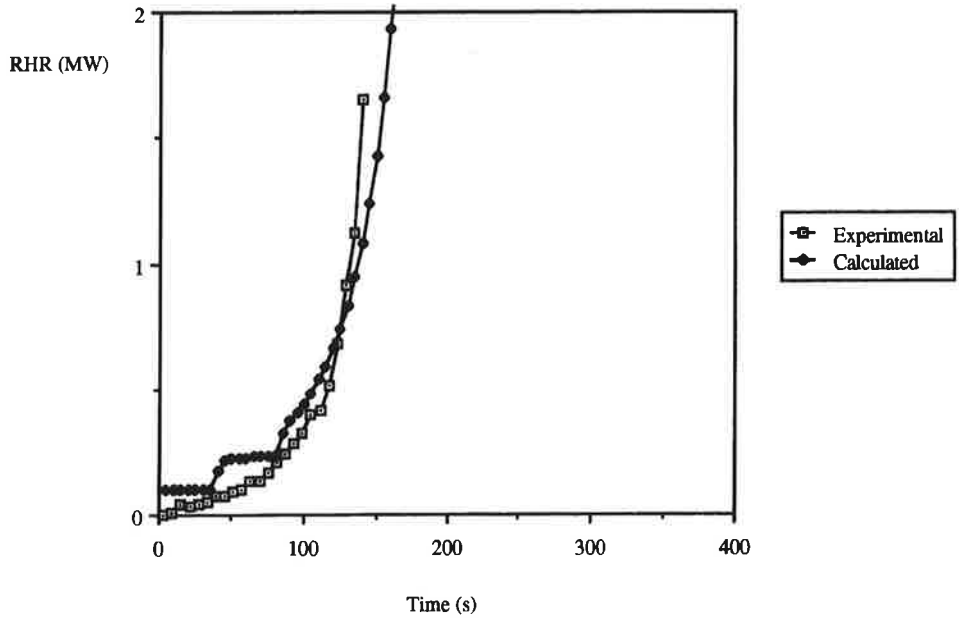

Material S2, full scale test, Model A
Gas temperature

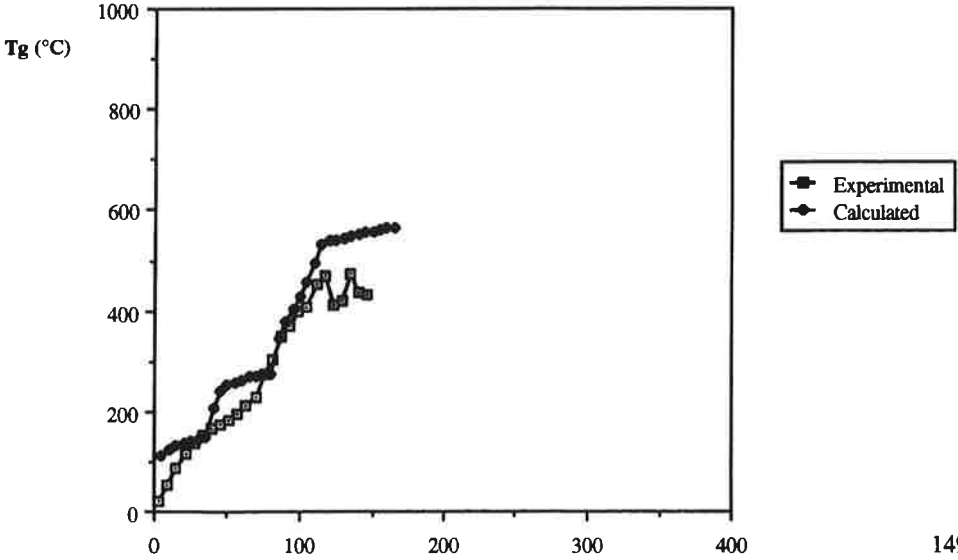

Material S3, full scale test, Model A
Rate of heat release

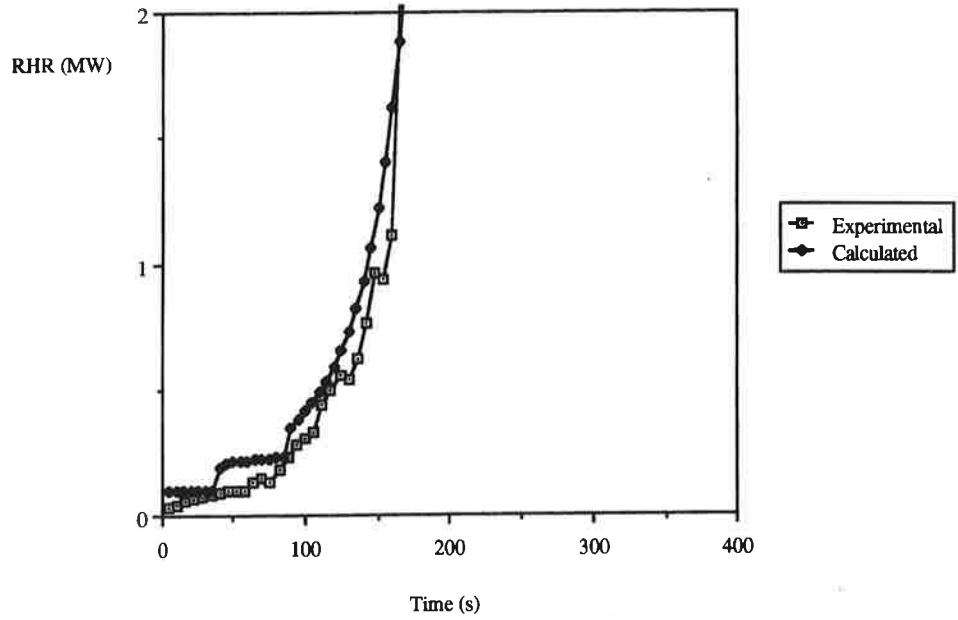

Material S3, full scale test, Model A
Gas temperature

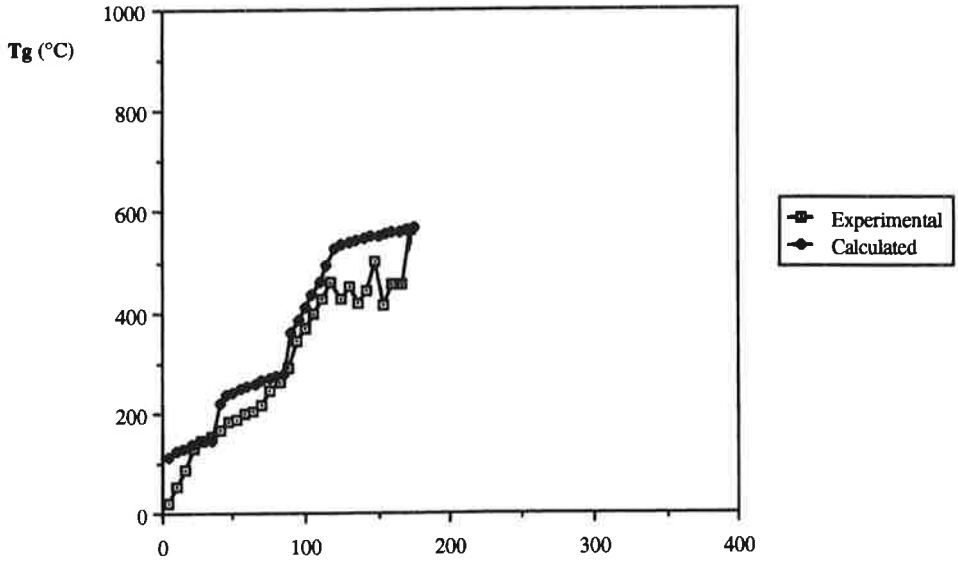

Material S4, full scale test, Model A
Rate of heat release

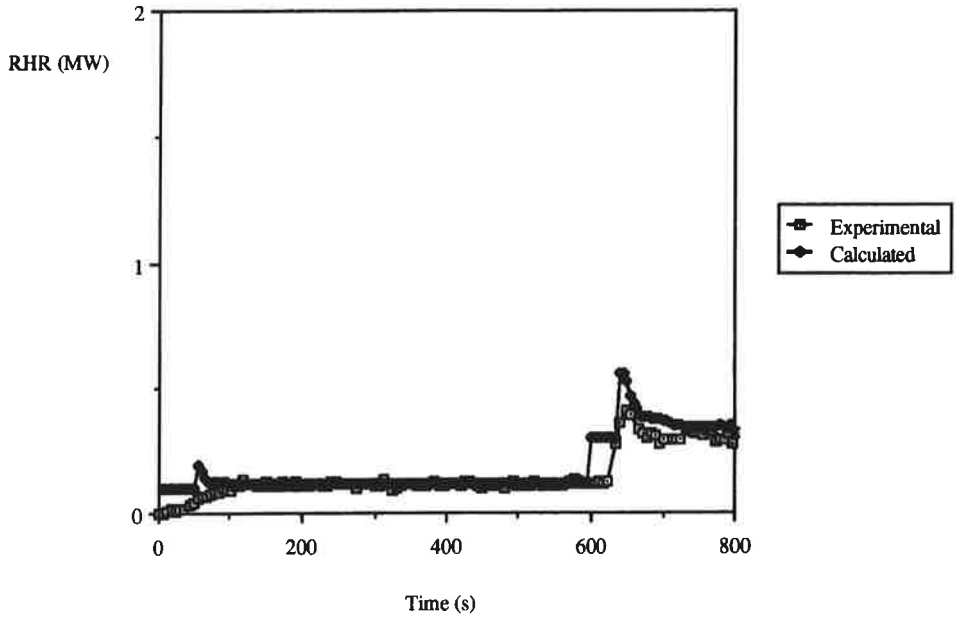

Material S4, full scale test, Model A
Gas temperature

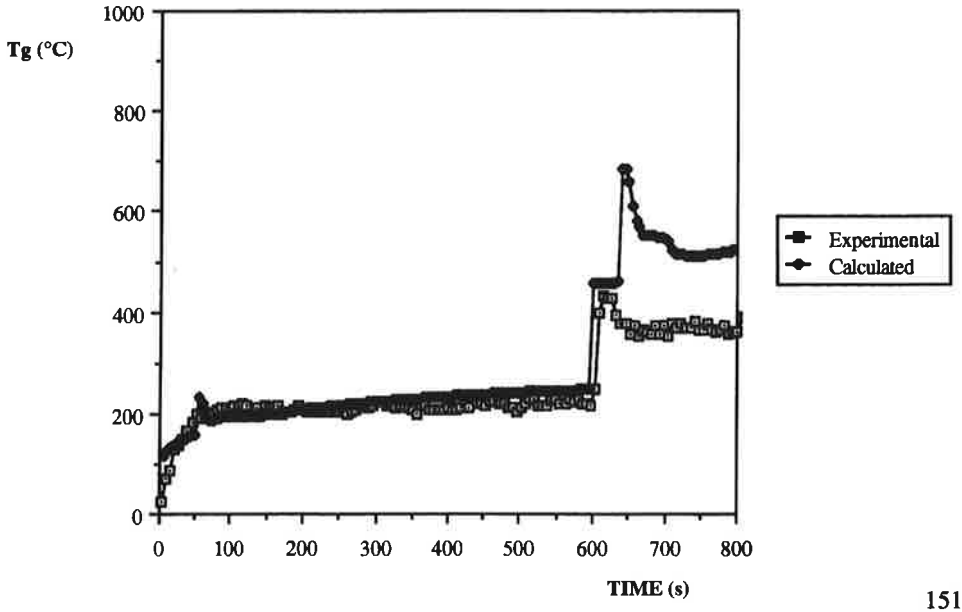

Material S5, full scale test, Model A

Rate of heat release

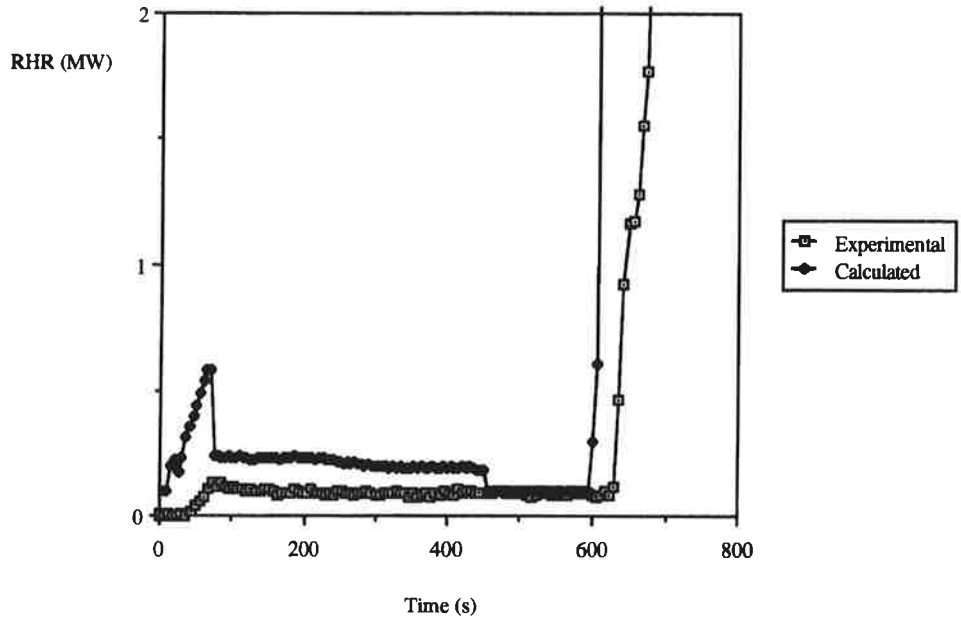

Material S5, full scale test, Model A

Gas temperature

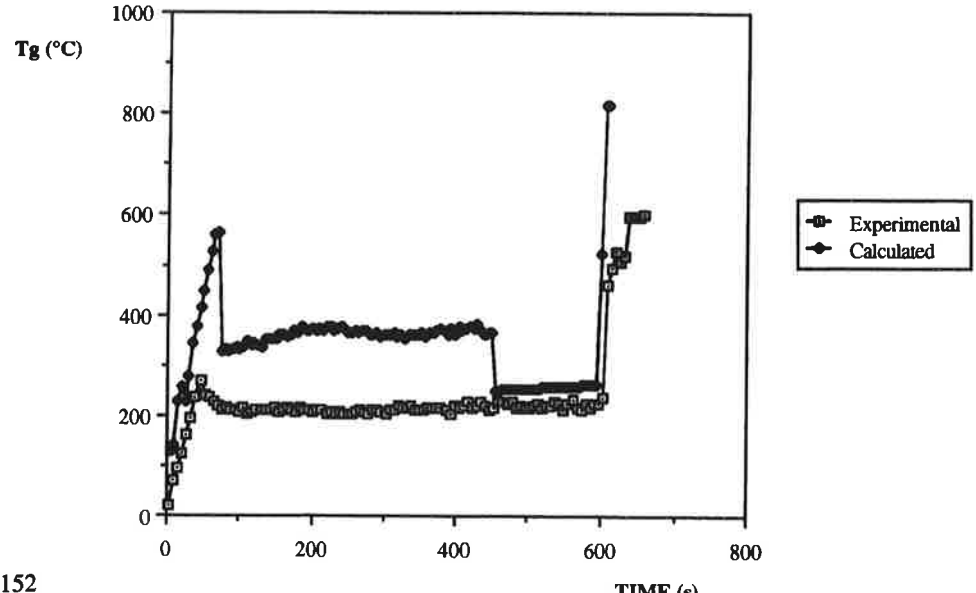

Material S6, full scale test, Model A
Rate of heat release

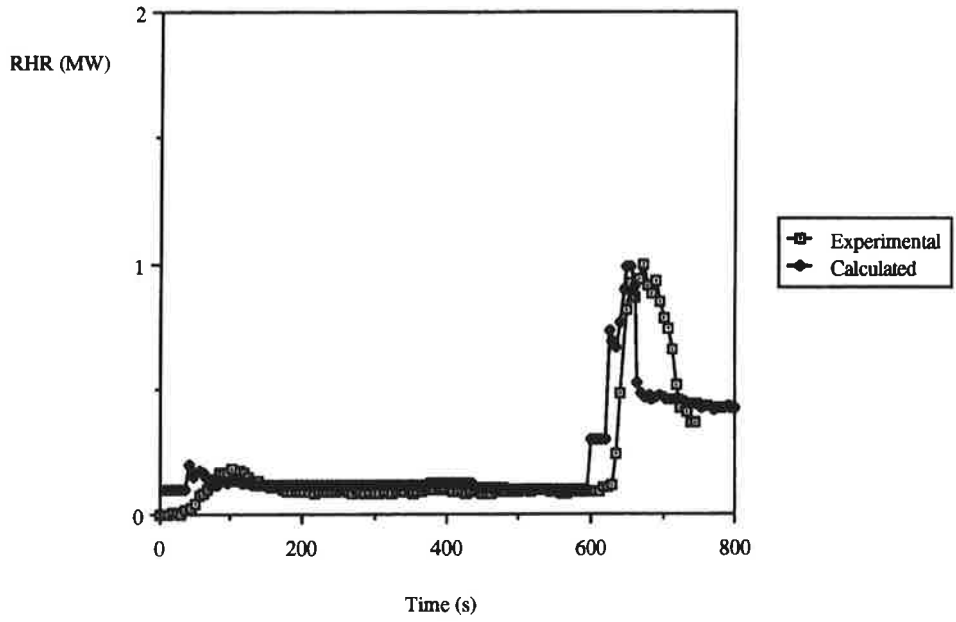

Material S6, full scale test, Model A
Gas temperature

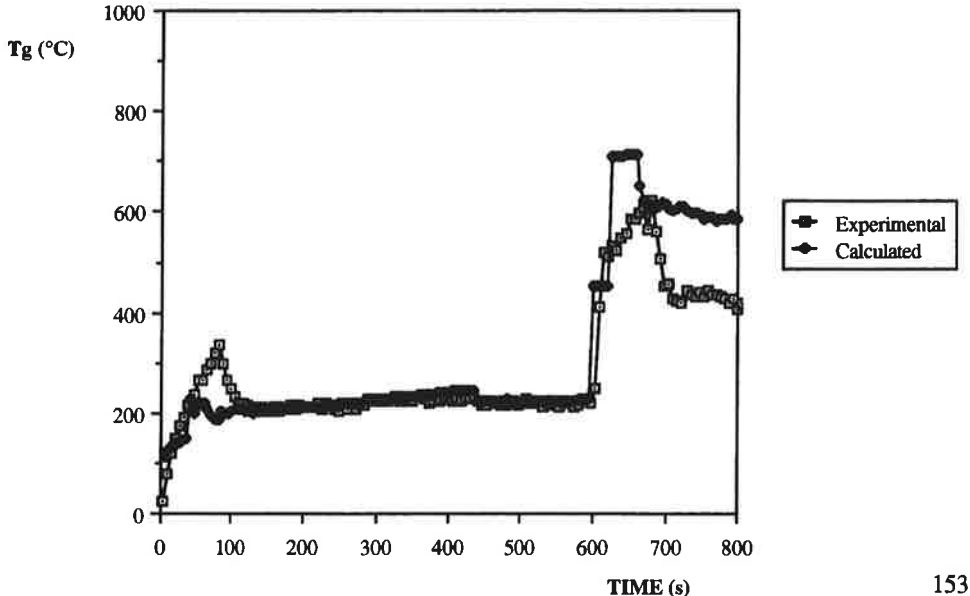

Material S7, full scale test, Model A
Rate of heat release

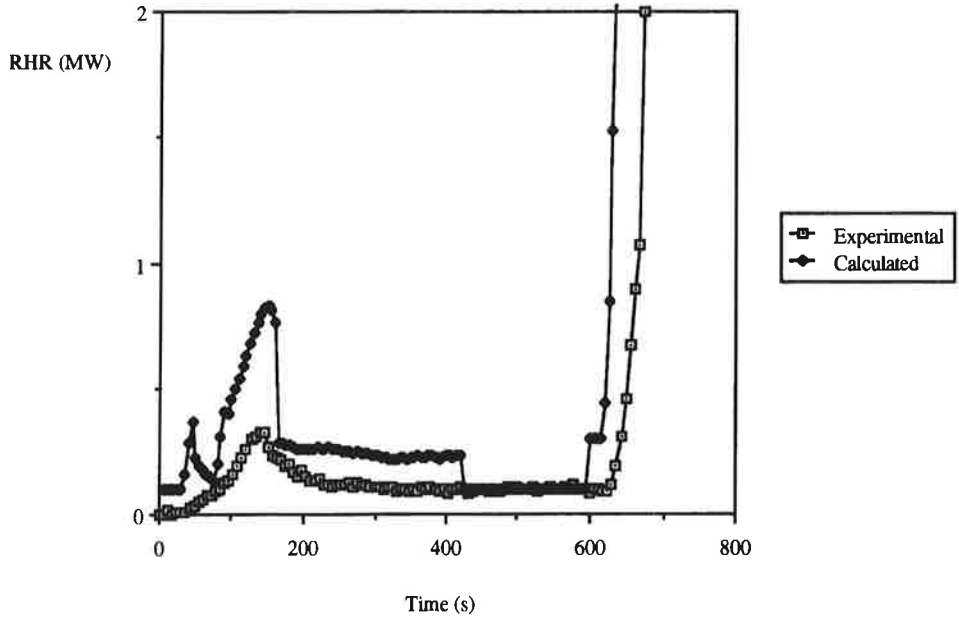

Material S7, full scale test, Model A
Gas temperature

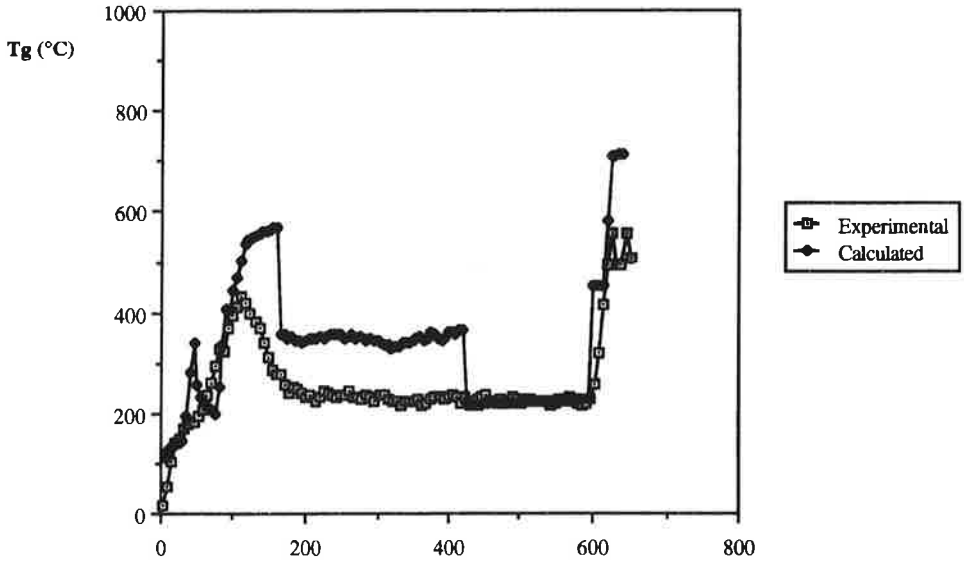

Material S8, full scale test, Model A
Rate of heat release

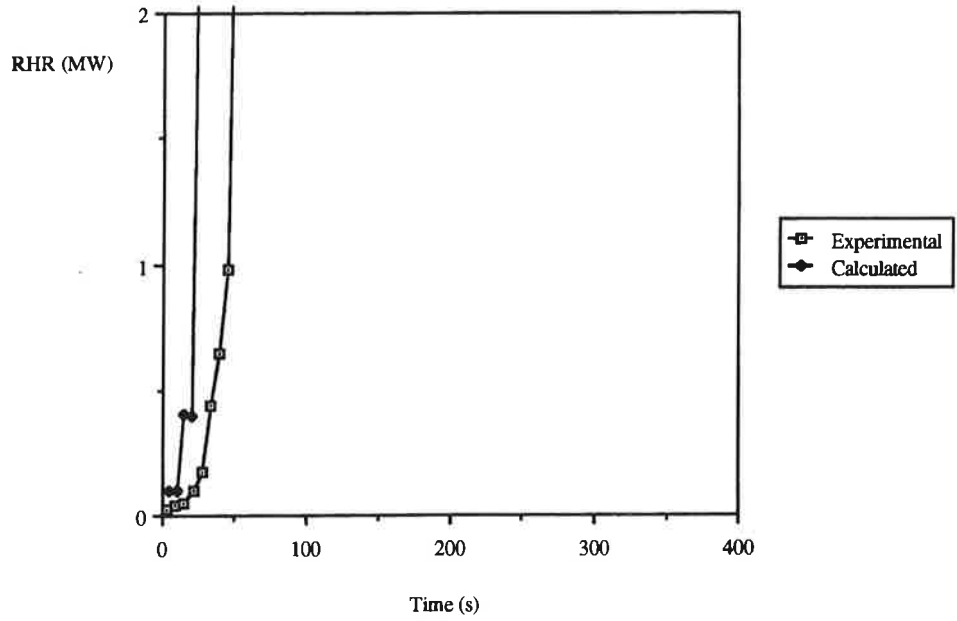

Material S8, full scale test, Model A
Gas temperature

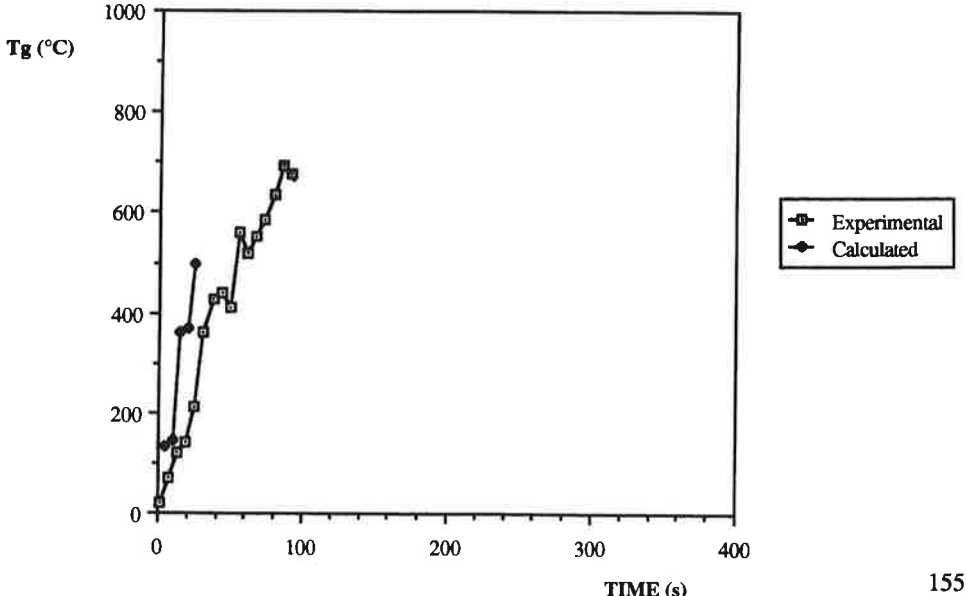

Material S9, full scale test, Model A
Rate of heat release

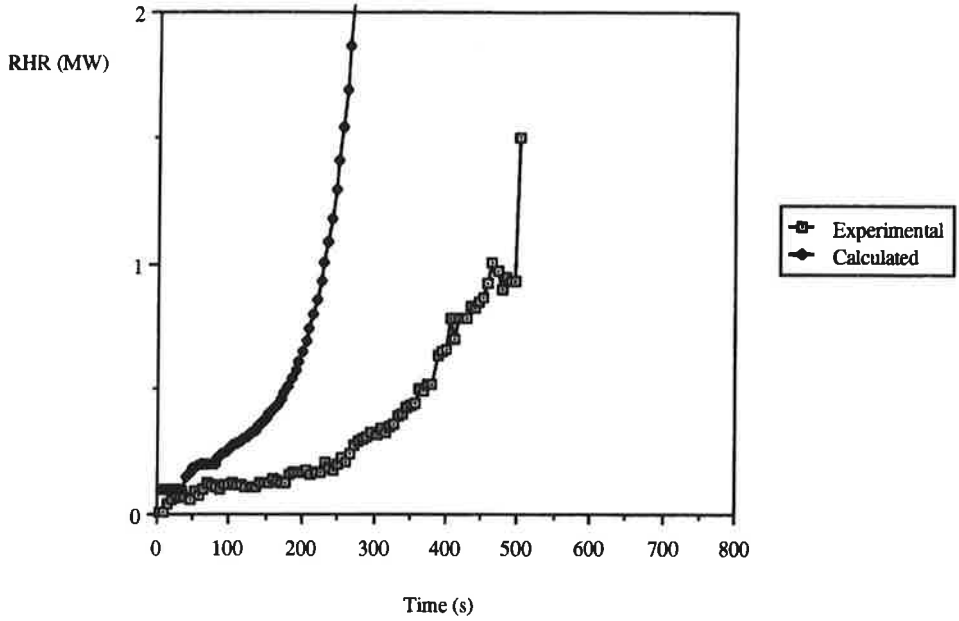

Material S9, full scale test, Model A
Gas temperature

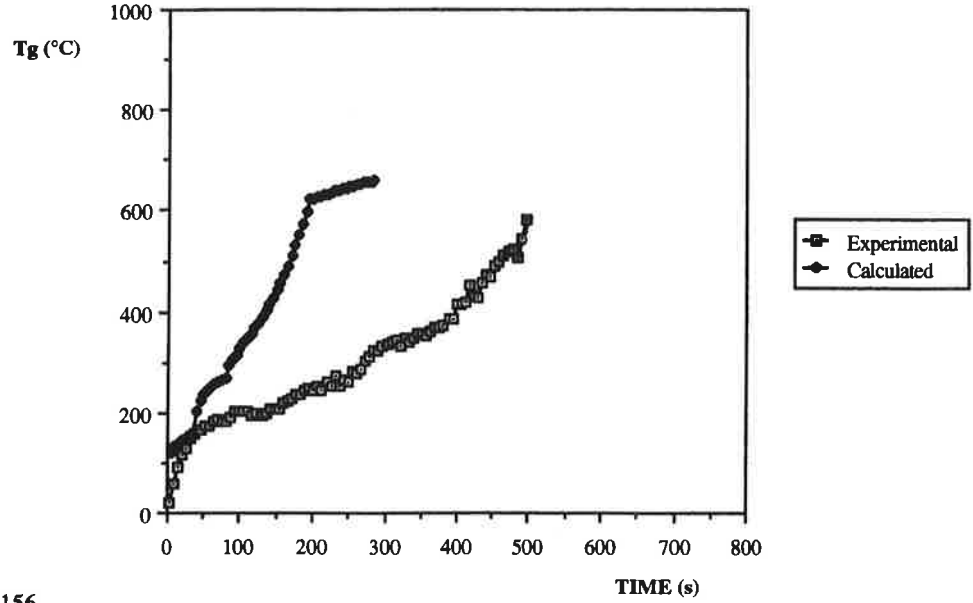

Material S10, full scale test, Model A

Rate of heat release

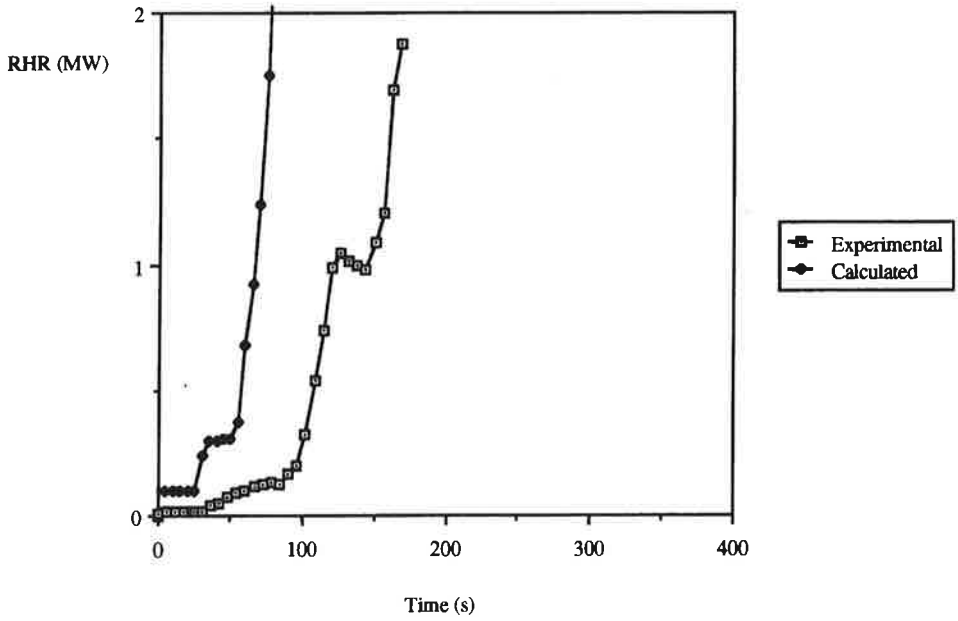

Material S10, full scale test, Model A

Gas temperature

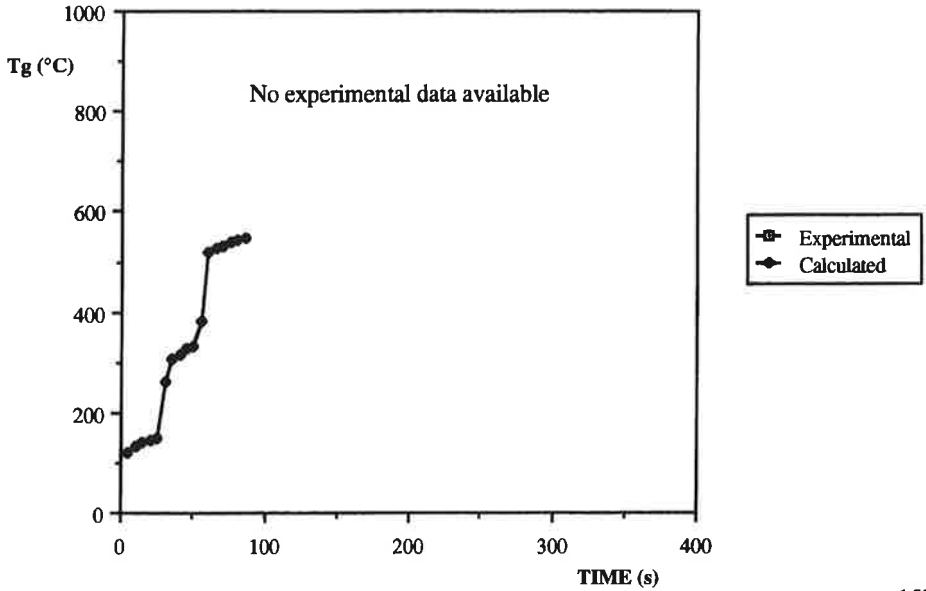

Material S11, full scale test, Model A
Rate of heat release

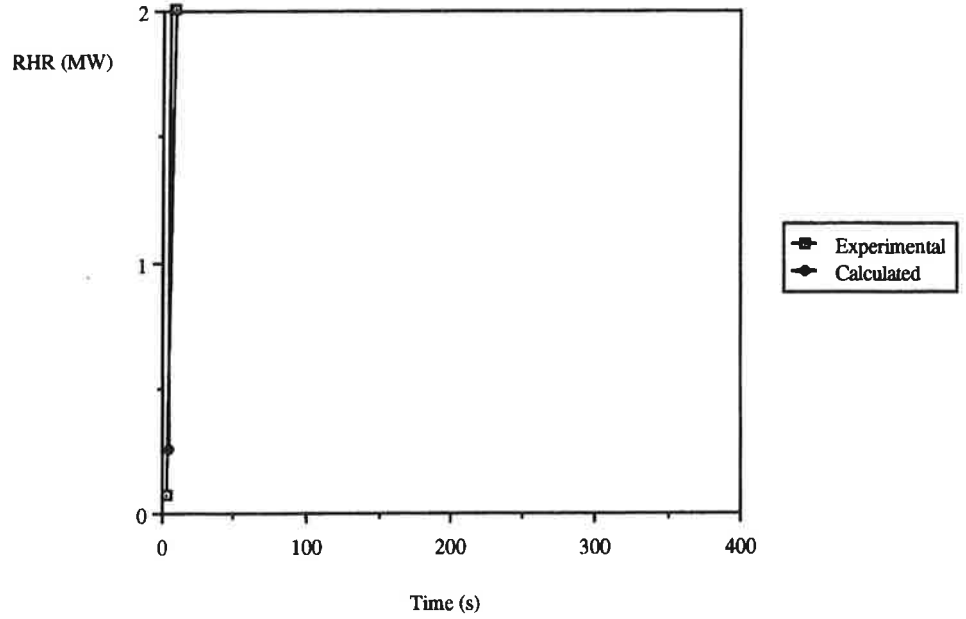

Material S11, full scale test, Model A
Gas temperature

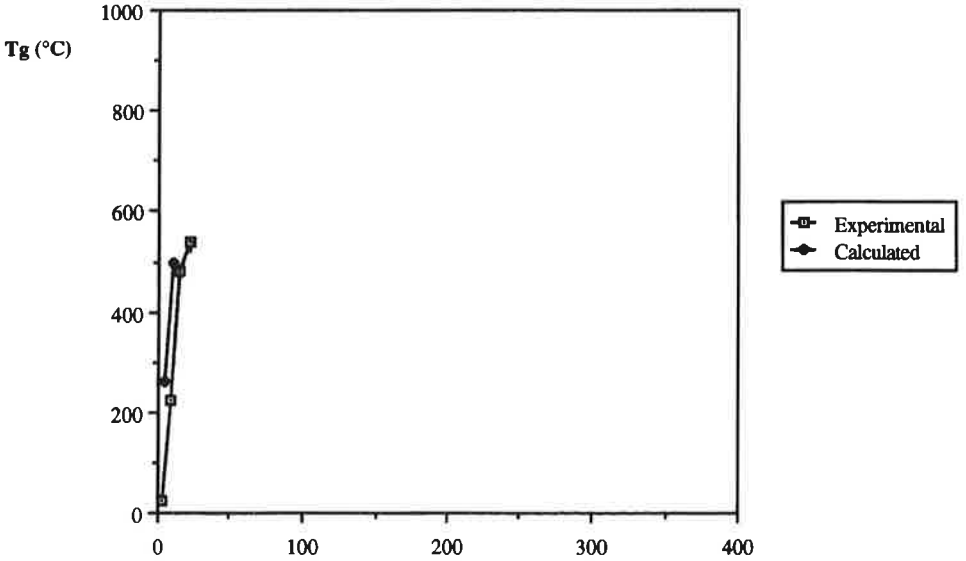

Material S12, full scale test, Model A
Rate of heat release

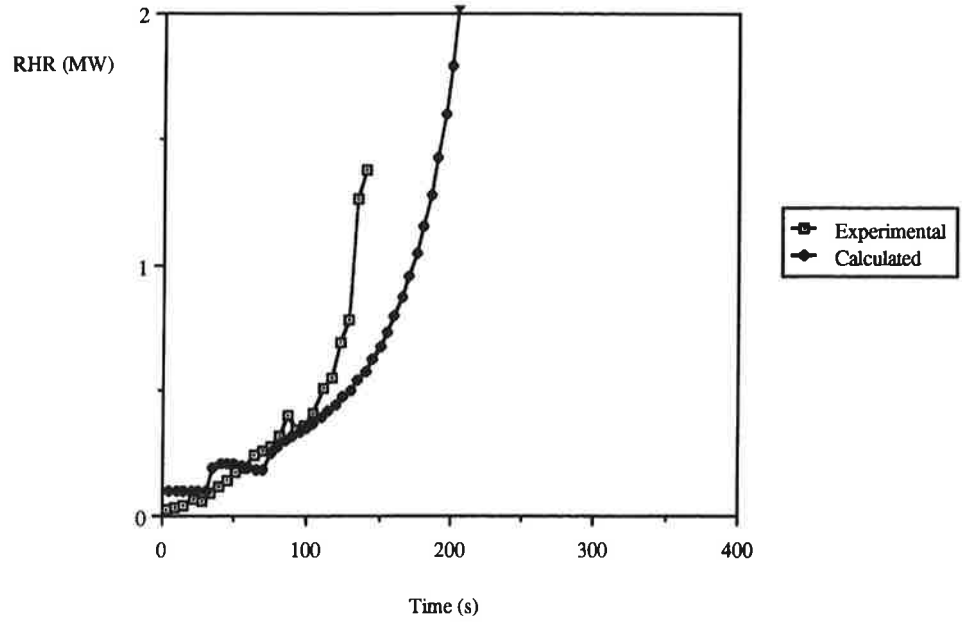

Material S12, full scale test, Model A
Gas temperature

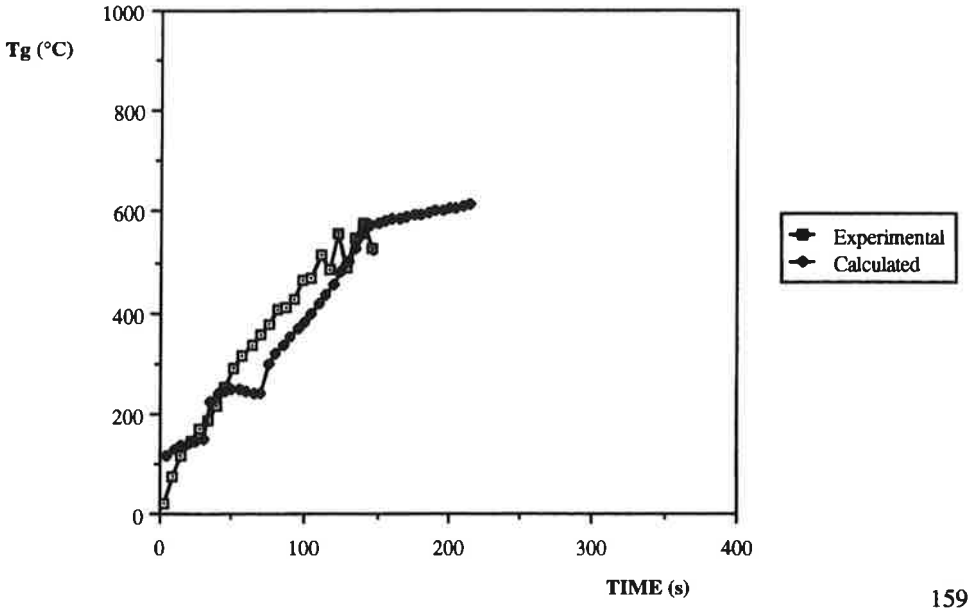

Material S13, full scale test, Model A
Rate of heat release

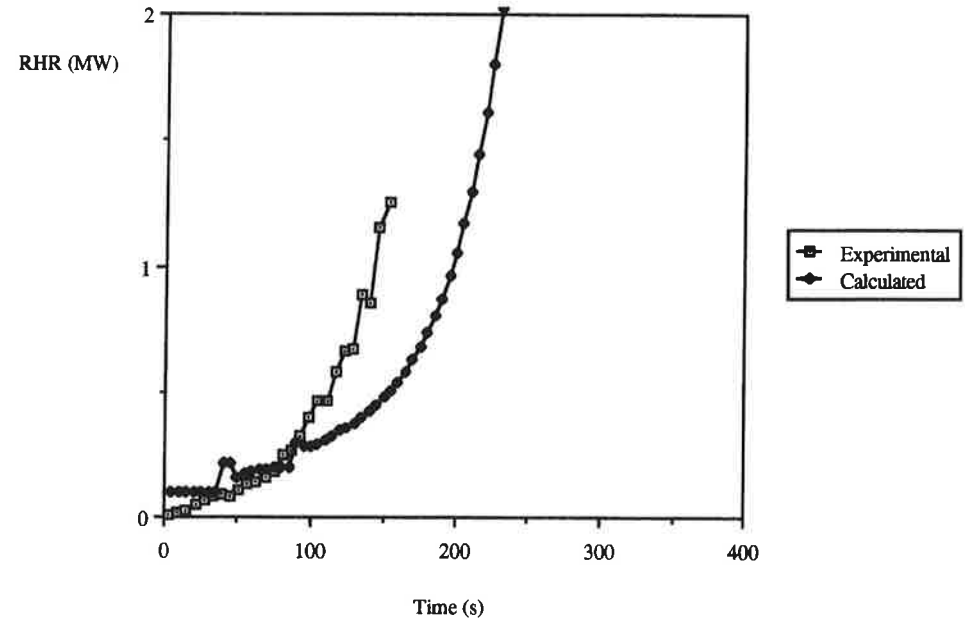

Material S13, full scale test, Model A
Gas temperature

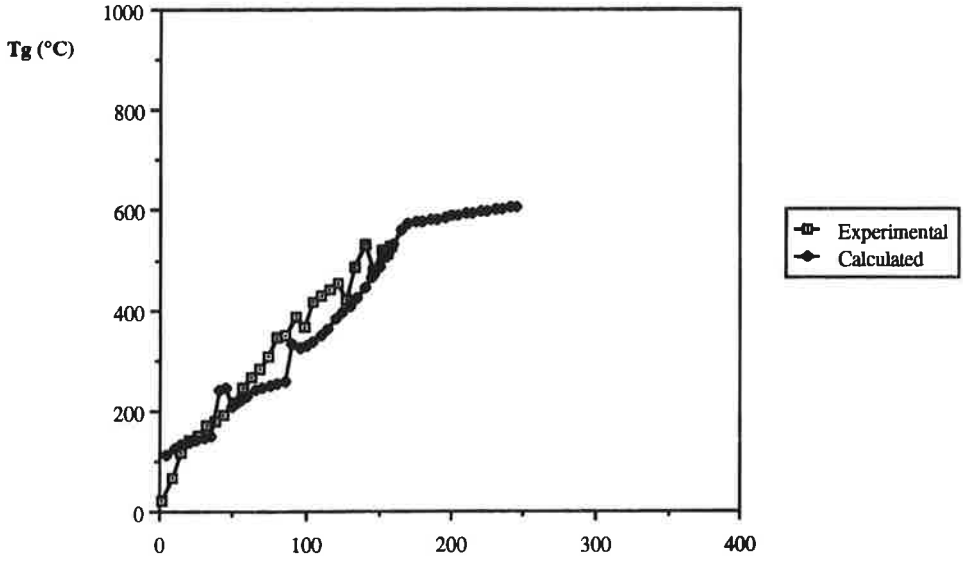

Material E1, full scale test, Model A

Rate of heat release

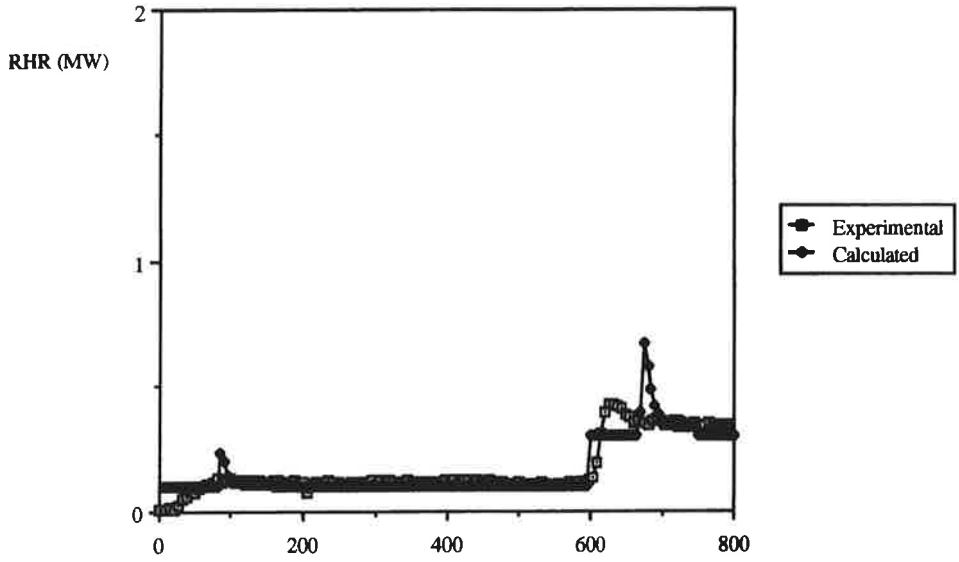

Material E2, full scale test, Model A

Gas temperature

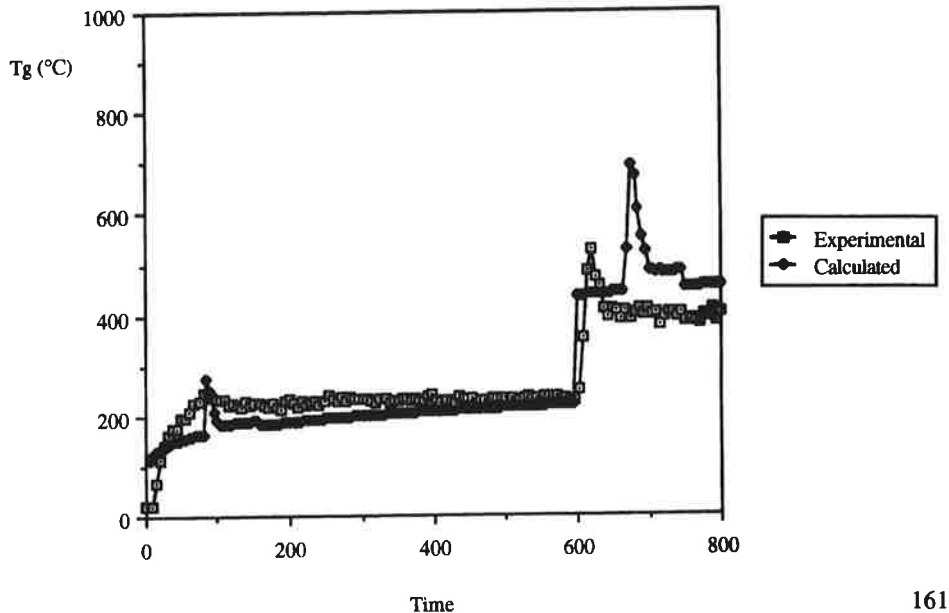

Material E2, full scale test, Model A
Rate of heat release

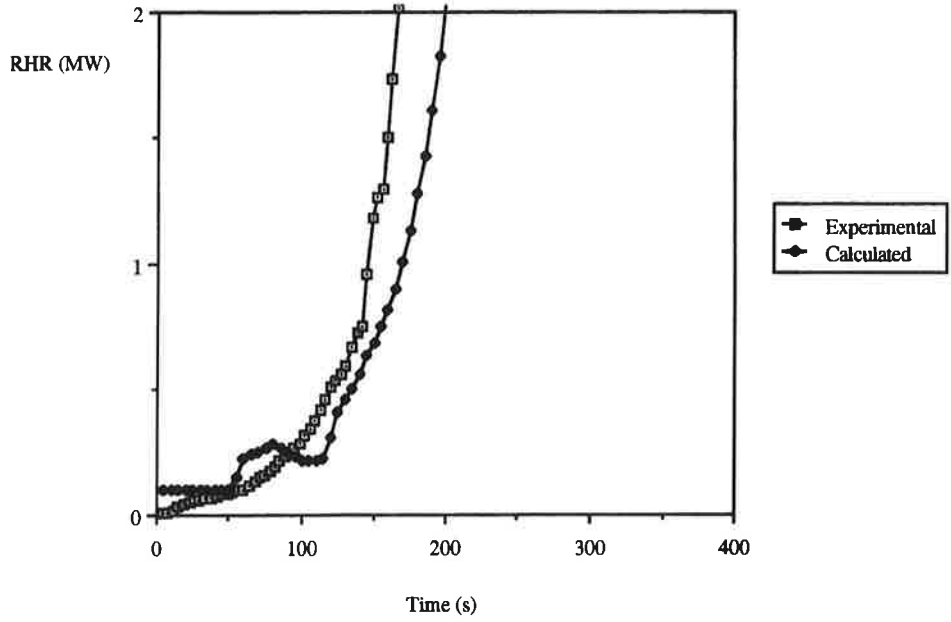

Material E2, full scale test, Model A
Gas temperature

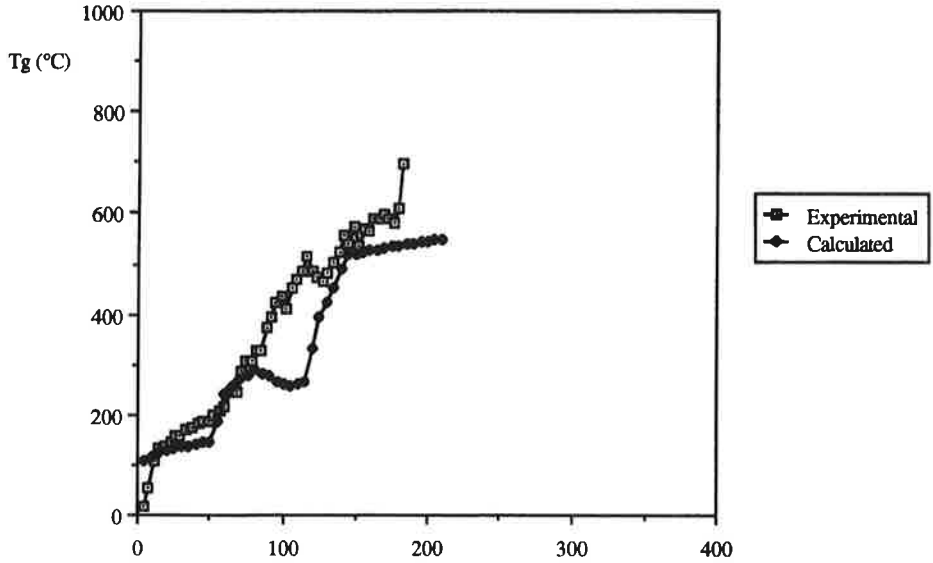

Material E3, full scale test, Model A
Rate of heat release

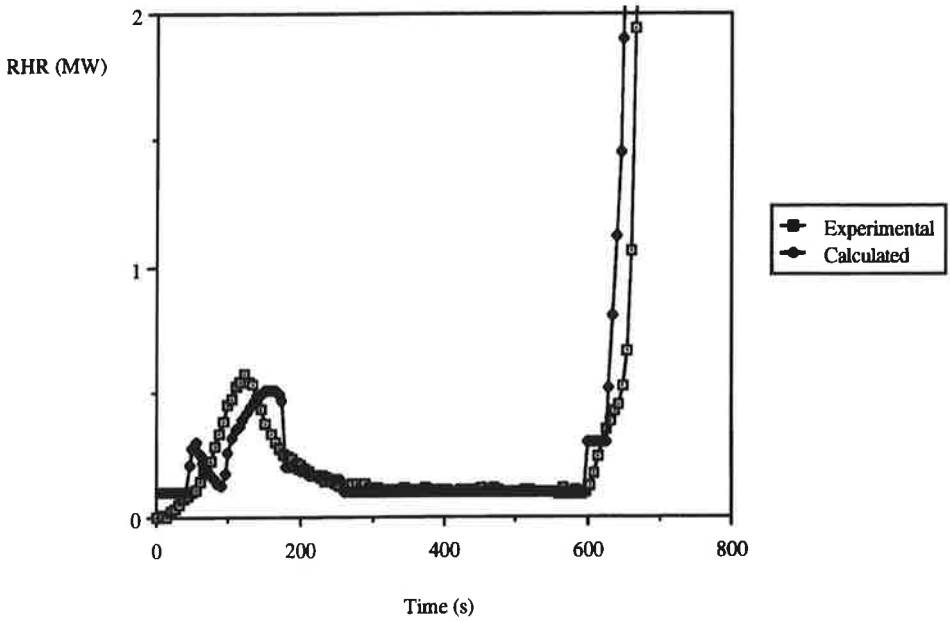

Material E3, full scale test, Model A
Gas temperature

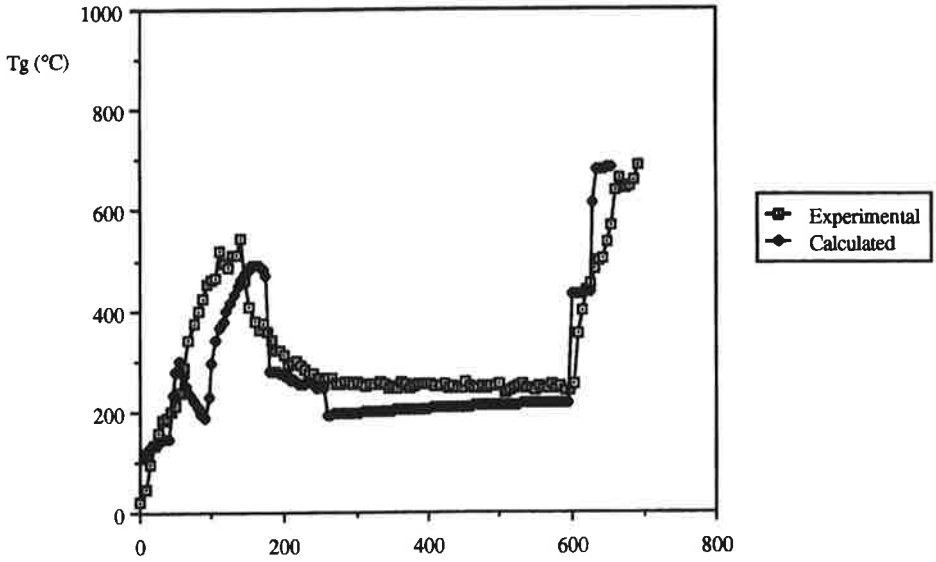

Material E4, full scale test, Model A
Rate of heat release

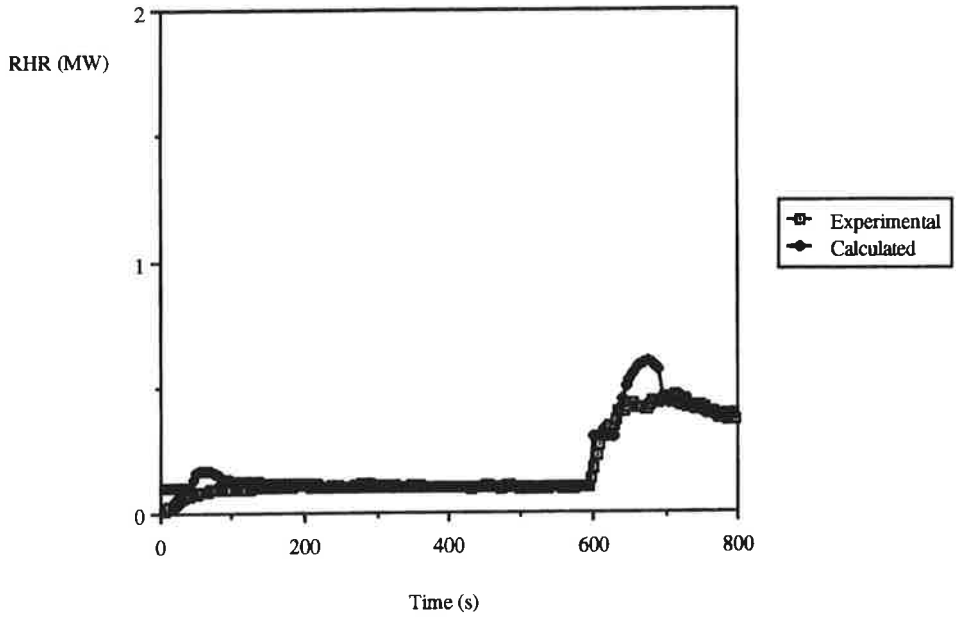

Material E4, full scale test, Model A
Gas temperature

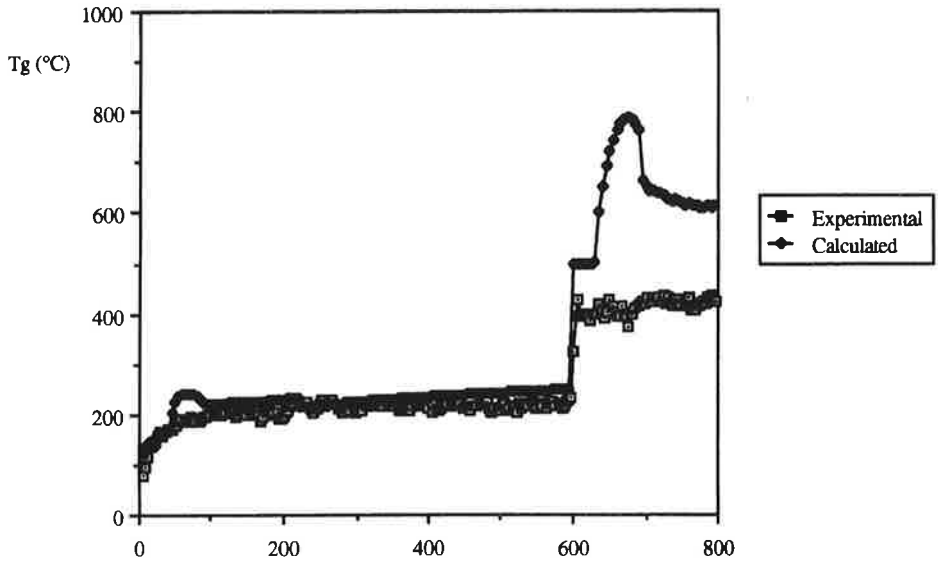

Material E5, full scale test, Model A
Rate of heat release

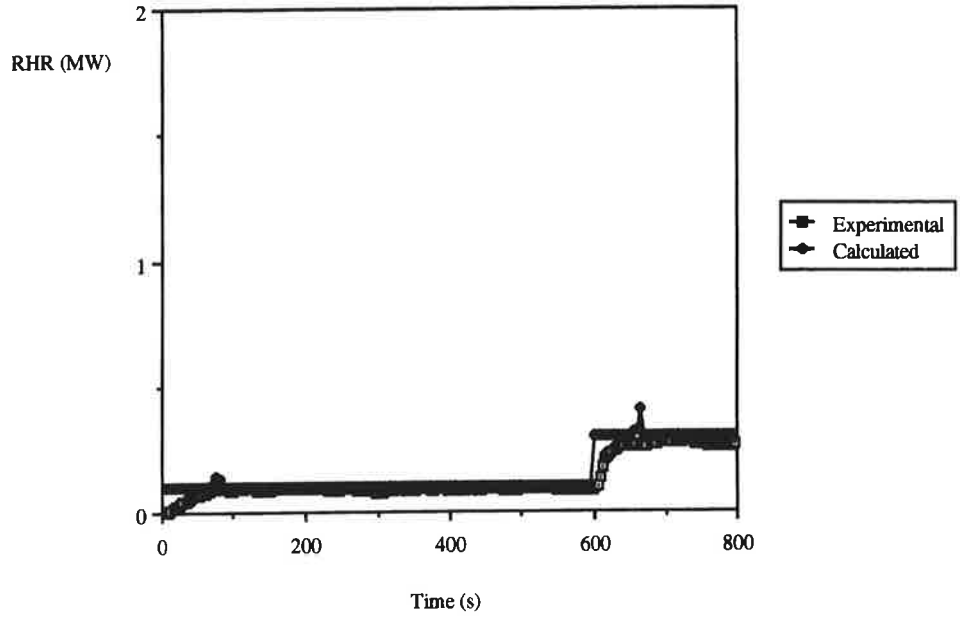

Material E5, full scale test, Model A
Gas temperature

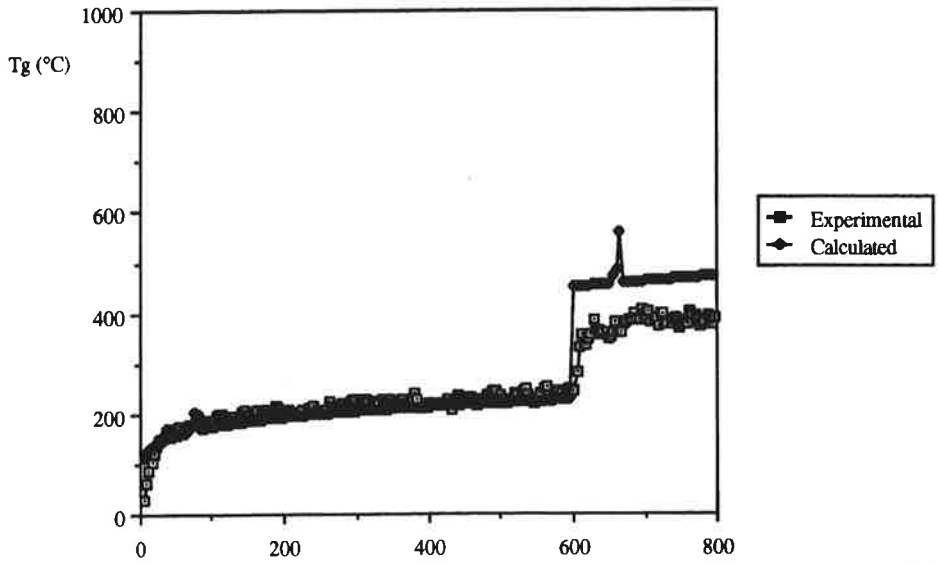

Material E7, full scale test, Model A
Rate of heat release

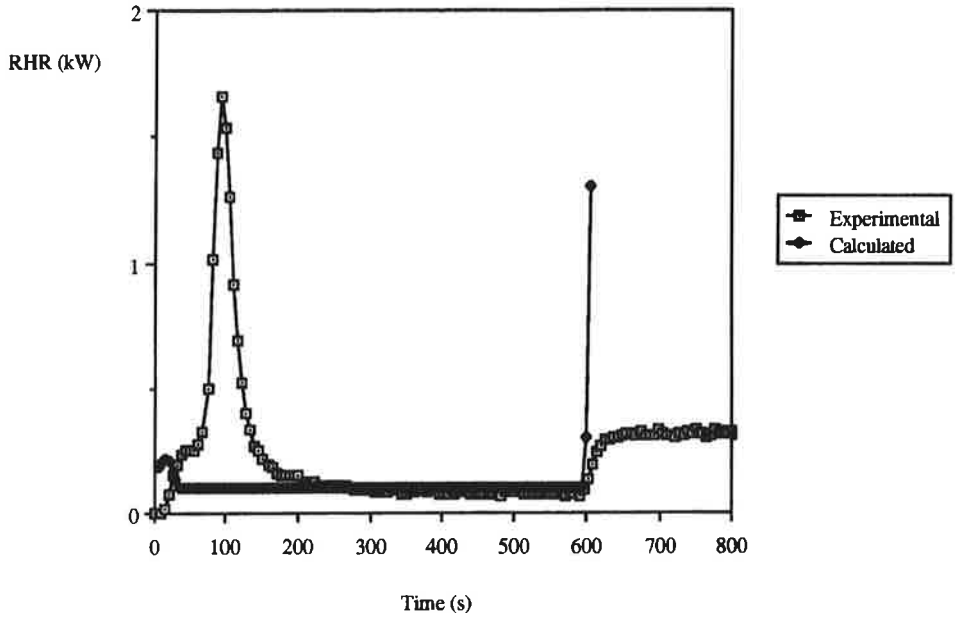

Material E7, full scale test, Model A
Gas temperature

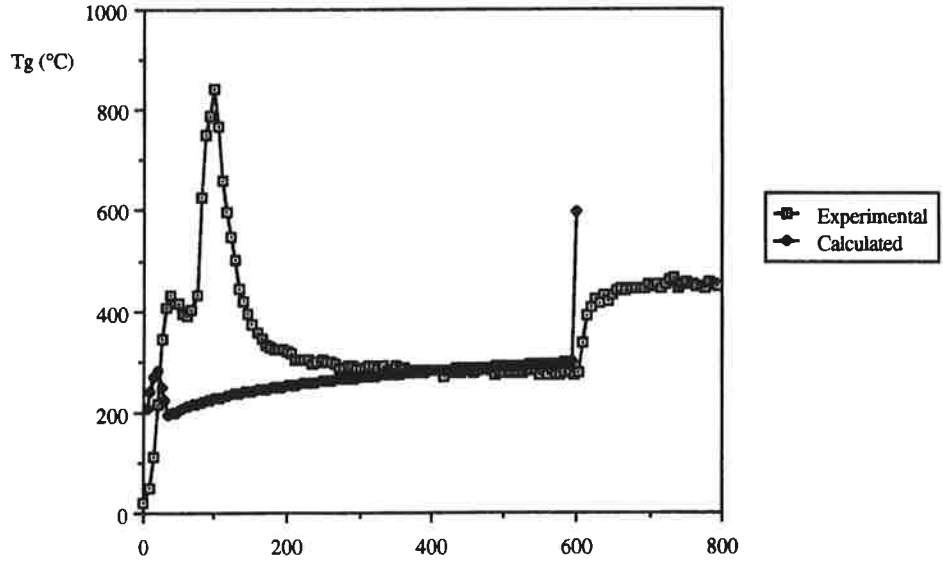

Material E9, full scale test, Model A
Rate of heat release

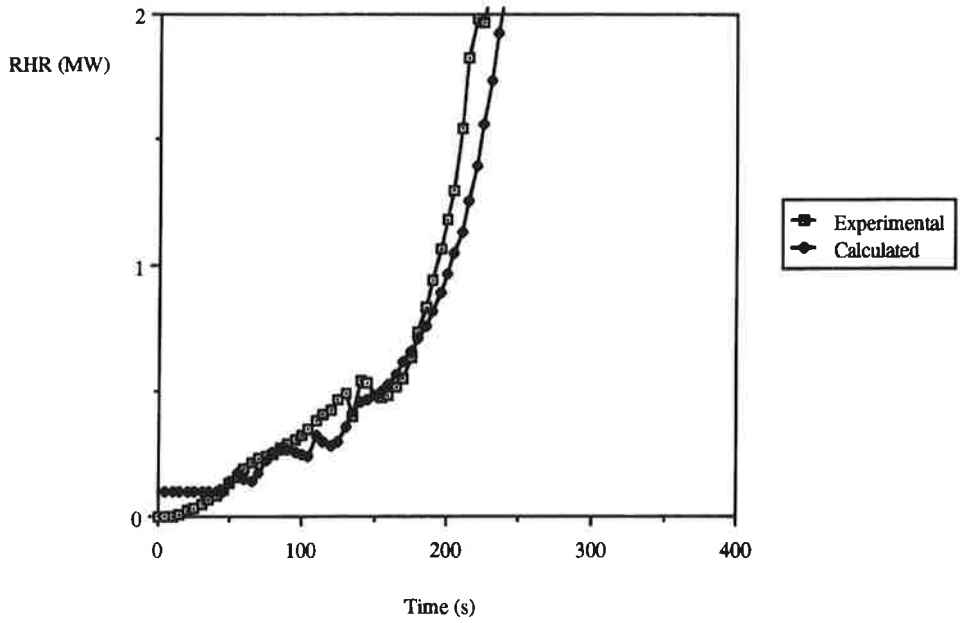

Material E9, full scale test, Model A
Gas temperature

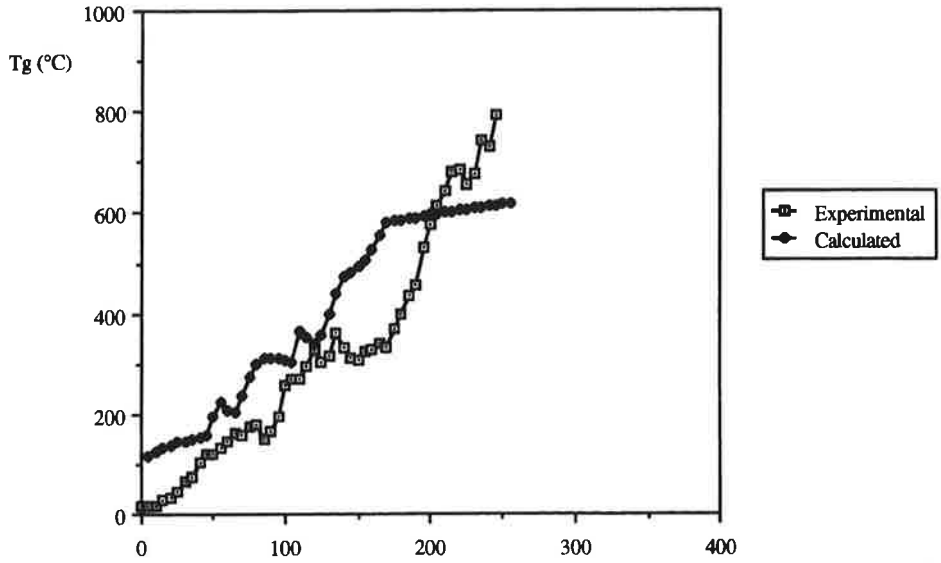

Material E10, full scale test, Model A
Rate of heat release

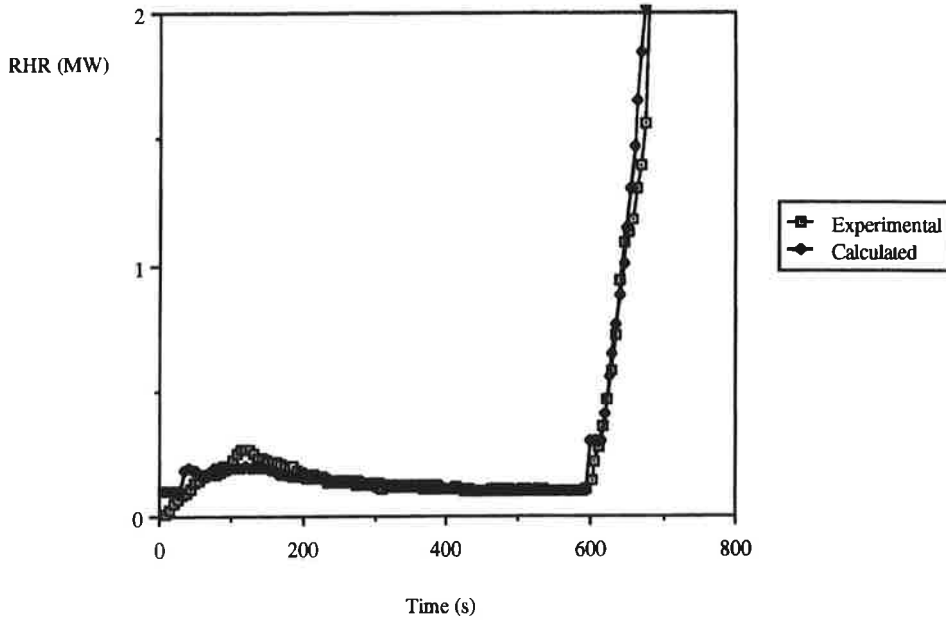

Material E10, full scale test, Model A
Gas temperature

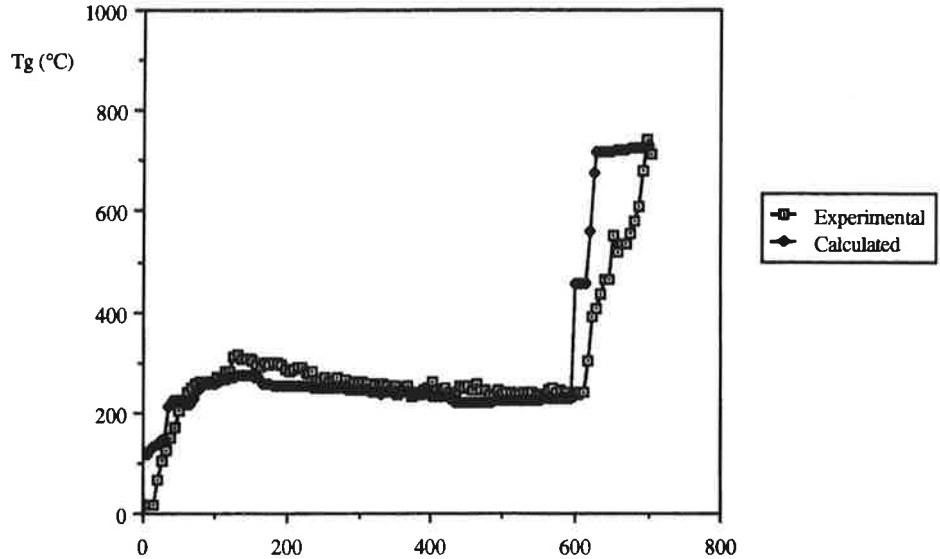

Material E11, full scale test, Model A
Rate of heat release

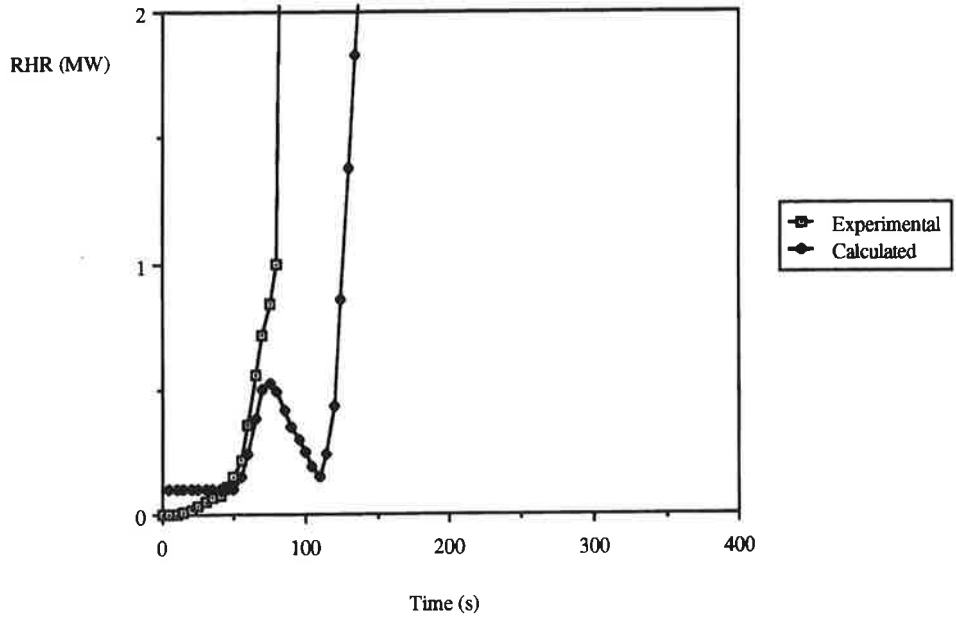

Material E11, full scale test, Model A
Gas temperature

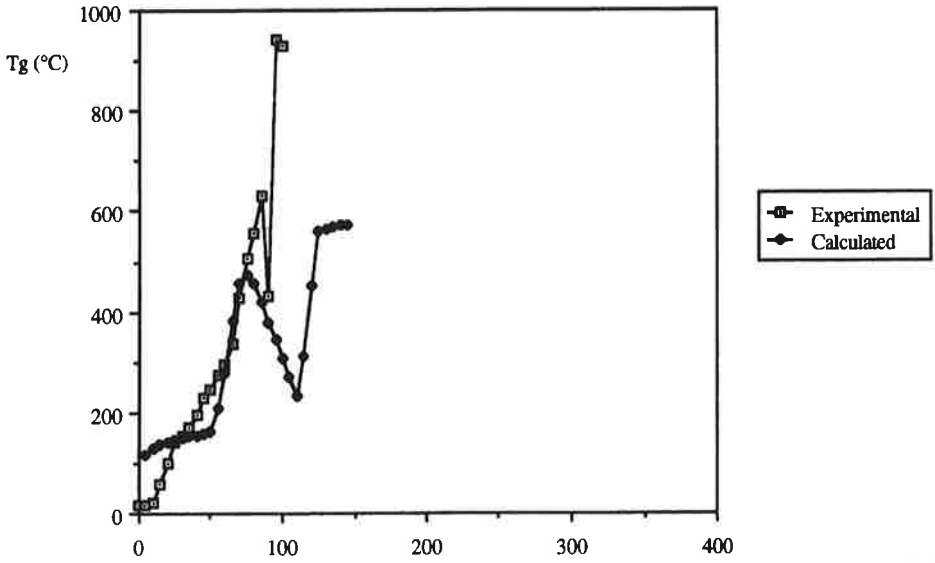

Appendix D

Results from Model A, 1/3 scale experiments

Comparison of experimental and calculated data from 1/3 scale test series, Scenario A.

Rate of heat release and gas temperatures, 13 materials.

Material S1, 1/3 scale test, Model A
Rate of heat release

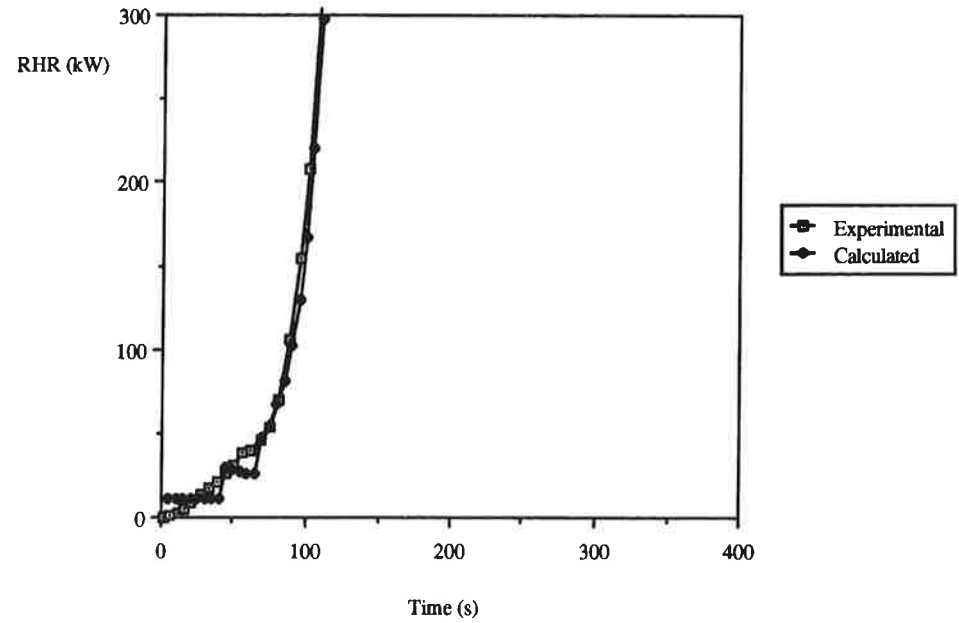

Material S1, 1/3 scale test, Model A
Gas temperature

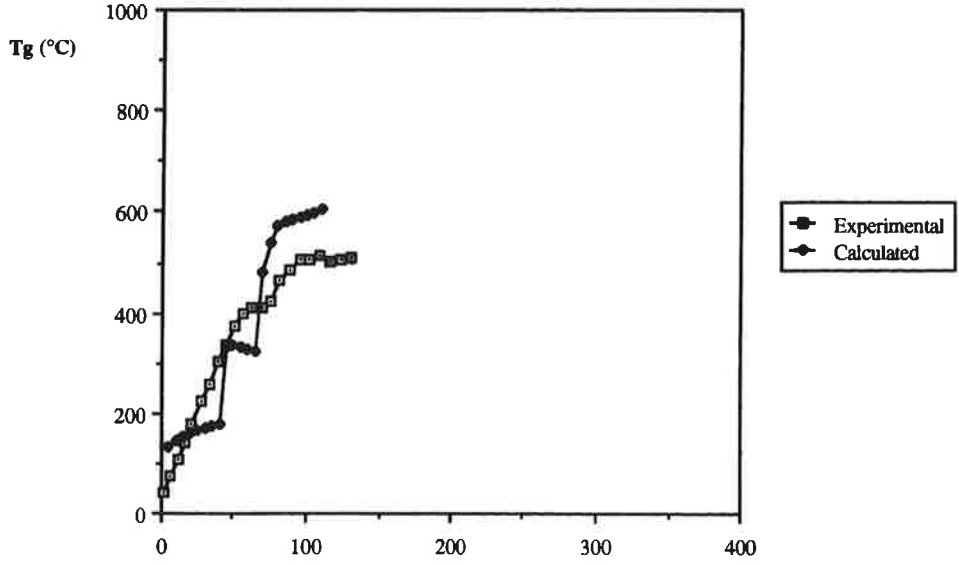

Material S2, 1/3 scale test, Model A

Rate of heat release

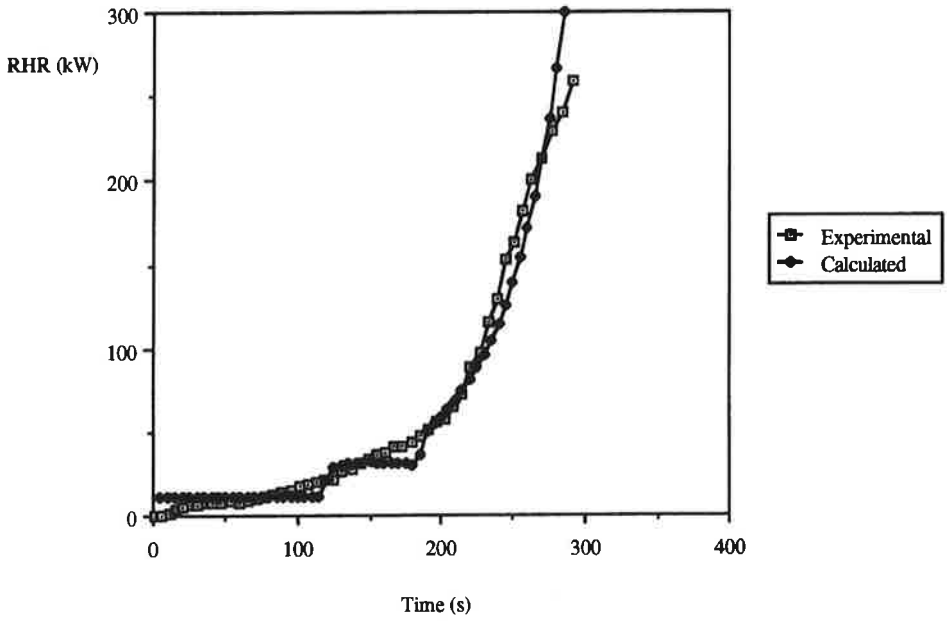

Material S2, 1/3 scale test, Model A

Gas temperature

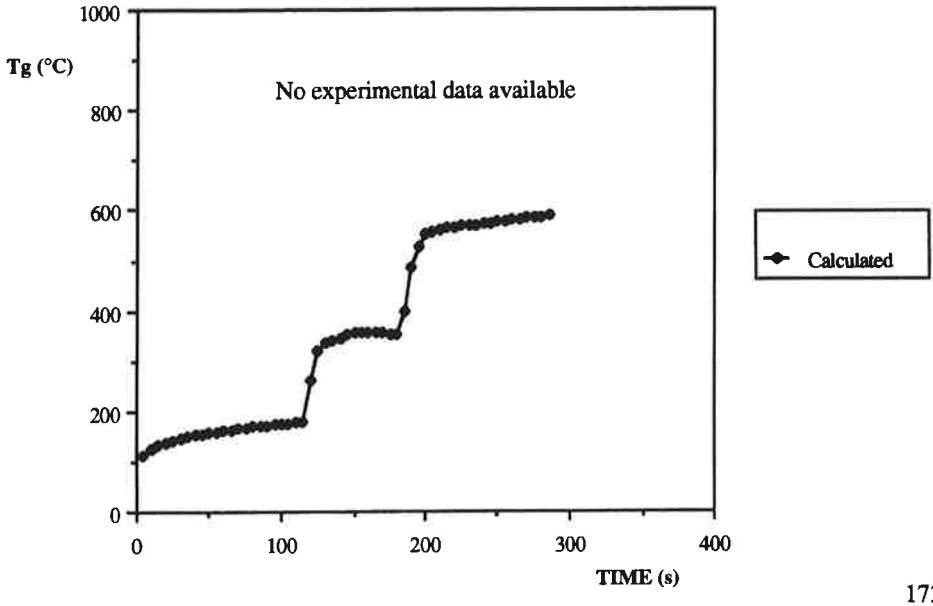

Material S3, 1/3 scale test, Model A
Rate of heat release

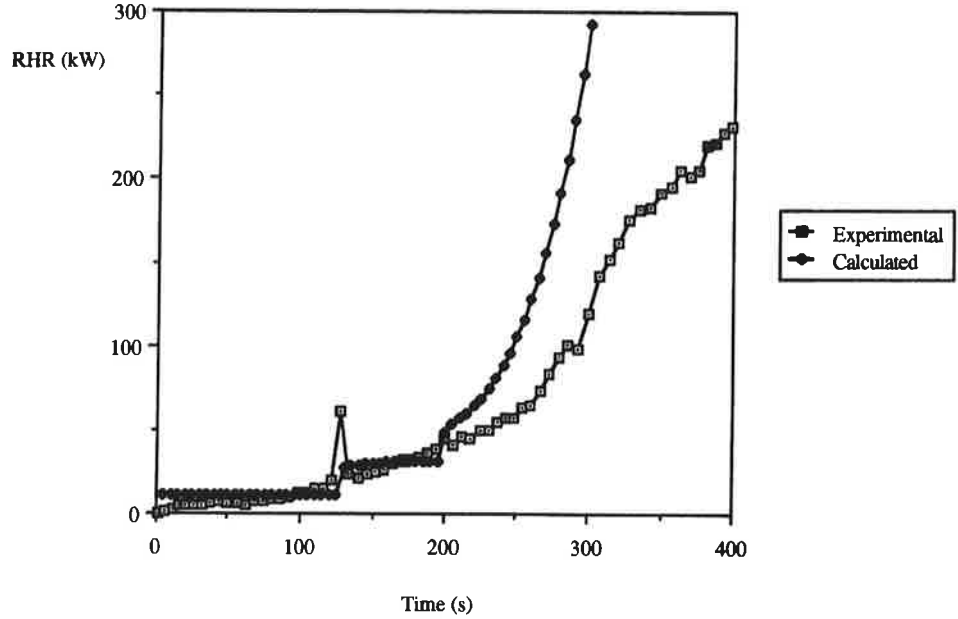

Material S3, 1/3 scale test, Model A
Gas temperature

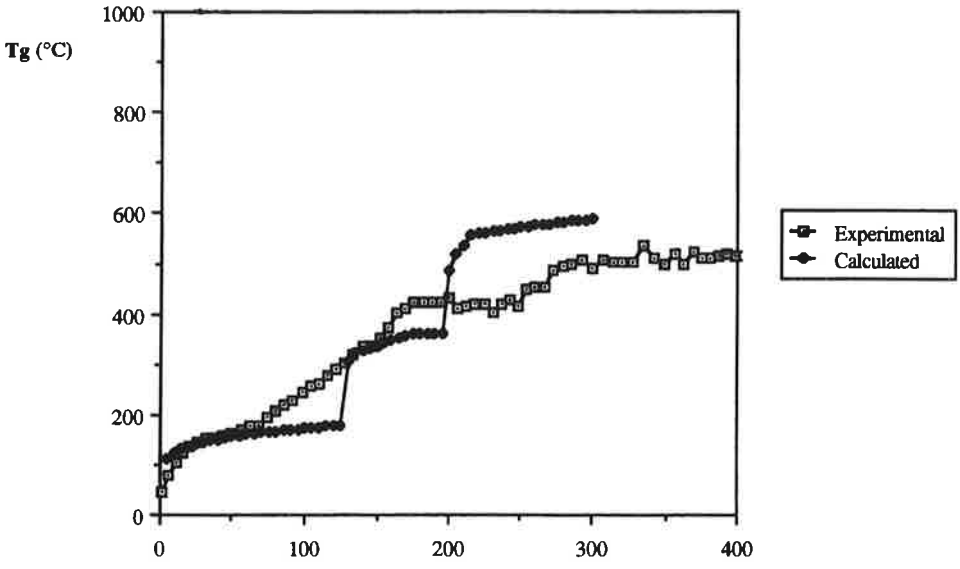

Material S4, 1/3 scale test, Model A

Rate of heat release

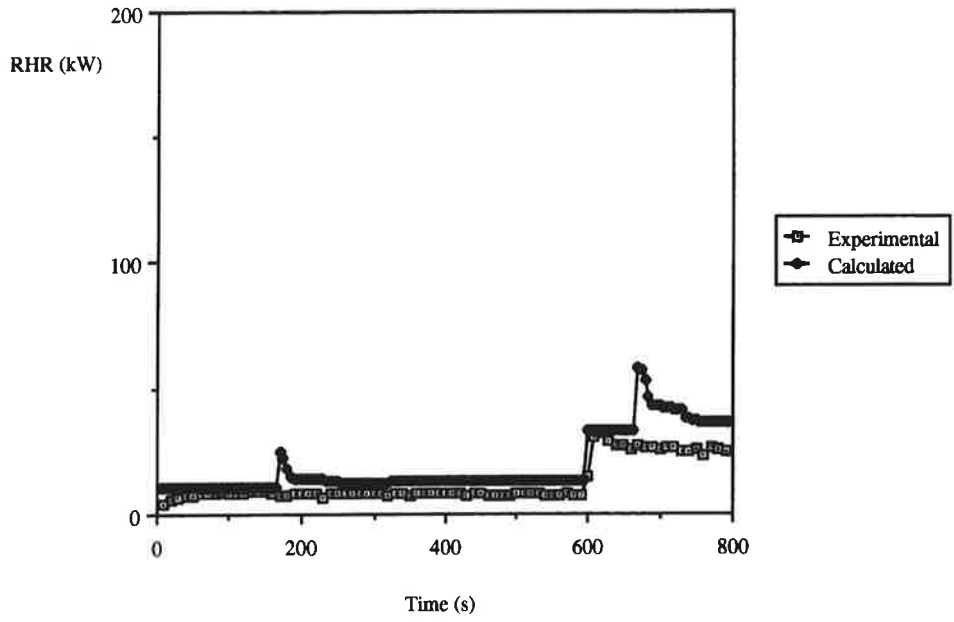

Material S4, 1/3 scale test, Model A

Gas temperature

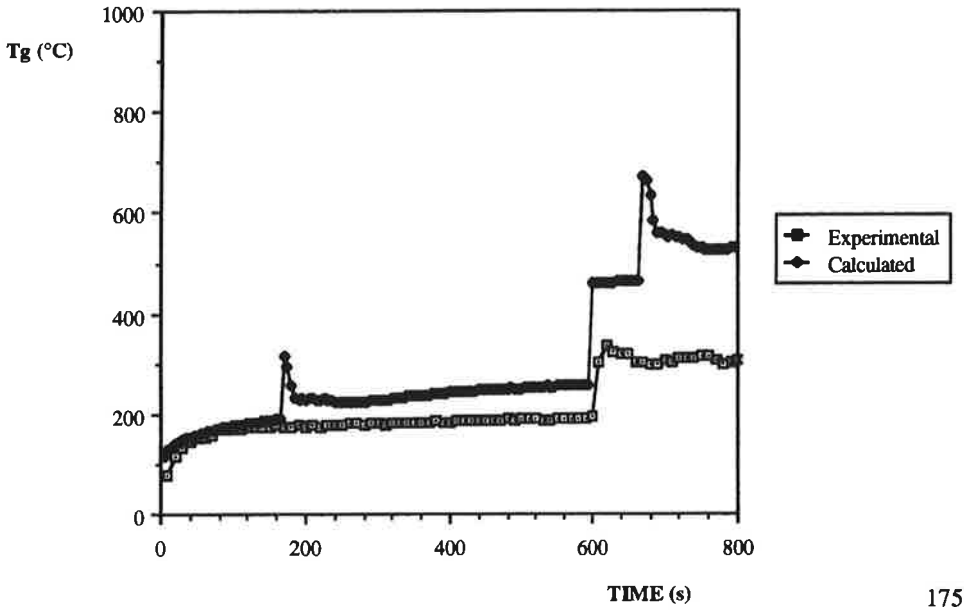

Material S5, 1/3 scale test, Model A
Rate of heat release

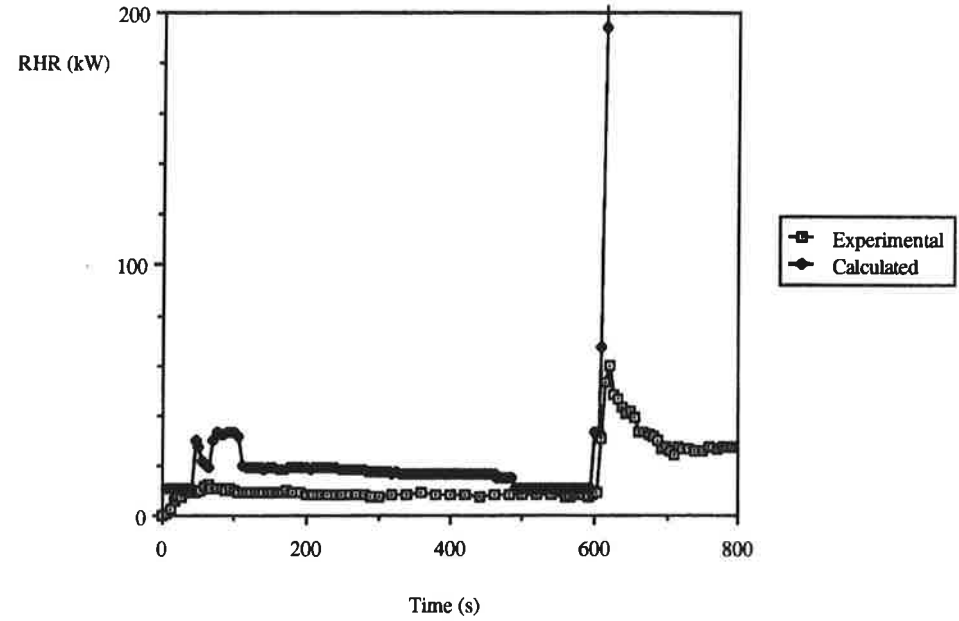

Material S5, 1/3 scale test, Model A
Gas temperature

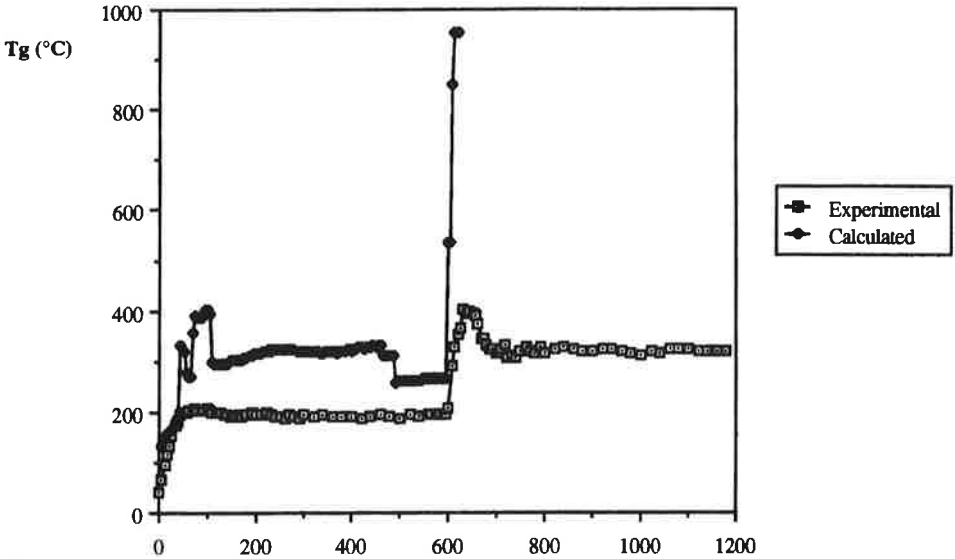

Material S6, 1/3 scale test, Model A
Rate of heat release

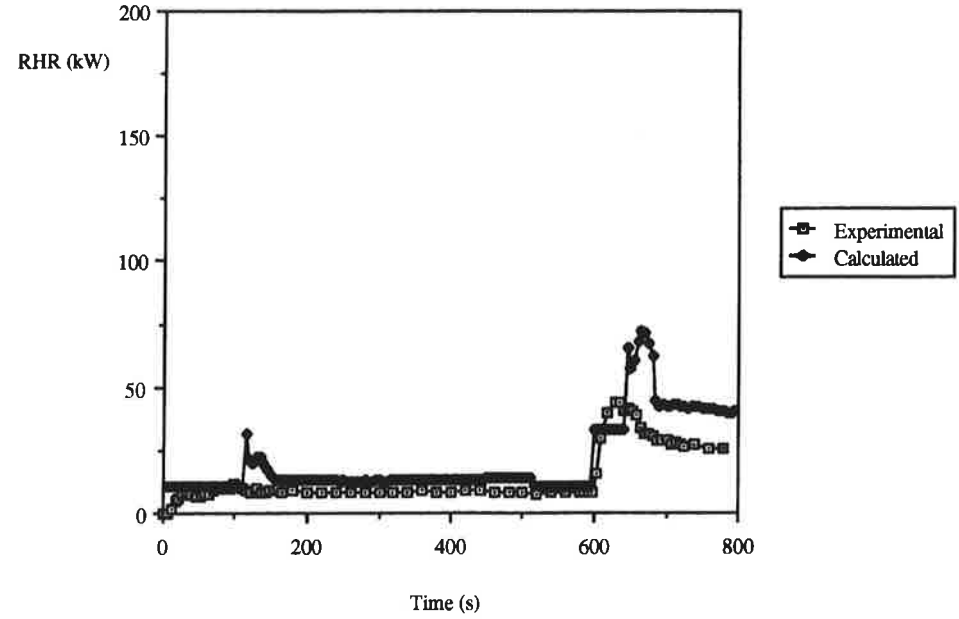

Material S6, 1/3 scale test, Model A
Gas temperature

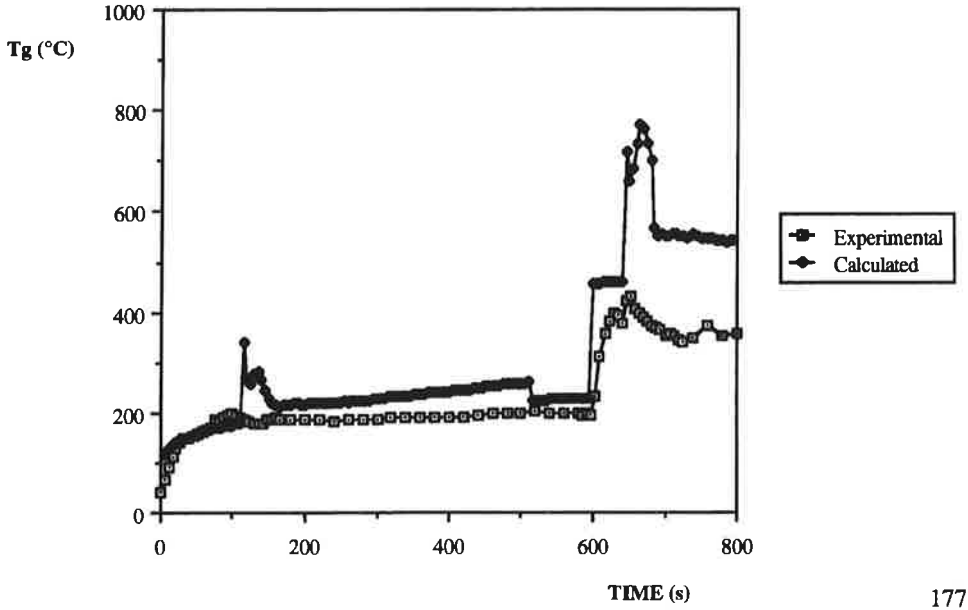

Material S7, 1/3 scale test, Model A
Rate of heat release

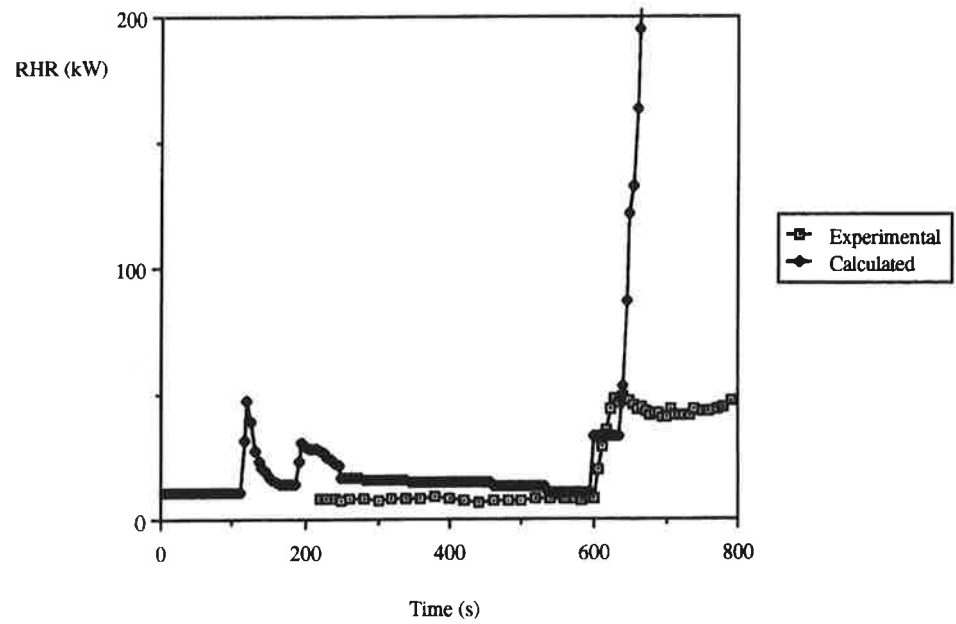

Material S7, 1/3 scale test, Model A
Gas temperature

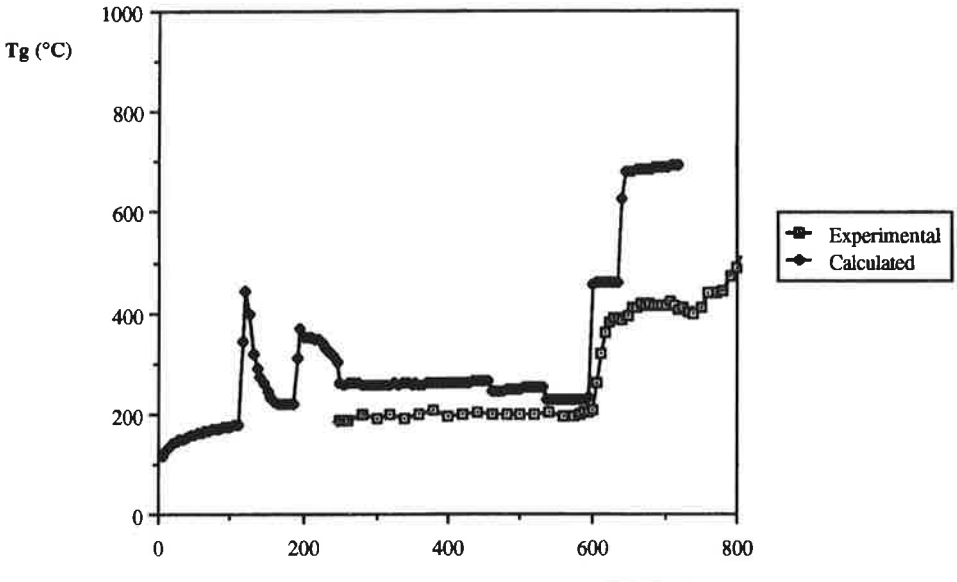

Material S8, 1/3 scale test, Model A
Rate of heat release

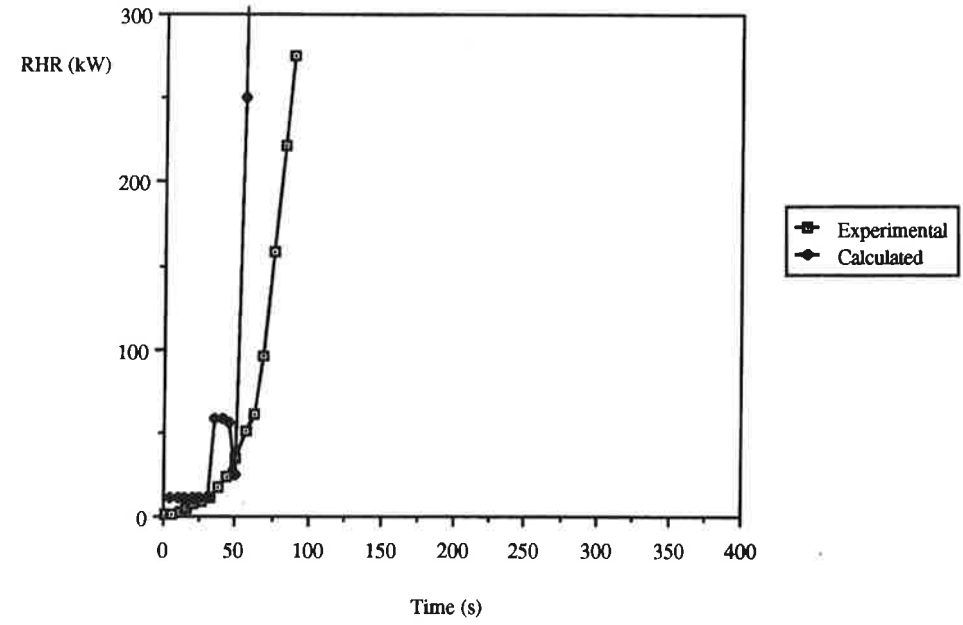

Material S8, 1/3 scale test, Model A
Gas temperature

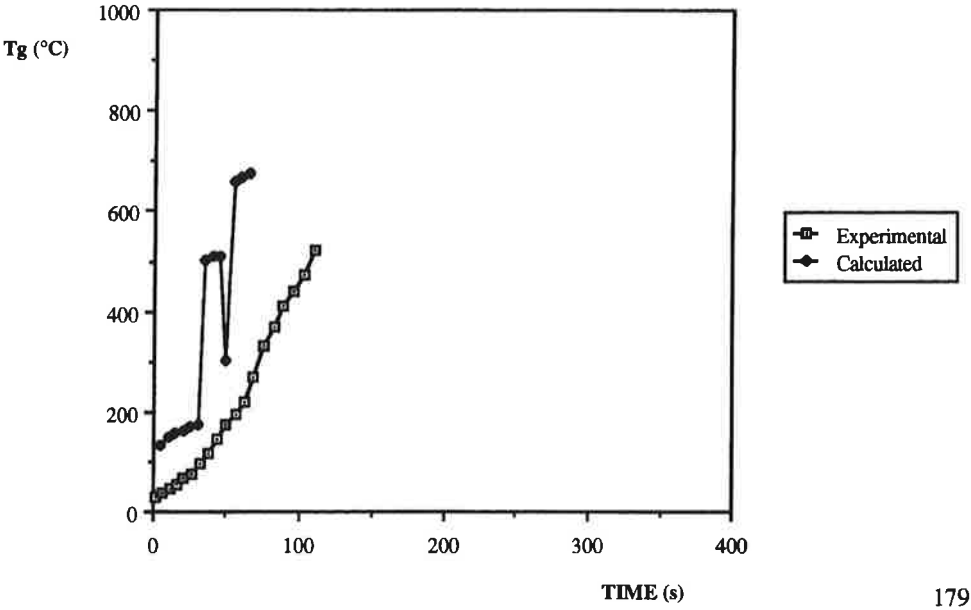

Material S9, 1/3 scale test, Model A
Rate of heat release

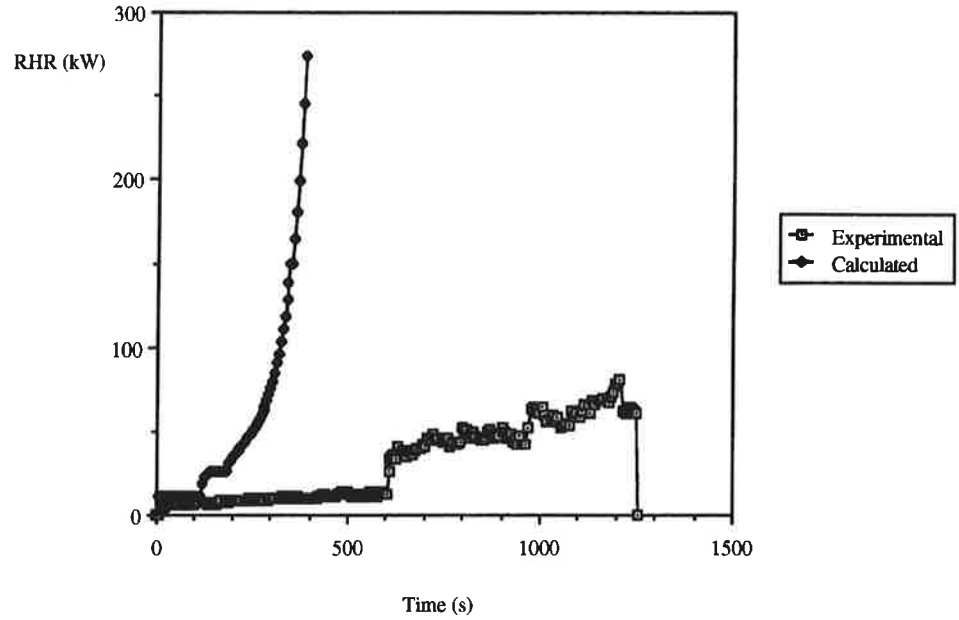

Material S9, 1/3 scale test, Model A
Gas temperature

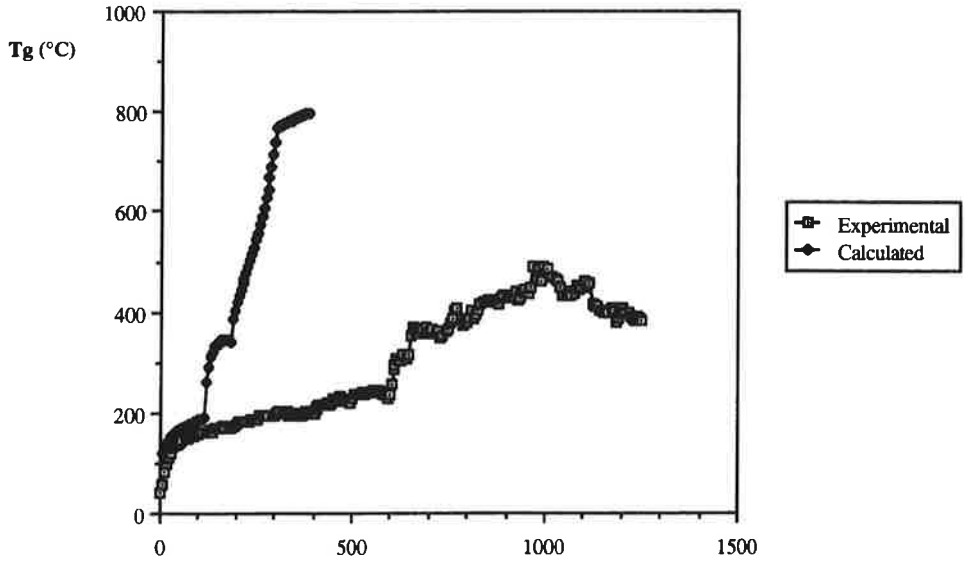

Material S10, 1/3 scale test, Model A
Rate of heat release

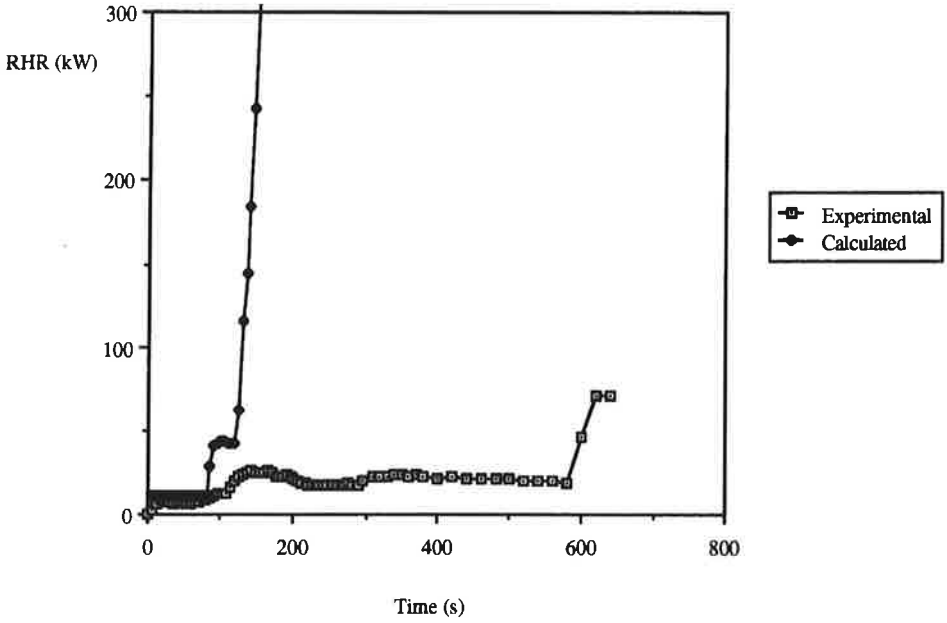

Material S10, 1/3 scale test, Model A
Gas temperature

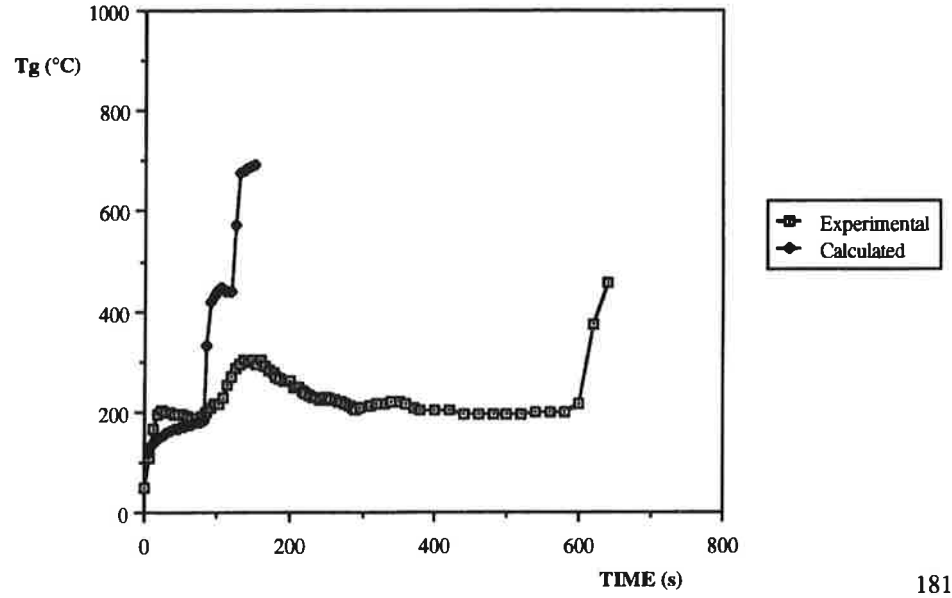

Material S11, 1/3 scale test, Model A
Rate of heat release

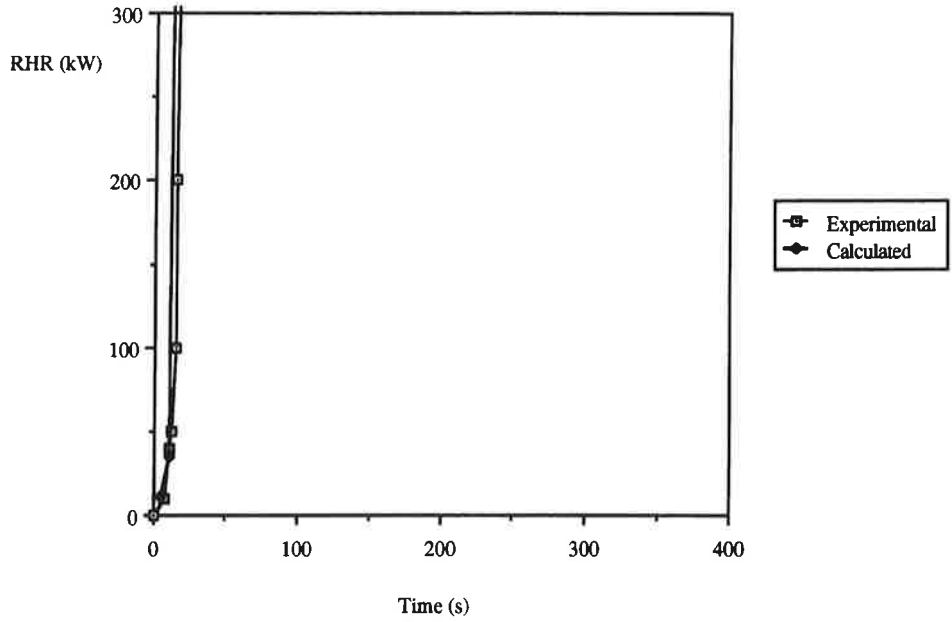

Material S11, 1/3 scale test, Model A
Gas temperature

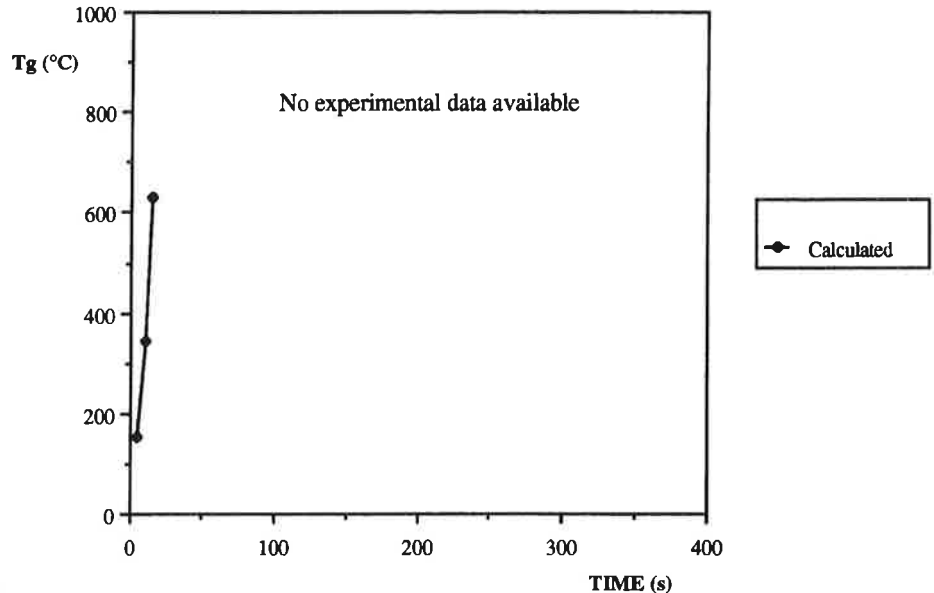

Material S12, 1/3 scale test, Model A
Rate of heat release

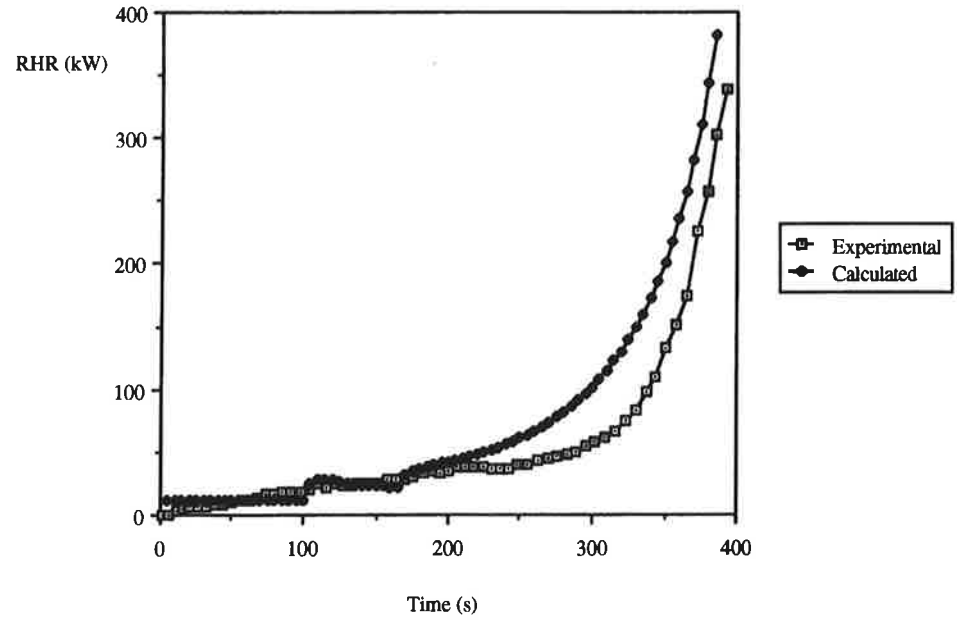

Material S12, 1/3 scale test, Model A
Gas temperature

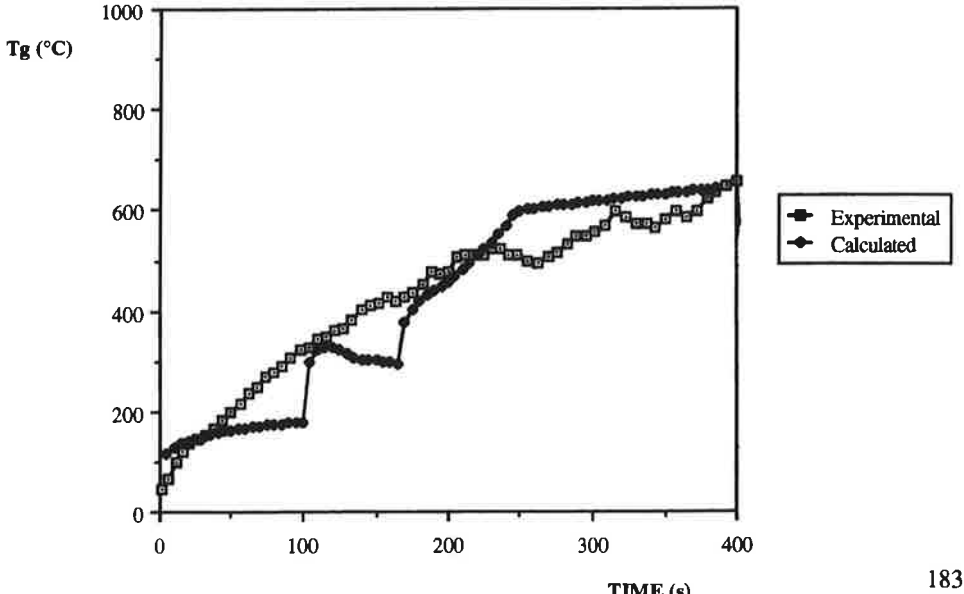

Material S13, 1/3 scale test, Model A
Rate of heat release

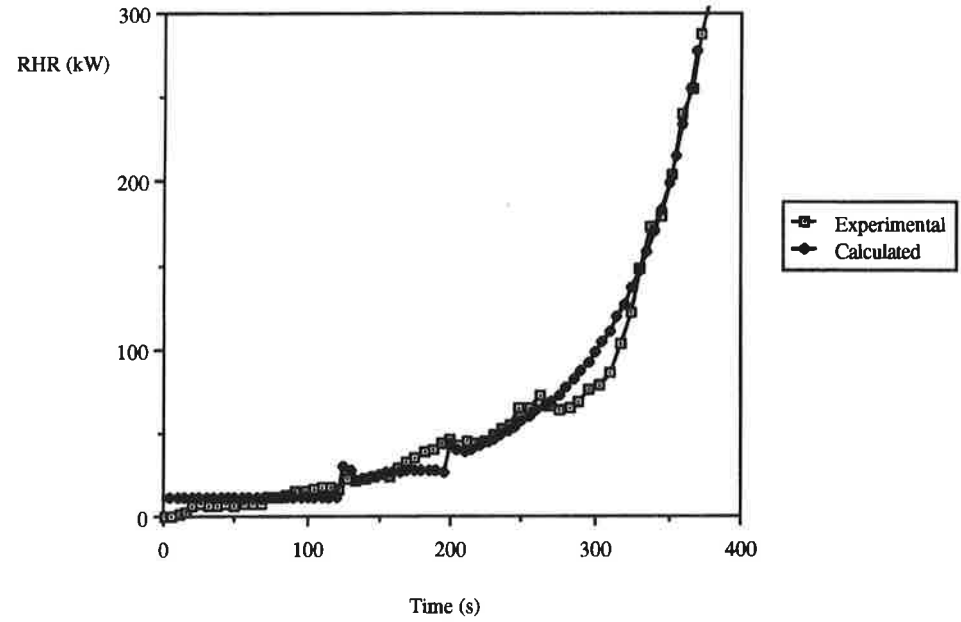

Material S13, 1/3 scale test, Model A
Gas temperature

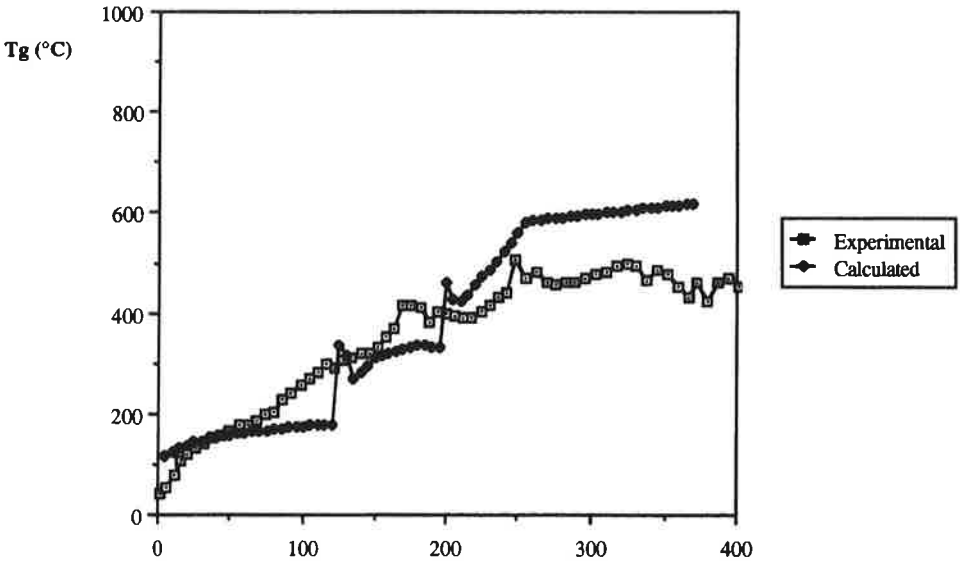

Appendix E

Results from Model B, full scale experiments

Comparison of experimental and calculated data from full scale test series, Scenario B.

Rate of heat release and gas temperatures, 4 materials.

Material S2, full scale test, Model B
Rate of heat release

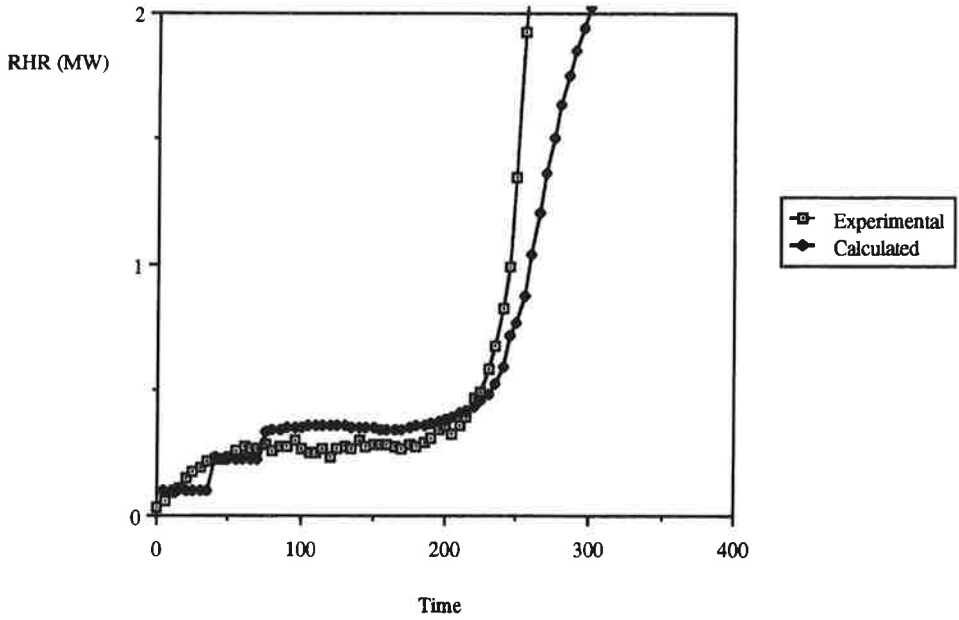

Material S2, full scale test, Model B
Gas temperature

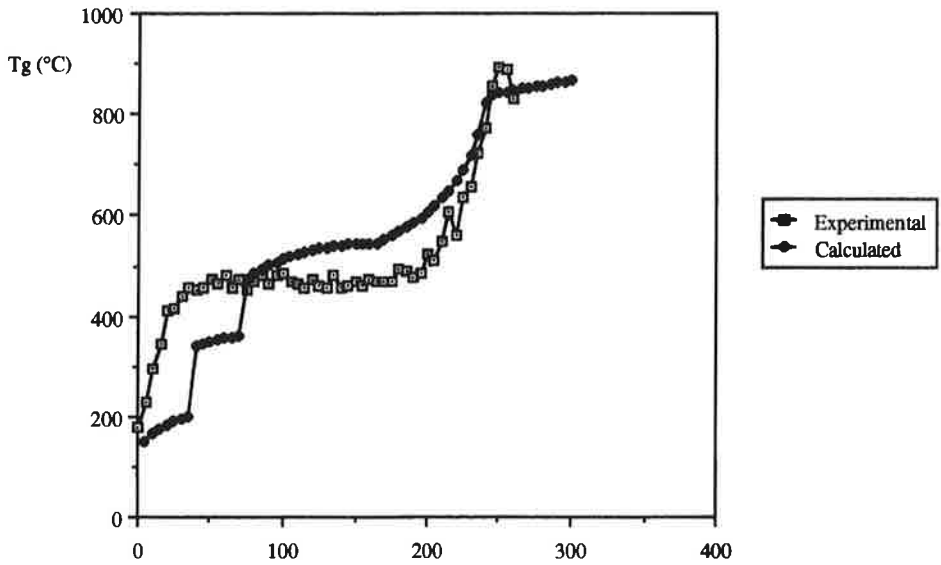

Material S3, full scale test, Model B
Rate of heat release

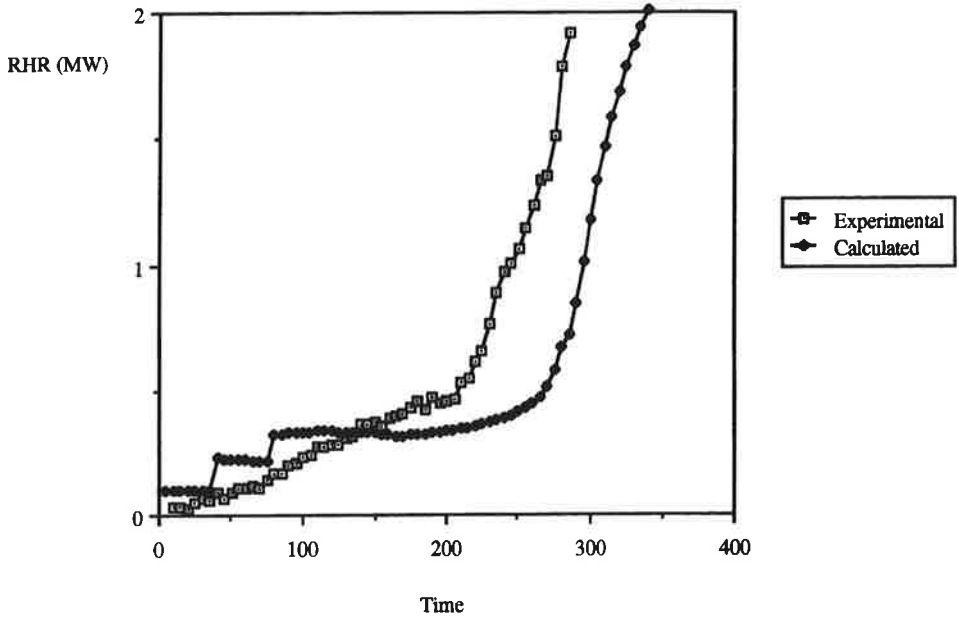

Material S3, full scale test, Model B
Gas temperature

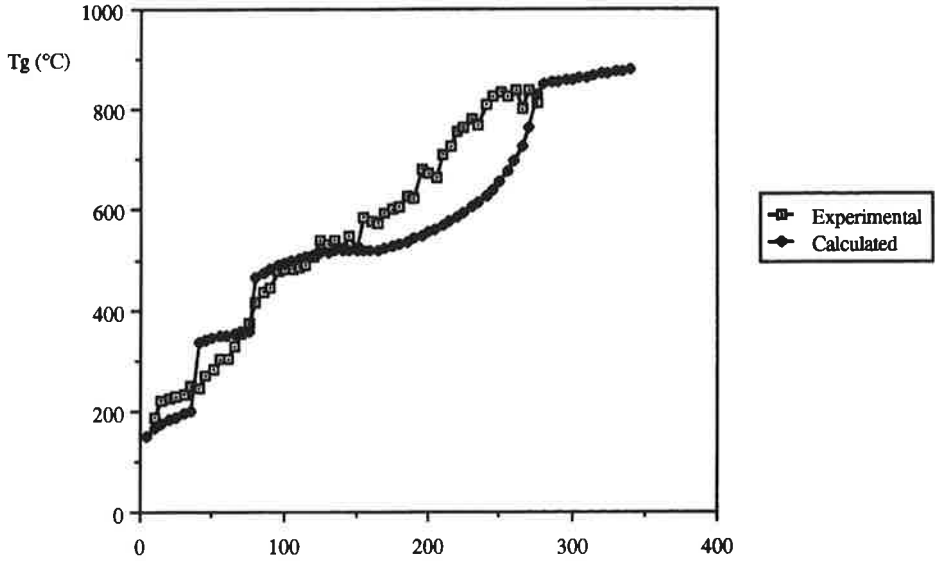

Material S6, full scale test, Model B
Rate of heat release

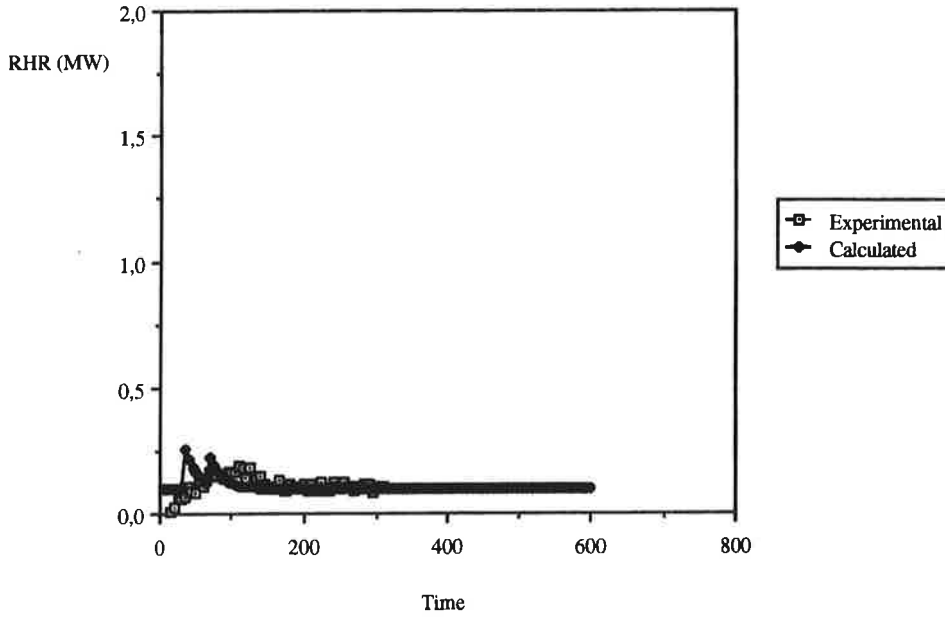

Material S6, full scale test, Model B
Gas temperature

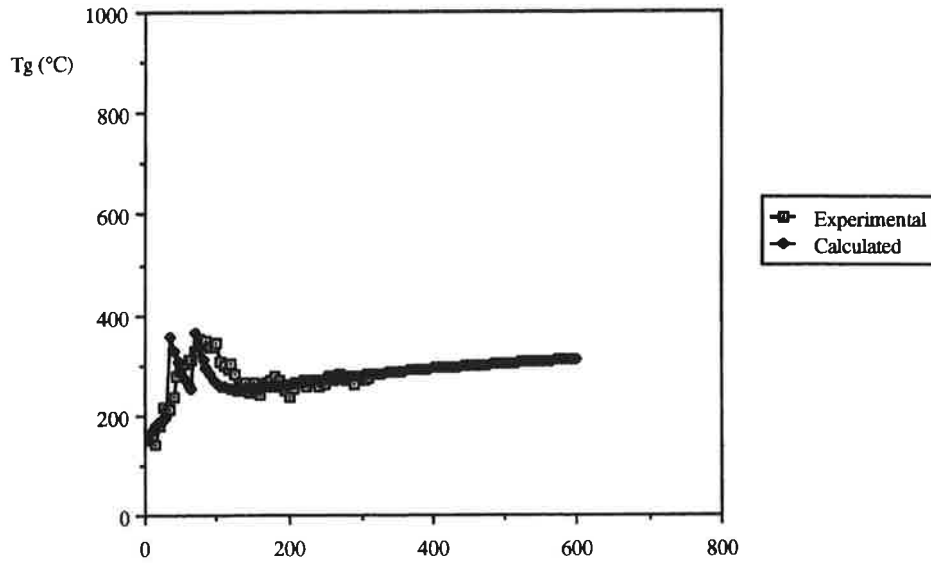

Material S8, full scale test, Model B
Rate of heat release

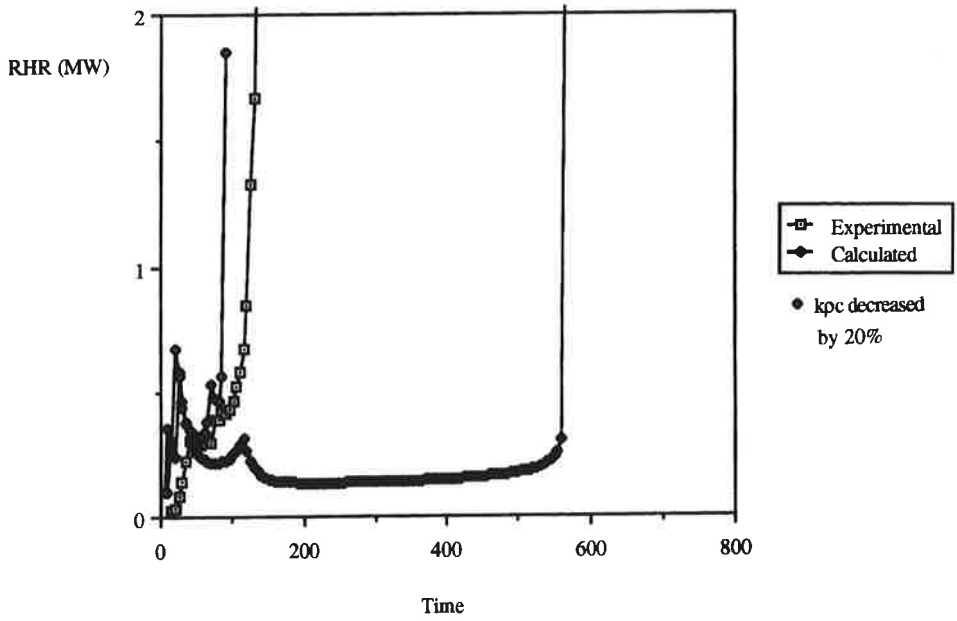

Material S8, full scale test, Model B
Gas temperature

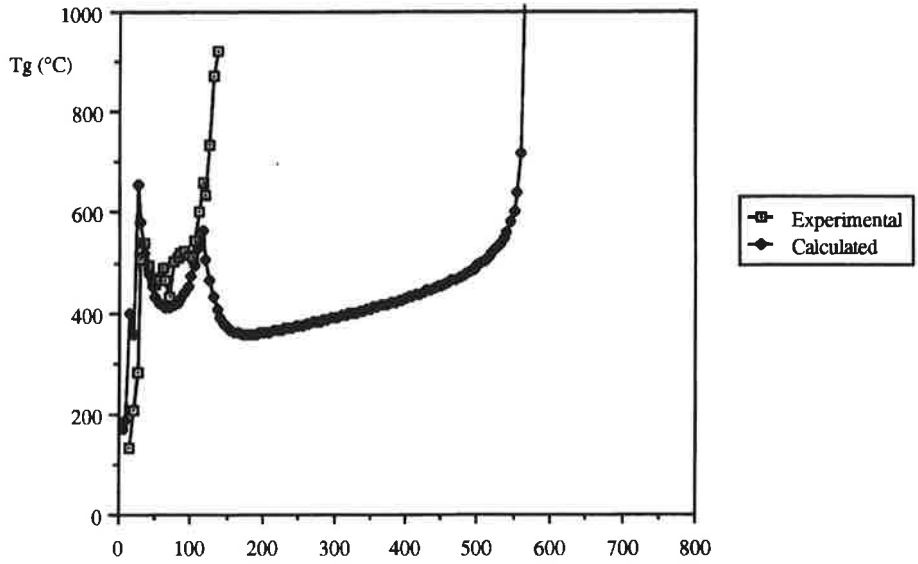

Appendix F

Results from Model B, 1/3 scale experiments

Comparison of experimental and calculated data from 1/3 scale test series, Scenario B.

Rate of heat release and gas temperatures, 10 materials.

Material S1, 1/3 scale test, Model B
Rate of heat release

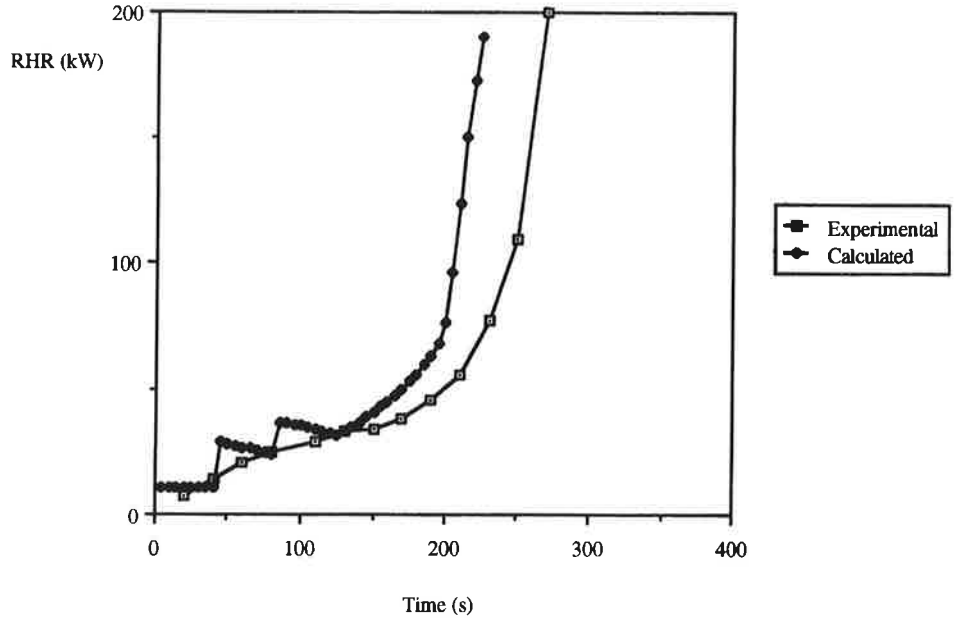

Material S1, 1/3 scale test, Model B
Gas temperature

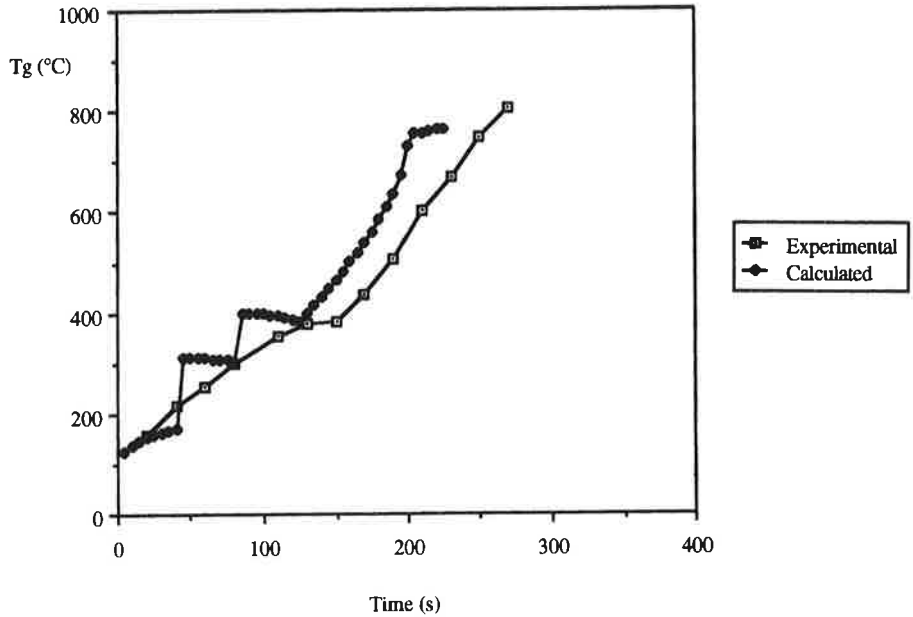

Material S2, 1/3 scale test, Model B
Rate of heat release

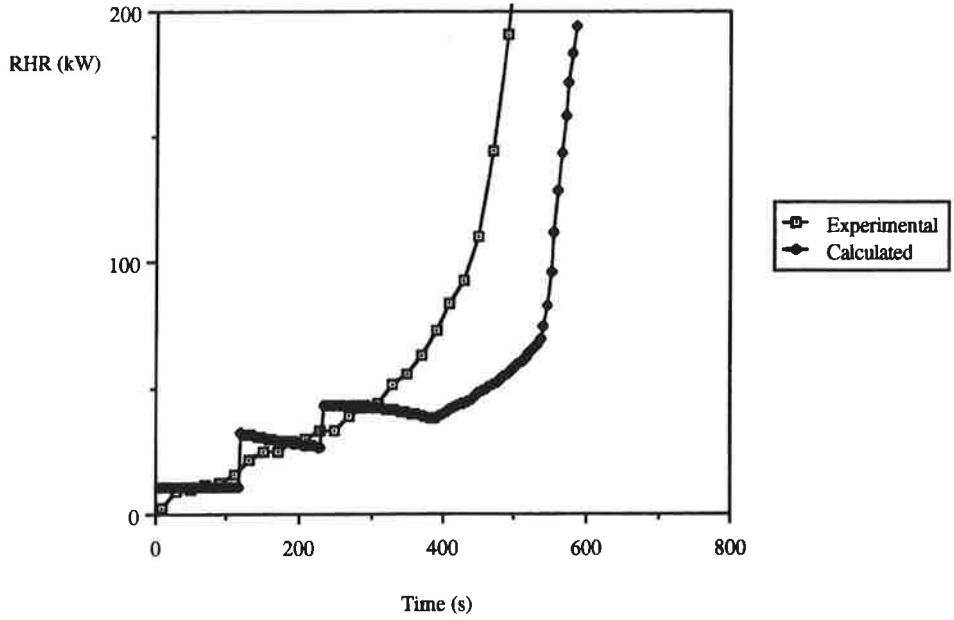

Material S2, 1/3 scale test, Model B
Gas temperature

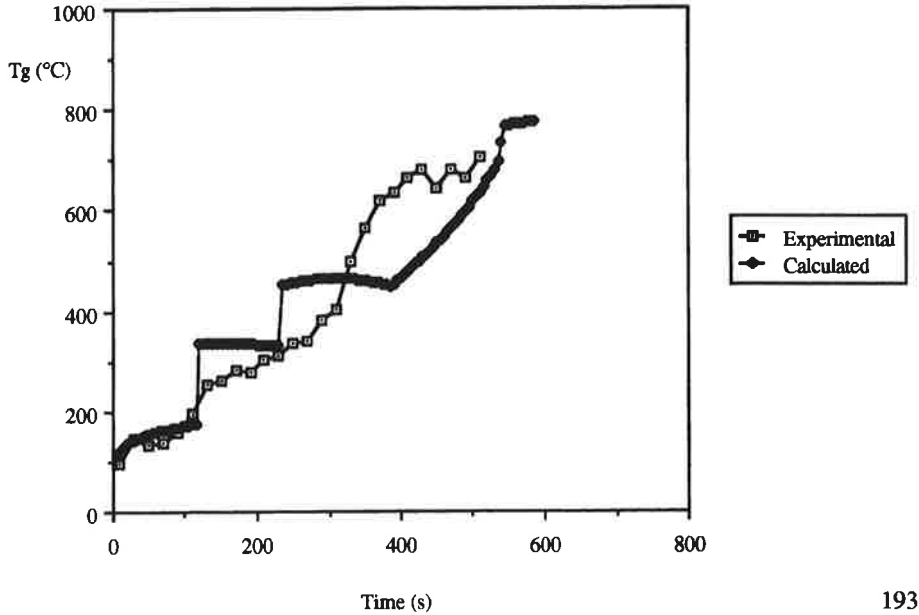

Material S3, 1/3 scale test, Model B
Rate of heat release

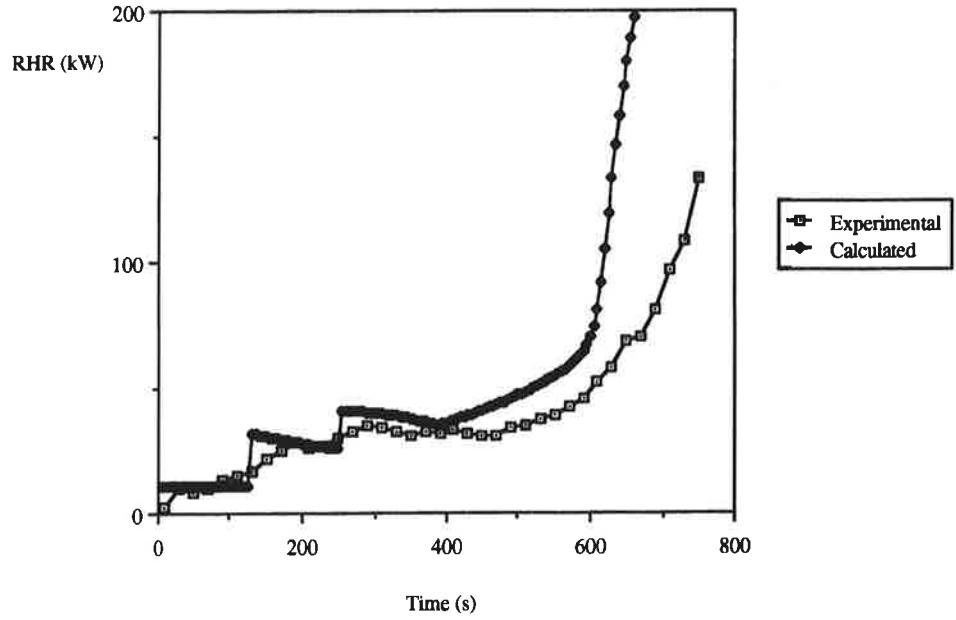

Material S3, 1/3 scale test, Model B
Gas temperature

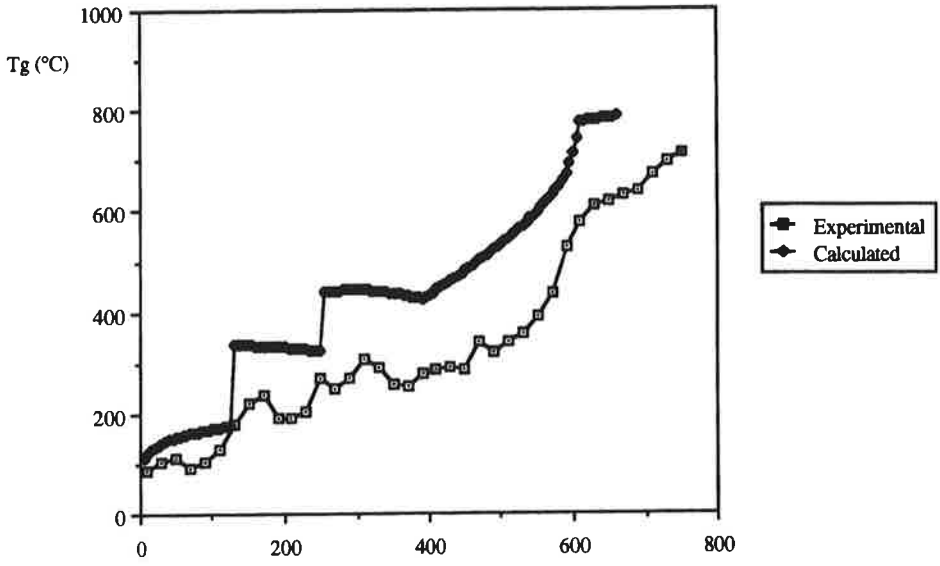

Material S5, 1/3 scale test, Model B
Rate of heat release

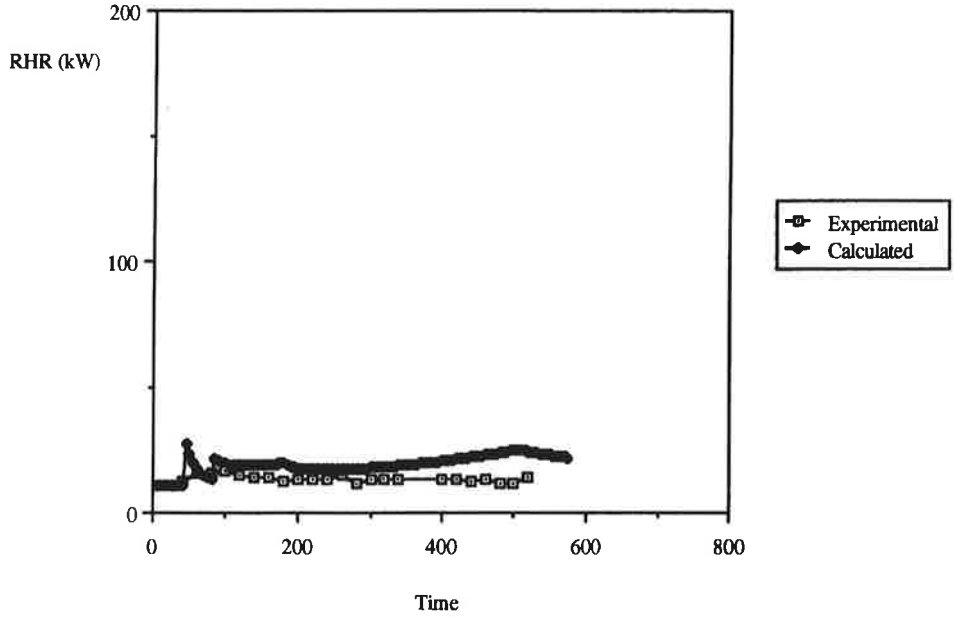

Material S5, 1/3 scale test, Model B
Gas temperature

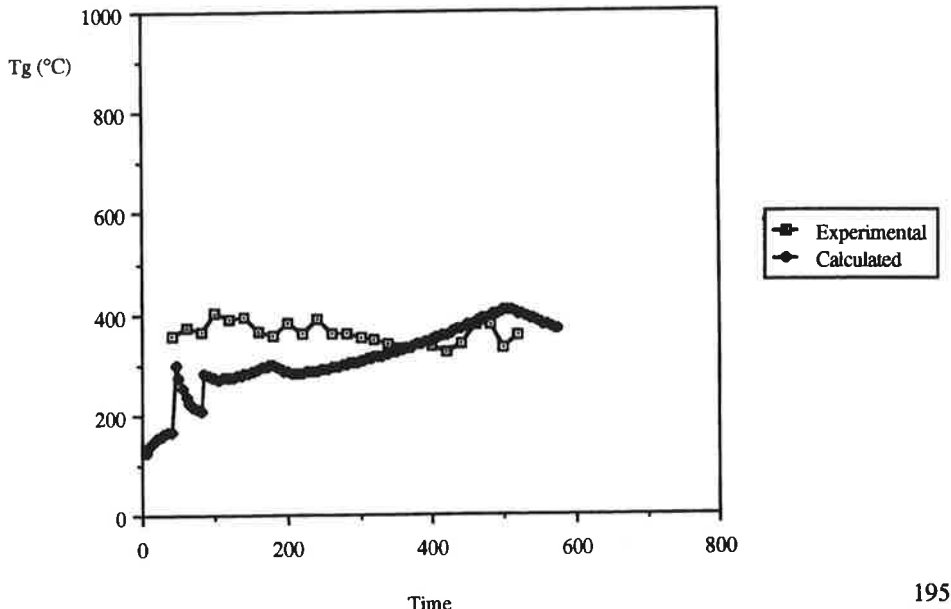

Material S7, 1/3 scale test, Model B
Rate of heat release

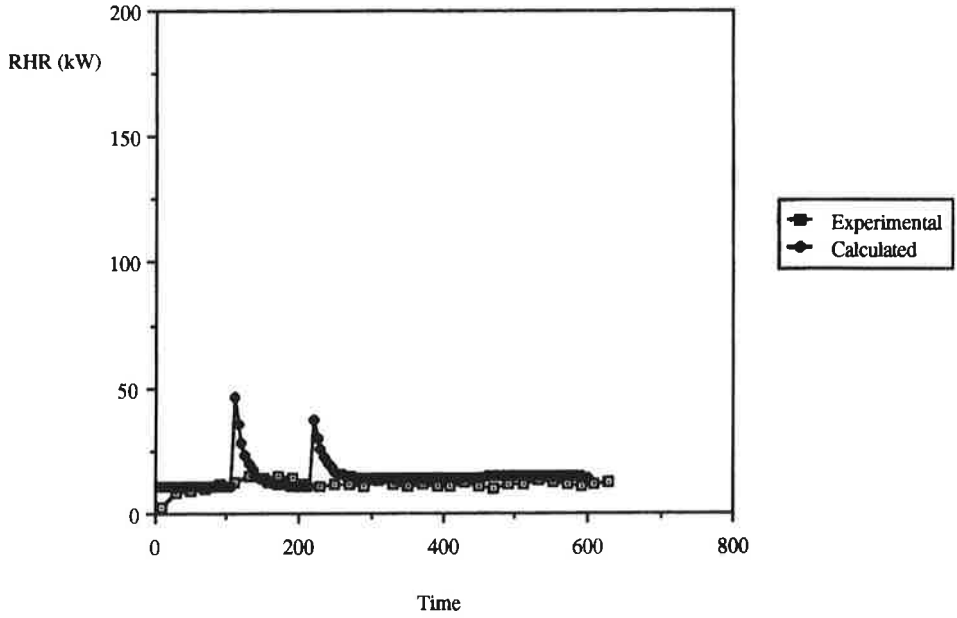

Material S7, 1/3 scale test, Model B
Gas temperature

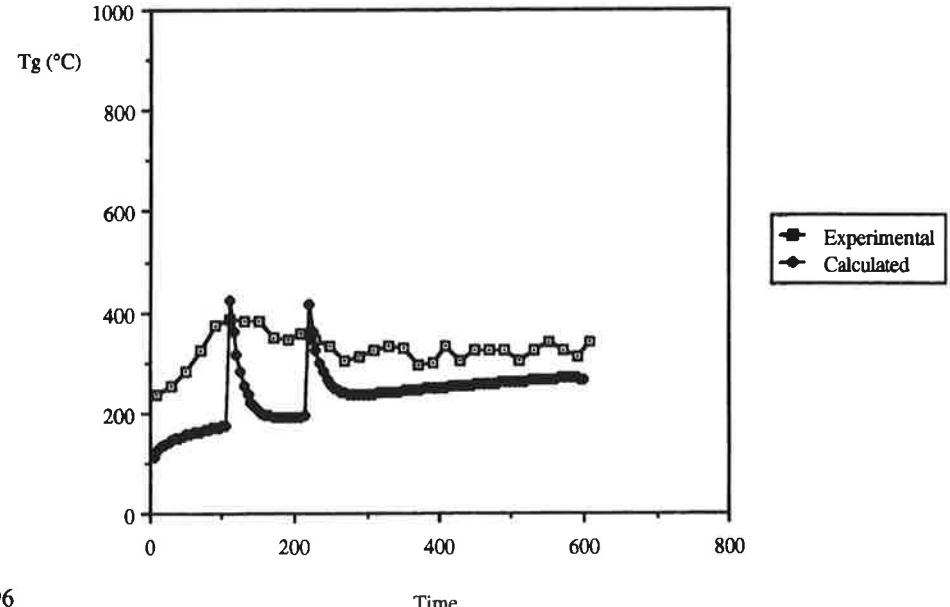

Material S8, 1/3 scale test, Model B
Rate of heat release

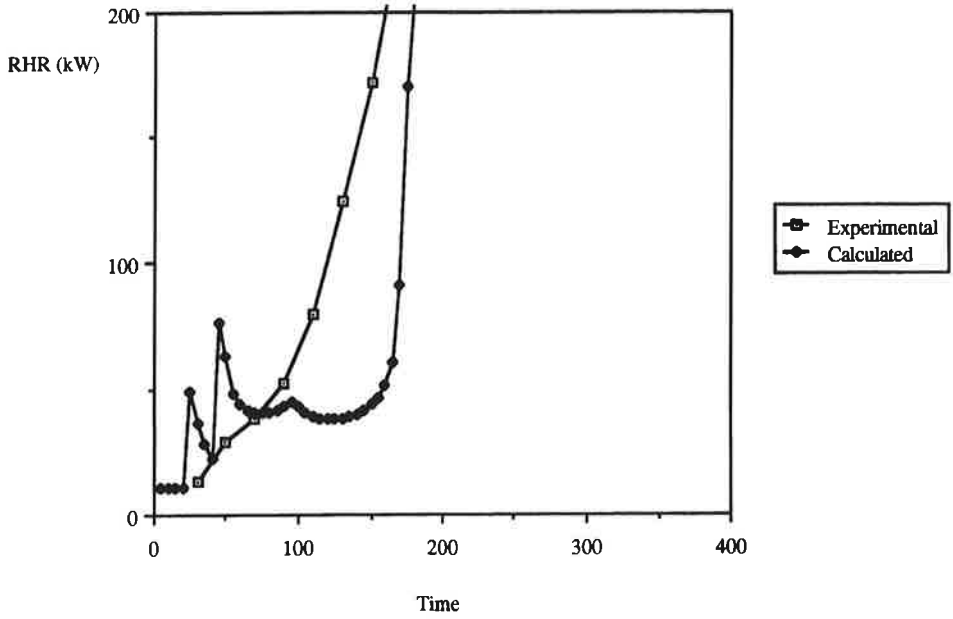

Material S8, 1/3 scale test, Model B
Gas temperature

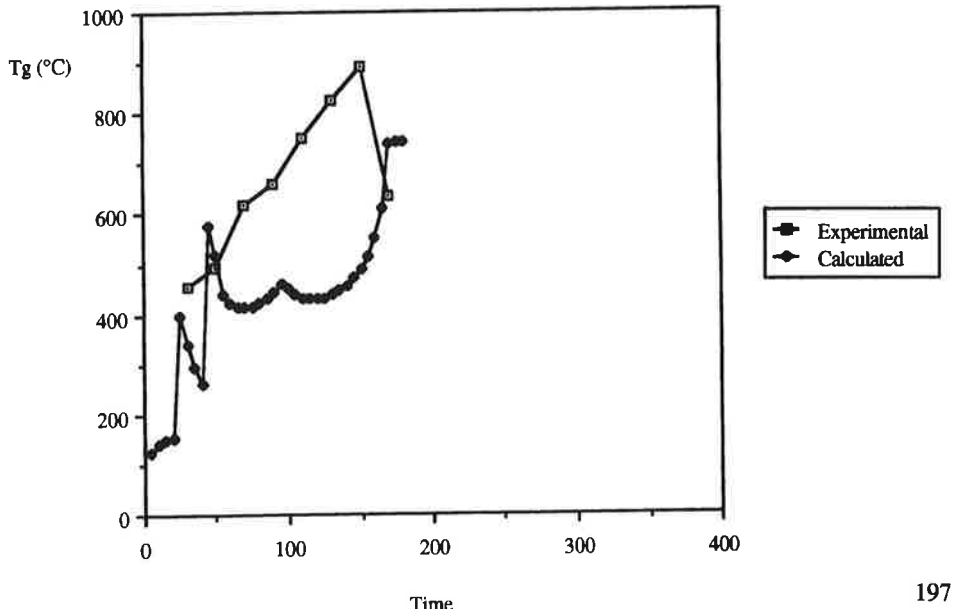

Material S9, 1/3 scale test, Model B
Rate of heat release

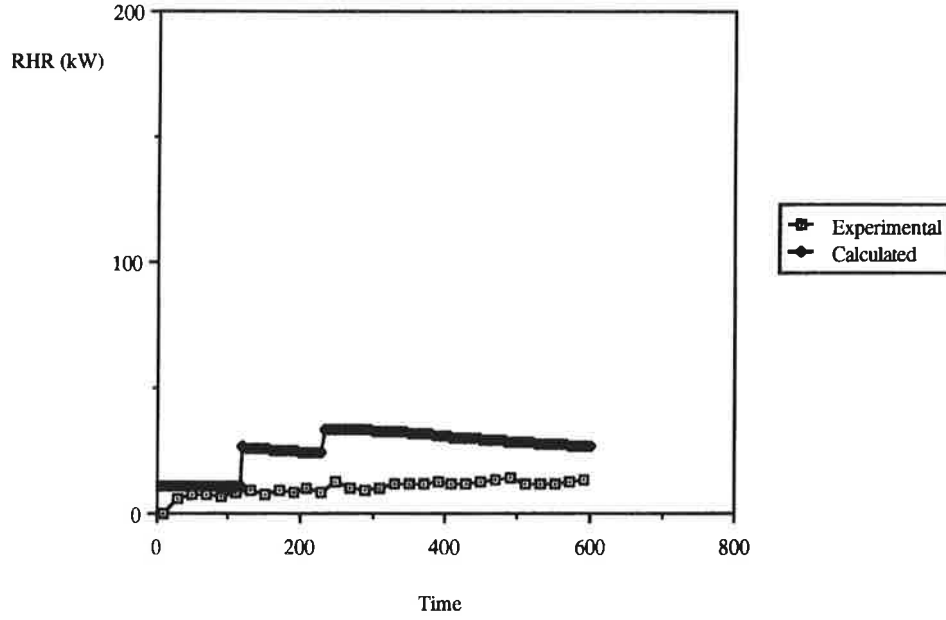

Material S9, 1/3 scale test, Model B
Gas temperature

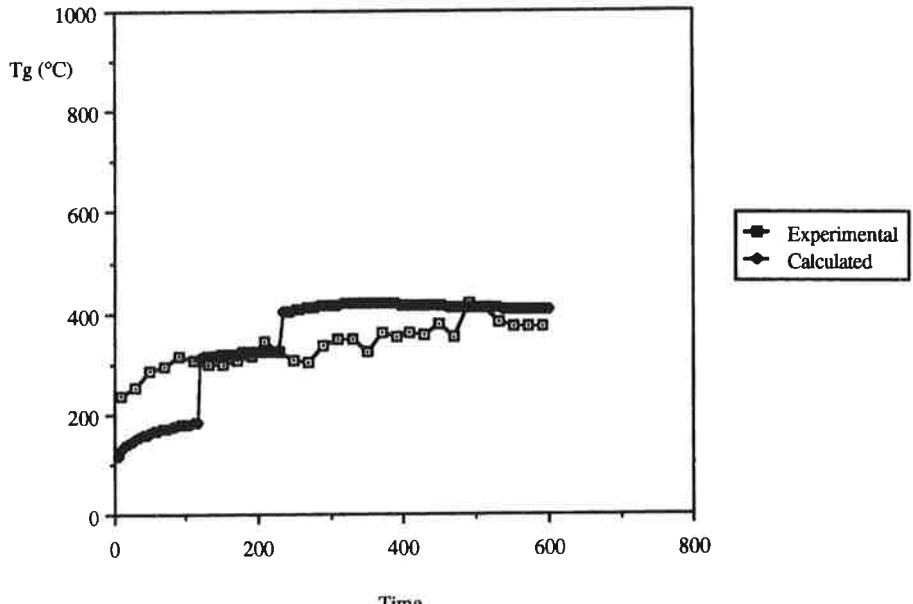

Material S11, 1/3 scale test, Model B

Rate of heat release

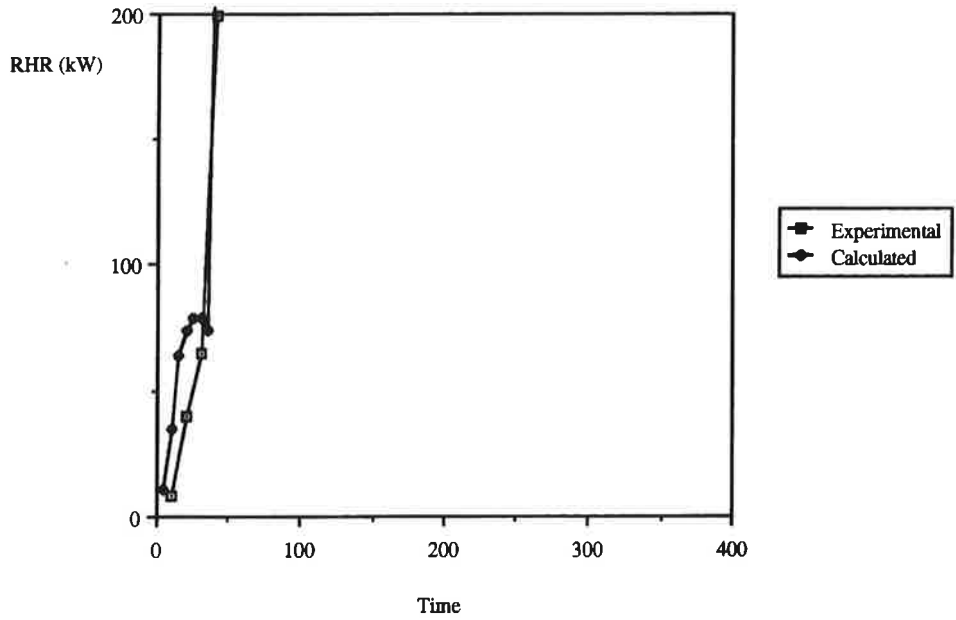

Material S11, 1/3 scale test, Model B

Gas temperature

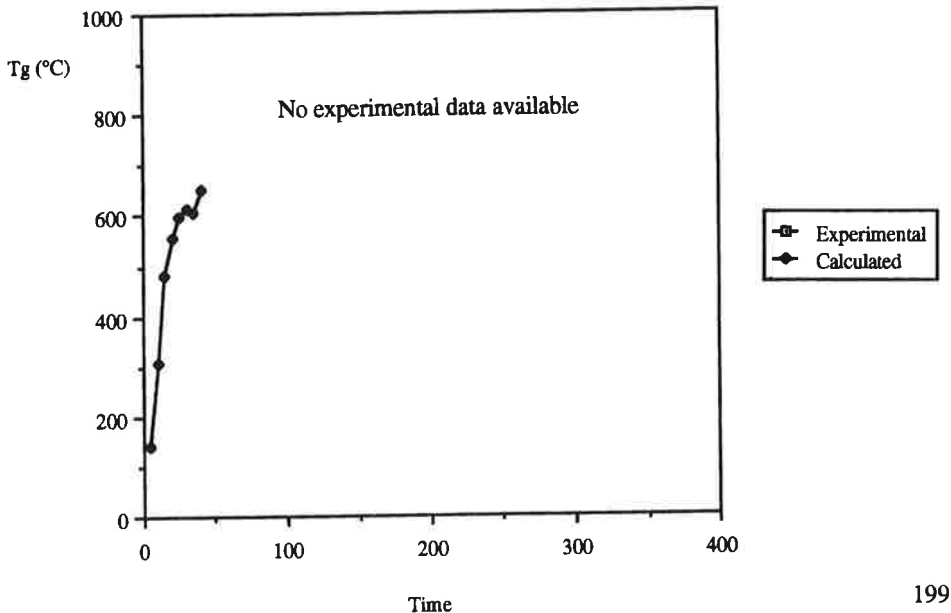

Material S12, 1/3 scale test, Model B
Rate of heat release

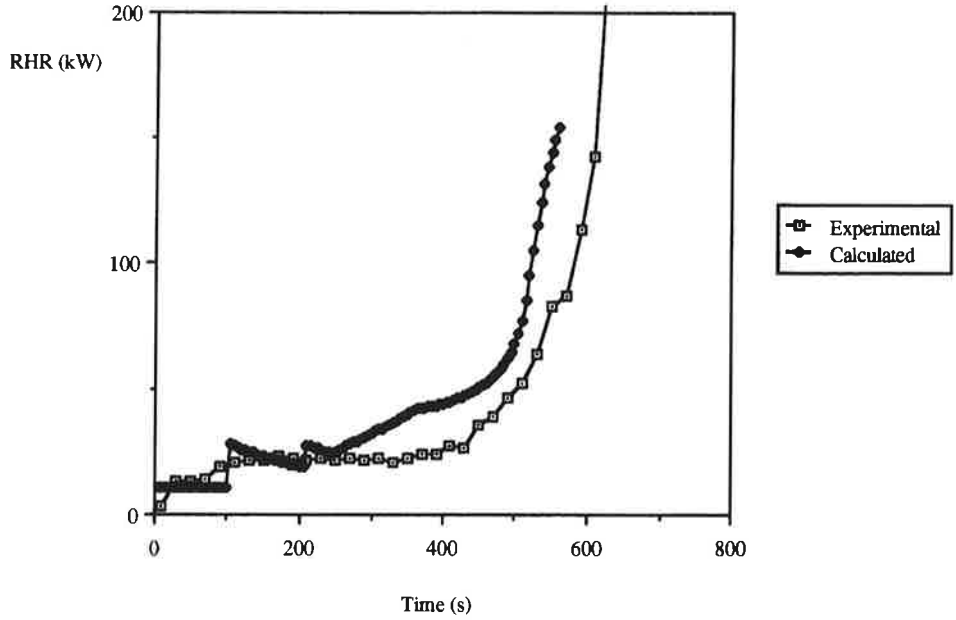

Material S12, 1/3 scale test, Model B
Gas temperature

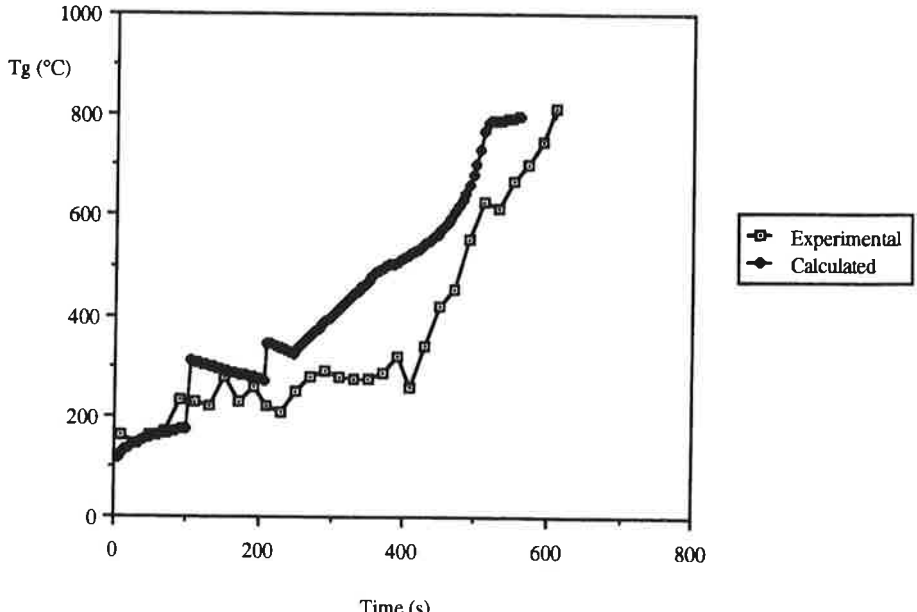

Material S13, 1/3 scale test, Model B
Rate of heat release

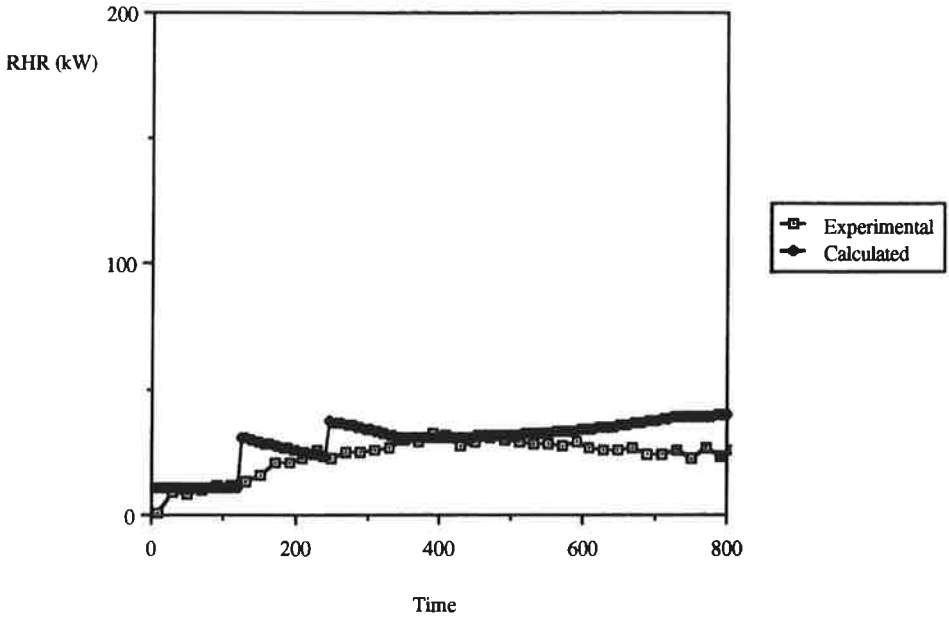

Material S13, 1/3 scale test, Model B
Gas temperature

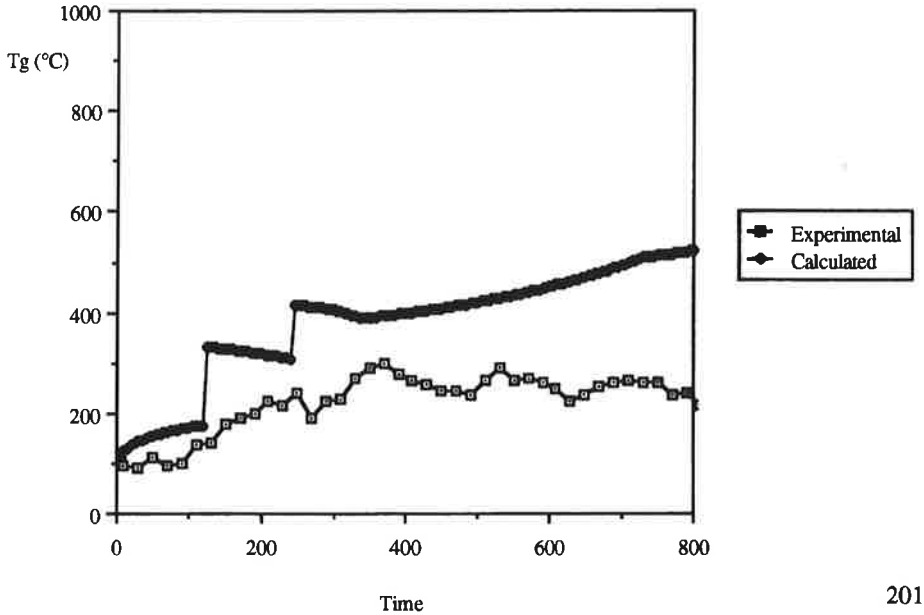

Report TVBB-1009
ISSN 1102-8246
ISRN LUTVDG/TVBB-- 1009--SE

KFS AB, Lund 1997